PROBABILISTIC ANALYSIS OF POWER SYSTEM WITH WIND GENERATORS

Ph.D. THESIS

by

NEERAJ GUPTA

DEPARTMENT OF ELECTRICAL ENGINEERING
INDIAN INSTITUTE OF TECHNOLOGY ROORKEE
ROORKEE – 247667 (INDIA)
DECEMBER, 2014

PROBABILISTIC ANALYSIS OF POWER SYSTEM WITH WIND GENERATORS

A THESIS

Submitted in partial fulfilment of the requirements for the award of the degree

of

DOCTOR OF PHILOSOPHY

in

ELECTRICAL ENGINEERING

by

NEERAJ GUPTA

DEPARTMENT OF ELECTRICAL ENGINEERING
INDIAN INSTITUTE OF TECHNOLOGY ROORKEE
ROORKEE – 247667 (INDIA)
DECEMBER, 2014

INDIAN INSTITUTE OF TECHNOLOGY ROORKEE
ROORKEE

CANDIDATE'S DECLARATION

I hereby certify that the work which is being presented in the thesis entitled **PROBABILISTIC ANALYSIS OF POWER SYSTEM WITH WIND GENERATORS** in partial fulfilment of the requirements for the award of the Degree of Doctor of Philosophy and submitted in the **Department of Electrical Engineering** of the **Indian Institute of Technology Roorkee** is an authentic record of my own work carried out during a period from Dec. 2009 to Dec. 2014 under the supervision of **Dr. Biswarup Das**, Professor and **Dr. Vinay Pant**, Assistant Professor, Department of Electrical Engineering, Indian Institute of Technology Roorkee. The matter presented in this thesis has not been submitted by me for the award of any other degree of this or any other Institute.

(Neeraj Gupta)

This is to certify that the above statement made by the candidate is correct to the best of our knowledge.

(Vinay Pant)
Supervisor

(Biswarup Das)
Supervisor

Dated:

Abstract

Owing to the great proliferation of intermittent generation (wind, solar) in power grid, open access system, deregulation and competitive power markets, the power system operation has become uncertain. Generally, the deterministic load flow (DLF) method using Newton Raphson technique is widely used for the planning and operation of a power system on a daily basis. DLF uses the crisp values of power generations and load demands corresponding to a particular network configuration to calculate the output variables of interest and as a result, it discounts the uncertainties in the power systems, e.g. load demand variation, generator outages and the change of network configurations. Further, DLF also does not take into account the fluctuating and uncertain power generated by the renewable energy sources such as wind, photovoltaic systems etc. For addressing various issues of power system operation and planning, while taking into account uncertainties, probabilistic load flow (PLF) was proposed in 1970s and has been widely used since then. PLF is used to find the probability that the various parameters of the system such as bus voltage magnitudes, line power flows and reactive power injection from the generators are within their respective specified limits. If the calculated probabilities of various limit violations are found to be unacceptable, suitable remedial measures are adopted to alleviate the problem. Additionally, by performing PLF studies in an open access system, the system planning engineers gain more confidence in making proper judgments concerning investments in an uncertain environment.

In the recent years, the power system industry has undergone a radical change i.e. transition to the horizontally operated system from a vertically operated power system. One of the major changes brought by this new structure is the incorporation of higher levels of non-dispatchable, stochastic generation in the system. The high penetration of intermittent generation in power grid has increased the uncertainty in power systems, which affects the medium and long term planning and day-ahead operation of the system. Now, among all the non-dispatchable intermittent distributed generation (DG) resources, wind energy has achieved substantial penetration level in the power grid. Therefore, for a system with large amount of wind power penetration, the probabilistic load flow analysis tool becomes even more important. However, the non-Gaussian probability density function (Weibull or Rayleigh) of wind speed and the correlation among the wind farms pose a major challenge for carrying out PLF for a system with high level of embedded wind power generation.

To address the above issues, different methods of PLF have been proposed in the literature. Among these methods, point estimate method (PEM) is an efficient method for estimating the mo-

ments of output variables of interest for a given set of input random variables. The point estimate method uses discrete locations on the probability density function (PDF) and the corresponding weights of the input random variables to calculate the statistical moments of the output variables using non-linear load flow (LF) equations. By this approximation, the contribution of each input random variable to the output variables is taken into account. The method can be applied to problems involving either continuous or discrete random variables. PEM has many variants, which use either 2, 3, 5 or 7 points to approximate a given PDF in the increasing order of their accuracies. As PEM requires less amount of statistical information about the random input data and is also computationally efficient with sufficient degree of accuracy, in this thesis, PLF using PEM has been carried out. To obtain the PDF and the cumulative distribution function (CDF) of the output variables from the moments calculated by the PEM based PLF, Gram-Charlier (GC) and Cornish-Fisher (CF) series have been used in the literature. Now, GC and CF series are quite accurate for approximating a unimodal PDF with CF being marginally better than GC. However, with the inclusion of generator reactive power limits and multimodal PDF of the loads, the resulting PDFs of the output variables also become multimodal which cannot be approximated satisfactorily by both GC and CF series, as both are based on Gaussian distribution. Hence, for constructing a multimodal PDF satisfactorily, spline based reconstruction technique has been adopted in this thesis along with 7PEM based PLF (because of its highest level of accuracy as compared to the other versions of PEM). Further, this method has also been augmented to consider the correlation among the loads of a power system.

Now, in the standard procedure of load flow, the real power outputs of all the generators except the slack bus are kept fixed. As a result, the slack bus absorbs (generates) all uncertainties in the total load of the system and thus, it has the widest possible variations of real power among all the generators. If the rating of the slack bus generator is adequately high to cover this wide variation, then the solution obtained by the probabilistic load flow is feasible. On the other hand, if the rating of the slack bus is not sufficient to cover the entire variation, then sometimes the slack bus generator would hit its maximum real power generation limit. Hence, it becomes necessary to consider the slack bus real power generation limit in PLF and towards this goal, necessary modifications in the basic PLF have been made. All the results obtained using the adopted methods have also been compared with those obtained by detailed Monte Carlo simulation (MCS) studies on two IEEE test systems and have been found to be reasonably satisfactory.

The PLF method, developed so far, has been suitably modified further to include the uncertain wind generation. In the literature, uncertain wind generation is usually modeled as random real and

reactive power injection (due to random variations of wind speed). However, to accurately estimate the reactive power consumption of wind turbine generator (WTG), detailed models of four types of WTGs have been included in the PLF. Further, as the generations from wind turbine generators are strongly correlated among adjacent wind farms due to the similar wind speed at that area, it is important to model the interdependence among the power generations from wind farms. Towards this goal, the correlation among the wind speeds experienced by WTGs has also been included in PLF.

Due to the operation of the WTGs, the reactive power consumed by the system increases which leads to the variations in the bus voltages and line flows. For the successful operation of the power system, it is mandatory to keep the bus voltages and line power flows of the system within the desired limits under various operating conditions. For this purpose, the power system operators use a number of reactive power control devices such as shunt capacitors and transformer taps. The optimal adjustment of these control devices has a significant influence on the security and economic operation of power system. Hence, proper reactive power planning is needed for ensuring the secure and economic operation of the system.

Traditionally, classical optimization techniques have been widely used for determining the optimal settings of the reactive power control devices. However, in modern power system problems, the objective functions and constraints are complex, non-smooth and non-differentiable and therefore, classical approaches often do not perform satisfactorily in these situations. To overcome the drawback of classical techniques, evolutionary algorithms, such as genetic algorithm (GA), particle swarm optimization (PSO), gravitational search algorithm (GSA), a combination of PSO and GSA (PSOGSA) etc. have been applied to reactive power planning problem. However, all these methods suffer from the problem of reproducibility of the results, i.e. if these techniques are run repeatedly, they tend to produce different results on each run. To overcome this limitation, in this thesis, a new modified PSOGSA (MPSOGSA) optimization method has been proposed and its performance has been compared with the other optimization methods such as GA, GSA and PSOGSA.

In all the above studies, network configuration of the power system has been assumed to be fixed and, consequently, the probability of the basic configuration of the system has been assumed to be unity. Thus, the probability of outage of any network element, such as transmission line, transformer, generator etc., is neglected. However, changes do occur in the network configuration because of generator and line outages owing to faults, overloads or scheduled maintenance. Therefore, the assumption of constant network configuration is unrealistic, particularly when the power generation

and load uncertainties are significant.

Now, any change in the power systems configuration will alter the set of functions relating the input and output variables and consequently, PDF of output variables may change substantially, which in turn, may affect the techno-economic decisions regarding the secure and optimal operation of power system. The outages of any power system element can be modeled as a random variable with an associated PDF. Subsequently, every network state caused by the outage of a power system component (generator/transmission line) has an associated probability of occurrence. In this thesis, the basic PEM based PLF procedure has also been modified to take into account the probability of occurrence of different network states. The effect of wind power injection with generator and line outages has also been studied.

Acknowledgements

I take this opportunity to express my sincere gratitude towards my august guides Prof. Biswarup Das and Dr. Vinay Pant, in the Department of Electrical Engineering, Indian Institute of Technology, Roorkee for their proficient and enthusiastic guidance, advice and encouragement, which were the constant source of inspiration for the completion of this research work. I am fortunate to have the guides with profound individualities, humanistic and warm personal approach, loving and the caring, which has given me the strength to carry out this research work. Their excellent and aesthetic oriented guidance has helped immensely in shaping up this thesis. I humbly acknowledge a lifetime gratitude to them. I am highly thankful to Dr. S. K. Jain for the encouragement and support to do the Ph.D. My express my deep sense of gratitude to Prof. Pramod Agrawal, Dean Research, Prof. S. P. Srivastava, Head, Electrical Engineering Department, Indian Institute of Technology, Roorkee, for providing the excellent computing facility in the department for the research work. I also express my indebtness to Prof. G. N. Pillai, Chairman, Department research committee, Electrical Engineering Department, Dr. Ganesh Kumbhar, of Electrical Engineering Department and Dr. Aditi Gangopadhya of Mathematics Department for being the members of my research committee and sparing their valuable time in reviewing and critically examining the whole work.

My special thanks to Prof. M. K. Vasantha, who always encourage me by saying Happy times. I am thankful Dr. Indra Gupta and to the technical staff of Power System Simulation Lab and Microprocessor Lab, in particular Mr. C. M. Joshi for his timely cooperation and needful help.

I acknowledge my sincere gratitude to MHRD Govt. of India, under which this research work is carried out. I thankfully appreciate and acknowledge my indebtness to the fellow research scholars Mr. Himanshu Chaudhary, Mr. Javed Dhillon, Mr. Pushker Tripathy, Mr. Dratha Novalio, Mr. K. S. Sajan, Mr. Ajay Shiv Sharma, Mr. Manmohan Garg, Mr. Amit Narwal, Mr. Akhilesh Mathur for the moral support rendered throughout the completion of research work during my stay at Roorkee. I would like to dedicate this thesis to my late father Dr. Bishan Dass Gupta, a symbol of love, care and dedication who always inspired to achieve high.

My special, sincere, heartfelt gratitude and indebtness to my family, mother for their sincere prayers , constant encouragement and blessings. They have been the main driving force in this endeavor for which no words of thanks would be sufficient. My heartiest gratitude goes to my brother Pankaj and Anshu and sister-in-law Sheetal for their constant support and encouragement. I am thankful to my in-laws for their constant support and encouragement during this period.

Above all, I am lucky to have such a nice wife, Rajni. I am immensely thankful to her for shouldering responsibilities, which lets me, concentrate on my research work and for the excellent cooperation during the whole stage of my work. Her loving, caring and sacrificing attitude has been the inspiring and driving force in this endeavor and hence no words of thanks are enough. I am thankful to my son Akshaj for giving me happiness with his smiles during the last seven months of my research.

I also wish to express my deep sense of gratitude to all persons who with their encouraging words, constructive criticism and suggestions have contributed directly or indirectly in a significant way towards the completion of this work.

I owe a deep sense of gratitude to all prevailing spirits whose divine light provided me the perseverance, guidance, inspiration, faith and strength to carry on even when time was tough for me.

(Neeraj Gupta)

Contents

List of Tables

List of Figures

Acronyms

CDF	Cumulative Distribution Function.
DG	Distributed Generation.
DLF	Deterministic Load Flow.
FFT	Fast Fourier Transform.
GA	Genetic Algorithm.
LF	Load Flow.
MCS	Monte Carlo Simulation.
ORPP	Optimal Reactive Power Planning.
PEM	Point Estimate Method.
PLF	Probabilistic Load Flow.
RV	Random Variables.
WTG	Wind Turbine Generator.

Chapter 1: Introduction

1.1 Overview

The Deterministic Load Flow (DLF) is used to undertake the planning exercise and assess the system operation of a power system on a daily basis. DLF uses the precise values of power generations and load demands for a particular network configuration to calculate the bus voltage magnitudes, angles as well as line power flows. Therefore, DLF discounts the uncertainties in the power systems, e.g. load demand variations, generator outage rates and the change in network configurations. Furthermore, with the integration of intermittent Distributed Generation (DG) units [1], such as Wind Turbine Generator (WTG) and photovoltaic systems in the modern power systems, additional power fluctuations are introduced into the system due to the uncertain generation from the DGs. Therefore, for the analysis of present day power system, the deterministic approach alone is not adequate and the results of the system performance studies based on DLF may not be sufficient for proper system planning. Probabilistic approach for computing load flow can take into account all the uncertainties discussed above and has been applied to address various issues in power system operation and planning [2]. Such an approach is called Probabilistic Load Flow (PLF). The main informations obtained by carrying out a PLF of a power system are:

- The probability that the voltage at any bus would be outside its operational limits.
- The probability that the flow in a line exceeds the thermal rating of the line.
- The probability that the reactive power injection at a generator bus would be between the specified limits.

These informations can then be used to evaluate the system performance in the presence of uncertainties.

By performing probabilistic load flow studies, the system planning engineers can anticipate the probable system operating conditions in a better way and therefore gain more confidence in making judgments concerning investment in an uncertain future. Further, the introduction of deregulation and competitive power markets has led to the increase in the uncertainty even more, as the well-known generation patterns cease to exist, the paths of supply are more diverse, and the injection of power into system nodes becomes more unpredictable. Consideration of uncertainty in power system planning (for long term studies) may lead to a more secure and less expensive network. Further, a

proper assessment of the system variables under uncertain operating conditions may lead to a better management of congestion in daily operation.

The PLF was first proposed in 1974 by Borkowska and Allan [3,4] and has been further developed and applied for addressing various operational and planning issues for both transmission [3, 4] and distribution systems [5, 6]. The inputs to the PLF are the probability density functions (PDF) of active and reactive power injections at different buses and the outputs are the PDF or Cumulative Distribution Function (CDF) of the bus voltages and the power flows in the lines. The PLF can be carried out by using either a numerical or an analytical approach.

1.2 Classification of PLF methods:

PLF methods can be broadly classified into three categories:

1. Simulation based PLF methods
2. Analytical approach based PLF methods
3. Moment based PLF methods

1.2.1 Simulation based PLF methods

In the simulation based approach, Monte Carlo Simulation (MCS) method [7] is widely used for the PLF analysis. In MCS, initially the bus active and reactive power injections are randomly generated (within a specified ranges and as per given PDF) and subsequently a deterministic load flow is carried out with these randomly generated power injections. This process is repeated thousands of times to get the probability distributions of the quantities of interest [2]. The results obtained from MCS are accurate, as it uses exact non-linear load flow equations, and are used as a benchmark for quantifying the effectiveness of other approximate PLF methods [8]. However, due to the large number of load flow calculations, the MCS method requires fairly large amount of computation time [2]. To reduce the computational burden, techniques such as Latin hypercube sampling technique based methods and Cholesky decomposition method has been proposed [9–12] for improving the computational efficiency of Monte Carlo simulation. Further, for this purpose, uniform design sampling based MCS method has also been proposed in the literature [13].

1.2.2 Analytical-approach based PLF methods

In the analytical-approach, the PDF of system states i.e. voltage, angle and line power flows are obtained analytically through the convolution of the PDFs of the input quantities. However, non-

linearity of load flow equations and interdependence of power system variables make it difficult to solve the PLF equations by the convolution of PDFs of the input variables [2, 14, 15]. Therefore, to perform PLF using an analytical approach, a number of assumptions are usually made, such as, totally independent or linearly-correlated variables and usually a constant network configuration. Further, the Load Flow (LF) equations are linearized with the first-order Taylor series expansion around the estimated mean of the input variables and the output system states are expressed as a linear combination of the input variables.

In the analytical approach based PLF methods, the linearization of non-linear LF equations is carried out around the mean value. Consequently, the accuracy of the results is adversely affected when values of the input variables are far from their corresponding mean values i.e. for input variables with large spread or standard deviation. The errors in the resulting PDF (due to the large value of standard deviation of input variables) are usually reflected in the tail regions, i.e. the two ends of the probability distribution curve of an output variable [16]. Therefore, to mitigate the error caused by the linearization of the LF equations, different methods have been proposed in the literature. Two typical solutions are: PLF using multi-linearization [17, 18] and the quadratic PLF [19, 20].

The PLF using multi-linearization involves the linearization of LF equations around several other points besides the mean value. Around each linearization point, a suitable convolution technique can be used to obtain the probability distributions of the desired output variables, which are then properly combined to obtain the final probabilistic representation of the results.

In quadratic PLF, the second-order term of the Taylor-series expansion of the LF equations is used. As a result, quadratic expressions for the LF equations are obtained due to the inclusion of second order terms in the Taylor-series expansion. The contribution of the quadratic terms is generally small. A technique for performing an efficient convolution using Laplace transformation of discrete and continuous stochastic variables has been given in [19], while, Fast Fourier Transform (FFT) used in [20] for convolution shows a better efficiency. Further, if the input variables are modelled as discrete random variables, then the convolution involves heavy computational burden [21]. Hence, for a power system with large number of load buses, the convolution method becomes computationally very expensive.

1.2.3 Moment based PLF methods

The use of moments and resulting cumulants of the input variables to estimate the PDFs and CDFs of the output variables is an attractive choice, because of the accuracy of the results and the convenience

to include dependence between the input random variables [21–24]. These methods are based on the concept that the cumulants of a sum of random variables is equal to the sum of the individual cumulants of the random variables. Using cumulants, the convolution of Random Variables (RV) is reduced to the addition of the cumulants of RV. As is well known [21], the first four cumulants denote the mean, variance, skewness and kurtosis repectively. In the methods based on the cumulants, cross cumulants are zero for independent RV and also higher order cumulants (>4) can be neglected if the distribution of RV is near Gaussian.

Another method namely the Point Estimate Method (PEM) as proposed in [25–28], is an efficient method for estimating the moments of the variables of interest. The point estimate method computes the moments of a random variable 'z' which in turn is a function of several other random input variables. This is achieved by approximating the PDF of an input random variable by 'h' discrete points and their associated weights. The pair comprising of a point and its associated weight is called a concentration. By this approximation, the contribution of each input random variable to the output variables is considered independently. The method can be applied either to continuous or discrete random variables [27, 28]. The advantages of PEM are [27] : (i) it requires smaller amount of information and (ii) it needs reduced computational effort. After the moments or cumulants of the output variables are obtained, the corresponding PDF and CDF can be determined by using Gram-Charlier (GC) series expansion [15,23], and Cornish-Fisher (CF) series expansion [29,30], Gaussian mixture model [31, 32] and Kernel density estimator [33].

1.3 Application and Extension of PLF

1.3.1 PLF integration with DG

Due to the random behavior of the wind speed, which follows either a Weibull or Rayleigh distribution [34], the power output of a WTG is also a random variable and therefore, the steady state analysis of the systems with such DG units requires a probabilistic approach. As a result, various approaches have been proposed in the literature for carrying out probabilistic analysis of power system with WTG units.

In [29, 30, 35], cumulant based convolution in conjunction with CF series has been used for calculating the PDF and CDF of the quantities of interest while in [36], cumulant based convolution and GC series have been used for the same purpose. In [37], DC load flow and Fourier Transform (FT) based convolution have been used for calculating the PDFs. In [38–40], different PEM based methods have been proposed for probabilistic analysis of a power system in the presence of WTGs.

In [38], PEM along with Nataf transformation has been used while in [39] and [40], discrete PEM and extended PEM have been employed respectively. Further, in majority of these works, the results obtained from PLF have also been compared with the results obtained by Monte-Carlo simulation studies.

1.3.2 Correlation in PLF

The generated power from the renewable energy systems such as wind are essentially intermittent, random [30] and also spatially correlated in a significant manner [35] within a given geographical area, as they are influenced by the same physical phenomena [41]. The different methods to generate the statistically dependent random variables (wind speeds and the load) are given in [42–45]. The significance of interdependence in modeling the stochastic generation is also demonstrated in [46]. The inclusion of correlation in wind generation and the loads for point estimate method is explained in [40]. Further, in [10–13, 31, 35, 37, 38] the correlation among the wind generator has also been considered. Moreover, since certain type of loads have similar behavior, input power variables are not completely independent from each other. A linear dependence was assumed in [47, 48], for modeling the correlation among the loads connected at different buses and between the active and reactive power of the loads.

1.3.3 Power system planning

Probabilistic power flow analysis of a power system is an important tool for planning and decision making for an electric grid under uncertain environment [49, 50]. Now, for the successful operation of the power systems, it is mandatory to keep the voltage of the system within the desired limits under various operating conditions. For this purpose, the power system operators use a number of reactive power control devices such as shunt capacitors and transformer taps [51,52]. The optimal adjustment of these control devices has a significant influence on the security and economic operation of power systems. The optimal values of the control devices are determined through Optimal Reactive Power Planning (ORPP). The setting and dimensioning of these control devices should be determined in a more realistic way than the traditional deterministic approach [53–59]. The stochastic reactive power planning considering the uncertainty is given in [60–62].

A method for reactive power planning using chance-constrained programming has been proposed in [60], which can accommodate uncertain factors and handle constraints easily. A model for long-term reactive power planning where a deterministic non-linear model is expanded into a multi-stage stochastic model under load uncertainty and N-k contingency is proposed in [61]. A method for

reactive power planning combining PLF and Genetic Algorithm (GA) is proposed in [62]. In this method the transformer taps and capacitor MVARs are considered as the decision variables.

A methodology for controlling the voltage using the system control devices through the PLF analysis has been investigated in [63]. The basic idea is to include a control variable, such as transformer taps, shunt compensation devices and voltages at PV buses, in a constrained LF analysis, so that some or all the elements of system states and line flows are within operating limits. In addition, operating constraint violations are obtained together with the probability of each violation.

With the increase in the penetration of WTGs in the system, the reactive power planning has to be carried out considering the uncertainties of the wind power generation. In [64–66], stochastic reactive power planning techniques for distribution system have been proposed while considering high wind penetration in the distribution grid. However, in these works, detailed wind generator models have not been used and as a result, the accurate estimation of the reactive power consumed by the WTGs has not been made.

1.3.4 Network outage rates

In all the works described above, the outages of the power system components (generator, transmission line etc.) have not been considered. However, for realistic planning exercise, the outages also need to be taken into account. The algorithm of the PLF considering network outage rates are discussed in [67], in which the network configuration is considered as a discrete stochastic variable with specified probability of each network component. Finally, the PDFs or CDFs of voltage, angle and line power flows are obtained from a weighted sum of the PDFs or CDFs obtained under each network configuration, respectively.

Another method of dealing with network outages is proposed in [68], where the line outage is simulated by modifying the injected powers at both ends of the line, so that the total power leaving the line is same as in the case of the actual line outage.

Another issue is the random variation of network parameters due to the variation of temperature, which is considered as a continuous stochastic variable and is not treated in the conventional PLF [28]. In this method line resistance and reactance are assumed to have uniform distributions with different mean values, while line susceptance is assumed to have a binary distribution. The line parameters are simulated to different degrees of variations and the results are compared with those obtained from the corresponding MCS study.

1.4 Contribution of the author

As discussed in the literature, the point estimate method has superior characteristics as compared to other methods of PLF. Hence, in this thesis, probabilistic load flow using point estimate method has been used. To obtain the PDF and the cumulative distribution function (CDF) of the output variables from the moments calculated by the PEM based PLF, Gram-Charlier (GC) and Cornish-Fisher (CF) series have been used in the literature. Now, GC and CF series are quite accurate for approximating a unimodal PDF with CF being marginally better than GC. However, with the inclusion of generator reactive power limits and multimodal PDF of the loads, the resulting PDFs of the output variables also become multimodal which cannot be approximated satisfactorily by both GC and CF series, as both are based on Gaussian distribution. Hence, for constructing a multimodal PDF satisfactorily, spline based reconstruction technique has been adopted in this thesis along with 7PEM based PLF (because of its highest level of accuracy as compared to the other versions of PEM).

Now, in the standard procedure of load flow, the real power outputs of all the generators except the slack bus are kept fixed. As a result, the slack bus absorbs (generates) all uncertainties in the total load of the system and thus, it has the widest possible variations of real power among all the generators. If the rating of the slack bus generator is adequately high to cover this wide variation, then the solution obtained by the probabilistic load flow is feasible. On the other hand, if the rating of the slack bus is not enough to cover the entire variation, then sometimes the slack bus generator would hit its maximum real power generation limit. Hence, it becomes necessary to consider the slack bus real power generation limit in PLF and towards this goal, necessary modifications in the basic PLF have been made.

The PLF method developed so far has been suitably modified further to include the uncertain wind generation. In the literature, uncertain wind generation is usually modeled as random real and reactive power injections (due to random variations of wind speed). However, to accurately estimate the reactive power consumption of wind turbine generator (WTG), detailed models of four types of WTGs have been included in the PLF. Further, as the generations from wind turbine generators are strongly correlated among adjacent wind farms due to the similar wind speed at that area, it is important to model the interdependence among the power generations from wind farms. Towards this goal, the correlation among the wind speeds experienced by the WTGs has also been included in PLF.

Due to the operation of the WTGs, the reactive power consumed by the system increases which

leads to the variations in the bus voltages and line flows. For successful operation of the power system, it is mandatory to keep the bus voltages and line power flows of the system within the desired limits under various operating conditions. For this purpose, the power system operators use a number of reactive power control devices such as shunt capacitors and transformer taps. The optimal adjustment of these control devices has a significant influence on the security and economic operation of power systems. So, reactive power planning is needed for ensuring the secure and economic operation of the system [53–56].

Traditionally, classical optimization techniques have been widely used for determining the optimal settings of the reactive power control devices. However, in modern power system problems, the objective functions and constraints are complex, non-smooth and non-differentiable and therefore, classical approaches often do not perform satisfactorily in these situations. To overcome the drawback of classical techniques, evolutionary algorithms, such as genetic algorithm (GA), particle swarm optimization (PSO), gravitational search algorithm (GSA), a combination of PSO and GSA (PSOGSA) etc. have been applied for reactive power planning [62, 69, 70]. However, all these methods suffer from the problem of reproducibility of the results, i.e. if these techniques are run repeatedly, they tend to produce different results in each run. To overcome this limitation, in this thesis, a new modified PSOGSA (MPSOGSA) optimization method has been proposed and its performance has been compared with the other optimization methods such as GA, GSA and PSOGSA.

In all the above studies, network configuration of the power system has been assumed to be fixed and, consequently, the probability of the basic configuration of the system has been assumed to be unity. Thus, the probability of outage of any network element, such as transmission line, transformer, generator etc., is neglected. However, changes do occur in the network configuration because of generator and line outages owing to faults, overloads or scheduled maintenance. Therefore, the assumption of constant network configuration is unrealistic, particularly when the power generation and load uncertainties are significant.

Now, any change in the power systems configuration will alter the set of functions relating the input and output variables and consequently, PDF of output variables may change substantially, which in turn, may affect the techno-economic decisions regarding the secure and optimal operation of power system. The outage of any power system element can be modeled as a random variable with an associated PDF. Subsequently, every network state caused by the outage of a power system component (generator/transmission line) has an associated probability of occurrence. In this thesis, the basic PEM based PLF procedure has also been modified to take into account the probability of

occurrence of different network states. The effect of wind power injection with generator and line outages has also been studied.

To summarize, the major contributions of this thesis are as follows:

- For including the reactive power limits of generators in probabilistic load flow, a point estimate based method incorporating reactive power limit violations has been proposed.
- For estimating a multi-modal PDF from the moments of variables of interest, a spline based reconstruction technique along with 7 point PEM based PLF has been adopted.
- To study the impact of wind power penetration into the grid, integration of detailed WTG models into the PEM based PLF has been carried out to obtain the PDFs of the reactive power consumed by the wind generators and other variables of interest. The correlation between the loads and the correlation between wind generators have also been included.
- A modified PSOGSA optimization method has been proposed for reactive power planning of a power system with embedded wind generation and the results of this developed method has been compared with those obtained with GA, GSA and PSOGSA.
- The PEM based PLF has been augmented to include the generator and line outages in the system in the presence of WTG.

The organization of the thesis is as follows:

In Chapter 2, detailed study of PLF with PEM and MCS with and without reactive power generation limit violations has been carried out. The PDF and CDF of the variables of interest have been constructed using Gram-Charlier and Cornish-Fisher series. With the inclusion of generator reactive limit violations, the resulting PDF is multimodal in nature. To reconstruct the multimodal PDFs, from the moments of the output variables, spline based reconstruction technique has been adopted in Chapter 3. The inclusion of correlation among the loads and slack bus power limit is also considered in this chapter. The inclusion of wind generation in the PLF is explained in Chapter 4. In this Chapter, detailed wind generator models have been included in the PEM based PLF. The effect of correlation among the wind speeds on the power outputs of the wind farms has also been considered in this chapter. With the inclusion of the WTGs in the PLF, the reactive power consumption in the system increases. This may cause the bus voltages and line power flows to cross their respective operating limits. Hence, reactive power planning is necessary for a secure and economic operation of

the power system. Towards this goal, in Chapter 5, a modified PSOGSA (MPSOGSA) optimization method has been proposed for probabilistic reactive power planning and its performance has been compared with those obtained with the other optimization methods such as GA, GSA and PSOGSA. As contingency analysis is an integral part of power system analysis and planning, inclusion of contingencies (generator and line outages) in the PLF is discussed in Chapter 6. Finally, Chapter 7 lists the major conclusions of this work, as well as, future scope of work.

In the next chapter, basic PEM based PLF is explained followed by construction of PDFs and CDFs of the variables of interest using GC and CF series.

Chapter 2: Probabilistic load flow

This chapter describes the basic probabilistic load flow techniques using Monte Carlo and point estimate method. Since the consideration of the generator reactive power limit violation is an essential aspect in load flow studies for planning, a point estimate method based PLF (upto seven points) which includes generator reactive power limit violation is proposed. In order to obtain the PDF and CDF of the output variables of interest, Gram-Charlier and Cornish-Fisher expansion series have been used. Further, the difficulties associated with these expansion series for approximation of multimodal PDFs have been identified.

2.1 Probabilistic load flow

In the last chapter, different types of PLF methods reported in the literature such as, simulation based PLF methods, analytical-approach based PLF methods and moment based PLF methods have been discussed briefly. In this work, out of these three methods, moment based PLF method has been chosen due to its non-dependence on the type of distribution, less complexity and low computational burden as compared to other two methods.

In PLF, the load is considered as a random variable whose modeling is given in the next section.

2.2 Load Modelling

The first step towards probabilistic load flow is the development of an appropriate probabilistic load model. The load can be modeled as a normally distributed load. The normally distributed load model for the i^{th} load is generally described by a normal distribution $N(\mu_i, \sigma_i)$, where, μ_i is the expected value of i^{th} load and σ_i is the standard deviation, describing the spread of the load values around the expected value μ_i. A typical normally distributed load is shown in Fig. 2.1 which has the mean value of 50 MW with standard deviation equal to 10% of the mean value.

Now, after the load modeling, the probabilistic load flow methods based on Monte Carlo simulation and point estimate method are explained in details.

2.3 Monte-Carlo based PLF

Monte-Carlo simulation method is the most basic and accurate form of PLF method, in which DLF is run thousands of times to obtain the probability distributions of the output variables of interest from the distributions of the input variables. Monte-Carlo based method is easy to implement and can be applied to any system. It has the properties such as insensitivity to the dimension of problems, avoidance of any constraining assumptions, and strong adaptability.

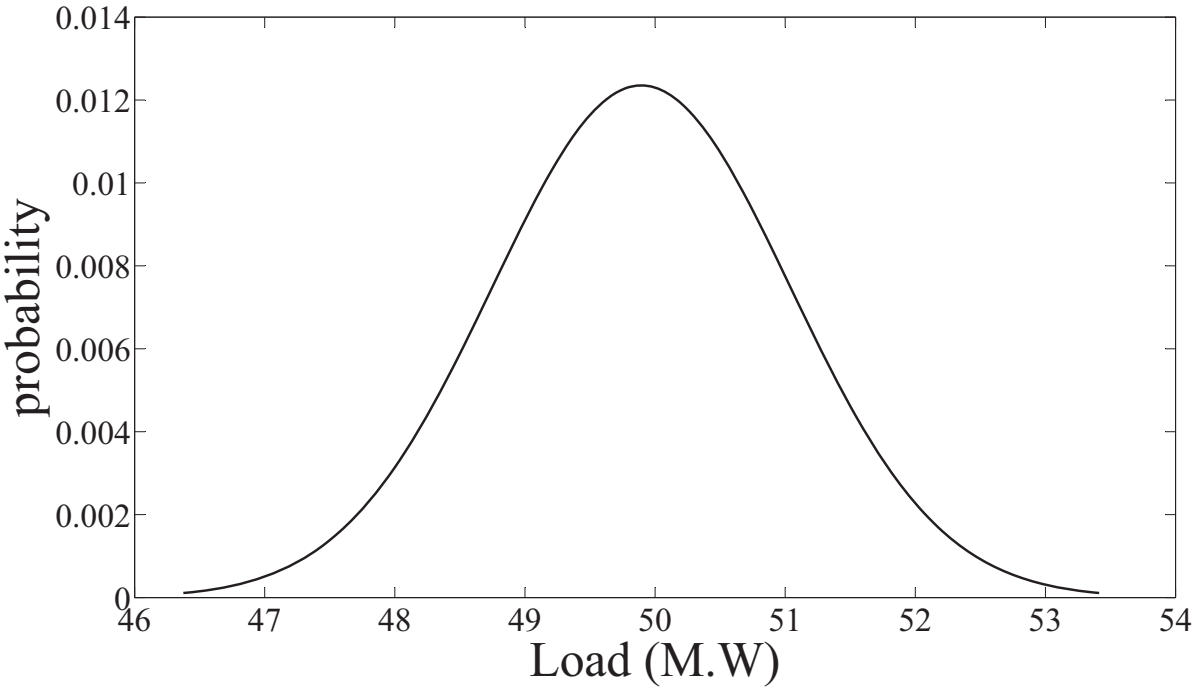

Figure 2.1: A normally distributed load

In MCS method, sampling is carried out to obtain the state of each component in the system, which includes various system equipments such as loads, generators, transmission lines, transformers, etc. Sampling can be carried out by either using inverse-transform method or acceptance rejection method [71]. Let the vector of input active and reactive power variables for i^{th} sample be represented as $\boldsymbol{x_i}$ and corresponding output voltages, angles and power flows be represented as $\boldsymbol{y_i}$. The main steps involved in MCS are:

1. Sample the input random variables i.e active and reactive loads, from the given probability distributions.

2. Obtain the output vector $\boldsymbol{y_i}$ for each input vector $\boldsymbol{x_i}$ by solving Newton Raphson Load Flow (NRLF).

3. Repeat steps 1 and 2 a sufficient number of times to obtain a large sample of output vector $\boldsymbol{y_i}$.

4. From the output vector $\boldsymbol{y_i}$ calculate the frequency distribution of each output variable $y_{i,k}$ and from the frequency distribution, find the probability distribution by converting the frequency values to probability values. Here, $y_{i,k}$ denotes the k^{th} component of the vector $\boldsymbol{y_i}$ with $k = 1, 2, .., N_T$, N_T being the total number of output variables of interest.

MCS suffers from the drawback of large computational time due to the large number of load flow calculations required, which increases with the increase in the size of the system. But due to its high accuracy, it is used as a benchmark for comparing the accuracy of other methods.

2.4 Point Estimate Based PLF

The PEM based PLF utilizes PEM to first generate the samples of the input random variables, and subsequently solves the DLF to generate the sample space of the output variables of interest. From the obtained sample space of the output variables of interest, different moments of each output variable are obtained [27]. This method has been successfully used for the probabilistic analysis of power system [72], [73]. In this method, points on the PDF are first estimated along with their corresponding weights and subsequently, from these estimated points and weights, the moments of variables of interest are calculated. Finally, using a suitable technique (Gram-Charlier or Cornish-Fisher series) the PDF of the variables is constructed. The general theory of point estimate method is as follows [74]:

2.4.1 Function of one variable

Let x be a random variable with a PDF $f_X(x)$ and let z be a function of x. If $z = h(x)$, it is desired to estimate the PDF of z ($f_Z(z)$). Further, let the j^{th} moments about the origin and about mean of the variable x be denoted as $m_{x,j}$ and $\mu_{x,j}$ respectively. The mean and variance of x is given by $\mu_x = m_{x,1}$ and $\sigma_x^2 = \mu_{x,2}$ respectively. The standardized moment can be obtained by:

$$\lambda_{x,j} = \frac{\mu_{x,j}}{\sigma_x^j} \tag{2.1}$$

where, $\lambda_{x,1} = 0$, $\lambda_{x,2} = 1$ and $\lambda_{x,3}$ and $\lambda_{x,4}$ are the skewness and kurtosis coefficients respectively.

Expanding $z = h(x)$ using Taylor series expansion around its mean μ_x, we obtain

$$h(x) = h(\mu_x) + \sum_{j=1}^{\infty} \frac{1}{j!} h^{(j)}(\mu_x)(x - \mu_x)^j \tag{2.2}$$

where, $h^{(j)}(\mu_x)$ is the derivative of order j of the function $h(x)$ evaluated at μ_x. Let μ_z be the mean

of z and can be obtained as:

$$\begin{aligned}\mu_z &= E[h(x)] = \int_{-\infty}^{\infty} h(x) f_X(x) dx \\ &= h(\mu_x) + \sum_{j=1}^{\infty} \frac{1}{j!} h^{(j)}(\mu_x) \int_{-\infty}^{\infty} (x-\mu_x)^j f_X(x) dx \\ &= h(\mu_x) + \sum_{j=1}^{\infty} \frac{1}{j!} h^{(j)}(\mu_x) \mu_{x,j} \\ &= h(\mu_x) + \sum_{j=1}^{\infty} \frac{1}{j!} h^{(j)}(\mu_x) \lambda_{x,j} \sigma_x^j\end{aligned} \tag{2.3}$$

where, $\int_{-\infty}^{\infty}(x-\mu_x)^j f_X(x)dx$ is the central moment $\mu_{x,j}$ of x of order j.

The point estimate method aims to approximate the mean and higher order moments by a linear combination of the values of function $h(x)$ at several points. For three point estimate this approximation can be written as:

$$\mu_z \simeq w_1 h(x_1) + w_2 h(x_2) + w_3 h(x_3) = \sum_{i=1}^{3} w_i h(x_i) \tag{2.4}$$

where, x_1, x_2 and x_3 are the points at which the function $h(x)$ is to be evaluated and w_1, w_2 and w_3 are the weights associated with these three points. The points x_1, x_2 and x_3 are given by the relations $x_1 = \mu_x + \xi_1\sigma_x$, $x_2 = \mu_x + \xi_2\sigma_x$ and $x_3 = \mu_x + \xi_3\sigma_x$, where, ξ_1, ξ_2 and ξ_3 are the coefficients that decide the locations of the three points.

Now for the points x_i, $\forall\, i = 1, .., 3$,

$$h(x_i) = h(\mu_x) + \sum_{j=1}^{\infty} \frac{1}{j!} h^{(j)}(\mu_x)(x_i - \mu_x)^j,$$

Next, eq. (2.4) can be expanded as

$$\begin{aligned}\mu_z \simeq w_1 h(x_1) + w_2 h(x_2) + w_3 h(x_3) = w_1 h(\mu_x) + \sum_{j=1}^{\infty} \frac{1}{j!} h^{(j)}(\mu_x) w_1 (x_1 - \mu_x)^j \\ + w_2 h(\mu_x) + \sum_{j=1}^{\infty} \frac{1}{j!} h^{(j)}(\mu_x) w_2 (x_2 - \mu_x)^j + w_3 h(\mu_x) + \sum_{j=1}^{\infty} \frac{1}{j!} h^{(j)}(\mu_x) w_3 (x_3 - \mu_x)^j\end{aligned} \tag{2.5}$$

As, $x_i = \mu_x + \xi_i\sigma_x$, eq. (2.5) can be written as

$$\mu_z \simeq w_1 h(x_1) + w_2 h(x_2) + w_3 h(x_3) = h(\mu_x)(w_1 + w_2 + w_3) + \sum_{j=1}^{\infty} \frac{1}{j!} h^{(j)}(\mu_x)(w_1\xi_1^j + w_2\xi_2^j + w_3\xi_3^j)\sigma_x^j \tag{2.6}$$

As, there are six unknowns i.e. ξ_1, ξ_2, ξ_3 and w_1, w_2, w_3, six equations are required to find the values of these unknown quantities. These equations are obtained by equating the first six terms of eq. (2.3) and eq. (2.6) and can be written as:

$$\begin{aligned} &h(\mu_x) + \frac{1}{1!}h^{(1)}(\mu_x)\lambda_{x,1}\sigma_x + \frac{1}{2!}h^{(2)}(\mu_x)\lambda_{x,2}\sigma_x^2 + \frac{1}{3!}h^{(3)}(\mu_x)\lambda_{x,3}\sigma_x^3 + \frac{1}{4!}h^{(4)}(\mu_x)\lambda_{x,4}\sigma_x^4 \\ &+ \frac{1}{5!}h^{(5)}(\mu_x)\lambda_{x,5}\sigma_x^5 = h(\mu_x)(w_1 + w_2 + w_3) + \frac{1}{1!}h^{(1)}(\mu_x)(w_1\xi_1 + w_2\xi_2 + w_3\xi_3)\sigma_x \\ &+ \frac{1}{2!}h^{(2)}(\mu_x)(w_1\xi_1^2 + w_2\xi_2^2 + w_3\xi_3^2)\sigma_x^2 \quad + \frac{1}{3!}h^{(3)}(\mu_x)(w_1\xi_1^3 + w_2\xi_2^3 + w_3\xi_3^3)\sigma_x^3 \\ &+ \frac{1}{4!}h^{(4)}(\mu_x)(w_1\xi_1^4 + w_2\xi_2^4 + w_3\xi_3^4)\sigma_x^4 + \frac{1}{5!}h^{(5)}(\mu_x)(w_1\xi_1^5 + w_2\xi_2^5 + w_3\xi_3^5)\sigma_x^5 \end{aligned} \tag{2.7}$$

On comparing the coefficients of $h(\mu_x)$ and $h^{(i)}(\mu_x)$ for $i = 1, 2.., 5$ on both sides of eq. (2.7), we get the following relations

$$\left.\begin{aligned} w_1 + w_2 + w_3 &= 1 \\ w_1\xi_1 + w_2\xi_2 + w_3\xi_3 &= \lambda_{x,1} \\ w_1\xi_1^2 + w_2\xi_2^2 + w_3\xi_3^2 &= \lambda_{x,2} \\ w_1\xi_1^3 + w_2\xi_2^3 + w_3\xi_3^3 &= \lambda_{x,3} \\ w_1\xi_1^4 + w_2\xi_2^4 + w_3\xi_3^4 &= \lambda_{x,4} \\ w_1\xi_1^5 + w_2\xi_2^5 + w_3\xi_3^5 &= \lambda_{x,5} \end{aligned}\right\} \tag{2.8}$$

In these equations, ξ_3 is taken as zero, as one of the locations i.e. x_3 is taken equal to the mean value μ_x and weight corresponding to this mean value w_μ is calculated using the first equation of eq. (2.8) as $1 - \sum_{i=1}^{2} w_i$. Finally, we have to calculate the four unknown quantities i.e $\xi_1,\ \xi_2$ and $w_1,\ w_2$, for which four equations are required. For this any four equations of the remaining five equations of eq. (2.8) can be selected and the selected equations are:

$$\left.\begin{aligned} w_1\xi_1 + w_2\xi_2 &= \lambda_{x,1} \\ w_1\xi_1^2 + w_2\xi_2^2 &= \lambda_{x,2} \\ w_1\xi_1^3 + w_2\xi_2^3 &= \lambda_{x,3} \\ w_1\xi_1^4 + w_2\xi_2^4 &= \lambda_{x,4} \end{aligned}\right\} \tag{2.9}$$

For a three point estimate method, four equations are required for the solution and in general, for an N point estimate method, $2N - 2$ equations are required for the solution, which can be obtained using the procedure described in [75]. A brief review of the procedure for solving eq. (2.9) is given next.

First, define a polynomial

$$\pi(\xi) = (\xi - \xi_1)(\xi - \xi_2)..(\xi - \xi_{N-1}) = \sum_{a=0}^{N-1} C_a \xi^a \tag{2.10}$$

where, N is the number of points to be estimated, which in present case is 3. Further, since, ξ_3 is taken as zero, a varies from 0 to $N-1$ instead of 0 to N.

It follows from eq. (2.10) that $C_{N-1} = 1$ and $\pi(\xi_i) = 0; \forall\, i = 1, 2, ..., N-1$

For three point estimate method, $N = 3$ and hence the first 3 equations of eq. (2.9) are multiplied with $C_0,\ C_1,\ C_2$ respectively and then added together to obtain

$$w_1\xi_1(C_2\xi_1^2 + C_1\xi_1 + C_0) + w_2\xi_2(C_2\xi_2^2 + C_1\xi_2 + C_0) = \sum_{a=0}^{N-1} C_a\lambda_{x,a+1}$$

$$\sum_{i=1}^{2} w_i\xi_i\pi(\xi_i) = \sum_{a=0}^{2} C_a\lambda_{x,a} = 0; \ \text{ since } \pi(\xi_i) = 0 \tag{2.11}$$

Similarly, multiplying 2^{nd}, 3^{rd} and 4^{th} equation of eq. (2.9) with $C_0,\ C_1,\ C_2$ respectively and then adding them together we get

$$\sum_{i=1}^{2} w_i\xi_i^2\pi(\xi_i) = \sum_{a=0}^{2} C_a\lambda_{x,a+2} = 0 \tag{2.12}$$

For an N point estimate this process is to be repeated $N-1$ number of times for the calculation of $C_0,\ C_1, ...C_{N-1}$. From eq. (2.11) and (2.12), we get

$$\left.\begin{aligned} C_0\lambda_{x,1} + C_1\lambda_{x,2} + C_2\lambda_{x,3} = 0 \\ C_0\lambda_{x,2} + C_1\lambda_{x,3} + C_2\lambda_{x,4} = 0 \end{aligned}\right\} \tag{2.13}$$

since, $C_2 = 1$, eq. (2.13) can be written as

$$\left.\begin{aligned} C_0\lambda_{x,1} + C_1\lambda_{x,2} = -\lambda_{x,3} \\ C_0\lambda_{x,2} + C_1\lambda_{x,3} = -\lambda_{x,4} \end{aligned}\right\} \tag{2.14}$$

or in matrix form as

$$\begin{bmatrix} \lambda_{x,1} & \lambda_{x,2} \\ \lambda_{x,2} & \lambda_{x,3} \end{bmatrix} \begin{bmatrix} C_0 \\ C_1 \end{bmatrix} = - \begin{bmatrix} \lambda_{x,3} \\ \lambda_{x,4} \end{bmatrix} \tag{2.15}$$

Since, $\lambda_{x,0}$, $\lambda_{x,1}$, $\lambda_{x,2}$ and $\lambda_{x,3}$ are known, C_0 and C_1 can be easily obtained from the above equation.

Substituting the values of C_0 and C_1 in eq. (2.10), the roots ξ_1 and ξ_2 of the polynomial are obtained. Next by substituting the values of ξ_1 and ξ_2 in eq. (2.9), we get four equations involving w_1 and w_2. To solve for w_1 and w_2 only two out of these four equations are required and the first two equations of eq. (2.9) are chosen as:

$$\begin{bmatrix} \xi_1 & \xi_2 \\ \xi_1^2 & \xi_2^2 \end{bmatrix} \begin{bmatrix} w_1 \\ w_2 \end{bmatrix} = \begin{bmatrix} \lambda_{x,1} \\ \lambda_{x,2} \end{bmatrix} \tag{2.16}$$

From the calculated values of ξ_1 and ξ_2 the points x_1 and x_2 are found out. Using the values of x_1, x_2 and weights w_1, w_2, higher order moments of random variable z can be calculated as:

$$\left.\begin{aligned} E[z^2] &\simeq w_1 h(x_1)^2 + w_2 h(x_2)^2 + + w_3 h(x_3)^2 \\ E[z^3] &\simeq w_1 h(x_1)^3 + w_2 h(x_2)^3 + w_3 h(x_3)^3 \\ \vdots \quad & \quad \vdots \quad \quad \vdots \quad \quad \vdots \\ E[z^j] &\simeq w_1 h(x_1)^j + w_2 h(x_2)^j + w_3 h(x_3)^j \end{aligned}\right\} \tag{2.17}$$

2.4.2 Function of more than one variable

Let $\boldsymbol{z}$ be a random variable which is a function of several independent random variables, and expressed as $\boldsymbol{z} = h(\boldsymbol{x})$, where $\boldsymbol{x} = (x_1, ..., x_n)$. Let the probability density functions of variable x_l be $f_{X_l}(x_l)$ for $l = 1, 2..n$, and the joint probability density functions of these variables be $f_{\boldsymbol{X}}(x_1..., x_n)$, and $\frac{\partial^{(ln)} f_x}{\partial x_{l1} ..... \partial x_{ln}} = 0$, if $l_i \neq l_j$. Let $\mu_{l,j}$ be the central moment of order j of variable x_l, whose mean and variance are μ_l and σ_l^2 respectively, with $\sigma_l^2 = \mu_{l,2}$.

Let us consider a point $x_{l,i} = \mu_l + \xi_{l,i}\sigma_l$ for $i = 1, ..., m$ points and $l = 1, ..., n$ variables. Each point will be associated with a weight $w_{l,i}$ such that $\sum_{l=1}^{n} \sum_{i=1}^{m} w_{l,i} = 1$. The function $\boldsymbol{z} = h(\boldsymbol{x})$ can be expanded by using multivariate Taylor series around the point $\boldsymbol{\mu}_x = (\mu_1, ..., \mu_n)$ and the mean of the $\boldsymbol{z}$ can be approximated as

$$\begin{aligned} \boldsymbol{\mu_z} = E[\boldsymbol{z}] = E[h(\boldsymbol{x})] &= \int_{-\infty}^{\infty} ... \int_{-\infty}^{\infty} h(\boldsymbol{x}) f_{\boldsymbol{X}}(\boldsymbol{x}) dx_1 dx_2 ... dx_n \\ &= \int_{-\infty}^{\infty} ... \int_{-\infty}^{\infty} f_{\boldsymbol{X}}(\boldsymbol{x}) \left[h(\boldsymbol{\mu}_x) + \sum_{j=1}^{\infty} \sum_{i=1}^{n} \frac{1}{j!} \left(\frac{\partial^j h}{\partial x_i^j} \right)_{\mu_i} (x_i - \mu_i)^j \right] d\boldsymbol{x} \end{aligned} \tag{2.18}$$

or,

$$\boldsymbol{\mu_z} = h(\boldsymbol{\mu}_x) + \sum_{j=1}^{\infty} \sum_{i=1}^{n} \frac{1}{j!} \left(\frac{\partial^j h}{\partial x_i^j} \right)_{\mu_i} \mu_{i,j} \tag{2.19}$$

as,

$$\int ... \int_{-\infty}^{\infty} f_{\boldsymbol{X}}(\boldsymbol{x})(x_i - \mu_i)^j d\boldsymbol{x} = \mu_{i,j}$$

Hence,

$$\boldsymbol{\mu_z} = h(\boldsymbol{\mu}_x) + \sum_{j=1}^{\infty} \sum_{i=1}^{n} \frac{1}{j!} \left(\frac{\partial^j h}{\partial x_i^j} \right)_{\mu_i} \lambda_{i,j} \sigma_i^j \tag{2.20}$$

Eq. (2.20) is written by utilizing the standardized moment given by

$$\lambda_{i,j} = \frac{\mu_{i,j}}{\sigma_i^j}$$

Further, let the function $\boldsymbol{z} = h(\boldsymbol{x})$ be approximated at points $x_{l,i} = \mu_l + \xi_{l,i}\sigma_l$ for $i = 1, ..., m$ points and $l = 1, ..., n$ variables. Each point is associated with a weight $w_{l,i}$ such that $\sum_{l=1}^{n} \sum_{i=1}^{m} w_{l,i} = 1$. The mean $\boldsymbol{\mu_z}$ can be approximated as

$$\begin{aligned} \boldsymbol{\mu_z} \cong \sum_{i=1}^{m} w_{1,i} h(x_{1,i}, \mu_2, .., \mu_n) + \sum_{i=1}^{m} w_{2,i} h(\mu_1, x_{2,i}, .., \mu_n) \\ + ... \sum_{i=1}^{m} w_{n,i} h(\mu_1, \mu_2, , ..., x_{n,i}) \end{aligned} \tag{2.21}$$

From the series expansion and equating the terms of eq. (2.20) and eq. (2.21) and using $x_{l,i} = \mu_l + \xi_{l,i}\sigma_l$, as in univariate case, we arrive at the following system of equations:

$$\sum_{i=1}^{m} w_{l,i} \xi_{l,i}^j = \lambda_{l,j}; \;\; j = 1, .., 2m-1, \; l = 1, .., n. \tag{2.22}$$

For a particular l^{th} variable and $m = 3$ (3PEM) these equations take the following form:

$$\left.\begin{aligned} w_{l,1}\xi_{l,1} + w_{l,2}\xi_{l,2} + w_{l,3}\xi_{l,3} &= \lambda_{l,1} \\ w_{l,1}\xi_{l,1}^2 + w_{l,2}\xi_{l,2}^2 + w_{l,3}\xi_{l,3}^2 &= \lambda_{l,2} \\ w_{l,1}\xi_{l,1}^3 + w_{l,2}\xi_{l,2}^3 + w_{l,3}\xi_{l,3}^3 &= \lambda_{l,3} \\ w_{l,1}\xi_{l,1}^4 + w_{l,2}\xi_{l,2}^4 + w_{l,3}\xi_{l,3}^4 &= \lambda_{l,4} \\ w_{l,1}\xi_{l,1}^5 + w_{l,2}\xi_{l,2}^5 + w_{l,3}\xi_{l,3}^5 &= \lambda_{l,5} \end{aligned}\right\} \tag{2.23}$$

Further, in these equations, $\xi_{l,3}$ is taken as zero, as one of the locations i.e. $x_{l,3}$ is taken equal to the mean value μ_l and weight corresponding to this mean value w_μ is calculated using $w_\mu = 1 - \sum_{l=1}^{n} \sum_{i=1}^{m-1} w_{l,i}$. Finally, we have to calculate the four unknowns for each variable for which a

set of four equations is required. From eq. (2.23), these four equations can be written as;

$$\left.\begin{aligned} w_{l,1}\xi_{l,1} + w_{l,2}\xi_{l,2} &= \lambda_{l,1} \\ w_{l,1}\xi_{l,1}^2 + w_{l,2}\xi_{l,2}^2 &= \lambda_{l,2} \\ w_{l,1}\xi_{l,1}^3 + w_{l,2}\xi_{l,2}^3 &= \lambda_{l,3} \\ w_{l,1}\xi_{l,1}^4 + w_{l,2}\xi_{l,2}^4 &= \lambda_{l,4} \end{aligned}\right\} \tag{2.24}$$

In the similar fashion as explained in single variable case (eq. (2.10)), a polynomial in ξ_l can be defined as:

$$\pi(\xi_l) = (\xi_l - \xi_1)(\xi_l - \xi_2)..(\xi_l - \xi_{m-1}) = \sum_{a=0}^{m-1} C_{l,a}\xi_l^a; \text{ with } C_{l,m-1} = 1 \tag{2.25}$$

Following the procedure similar to single variable case (eq. (2.13)), the set of equations as given in eq. (2.26) are obtained for three point estimate:

$$\left.\begin{aligned} C_{l,0}\lambda_{l,1} + C_{l,1}\lambda_{l,2} + C_{l,2}\lambda_{l,3} &= 0 \\ C_{l,0}\lambda_{l,2} + C_{l,1}\lambda_{l,3} + C_{l,2}\lambda_{l,4} &= 0 \end{aligned}\right\} \tag{2.26}$$

since, $C_{l,2} = 1$, eq. (2.26) can be written as

$$\begin{bmatrix} \lambda_{l,1} & \lambda_{l,2} \\ \lambda_{l,2} & \lambda_{l,3} \end{bmatrix} \begin{bmatrix} C_{l,0} \\ C_{l,1} \end{bmatrix} = - \begin{bmatrix} \lambda_{l,3} \\ \lambda_{l,4} \end{bmatrix} \tag{2.27}$$

The above equation can be solved for $C_{l,0}$ and $C_{l,1}$. Once the coefficients $C_{l,i}$ are known, the polynomial $\sum_{a=0}^{m-1} C_{l,a}\xi_l^a$ can be solved for the roots $\xi_{l,1}$ and $\xi_{l,2}$. Now, the values of the weights $w_{l,1}$ and $w_{l,2}$ can be found out from the following matrix equation.

$$\begin{bmatrix} \xi_{l,1} & \xi_{l,2} \\ \xi_{l,1}^2 & \xi_{l,2}^2 \end{bmatrix} \begin{bmatrix} w_{l,1} \\ w_{l,2} \end{bmatrix} = \begin{bmatrix} \lambda_{l,1} \\ \lambda_{l,2} \end{bmatrix} \tag{2.28}$$

Next, the location $x_{l,i} = \mu_l + \xi_{l,i}\sigma_l$ are calculated for $l = 1, 2..n$ and $i = 1, ..2$. Once the locations are known, the moments of random variable $\boldsymbol{z}$ of order j can be estimated as;

$$\begin{aligned} E[\boldsymbol{z}^j] \cong &\sum_{i=1}^{m-1} w_{1,i} h(x_{1,i}, \mu_2, .., \mu_n)^j + \sum_{i=1}^{m-1} w_{2,i} h(\mu_1, x_{2,i}, .., \mu_n)^j \\ &+ .... \sum_{i=1}^{m-1} w_{n,i} h(\mu_1, \mu_2, , ..., x_{n,i})^j + w_\mu h(\mu_1, \mu_2, , ..., \mu_n)^j \end{aligned} \tag{2.29}$$

This method can be extended to five and seven point estimate as explained next.

2.4.3 Five point estimate Method (5PEM)

1. Find the standard central moments as [27];

$$\lambda_{l,i} = \frac{E\left[(x_l - \mu_l)^i\right]}{\sigma_l^i}, \quad i = 3, .., 8. \tag{2.30}$$

2. Find the four standard locations $\xi_{l,1}$, $\xi_{l,2}$, $\xi_{l,3}$ and $\xi_{l,4}$, other than mean, by obtaining the roots of the polynomial (as explained in the previous section)

$$\pi(\xi_l) = \xi_l^4 + C_{l,3}\xi_l^3 + C_{l,2}\xi_l^2 + C_{l,1}\xi_l + C_{l,0} \tag{2.31}$$

where, the cofficients $C_{l,0}, C_{l,1}, C_{l,2}, C_{l,3}$ are the solutions of the system of equations shown below:

$$\begin{bmatrix} \lambda_{l,1} & \lambda_{l,2} & \lambda_{l,3} & \lambda_{l,4} \\ \lambda_{l,2} & \lambda_{l,3} & \lambda_{l,4} & \lambda_{l,5} \\ \lambda_{l,3} & \lambda_{l,4} & \lambda_{l,5} & \lambda_{l,6} \\ \lambda_{l,4} & \lambda_{l,5} & \lambda_{l,6} & \lambda_{l,7} \end{bmatrix} \begin{bmatrix} C_{l,0} \\ C_{l,1} \\ C_{l,2} \\ C_{l,3} \end{bmatrix} = - \begin{bmatrix} \lambda_{l,5} \\ \lambda_{l,6} \\ \lambda_{l,7} \\ \lambda_{l,8} \end{bmatrix} \tag{2.32}$$

3. After the calculation of standard locations $\xi_{l,1}$, $\xi_{l,2}$, $\xi_{l,3}$ and $\xi_{l,4}$, obtain $x_{l,1}$, $x_{l,2}$, $x_{l,3}$ and $x_{l,4}$ using $x_{l,i} = \mu_l + \xi_{l,i}\sigma_l$, where $i = 1, 2..4$. The weight factors $w_{l,1}, w_{l,2}, w_{l,3}, w_{l,4}$ and w_μ are then determined by solving the following equations:

$$\begin{bmatrix} w_{l,1} \\ w_{l,2} \\ w_{l,3} \\ w_{l,4} \end{bmatrix} = \begin{bmatrix} \xi_{l,1} & \xi_{l,2} & \xi_{l,3} & \xi_{l,4} \\ \xi_{l,1}^2 & \xi_{l,2}^2 & \xi_{l,3}^2 & \xi_{l,4}^2 \\ \xi_{l,1}^3 & \xi_{l,2}^3 & \xi_{l,3}^3 & \xi_{l,4}^3 \\ \xi_{l,1}^4 & \xi_{l,2}^4 & \xi_{l,3}^4 & \xi_{l,4}^4 \end{bmatrix}^{-1} \begin{bmatrix} 0 \\ 1 \\ \lambda_{l,3} \\ \lambda_{l,4} \end{bmatrix} \tag{2.33}$$

$$w_\mu = 1 - \sum_{l=1}^{n} \sum_{k=1}^{4} w_{l,k} \tag{2.34}$$

2.4.4 Seven point estimate Method (7PEM)

1. Find the standard central moments as [27];

$$\lambda_{l,i} = \frac{E\left[(x_l - \mu_l)^i\right]}{\sigma_l^i}, \quad i = 3, .., 12. \tag{2.35}$$

2. Find the six standard locations $\xi_{l,1}$, $\xi_{l,2}$, $\xi_{l,3}$, $\xi_{l,4}$, $\xi_{l,5}$ and $\xi_{l,6}$, other than mean, by obtaining the roots of the polynomial

$$\pi(\xi_l) = \xi_l^6 + C_{l,5}\xi_l^5 + C_{l,4}\xi_l^4 + C_{l,3}\xi_l^3 + C_{l,2}\xi_l^2 + C_{l,1}\xi_l + C_{l,0} \tag{2.36}$$

where, the coefficients $C_{l,0}, C_{l,1}, C_{l,2}, C_{l,3}, C_{l,4}, C_{l,4}$ are the solutions of the system of equations shown below:

$$\begin{bmatrix} \lambda_{l,1} & \lambda_{l,2} & \lambda_{l,3} & \lambda_{l,4} & \lambda_{l,5} & \lambda_{l,6} \\ \lambda_{l,2} & \lambda_{l,3} & \lambda_{l,4} & \lambda_{l,5} & \lambda_{l,6} & \lambda_{l,7} \\ \lambda_{l,3} & \lambda_{l,4} & \lambda_{l,5} & \lambda_{l,6} & \lambda_{l,7} & \lambda_{l,8} \\ \lambda_{l,4} & \lambda_{l,5} & \lambda_{l,6} & \lambda_{l,7} & \lambda_{l,8} & \lambda_{l,9} \\ \lambda_{l,5} & \lambda_{l,6} & \lambda_{l,7} & \lambda_{l,8} & \lambda_{l,9} & \lambda_{l,10} \\ \lambda_{l,6} & \lambda_{l,7} & \lambda_{l,8} & \lambda_{l,9} & \lambda_{l,10} & \lambda_{l,11} \end{bmatrix} \begin{bmatrix} C_{l,0} \\ C_{l,1} \\ C_{l,2} \\ C_{l,3} \\ C_{l,4} \\ C_{l,5} \end{bmatrix} = - \begin{bmatrix} \lambda_{l,7} \\ \lambda_{l,8} \\ \lambda_{l,9} \\ \lambda_{l,10} \\ \lambda_{l,11} \\ \lambda_{l,12} \end{bmatrix} \tag{2.37}$$

3. After the calculation of standard locations $\xi_{l,1}$, $\xi_{l,2}$, $\xi_{l,3}$, $\xi_{l,4}$, $\xi_{l,5}$ and $\xi_{l,6}$, obtain $x_{l,1}$, $x_{l,2}$, $x_{l,3}$, $x_{l,4}$, $x_{l,5}$ and $x_{l,6}$ using $x_{l,i} = \mu_l + \xi_{l,i}\sigma_l$, where $i = 1, 2..6$. The weight factors $w_{l,1}, w_{l,2}, w_{l,3}, w_{l,4}$, $w_{l,5}$, $w_{l,6}$ and w_μ are determined by the following equations:

$$\begin{bmatrix} w_{l,1} \\ w_{l,2} \\ w_{l,3} \\ w_{l,4} \\ w_{l,5} \\ w_{l,6} \end{bmatrix} = \begin{bmatrix} \xi_{l,1} & \xi_{l,2} & \xi_{l,3} & \xi_{l,4} & \xi_{l,5} & \xi_{l,6} \\ \xi_{l,1}^2 & \xi_{l,2}^2 & \xi_{l,3}^2 & \xi_{l,4}^2 & \xi_{l,5}^2 & \xi_{l,6}^2 \\ \xi_{l,1}^3 & \xi_{l,2}^3 & \xi_{l,3}^3 & \xi_{l,4}^3 & \xi_{l,5}^3 & \xi_{l,6}^3 \\ \xi_{l,1}^4 & \xi_{l,2}^4 & \xi_{l,3}^4 & \xi_{l,4}^4 & \xi_{l,5}^4 & \xi_{l,6}^4 \\ \xi_{l,1}^5 & \xi_{l,2}^5 & \xi_{l,3}^5 & \xi_{l,4}^5 & \xi_{l,5}^5 & \xi_{l,6}^5 \\ \xi_{l,1}^6 & \xi_{l,2}^6 & \xi_{l,3}^6 & \xi_{l,4}^6 & \xi_{l,5}^6 & \xi_{l,6}^6 \end{bmatrix}^{-1} \begin{bmatrix} 0 \\ 1 \\ \lambda_{l,3} \\ \lambda_{l,4} \\ \lambda_{l,5} \\ \lambda_{l,6} \end{bmatrix} \tag{2.38}$$

$$w_\mu = 1 - \sum_{l=1}^{n} \sum_{k=1}^{6} w_{l,k} \tag{2.39}$$

This method can be applied to solve the PLF for a power system as explained next.

2.4.5 PLF using PEM without reactive limit violations

It is assumed that in a power system there are total 'n' number of random input variables. For instance, if there are 'L' load buses in a power system, each having both real and reactive power loads which are randomly fluctuating, then n = 2L. The objective of PLF is to calculate the PDFs of bus voltage magnitudes and angles from the given PDFs of these 'n' variables.

Let the l^{th} random variable x_l $(l = 1, 2, ..n)$ having PDF f_l be defined as

$$x_{l,k} = \mu_l + \xi_{l,k}\sigma_l \quad \text{for } k = 1, 2...\text{no. of points} \tag{2.40}$$

In eq. (2.40), μ_l and σ_l are mean and standard deviation of x_l respectively and $\xi_{l,k}$ can be obtained as explained in the previous section.

Once the points and weights corresponding to 3PEM, 5PEM and 7PEM are estimated, the following procedure is adopted for PLF:

1. Form the input matrices $\boldsymbol{X_1}, \boldsymbol{X_2}, .., \boldsymbol{X_k}$ as;

$$\boldsymbol{X_k} = \begin{bmatrix} x_{1,k} & \mu_2 & \dots & \mu_n \\ \mu_1 & x_{2,k} & \dots & \mu_n \\ \vdots & \vdots & \ddots & \vdots \\ \mu_1 & \mu_2 & \dots & x_{n,k} \end{bmatrix} \tag{2.41}$$

   where, $k = 1, .., m$, $m = 2, 4$ and 6 for 3PEM, 5PEM and 7PEM respectively.

2. For each row of $\boldsymbol{X_k}$, a deterministic load flow is carried out.

3. Repeat step 2 for all the rows of the matrices $\boldsymbol{X_1}, \boldsymbol{X_2}, .., \boldsymbol{X_k}$. As a result, a total of 'nm' load flow computations would be carried out.

4. For each output variable of interest $y_{i,lk}$, calculate the j^{th} moment as,

$$E(y_{i,lk}^j) = \sum_{l=1}^{n}\sum_{k=1}^{m} w_{l,k} E\left[(y_{i,lk})^j\right], \quad j = 1, .., \text{no. of moments.} \tag{2.42}$$

   In this work the first eight moments have been used. It is to be noted that in eq. (2.42), $y_{i,lk}$ denotes the value of i^{th} variable of interest corresponding to $(lk)^{th}$ load flow, where $l = 1, ...n$ and $k = 1, ...m$.

5. Lastly, a deterministic load flow is carried out with an input vector $\boldsymbol{X_{mean}}$, as given in eq. (2.43)

$$\boldsymbol{X_{mean}} = [\mu_1, \mu_2, ..., \mu_l, .., \mu_n] \tag{2.43}$$

Let $y_{i,\mu}$ denotes the value of i^{th} output variable of interest corresponding to this load flow and the j^{th} moment $E(y_{i,lk}^j)$ is updated as:

$$E(y_{i,lk}^j) = E(y_{i,lk}^j) + w_\mu \left(y_{i,\mu}\right)^j \tag{2.44}$$

w_μ represent the weight corresponding to the location $\xi_{l,3},\ \xi_{l,5}$ and $\xi_{l,7}$ of 3PEM, 5PEM and 7PEM respectively.

6. With the above calculated moments, the CDF and PDF of y_i is computed using Cornish-Fisher series [30] or Gram-Charlier expansion series [76] described in the subsequent section. The flowchart of basic PLF with PEM is shown in the Fig. 2.2.

2.5 Gram-Charlier and Cornish-Fisher series for the construction of distribution of output variable

Once the moments of output variables are obtained, the probability distribution of the output variables can be obtained by using Gram-Charlier and Cornish-Fisher expansion series. Both series are based on the standard normal distribution and can be obtained from the cumulants of the output variables.

The probability distribution of any random variable expressed by the Gram-Charlier series is given in eq. (2.45). The detail of the series is given in Appendix A [21].

$$f(x) = \phi(x)\left(1 + \frac{g_3}{3!}H_3(\bar{x}) + \frac{g_4}{4!}H_4(\bar{x}) + \frac{g_5}{5!}H_5(\bar{x}) + \frac{g_6 + 10g_3^2}{6!}H_6(\bar{x}) + \frac{g_7 + 35g_3g_4}{7!}H_6(\bar{x}) + ...\right) \tag{2.45}$$

where, ϕ is the standard normal distribution function $N(0,1)$, $H_n(\bar{x})$ is the Hermite polynomial and g_n is the normalized cumulant of the order n.

The Cornish-Fisher expansion series provides an approximation of a quantile of a distribution function $f(x)$ in terms of the quantile of a standard normal distribution $(\phi(x))$ and the cumulants of $f(x)$ [77].

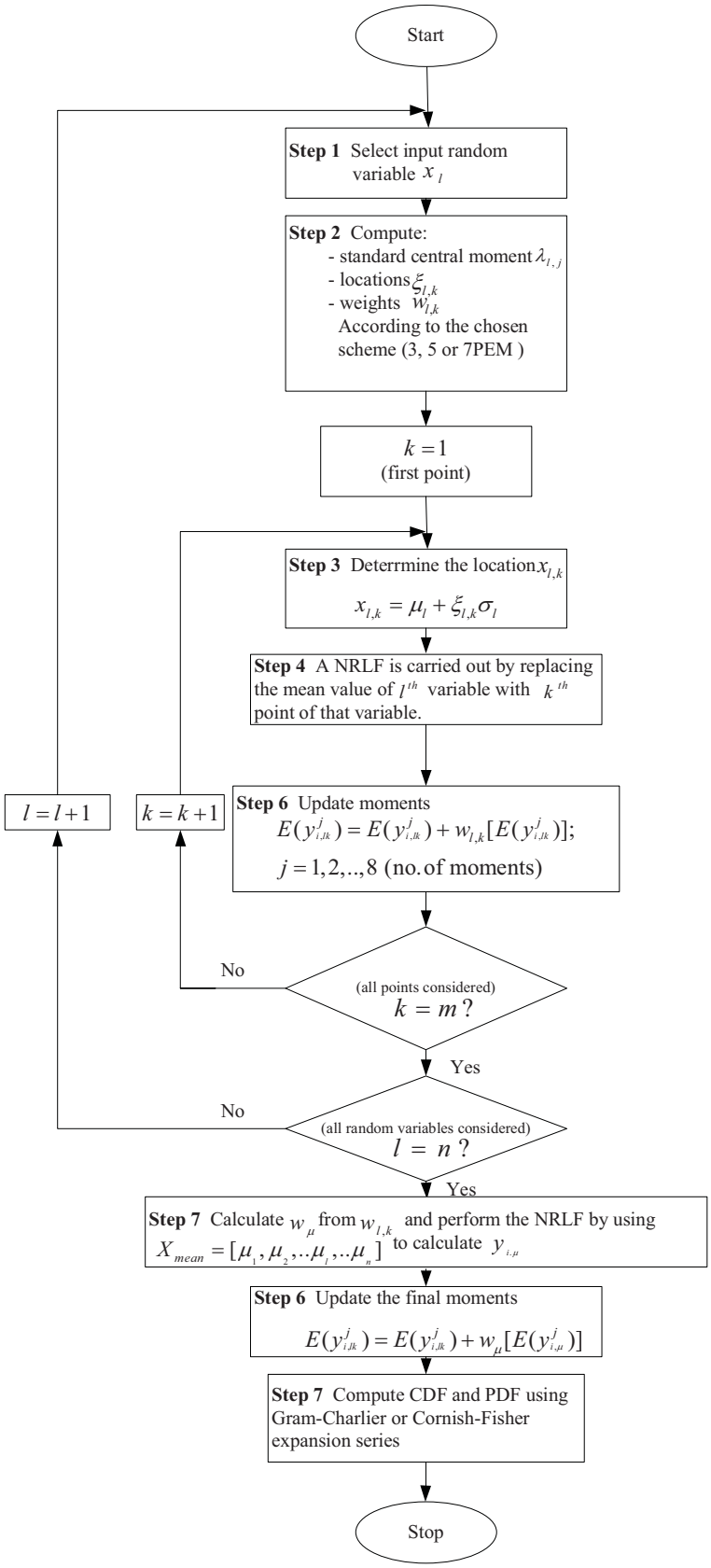

Figure 2.2: Flowchart of basic PLF with PEM

The Cornish-Fisher series expansion can be written using the first five cumulants as [76];

$$\begin{aligned} x(\alpha) \approx \zeta(\alpha) &+ \frac{1}{6}\left(\zeta^2(\alpha)-1\right)\kappa_3 \\ &+ \frac{1}{24}\left(\zeta^3(\alpha)-3\zeta(\alpha)\right)\kappa_4 \\ &- \frac{1}{36}\left(2\zeta^3(\alpha)-5\zeta(\alpha)\right)\kappa_3^2 \\ &+ \frac{1}{120}\left(\zeta^4(\alpha)-6\zeta^2(\alpha)+3\right)\kappa_5 \\ &- \frac{1}{24}\left(\zeta^4(\alpha)-5\zeta^2(\alpha)+2\right)\kappa_3\kappa_4 \\ &+ \frac{1}{324}\left(12\zeta^4(\alpha)-53\zeta^2(\alpha)+17\right)\kappa_3^3 \end{aligned} \tag{2.46}$$

where, α is the quantile of distribution function $f(x)$, $x(\alpha) = f^{-1}(\alpha)$ and $\zeta(\alpha) = \phi^{-1}(\alpha)$ and κ_n is the n^{th} order cumulant of the distribution function $f(x)$. Finally, $x(\alpha)$ is plotted with quantile α to get the distribution from commulants. The details of the quantile of a distribution function are given in Appendix A [78].

The convergence property of the Cornish-Fisher expansion series is superior to that of the Gram-Charlier series for the non-gaussian distribution functions due to smaller numerical errors [79].

Now, in the literature, generator reactive power limits have not been considered in the PLF using PEM. This work, therefore, proposes to include generator reactive power limits in PEM based PLF. The steps of the proposed PLF are described next.

2.6 Proposed PLF using PEM with reactive limit violations

The steps for the proposed PLF are as follows:

1. Form the input matrices $\boldsymbol{X_1}, \boldsymbol{X_2}, .., \boldsymbol{X_k}$ as;

$$\boldsymbol{X_k} = \begin{bmatrix} x_{1,k} & \mu_2 & \dots & \mu_n \\ \mu_1 & x_{2,k} & \dots & \mu_n \\ \vdots & \vdots & \ddots & \vdots \\ \mu_1 & \mu_2 & \dots & x_{n,k} \end{bmatrix} \tag{2.47}$$

   where, $k = 1, .., m$, $m = 2, 4$ and 6 for 3PEM, 5PEM and 7PEM respectively.

2. For each row of $\boldsymbol{X_k}$, a deterministic load flow is carried out and the reactive power limits on

the generator bus are checked in every iteration of the load flow according to:-

$$Q_i = \begin{cases} Q_i^{min} & Q_i < Q_i^{min} \\ Q_i^{max} & Q_i > Q_i^{max} \\ Q_i & Q_i^{min} \leq Q_i \leq Q_i^{max} \end{cases} \tag{2.48}$$

In eq. (2.48), Q_i is the injected reactive power at the i^{th} generator bus and Q_i^{min} and Q_i^{max} are the minimum and the maximum reactive power limits of i^{th} generator respectively. If the reactive power limits are not violated, the bus voltage magnitude is maintained at the specified value. Otherwise, the generator bus is considered as a load bus and the change in voltage magnitude on that bus is calculated by,

$$\Delta V_i = \frac{V_i}{L_{ii}} \left[\Delta Q_i - \sum_{k=2}^{nb} J_{ik} \Delta \delta_k - \sum_{\substack{k=nv+1 \\ k \neq i}}^{nb} L_{ik} \frac{\Delta V_k}{V_k} \right] \tag{2.49}$$

In eq. (2.49), L_{ii}, J_{ik}, L_{ik} are the elements of the jacobian submatrices, $L_{ii} = V_i \frac{\partial Q_i}{\partial V_i}$, $J_{ik} = \frac{\partial Q_i}{\partial \delta_k}$, $L_{ik} = V_k \frac{\partial Q_i}{\partial V_k}$, δ_k is the voltage angle of k^{th} bus (in radians), nb is the number of buses, nv is the number of generator buses, and ΔQ_i is the change in the injected reactive power at i^{th} bus. After ΔV_i is calculated, the voltage magnitude of this generator bus is updated as $V_i = V_i^{sp} + \Delta V_i$ where, V_i^{sp} is the specified voltage magnitude of i^{th} bus. By following a similar procedure, the deterministic load flow with reactive power limit violations are carried out for all the rows of $\boldsymbol{X_k}$ to determine the corresponding values of the output variables of interest.

3. Repeat step 2 for all the rows of the matrices $\boldsymbol{X_1}, \boldsymbol{X_2}, .., \boldsymbol{X_k}$. As a result, a total of 'nm' load flow computations would be carried out.

4. For each output variable of interest $y_{i,lk}$, calculate the j^{th} moment as,

$$E(y_{i,lk}^j) = \sum_{l=1}^{n} \sum_{k=1}^{m} w_{l,k} E\left[(y_{i,lk})^j \right], \; j = 1, .., \text{no. of moments.} \tag{2.50}$$

In this work, first eight moments have been used. It is to be noted that in eq. (2.50), $y_{i,lk}$ denotes the value of i^{th} variable of interest corresponding to $(lk)^{th}$ load flow, where $l = 1, ...n$ and $k = 1, ...m$.

5. Lastly, a deterministic load flow is carried out (along with the checking of reactive power limit as given in eq. (2.48) and calculation of change in voltage magnitude as in eq. (2.49) if required) with an input vector as given in eq. (2.51)

$$\boldsymbol{X_{mean}} = [\mu_1, \mu_2, ..., \mu_l, , .., \mu_n] \tag{2.51}$$

Let $y_{i,\mu}$ denotes the value of i^{th} output variable of interest corresponding to this load flow and the moment $E(y^j_{i,lk})$ is updated as:

$$E(y^j_{i,lk}) = E(y^j_{i,lk}) + w_\mu \left(y_{i,\mu}\right)^j \tag{2.52}$$

w_μ represent the weight corresponding to the location $\xi_{l,3},\ \xi_{l,5}$ and $\xi_{l,7}$ of 3PEM, 5PEM and 7PEM respectively.

6. With the above calculated moments, the CDF and PDF of y_i is computed using appropriate expansion series.

The developed method has been applied to IEEE-118 bus system to check its performance. The results of this study along with the relevant discussions are given next.

2.7 Results and discussion

2.7.1 Without generator reactive power limits

The distributions (PDFs and CDFs) of variables of interest have been obtained using PLF with PEM without considering generator reactive power limit violations, as described in Section 2.4.5. The method has been applied to IEEE-118 bus system (Appendix B [80]) and PLF has been solved by using 3PEM, 5PEM and 7PEM. The loads have been assumed to have normal distribution with mean value equal to the load data given in Appendix B and standard deviation equal to 10% of the corresponding mean value of the load. All the simulation studies have been carried out on an Intel Dual-core 2.67 GHz, 2 GB RAM machine, using the MATLAB environment [81].

It is known that the Gram-Charlier expansion series has a tendency to produce small negative probability values particularly in the extremes [82]. As an illustration, the PDF of the active power flow over the line between the buses 4-13 obtained using Gram-Charlier expansion, is shown in Fig. 2.3. As can be seen from this figure, the probability value is negative in the initial region of the PDF. Further, it has been already pointed out earlier that Gram-Charlier series has poor convergence property as compared to Cornish-Fisher series for non-gaussian distribution function [29]. Due to

these two reasons, in this work, the CDFs and PDFs have been computed using Cornish-Fisher (CF) series [30, 35].

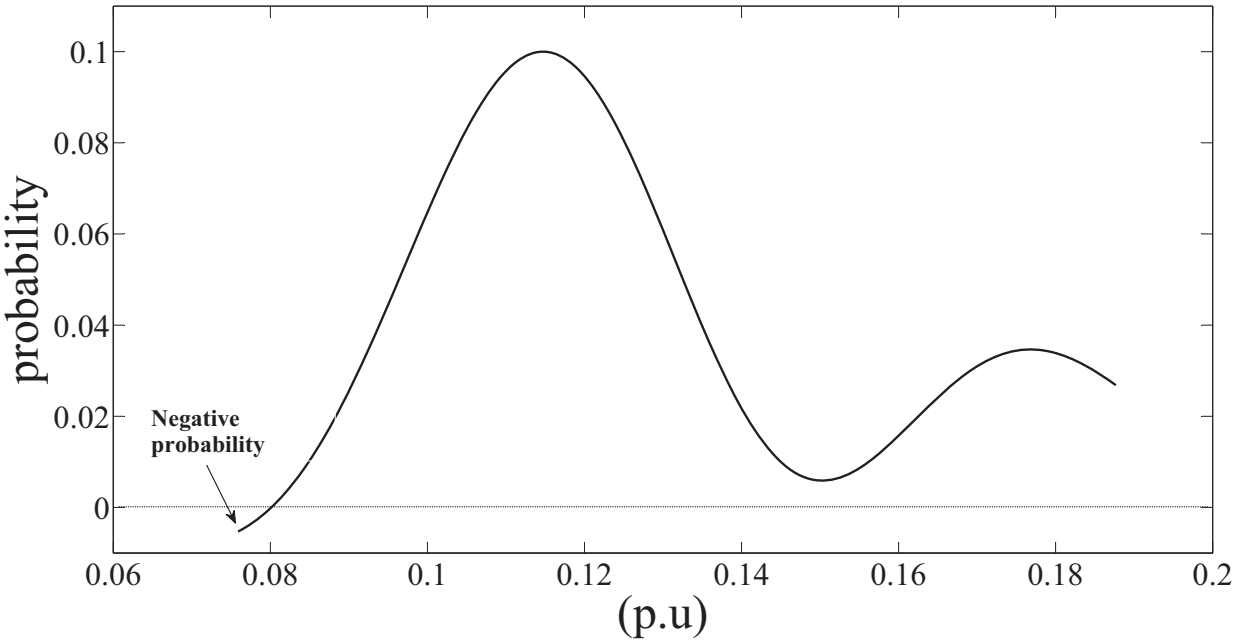

Figure 2.3: PDF of active power flow in the line between the buses 4-13 obtained by Gram-Charlier series

The PDFs and the CDFs of voltage at bus no. 3 (as a representative case), as obtained by the different point estimate methods (3PEM, 5PEM, 7PEM) and CF series are shown in Figs. 2.4 and 2.5 respectively.

For comparing the performance of the developed method, the results were compared with those obtained through MCS study. In MCS study, deterministic load flow was carried out 100000 times with the input variables sampled randomly within the corresponding specified ranges. The resulting PDF and CDF as obtained by MCS study are also shown in Figs. 2.4 and 2.5 respectively.

The four basic statistical parameters of a PDF, i.e. mean, variance, skewness and kurtosis, as computed by the different point estimate methods (3, 5 and 7 PEM) and MCS are shown in Table 2.1 for comparison. From this table, it can be observed that 7PEM results are closest to those obtained by MCS and are in very good agreement with each other. Also, from Figs. 2.4 and 2.5, it can be seen that the PDF and CDF as obtained by 7PEM and Cornish-Fisher series is closest to the PDF and CDF obtained by MCS respectively. Similarly, probability distributions have also been obtained for the active power flow in the line between the buses 2-4, reactive power flow in the line between

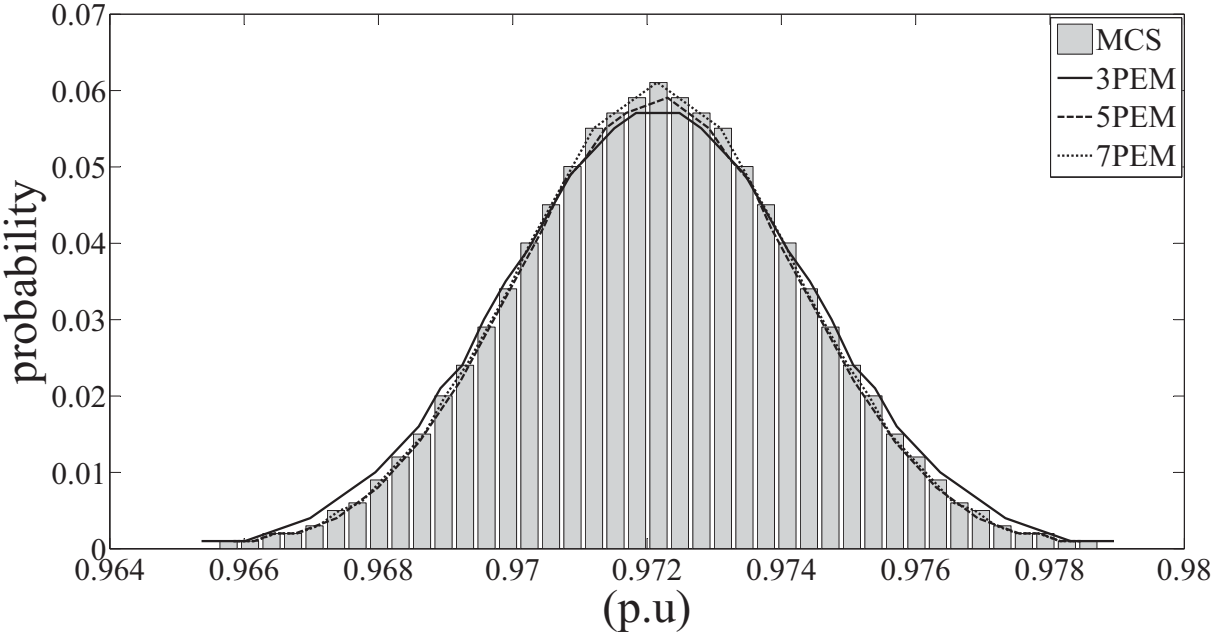

Figure 2.4: PDF of voltage magnitude at bus no. 3

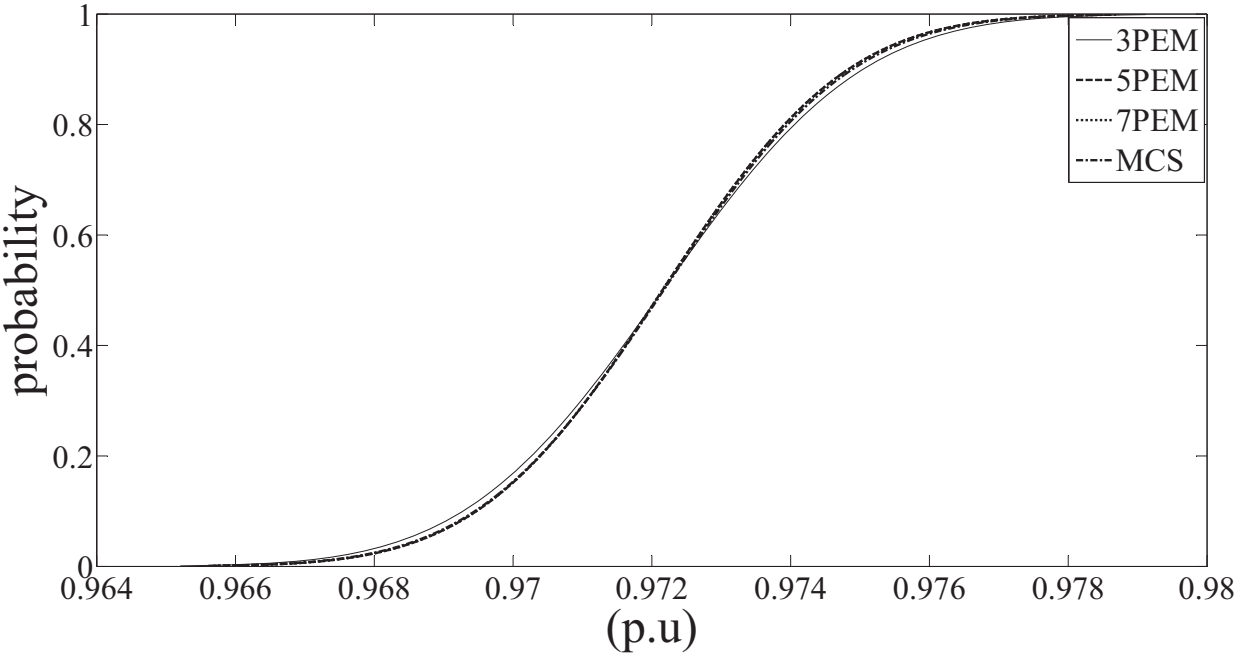

Figure 2.5: CDF of voltage magnitude at bus no. 3

the buses 12-13 and reactive power at generator bus no. 13. These are shown in Figs. 2.6, 2.7 and 2.8 respectively.

Again, from these three figures, it can be observed that the results of 7PEM based PLF are in best

Table 2.1: Statistical parameters of the voltage magnitude at bus no. 3

Schemes	Mean	S. dev.	Skewness	Kurtosis	Confidence level	
	μ	σ	sk	ku	10%	90%
3PEM	0.9722	0.0041	0.4329	1.6620	0.9659	0.9784
5PEM	0.9722	0.0038	0.4301	1.6526	0.9663	0.9780
7PEM	0.9722	0.0038	0.4324	1.6642	0.9663	0.9780
MCS	0.9722	0.0038	0.4325	1.6643	0.9663	0.9781

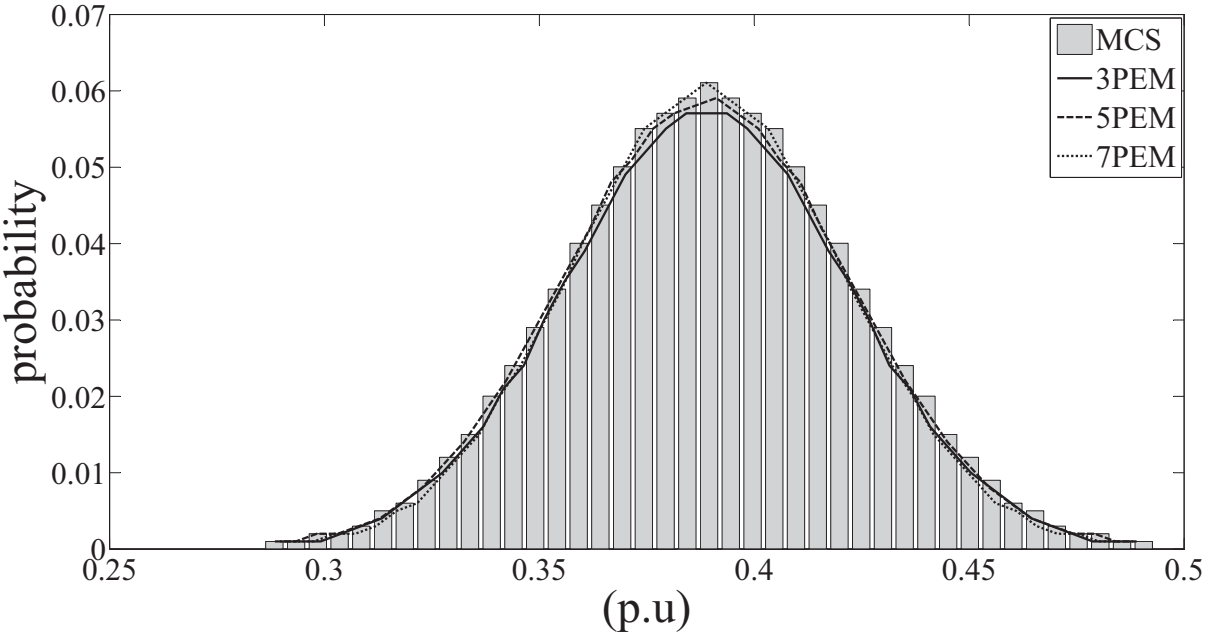

Figure 2.6: PDF of active power flow in the line between the buses 2-4

agreement with the results of MCS. Further, for normally distributed loads, the time taken by the MCS study with 100000 deterministic load flows is approximately 6 hours, while the 7PEM based PLF takes only about 6 minutes.

Thus it can be safely concluded that 7PEM based PLF is a good alternative to MCS based PLF.

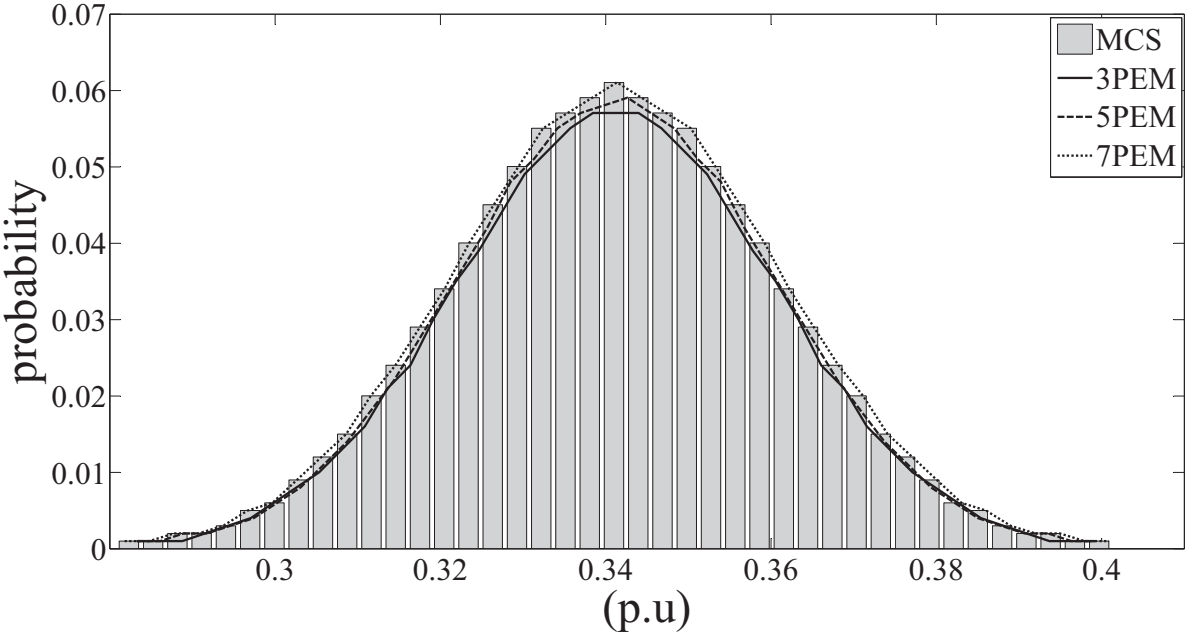

Figure 2.7: PDF of reactive power flow in the line between the buses 12-13

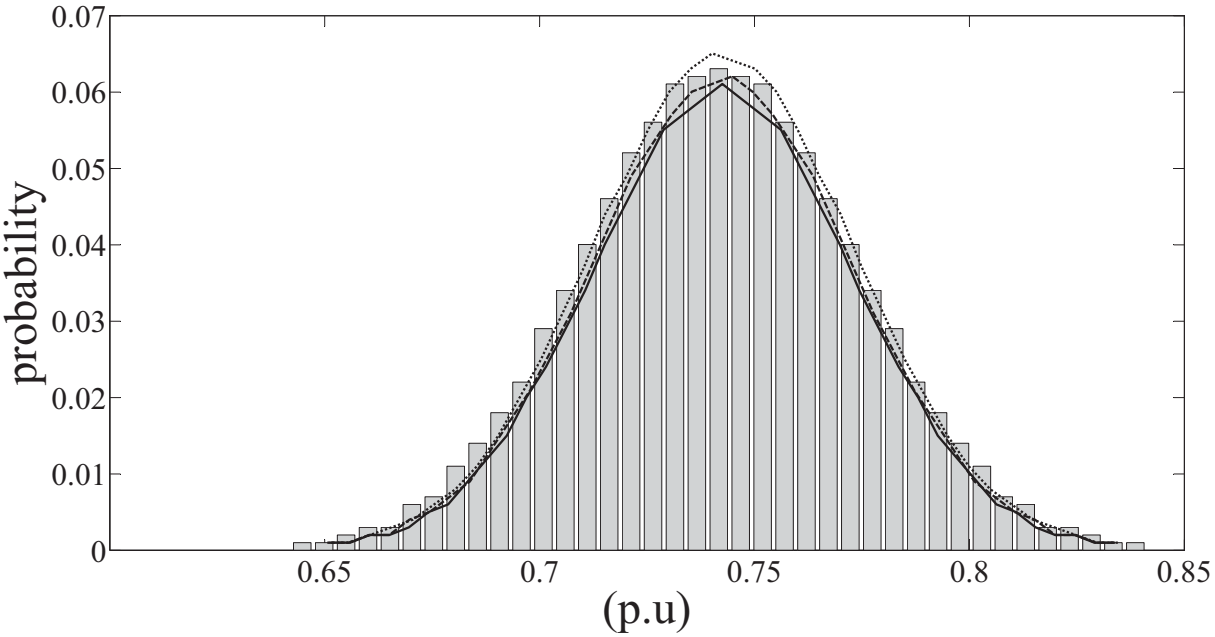

Figure 2.8: PDF of injected reactive power at the generator bus no. 13

2.7.2 With generator reactive power limits

For IEEE-118 bus system, with normally distributed loads at all the buses, the load values have been increased to 1.5 times of the base loading condition (as given in [80]) so that reactive power

violations may occur at few generator buses. For this loading condition, the PLF has been computed using 3PEM, 5PEM and 7PEM methods. The results have also been compared with those obtained by MCS.

The PDF and CDF of voltage magnitude at bus no. 92 (one of the buses where the reactive power limits are violated), as obtained from these three methods and MCS, are shown in Fig. 2.9 and Fig. 2.10 respectively.

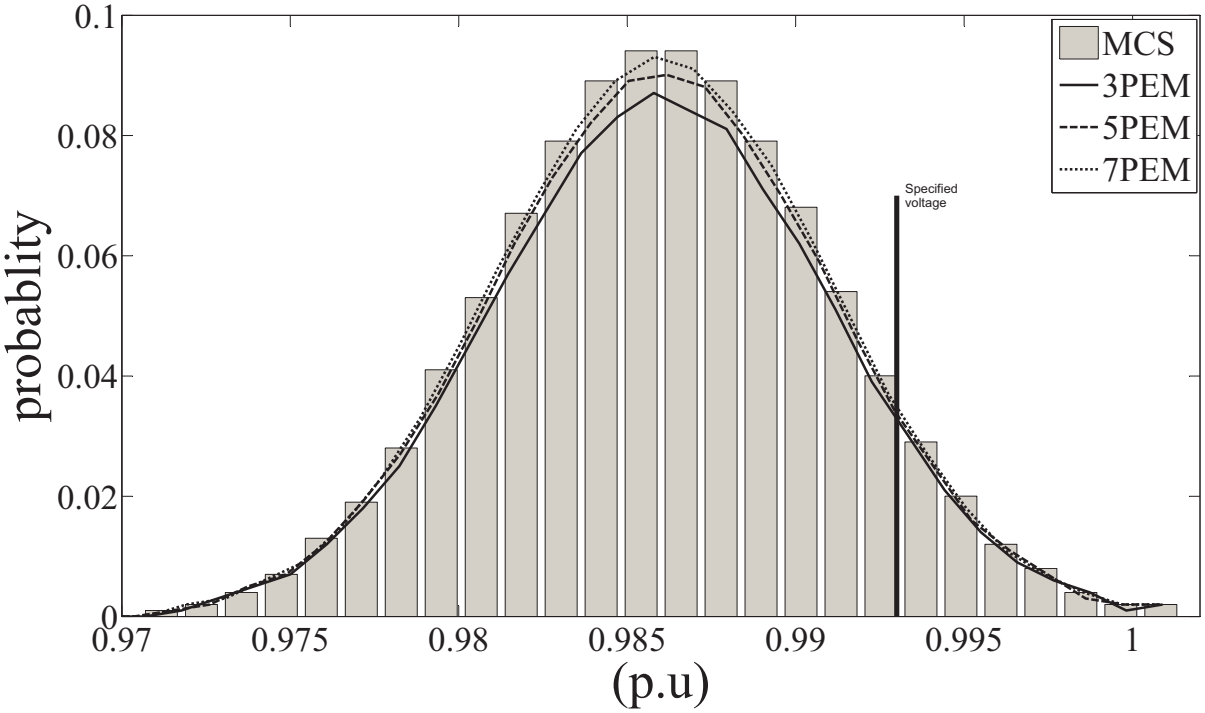

Figure 2.9: PDF of voltage magnitude at bus no. 92

From these two figures, it can be clearly observed that the 7PEM along with Cornish-Fisher expansion gives the best approximation of PDF and CDF of the bus voltage magnitude in comparison to 3PEM and 5PEM, and is closest to the PDF obtained by MCS. For further insight, some pertinent statistical parameters of the voltage magnitude at bus 92 are given in Table 2.2. From these results also, it is observed that the results obtained by 7PEM give the values of the four statistical parameters closest to those obtained by MCS. Consequently, for all subsequent results shown for the IEEE-118 bus system, the moments have been calculated using 7PEM.

The PDF of reactive power at bus no. 92 is shown in Fig. 2.11. Now, the maximum and minimum reactive power limit at bus no. 92 is 0.09 p.u and -0.03 p.u. respectively, with a specified voltage of 0.993 p.u. As observed from Fig. 2.11, the probability of violation of the upper generator reactive

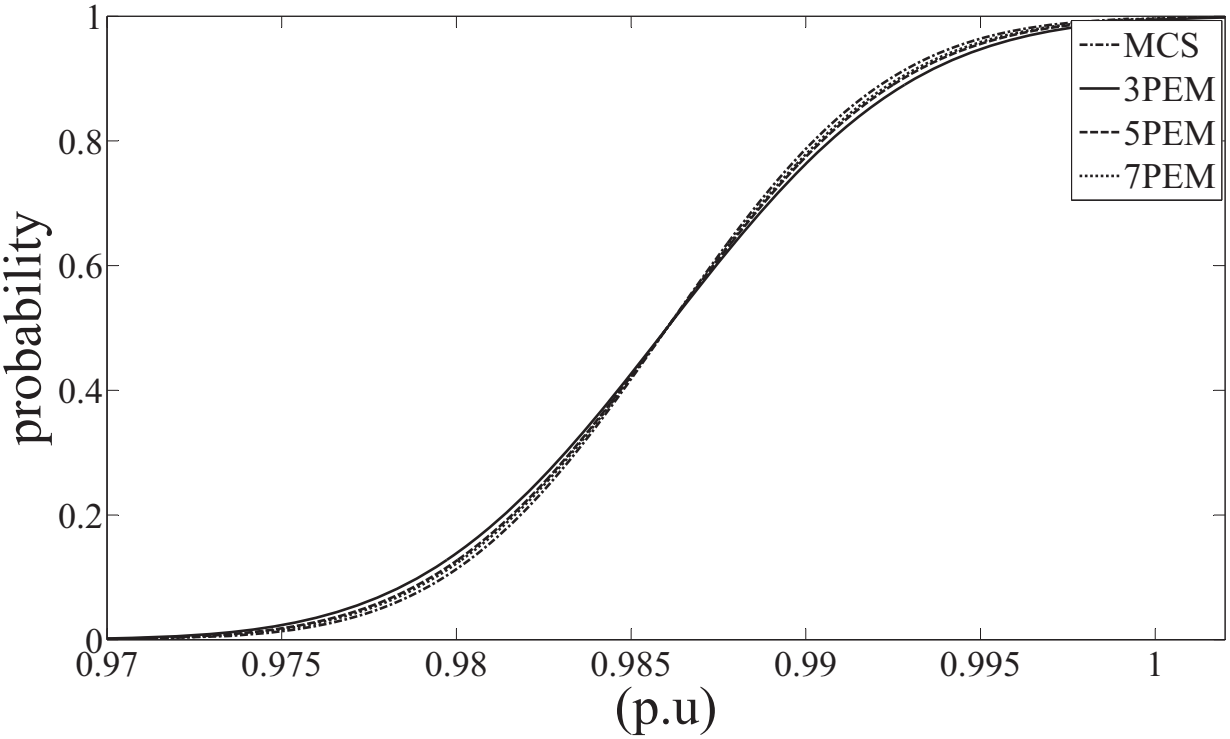

Figure 2.10: CDF of voltage magnitude at bus no. 92

Table 2.2: Statistical parameters of the voltage magnitude at bus no. 92

Schemes	**Mean**	**S. dev.**	**Skewness**	**Kurtosis**	**Confidence level**	
	μ	σ	sk	ku	10%	90%
3PEM	0.9851	0.0512	0.43014	1.6568	0.9812	0.9925
5PEM	0.9857	0.0518	0.43006	1.6526	0.9823	0.9937
7PEM	0.9862	0.0521	0.43258	1.6643	0.9827	0.9942
MCS	0.9871	0.0529	0.43308	1.6601	0.9832	0.9945

power limit at this bus is more as compared to lower limit violation. Therefore, the probability that the bus voltage magnitude is lower than the specified value of 0.993 p.u should be more than the probability of the bus voltage magnitude being higher than the specified voltage magnitude. From Fig. 2.9, it is observed that this indeed is the case.

In Fig. 2.11, the PDF of generator bus reactive power obtained by MCS is discrete, with two peaks occuring at the two reactive power limits. The approximation of this discrete distribution using

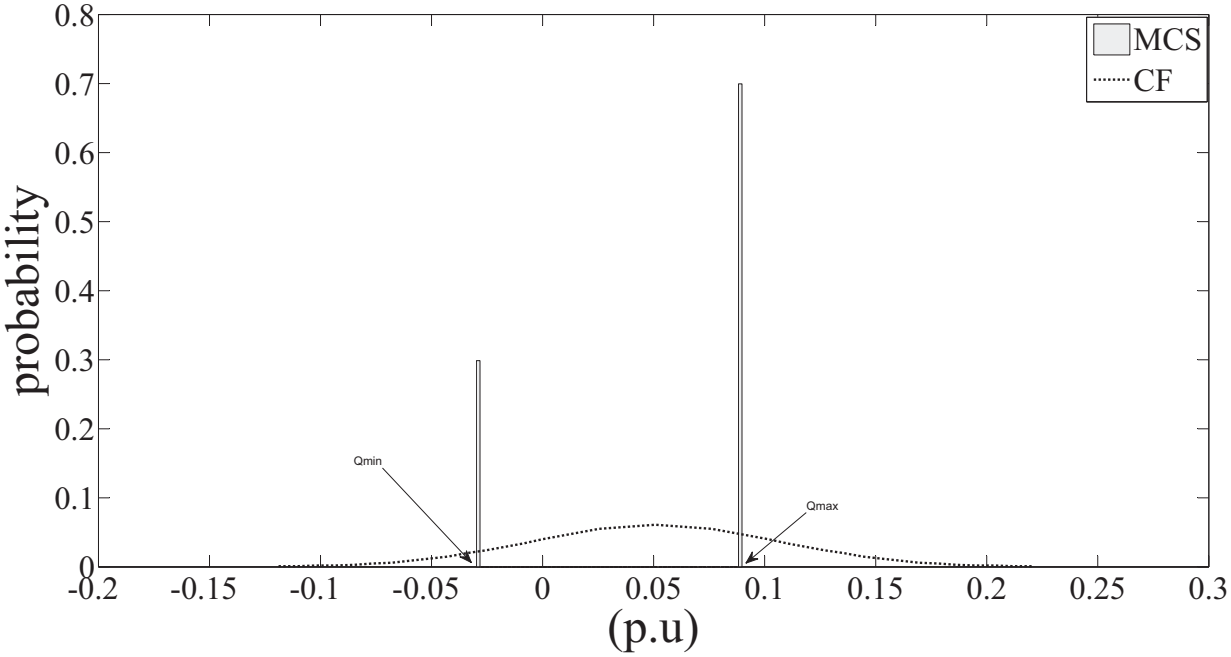

Figure 2.11: PDF of reactive power at generator bus no. 92

Cornish-Fisher (CF) expansion series is also shown in Fig. 2.11. It is observed that the approximation obtained by CF series is quite poor. This is due to the fact that the CF series is good for approximating only unimodal distributions, and not a multi-modal distribution as shown in Fig. 2.11. Hence, for approximating the multi-modal distributions from the moments more accurately, the application of spline based reconstruction method is explored in the next chapter.

2.8 Conclusion

In this chapter, the PEM based PLF technique incorporating reactive power limit violations with 3PEM, 5PEM and 7PEM has been developed. The results obtained by these three methods have also been compared with those obtained by MCS method. Further, the PDFs and CDFs of the output variables of interest have been determined by using Gram-Charlier and Cornish-Fisher expansion series. All these studies have been carried out on IEEE-118 bus system with normally distributed loads. From these studies, it has been observed that the unimodal distributions are satisfactorily approximated using Cornish-Fisher expansion series as compared to Gram-Charlie series, which produces small negative probability values at the extreme points. However, there is a problem in approximating the multi-modal distributions using Cornish-Fisher expansion series. Hence, a method is required for approximating a multi-modal distribution and towards this goal, a spline based method for the reconstruction of multi-modal distributions is explored in the next chapter.

Chapter 3: Spline based technique for reconstruction of PDF

This chapter describes a spline based method for the reconstruction of multi-modal distribution functions for the variables of interest in a PLF. The correlation among the bus loads and slack bus power limits has also been considered and included in the PLF. The spline based reconstruction technique has been tested with different types of loads and the reconstructed PDFs have been compared with the PDFs obtained from MCS.

As discussed in Chapter 2, the Cornish-Fisher expansion series is suitable for constructing the PDF of unimodal distribution and also provides a reasonable normal approximation of non-normal distributions which are only slightly deviated from the normal distribution. However, the normal approximation does not lead to satisfactory results for estimating the PDF of variables which are multi-modal in nature. Therefore, in order to obtain a reasonably accurate estimate for the multi-modal distribution functions, the application of spline based reconstruction technique is explored in this chapter.

3.1 Spline

A spline is basically a smooth polynomial function composed of several polynomial segments. A spline exhibits a high degree of smoothness at the points (known as knots) where the polynomial segments connect with each other. A spline is defined as [83]:

A piecewise-polynomial real function $S : [a, b] \Rightarrow R$ on an interval [a,b] is called a spline and is composed of 'v' number of ordered disjoint subintervals $[x_i, x_{i+1}]$ with $a = x_1 < x_2 < ...x_v < x_{v+1} = b$. In the i^{th} interval, S consists of a polynomial $S_i : [x_i, x_{i+1}] \Rightarrow R$, so that

$S(x) = S_1(x), x_1 \leq x < x_2,$

$S(x) = S_2(x), x_2 \leq x < x_3,$

$\vdots$

$S(x) = S_v(x), x_v \leq x \leq x_{v+1},$

Order of the spline is the highest order of the polynomial $S_i(x)$ and these polynomials are chosen in such a way so that sufficient smoothness of S is guaranteed. The most commonly used spline is cubic spline, i.e., of order 3 (as shown in Fig. 3.1).

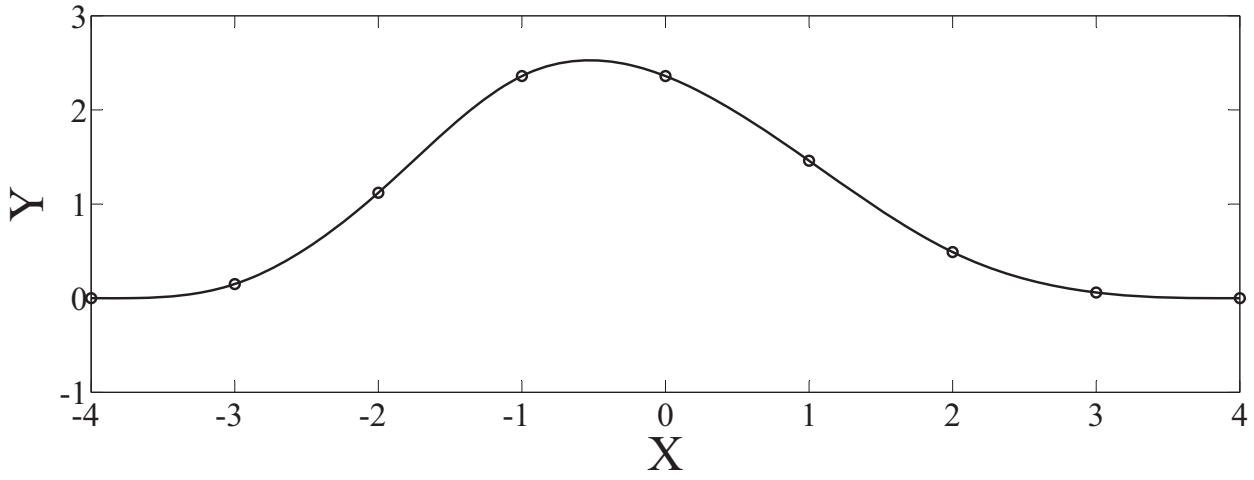

Figure 3.1: Cubic spline

3.2 Spline based reconstruction technique

After the moments of variables of interest are obtained using PEM based PLF, the next task is to reconstruct the PDF of these variables. Let this PDF be denoted as $f(x)$. The key features of reconstruction by splines are as follows [84]:

- For the shape of the function $f(x)$, which is to be reconstructed, no a priori assumptions are needed and a piecewise polynomial function is used to approximate its shape.
- A rough priori information about the interval, where $f(x)$ has positive values is required.
- Since, the reconstruction of a distribution function by a finite number of its moments is a severely ill-conditioned problem (small changes of the data might lead to rather large changes in the reconstruction), only reliable moments need to be used.

The possible range over which $f(x)$ exists, is divided into v sub-intervals (shown in Fig. 3.2) such that $a = x_1 < x_2 < ...x_{v+1} = b$, where, v, the number of sub-intervals, is the sum of number of moments considered and the order of spline. In this work, $v = 11$, as eight moments have been used and the reconstruction has been carried out with the help of piecewise polynomials of order 3. Let the expression for the estimated curve in the i^{th} interval $s_i(x)$ be given as;

$$s_i(x) = \sum_{j=0}^{3} s_{ij}(x - x_i)^j, x \in [x_i, x_{i+1}], i = 1, ..., v \tag{3.1}$$

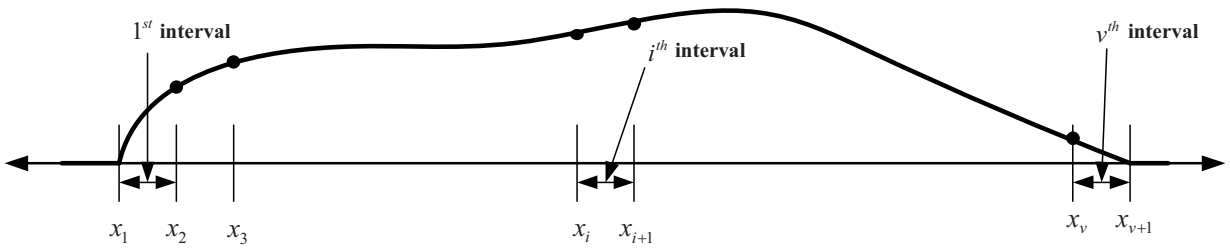

Figure 3.2: Sub-intervals for the spline based reconstruction method

From eq. (3.1), the first and second order derivatives (denoted as $s_i'(x)$ and $s_i''(x)$ respectively) can be easily calculated. In each sub-interval the four coefficients s_{ij} are not known and hence for v sub-intervals we have a total of $4v$ unknowns. The set of $4v$ equations required for determining these $4v$ unknowns is generated as follows:

- $f(x)$ is to be reconstructed with the assumption that it exists only in the interval $[x_1, x_{v+1}]$, and is zero beyond it. Further, at the interval boundaries the transition from zero to non zero values is smooth. Hence, the conditions at the left boundary point x_1 are;

$$s_1(x_1) = 0;\ s_1^{'}(x_1) = 0;\ s_1^{''}(x_1) = 0 \tag{3.2}$$

  Using these conditions in eq. (3.1), we get the following three equations:

$$s_1(x_1) = s_{10} = 0, s_1'(x_1) = s_{11} = 0, s_1''(x_1) = 2s_{12} = 0 \tag{3.3}$$

- Similarly with the same assumption, three equations are generated at the right boundary point x_{v+1} as;

$$s_v(x_{v+1}) = 0;\ s_v^{'}(x_{v+1}) = 0;\ s_v^{''}(x_{v+1}) = 0 \tag{3.4}$$

  Substituting these equations in eq. (3.1), we get the following three equations:

$$\begin{bmatrix} 1 & x_{v+1} - x_v & (x_{v+1} - x_v)^2 & (x_{v+1} - x_v)^3 \\ 0 & 1 & 2(x_{v+1} - x_v) & 3(x_{v+1} - x_v)^2 \\ 0 & 0 & 2 & 6(x_{v+1} - x_v) \end{bmatrix} \begin{bmatrix} s_{v0} \\ s_{v1} \\ s_{v2} \\ s_{v3} \end{bmatrix} = \begin{bmatrix} 0 \\ 0 \\ 0 \end{bmatrix} \tag{3.5}$$

- $(v-1)$ equations are obtained by using the continuity condition of the function s_i,

$$s_i(x_{i+1}) = s_{i+1}(x_{i+1}), \;\; i = 1, ..., v-1 \tag{3.6}$$

On applying the conditions given in eq. (3.6) to eq. (3.1), we get $v-1$ equations as:

$$\begin{bmatrix} 1 & (x_{i+1}-x_i) & (x_{i+1}-x_i)^2 & (x_{i+1}-x_i)^3 & -1 \end{bmatrix} \begin{bmatrix} s_{i0} \\ s_{i1} \\ s_{i2} \\ s_{i3} \\ s_{(i+1)0} \end{bmatrix} = 0; \;\; i = 1, ..., v-1 \tag{3.7}$$

- Next $2(v-1)$ equations are obtained by using the continuity condition of the first and second order derivatives of s_i, i.e.

$$s_i^{'}(x_{i+1}) = s_{i+1}^{'}(x_{i+1}) \text{ and } s_i^{''}(x_{i+1}) = s_{i+1}^{''}(x_{i+1}) \tag{3.8}$$

Using eq. (3.8) and eq. (3.1), following sets of equations are obtained:

$$\begin{bmatrix} 1 & 2(x_{i+1}-x_i) & 3(x_{i+1}-x_i)^2 & -1 \end{bmatrix} \begin{bmatrix} s_{i1} \\ s_{i2} \\ s_{i3} \\ s_{(i+1)1} \end{bmatrix} = 0; \;\; i = 1, ..., v-1 \tag{3.9}$$

$$\begin{bmatrix} 2 & 6(x_{i+1}-x_i) & -2 \end{bmatrix} \begin{bmatrix} s_{i2} \\ s_{i3} \\ s_{(i+1)2} \end{bmatrix} = 0; \;\; i = 1, ..., v-1 \tag{3.10}$$

- Eqs. (3.3), (3.5), (3.7), (3.9) and (3.10) give a total of $3(v-1)+3+3 = 3v+3$ equations for $4v$ unknowns. The remaining $v-3$ equations are obtained by equating the known moments and the moments of the fitted splines by using the following equations:

The k^{th} moment of a cubic spline ($s^{(3)}$) is given by,

$$\int_{x_1}^{x_{v+1}} x^k s^{(3)}(x)dx = \sum_{i=1}^{v} \int_{x_1}^{x_{i+1}} x^k s_i(x)dx = \sum_{i=1}^{v} \sum_{j=0}^{3} s_{ij} \int_{x_1}^{x_{i+1}} x^k (x - x_i)^j dx$$

$$= \sum_{i=1}^{v} \left[I_1 s_{i0} + (I_2 - x_i I_1) s_{i1} + (I_3 - 2x_i I_2 + x_i^2 I_1) s_{i2} + (I_4 - 3x_i I_3 + 3x_i^2 I_2 - x_i^3 I_1) s_{i3} \right] \tag{3.11}$$

where, the coefficients $I_1, ..., I_4$ are

$$I_1 = \frac{x_{i+1}^{k+1} - x_i^{k+1}}{k+1}, I_2 = \frac{x_{i+1}^{k+2} - x_i^{k+2}}{k+2}$$
$$I_3 = \frac{x_{i+1}^{k+3} - x_i^{k+3}}{k+3}, I_4 = \frac{x_{i+1}^{k+4} - x_i^{k+4}}{k+4} \tag{3.12}$$

The expression given in eq. (3.11) is equal to the k^{th} moment $\mu_{x,k}$ of $f_X(x)\ \forall\ k = 1, ..., 8$. Thus, a $4v \times 4v$ linear system of equations is obtained and can be solved for the coefficients of the spline.

The following points are kept in mind while reconstructing the function:

1. The reconstruction is done in the smallest possible interval $[a, b]$ in which the values of the function are greater than zero.

2. If the linear system of equations for calculating the unknown coefficients of splines is ill-conditioned, it should be regularized. For this, the system of equations is usually solved using a pseudo-inverse procedure by neglecting the smallest singular values.

The finer details of the procedure are given in [84].

3.3 Inclusion of correlation among the loads in PLF

In the PLF with PEM, discussed in the Chapter 2, the correlation among the loads has not been considered. However, in this work, the correlation among the loads has also been taken into account. The detailed procedure for this is given in [40] and is discussed in brief below:

Let a vector of z correlated random variables $\boldsymbol{x} = (x_1, x_2...x_z)^T$ be considered with the corresponding mean vector $\boldsymbol{\mu_x}$ as $\boldsymbol{\mu_x} = [\mu_1\ \mu_2...\mu_z]^T$, where the subscript 'T' denotes the transpose of a

vector. Let the correlation matrix be denoted as

$$\boldsymbol{P_x} = \begin{array}{c} \\ x_1 \\ x_2 \\ \vdots \\ x_z \end{array} \begin{array}{c} \begin{array}{cccc} x_1 & x_2 & \cdots & x_z \end{array} \\ \begin{bmatrix} 1 & \rho_{12} & \cdots & \rho_{1z} \\ \rho_{21} & 1 & \cdots & \rho_{2z} \\ \vdots & \vdots & \ddots & \vdots \\ \rho_{z1} & \rho_{z2} & \cdots & 1 \end{bmatrix} \end{array} \tag{3.13}$$

where ρ_{ij} is the correlation between i^{th} and j^{th} random variable. From the correlation matrix and known standard deviations the variance-covariance matrix can be obtained as [45],

$$\boldsymbol{C_x} = \begin{bmatrix} \sigma_{x_1}^2 & \rho_{12}\sigma_{x_1}\sigma_{x_2} & \cdots & \rho_{1z}\sigma_{x_1}\sigma_{x_z} \\ \rho_{21}\sigma_{x_2}\sigma_{x_1} & \sigma_{x_2}^2 & \cdots & \rho_{2z}\sigma_{x_2}\sigma_{x_z} \\ \vdots & \vdots & \ddots & \vdots \\ \rho_{z1}\sigma_{x_z}\sigma_{x_1} & \rho_{z2}\sigma_{x_z}\sigma_{x_2} & \cdots & \sigma_{x_z}^2 \end{bmatrix} \tag{3.14}$$

where $\sigma_{x_1}, \sigma_{x_2} \cdots, \sigma_{x_z}$ are the standard deviations of the random variables $x_1, x_2 \cdots, x_z$ respectively.

For including the correlation in the input variables using point estimate method, following procedure is adopted [40] :

1. Carry out the Cholesky decomposition of $\boldsymbol{C_x}$ as

$$\boldsymbol{C_x} = \boldsymbol{L}\boldsymbol{L}^T \tag{3.15}$$

2. Compute the matrix $\boldsymbol{B}$ as

$$\boldsymbol{B} = \boldsymbol{L}^{-1} \tag{3.16}$$

3. Using the above matrix $\boldsymbol{B}$, the original vector $\boldsymbol{x}$ of correlated variables is transformed into a vector of uncorrelated variables $\boldsymbol{y}$ as

$$\boldsymbol{y} = \boldsymbol{B}\boldsymbol{x} \tag{3.17}$$

4. Transform the central moments of $\boldsymbol{x}$ to the new space as

$$\boldsymbol{\mu_y} = \boldsymbol{L}^{-1}\boldsymbol{\mu_x}, \tag{3.18}$$

$$\lambda_{yi,s} = \sum_{r=1}^{z} B_{ir}^{s} \lambda_{xr,s} \sigma_{xr}^{s} \tag{3.19}$$

$s = 3, 4$ for the transformed skewness and kurtosis respectively, B_{ir} represents the element located at i^{th} row and r^{th} column of the matrix $\boldsymbol{B}$, $\lambda_{xr,3}$ and $\lambda_{xr,4}$ are the skewness and kurtosis of x_r respectively and σ_{xr} is the standard deviation of x_r. Further, $\lambda_{y_i,3}$ and $\lambda_{y_i,4}$ are the skewness and kurtosis of i^{th} transformed correlated variable respectively, and $\hat{\boldsymbol{\mu}}_{\boldsymbol{y}}$ is vector of mean values of $\boldsymbol{y}$.

5. In the transformed space, compute the points $(y_{i,k})$ and corresponding weights $(w_{i,k})$ using the point estimate method as explained in Chapter 2.

6. Form the $(2m+1)$, $(4m+1)$ and $(6m+1)$ vectors (corresponding to 3PEM, 5PEM and 7PEM respectively) in the transformed space $\boldsymbol{y}$, following step 1 of Section 2.6 as,

$$\boldsymbol{Y_k} = \begin{bmatrix} y_{1,k} & \mu_{2y} & \cdots & \mu_{zy} \\ \mu_{1y} & y_{2,k} & \cdots & \mu_{zy} \\ \vdots & \vdots & \ddots & \vdots \\ \mu_{1y} & \mu_{2y} & \cdots & y_{z,k} \end{bmatrix} \tag{3.20}$$

where, $k = 1, .., m$, $m = 2, 4$ and 6 for 3PEM, 5PEM and 7PEM respectively.

7. Transform the vector $\boldsymbol{Y_k}$ back into the original space by using the transformation

$$\boldsymbol{X_k} = \boldsymbol{B}^{-1} \boldsymbol{Y_k}. \tag{3.21}$$

8. For the remaining $n - z$ uncorrelated variables the vector $\boldsymbol{X_k}$ is generated as given in eq. (2.47).

9. Follow steps 2, 3, 4, 5 and 6 of Section 2.6 of Chapter 2 for obtaining the moments of the variables of interest.

For including correlation in Monte Carlo simulation the following procedure is adopted [43] :

Let us suppose that we have z correlated loads with a given correlation matrix. For each load, a set of values has been generated randomly according to its mean and standard deviation. The correlation between these independently generated random variables is close to zero. Let $\boldsymbol{x}$ be the

vector of uncorrelated variables stochastically generated, $\boldsymbol{x} = (x_1, x_2, .., x_z)^T$ with the vector of mean values $\boldsymbol{\mu_x} = (\mu_1, \mu_2, .., \mu_z)^T$, Now the correlation can be accommodated in the stochastically generated series by first obtaining the Cholesky decomposition of variance-covariance matrix (C_x) given in eq. (3.14).

By Cholesky decomposition of $\boldsymbol{C_x}$, $\boldsymbol{C_x} = \boldsymbol{L}\boldsymbol{L}^T$, where $\boldsymbol{L}$ is the lower triangular matrix. The new vector $\boldsymbol{y} = (y_1, y_2, ..y_z)^T$ of correlated variables can be obtained by using the operation $\boldsymbol{y} = \boldsymbol{L}\boldsymbol{x}$.

3.4 Results and discussion

For calculating the moments of the variables of interest in a power system, the method as described in Section 2.6 of Chapter 2 has been used for carrying out the PLF by using 3PEM, 5PEM and 7PEM methods. The results obtained by these methods have also been compared with those obtained by the Monte Carlo simulation (MCS) studies. The method has been applied to IEEE-118 and IEEE-300 bus systems [80]. For modelling the variations in loads, three different load PDFs have been considered in this work. These are:

1. A normal distribution with the mean values equal to the load data given in [80] and a standard deviation equal to 10% of the corresponding mean value of the load.

2. A non-normal distribution taken from the IEEE Reliability test system hourly load data [85].

3. A non-normal distribution taken from the PJM load data [86].

For the cases (ii) and (iii), the load values given in [85] and [86] have been assumed as peak loads. Further, the load values in IEEE-118 bus system have been increased to 1.5 times of the base loading condition and for IEEE-300 bus system these have been increased to 1.05 times the base loading condition so that in some cases reactive power violations may occur at few generator buses.

3.4.1 Loads with normal distribution only

As already observed in the previous Chapter, the reactive power at the generator bus no. 92 of IEEE-118 bus system is multimodal in nature (Fig. 2.11) and CF series is unable to provide an accurate estimate of this multi-modal PDF.

For a better approximation of this multi-modal distribution, the spline based reconstruction technique (described in Section 3.2) has been used and the approximated distribution is also shown in Fig. 3.3.

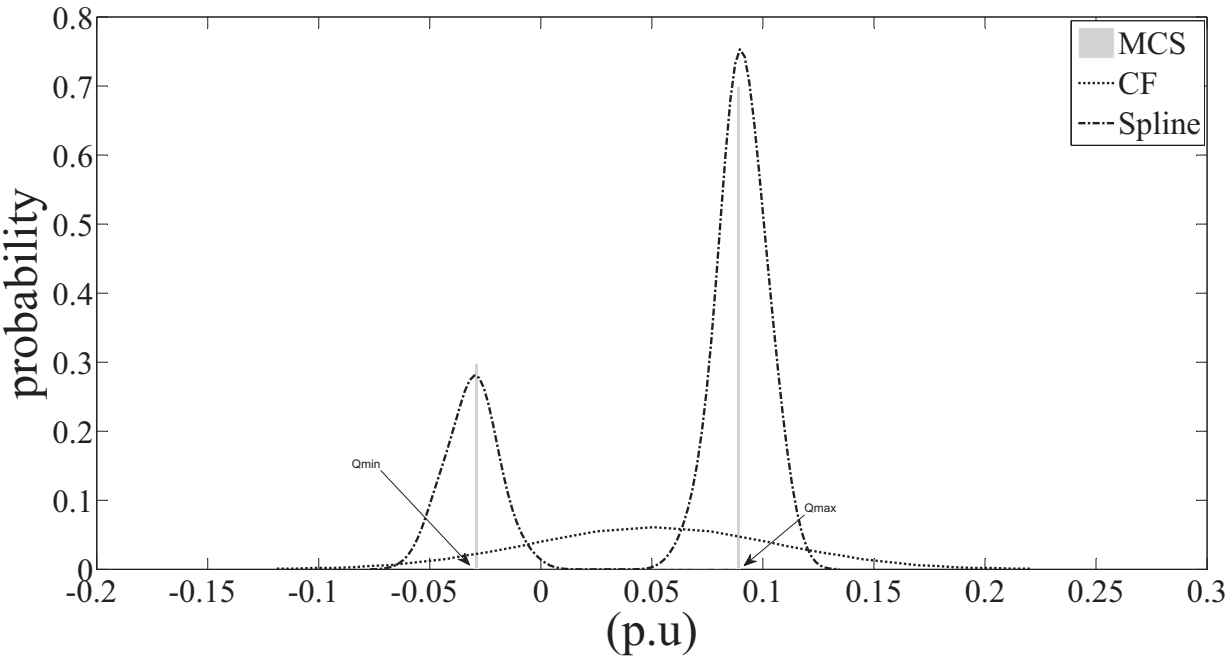

Figure 3.3: PDF of reactive power injected at generator bus no. 92

From this figure, it is observed that the spline based approximate distribution also has two peaks similar to the distribution obtained through MCS. Therefore, the spline based technique gives a much better approximation to the multimodal PDF than the CF series based method which provides a unimodal approximation only.

To investigate the effectiveness of the spline based technique for approximating a unimodal distribution, the PDF of voltage magnitude of bus 92 has also been approximated by using the spline based technique. The resulting distribution, along with the distributions obtained by CF series (using 7PEM) and MCS study, is shown in Fig. 3.4.

From this figure it is observed that these three distributions are quite close to each other with the spline based PDF being marginally better than that obtained by CF series. Therefore, the spline based method is found to be equally efficient in approximating a unimodal distribution also. It can also be observed that the probability of violation of the upper limit of the reactive power generation (Q_{max}) is higher than the probability of violation of the lower limit of reactive power generation (Q_{min}). This implies that the probability of the voltage being lower than the specified limit should be high. This is clearly established by the plot shown in Fig. 3.4.

For IEEE-300 bus system, as a representative case, the PDF of voltage magnitude at generator bus no. 267 has been estimated using MCS, CF and spline based reconstruction method for normally

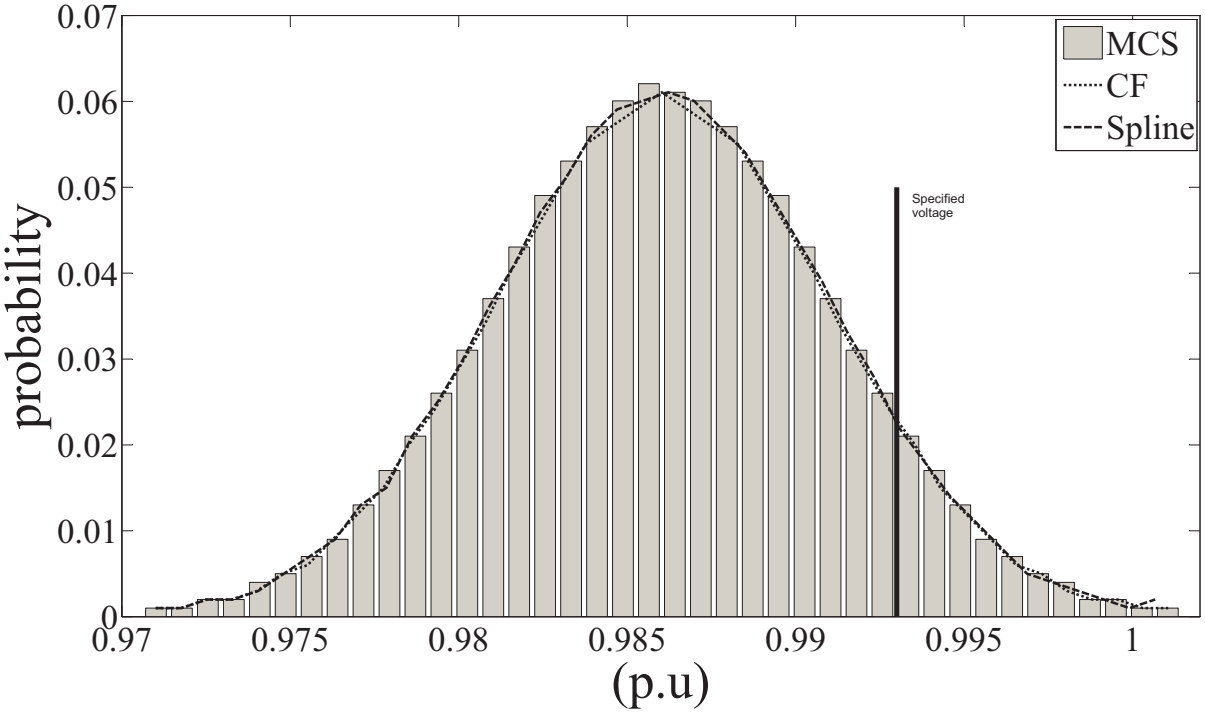

Figure 3.4: PDF of voltage magnitude at bus no. 92

distributed loads, and is shown in Fig. 3.5. The specified voltage at bus no. 267 is 0.9545 p.u and the lower and upper generator reactive power limits are -0.02 p.u and 0.02 p.u respectively.

The PDFs of the reactive power at generator bus no. 267 (Q_{267}) obtained by MCS, spline based technique and CF series are shown in Fig. 3.6. From this figure it is observed that the PDF of Q_{267} is a multimodal one and the spline based technique is able to approximate it reasonably well while CF series is unable to do so.

In this case, the lower reactive power limit is violated more as compared to the upper limit and therefore, the probability that the voltage magnitude is greater than the specified value of 0.9545 p.u. should be more. This is also reflected in the PDF of the bus voltage magnitude as shown in Fig. 3.5. The corresponding statistical parametres of bus voltage magnitude obtained from 3PEM, 5PEM, 7PEM and MCS are given in Table 3.1.

From Table 3.1 it is observed that in this case also, among the three different point estimate methods, 7PEM is most accurate in approximating the various statistical parameters of the random variable, the voltage magnitude of bus no. 267. Further, from Fig. 3.5 it is observed that the spline based technique and CF series with 7PEM are equally effective in approximating the PDF of voltage magnitude properly.

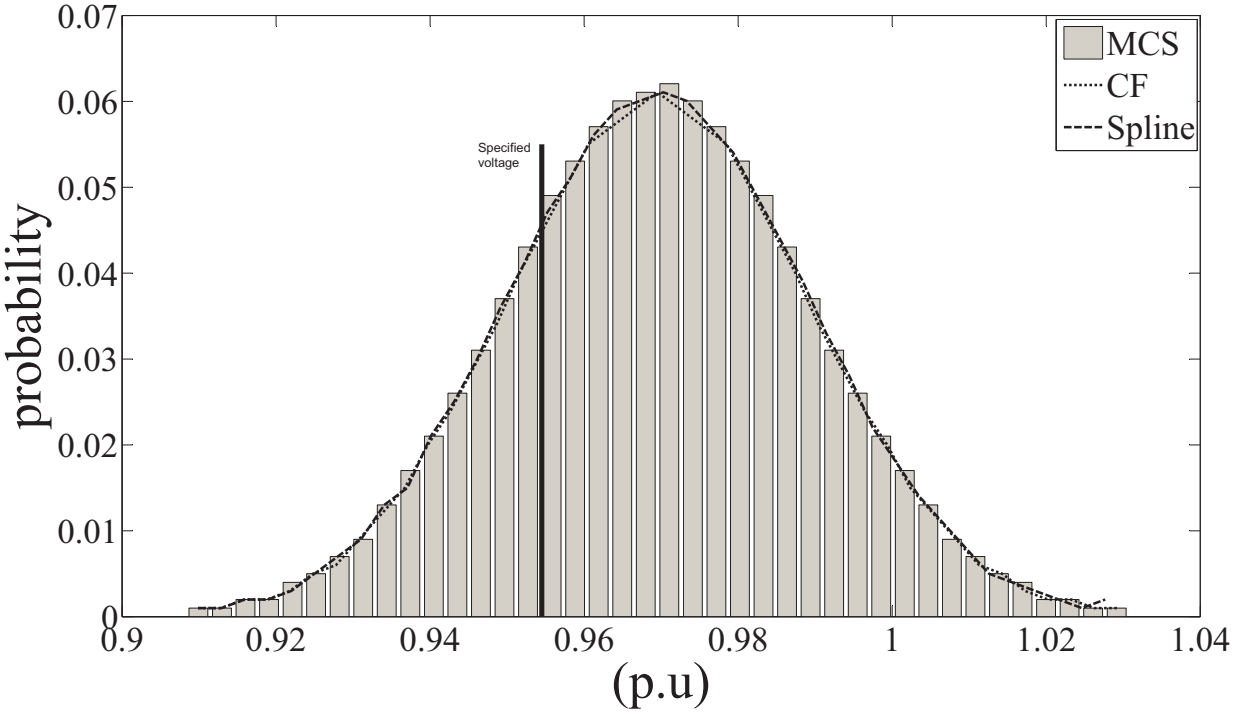

Figure 3.5: PDF of voltage magnitude at bus no. 267

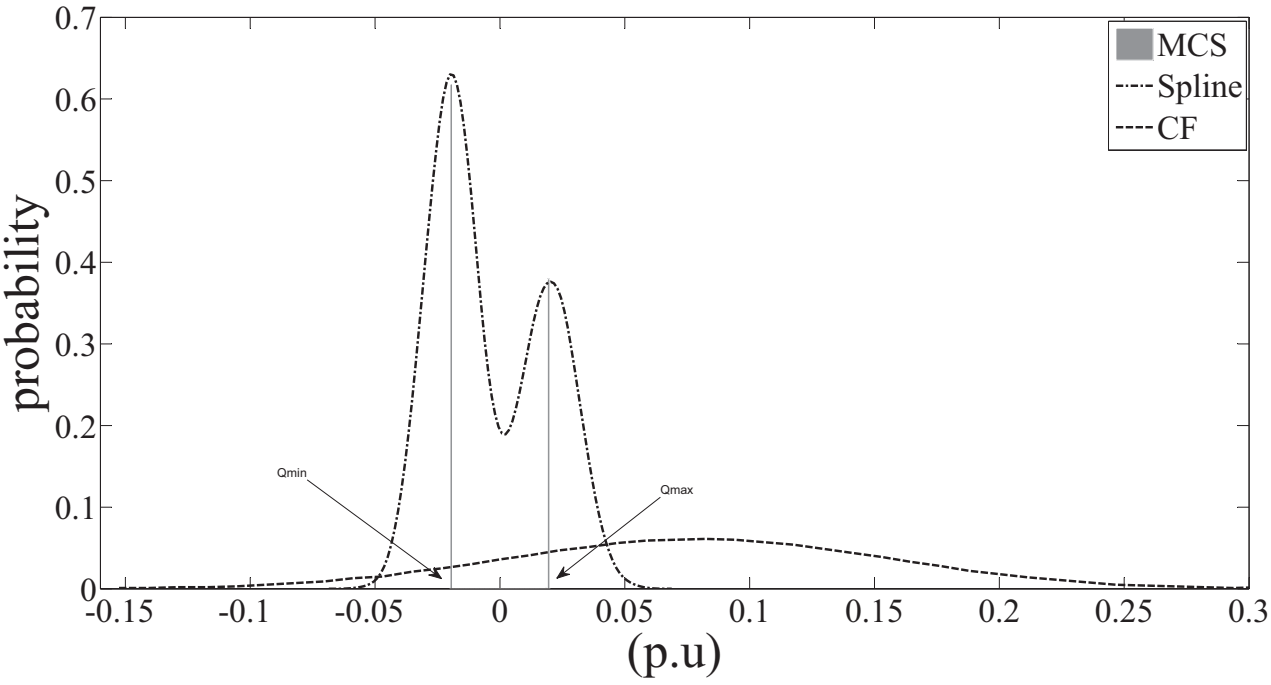

Figure 3.6: PDF of reactive power at generator bus no. 267

Table 3.1: Statistical parameters of the voltage magnitude at bus no. 267

Schemes	Mean	S. dev.	Skewness	Kurtosis	Confidence level	
	μ	σ	sk	ku	10%	90%
3PEM	0.9672	0.0172	0.42148	1.6512	0.9421	0.9882
5PEM	0.9685	0.0181	0.42157	1.6527	0.9427	0.9891
7PEM	0.9689	0.0185	0.43218	1.6664	0.9431	0.9895
MCS	0.9693	0.0188	0.43230	1.6691	0.9435	0.9897

Next, the proposed method has been tested for different values of standard deviation or coefficient of variations (CV), with normally distributed loads. A low value of CV indicates that the nodal data is reasonably accurately known (e.g. for short term planning) while a high value of CV represents the long term planning exercise with a greater amount of uncertainity. The effect of variation of CV and system size on the maximum amount of error in the average values of the voltage magnitudes has been investigated on IEEE-118 and IEEE-300 bus system for the following three methods: i) 5PEM with CF series, ii) 7PEM with CF series and iii) 7PEM with spline based reconstruction technique. For quantifying the accuracy of these three methods vis-a-vis the MCS study, the absolute maximum error in the estimated value of probability (Em) has been calculated by the following procedure.

Initially, each of the four PDFs obtained by 5PEM with CF series, 7PEM with CF series, 7PEM with spline based reconstruction technique and MCS study is discretized at points x_i with corresponding value of probability (p_i), where, $i = 1, .., N$, N being the total number of points used for discretization. Let the values of (p_i) obtained from the curves of MCS, 5PEM with CF series, 7PEM with CF series and 7PEM with spline based reconstruction technique be denoted as p_i^{MCS}, p_i^{5PEMCF}, p_i^{7PEMCF} and p_i^{7PEMSP} respectively. Lastly, the absolute maximum errors in the estimated values of probability (p_i) for 5PEM with CF series, 7PEM with CF series and 7PEM with spline based method are calculated as:

$$Em_{5PEMCF} = max \left| p_i^{MCS} - p_i^{5PEMCF} \right| ; \forall i = 1, 2, ...N$$

$$Em_{7PEMCF} = max \left| p_i^{MCS} - p_i^{7PEMCF} \right| ; \forall i = 1, 2, ...N$$

$$Em_{7PEMSP} = max \left| p_i^{MCS} - p_i^{7PEMSP} \right| ; \forall i = 1, 2, ...N$$

In this study the value of N has been taken as 1000.

The absolute maximum errors for the voltage magnitudes at some selected buses for IEEE-118 and IEEE-300 bus system are tabulated in Tables 3.2 and 3.3 respectively.

Table 3.2: Absolute maximum error ($\times 10^{-3}$) calculated for the IEEE-118 bus system

Bus no.	**CV 5%**			**CV 10%**			**CV 15%**		
	Em_{5PEMCF}	Em_{7PEMCF}	Em_{7PEMSP}	Em_{5PEMCF}	Em_{7PEMCF}	Em_{7PEMSP}	Em_{5PEMCF}	Em_{7PEMCF}	Em_{7PEMSP}
2	1.9784	1.9752	1.9749	1.9985	1.9973	1.9971	2.0184	2.0180	2.0178
7	1.9543	1.9512	1.9507	2.0010	2.0003	2.0001	2.1658	2.1642	2.1635
9	1.9641	1.9634	1.9629	1.9921	1.9915	1.9909	2.1100	2.1098	2.1095
113	1.9872	1.9865	1.9863	2.0012	2.0007	2.0003	2.1298	2.1287	2.1282
116	1.9771	1.9764	1.9759	1.9981	1.9979	1.9976	2.0931	2.0925	2.0922

Table 3.3: Absolute maximum error ($\times 10^{-3}$) calculated for the IEEE-300 bus system

Bus no.	**CV 5%**			**CV 10%**			**CV 15%**		
	Em_{5PEMCF}	Em_{7PEMCF}	Em_{7PEMSP}	Em_{5PEMCF}	Em_{7PEMCF}	Em_{7PEMSP}	Em_{5PEMCF}	Em_{7PEMCF}	Em_{7PEMSP}
9	2.5289	2.5274	2.5269	3.1849	3.1835	3.1832	4.0011	4.0005	4.0002
11	2.3892	2.3858	2.3849	3.4295	3.4291	3.4287	4.0491	4.0485	4.0483
70	2.5261	2.5248	2.5242	3.3125	3.3121	3.3118	4.3120	4.3105	4.3102
81	2.7298	2.7156	2.7148	3.6124	3.6101	3.6100	4.4013	4.4005	4.4003
219	2.2013	2.2002	2.2000	3.6421	3.6415	3.6412	4.7321	4.7305	4.7300

From the values of maximum errors in Table 3.2 and Table 3.3 for IEEE-118 and IEEE-300 bus system at different nodes, it is seen that the maximum error increases with the increase in the coefficient of variation or standard deviation. Moreover, this error also increases with the increase

in system size as observed from Table 3.2 and Table 3.3, but the increase in error with the increase in system size is marginal. The maximum error in all the cases is minimum for the 7PEM with spline based reconstruction method. Therefore, for all subsequent results shown in this chapter, the moments have been calculated by 7PEM.

3.4.2 With IEEE non-normal load distribution

In this case loads having non-normal distribution with a PDF as shown in Fig. 3.7 have been used. The PDF shown in Fig. 3.7 represents the PDF of IEEE Reliability test system hourly load data [85].

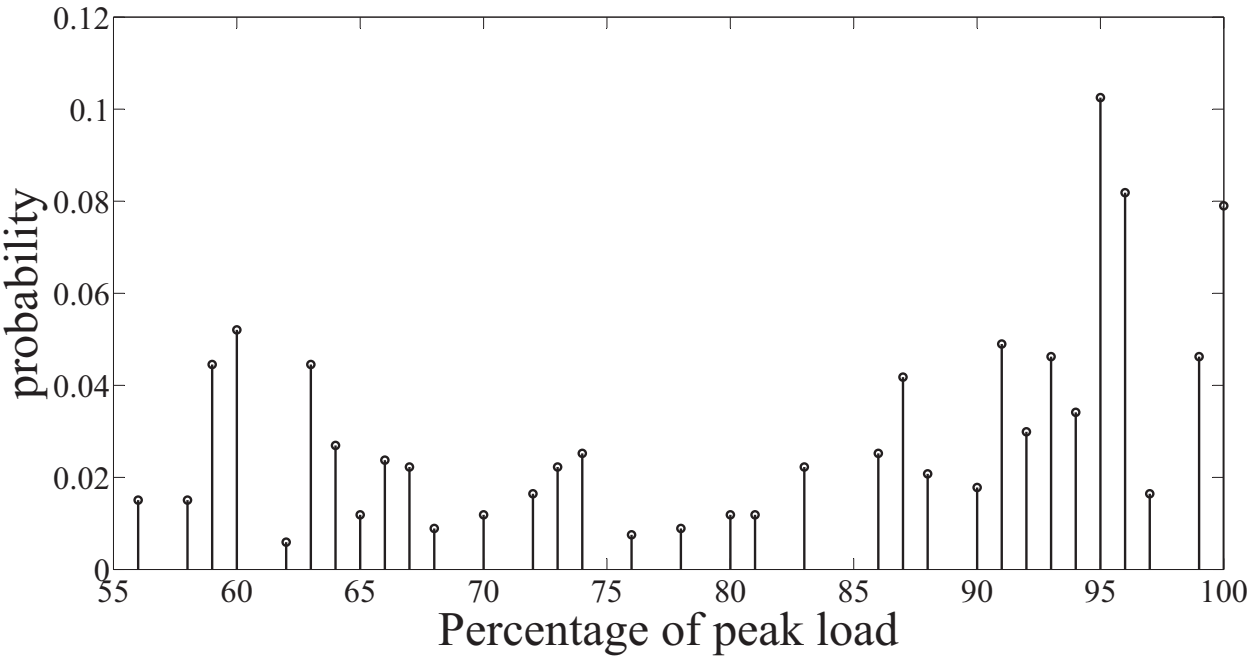

Figure 3.7: IEEE load probability distribution function

To investigate the effectiveness of the spline based technique for this type of loads, the PLF, using 7PEM, was carried out initially for IEEE-118 bus system assuming the shapes of the load PDFs at all the buses to be the same as shown in the Fig. 3.7. The resultant multi-modal PDFs of voltage magnitude at bus no. 42, active power flow in the line between the buses 6-12, reactive power flow in the line between the buses 27-31 (as representative cases) estimated using MCS, CF series and spline based method are shown in Figs. 3.8, 3.9 and 3.10 respectively.

It can be observed that in this case also, the spline based method estimates the PDF quite nicely while CF series is unable to do so.

The results for the PDF of voltage magnitude at the load bus no. 61 for IEEE-300 bus system

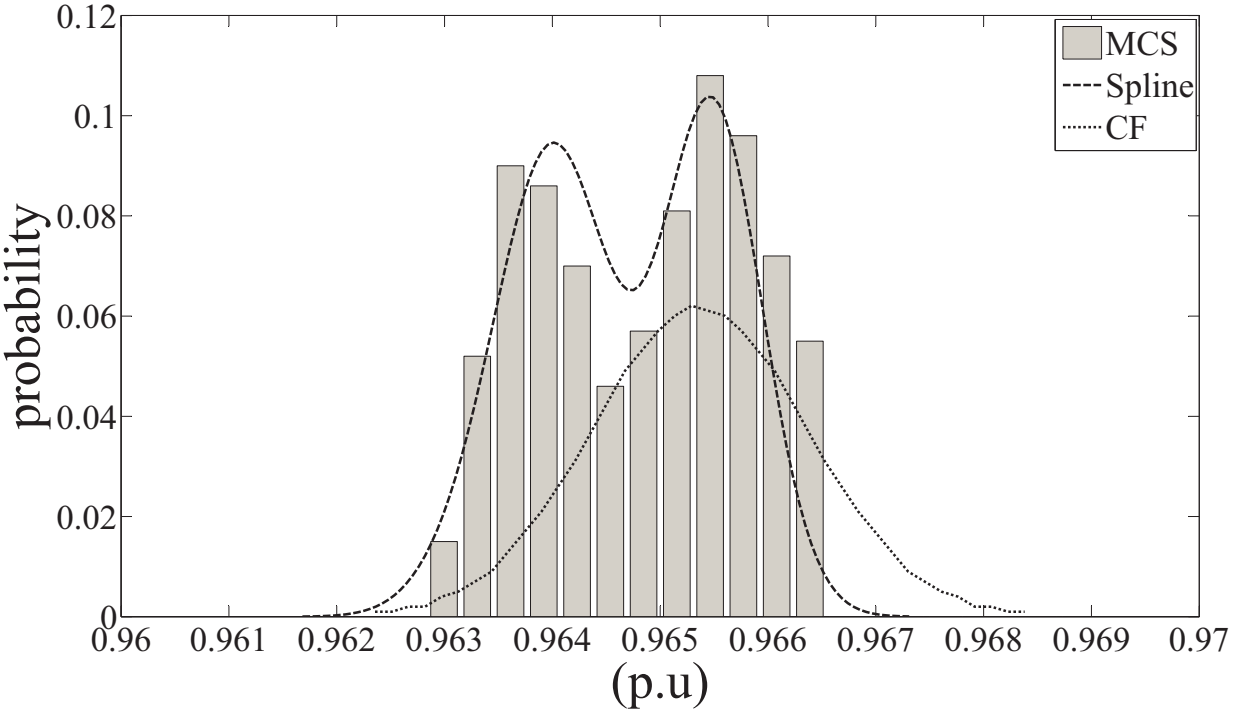

Figure 3.8: PDF of voltage magnitude at bus no. 42

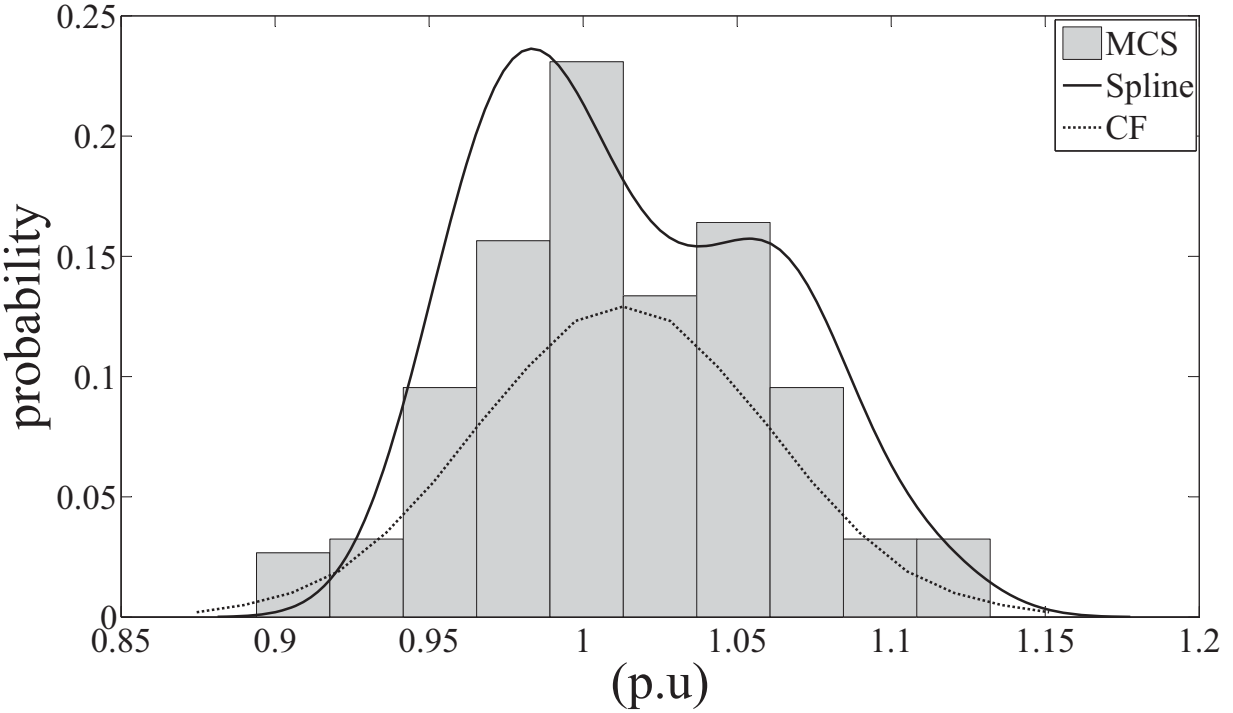

Figure 3.9: PDF of active power flow in the line between the buses 6-12

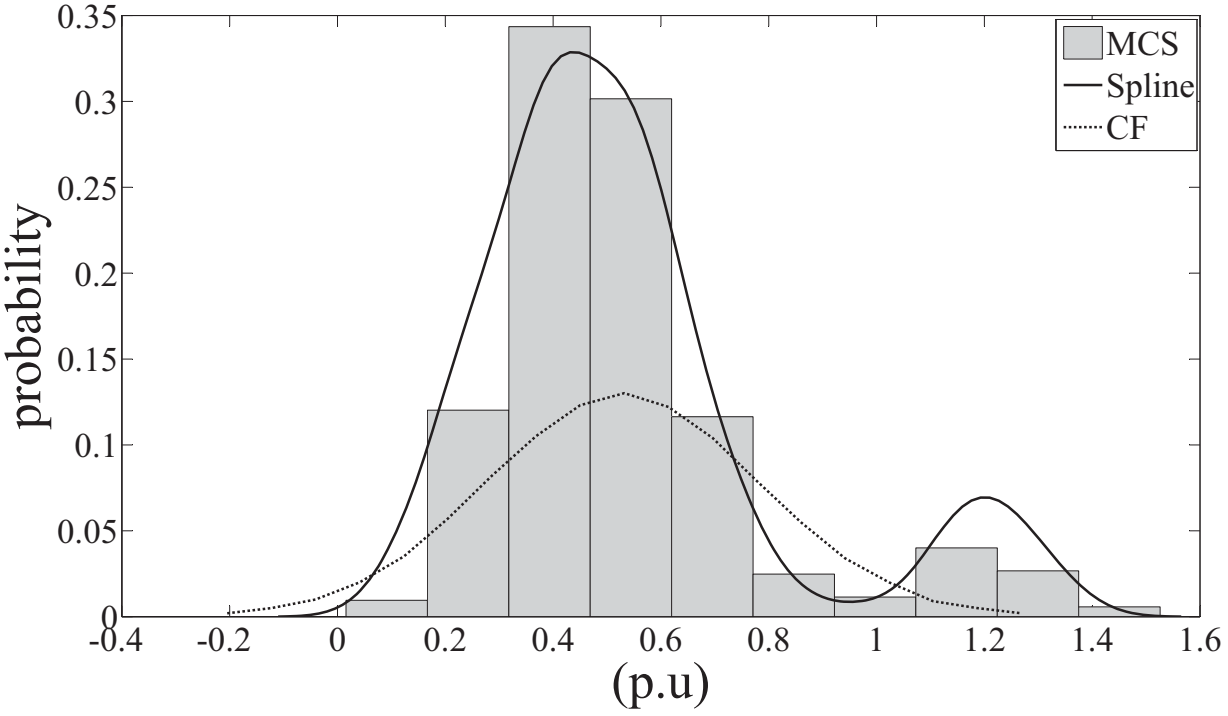

Figure 3.10: PDF of reactive power flow in the line between the buses 27-31

for non-normal load distribution (as in Fig. 3.7) are shown in Fig. 3.11. These results also show that spline based reconstruction technique is successful in estimating the multimodal PDF of voltage magnitude from its moments while the CF series fails to do so. Similar results are obtained for the active power flow in the line between the buses 12-93 and reactive power flow in the line between the buses 12-88 for IEEE-300 bus system (shown in the Figs. 3.12 and 3.13 respectively).

3.4.3 With mixed and correlated loads

In this case, the mixed loads considered are (i) normally distributed loads, (ii) loads having non-normal IEEE distribution as shown in Fig. 3.7, and (iii) loads having non-normal PJM distribution [86] (as shown in Fig. 3.14). Further, a correlation among the loads of 4 selected buses having same type of loads has been considered for both 118 and 300 bus systems. The corresponding correlation matrix is given in eq. (3.22).

$$\boldsymbol{Cr_{load}} = \begin{bmatrix} 1.0000 & -0.4529 & 0.9058 & 0.0234 \\ -0.4529 & 1.0000 & -0.4978 & 0.1036 \\ 0.9058 & -0.4978 & 1.0000 & -0.0068 \\ 0.0234 & 0.1036 & -0.0068 & 1.0000 \end{bmatrix} \tag{3.22}$$

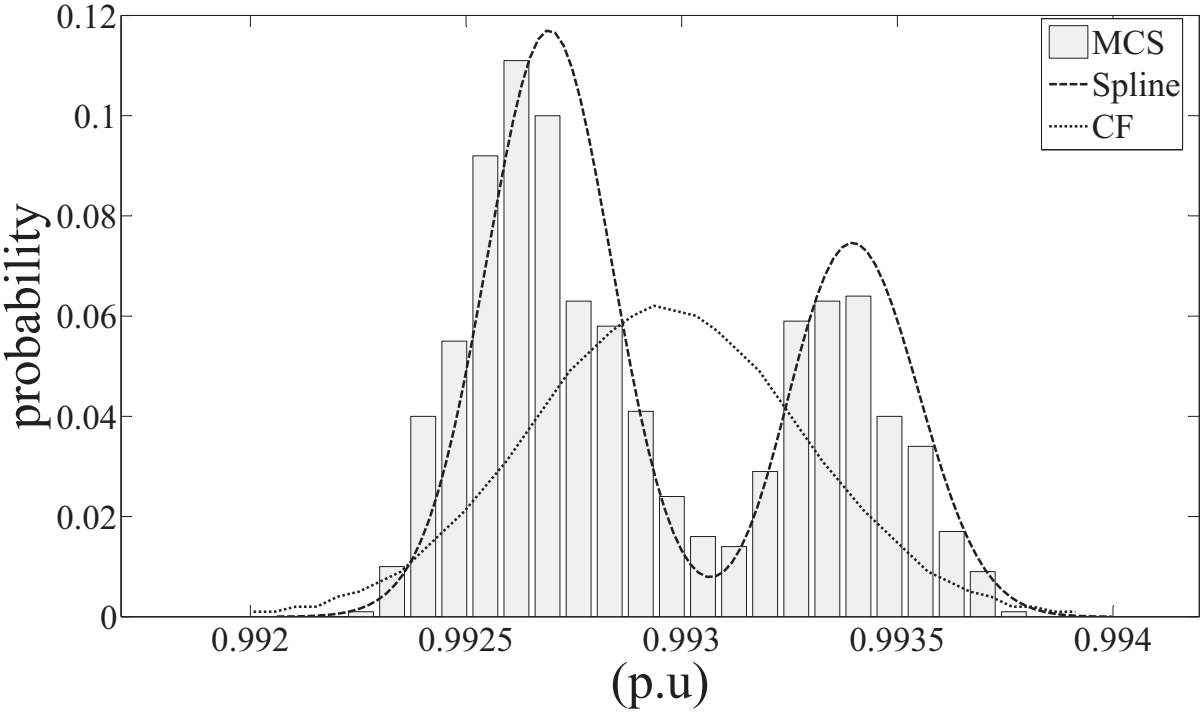

Figure 3.11: PDF of voltage magnitude at bus no. 61

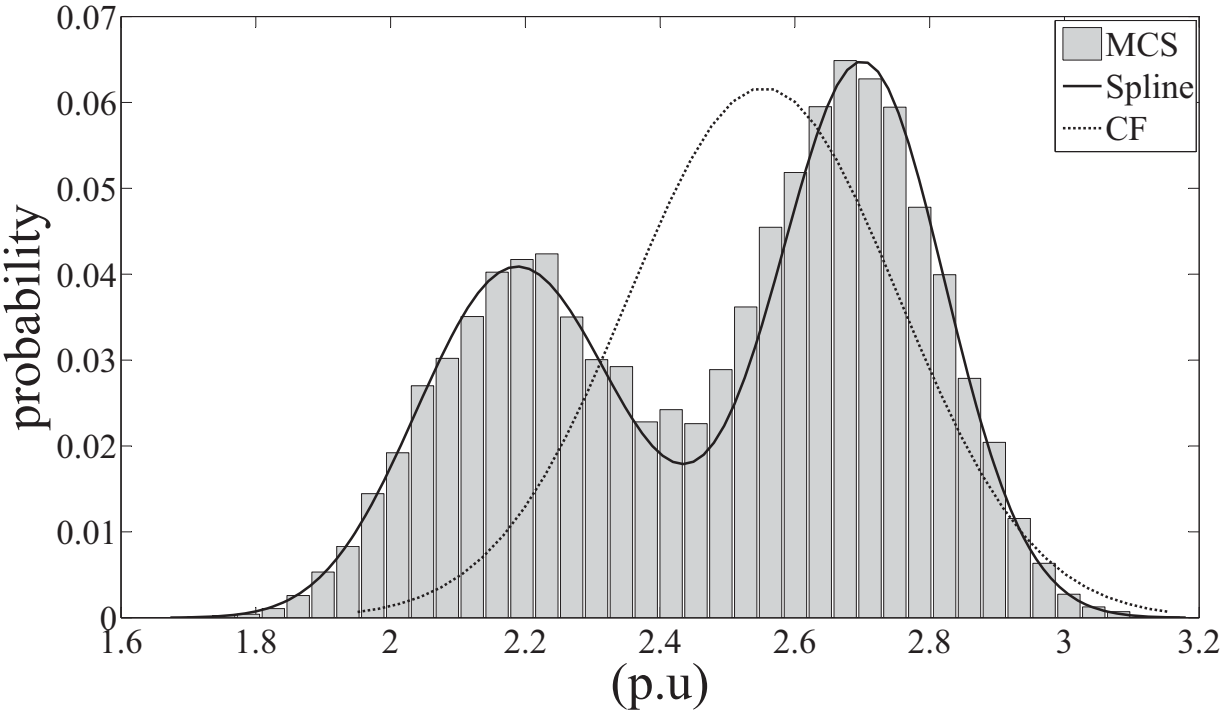

Figure 3.12: PDF of active power flow in the line between the buses 12-93

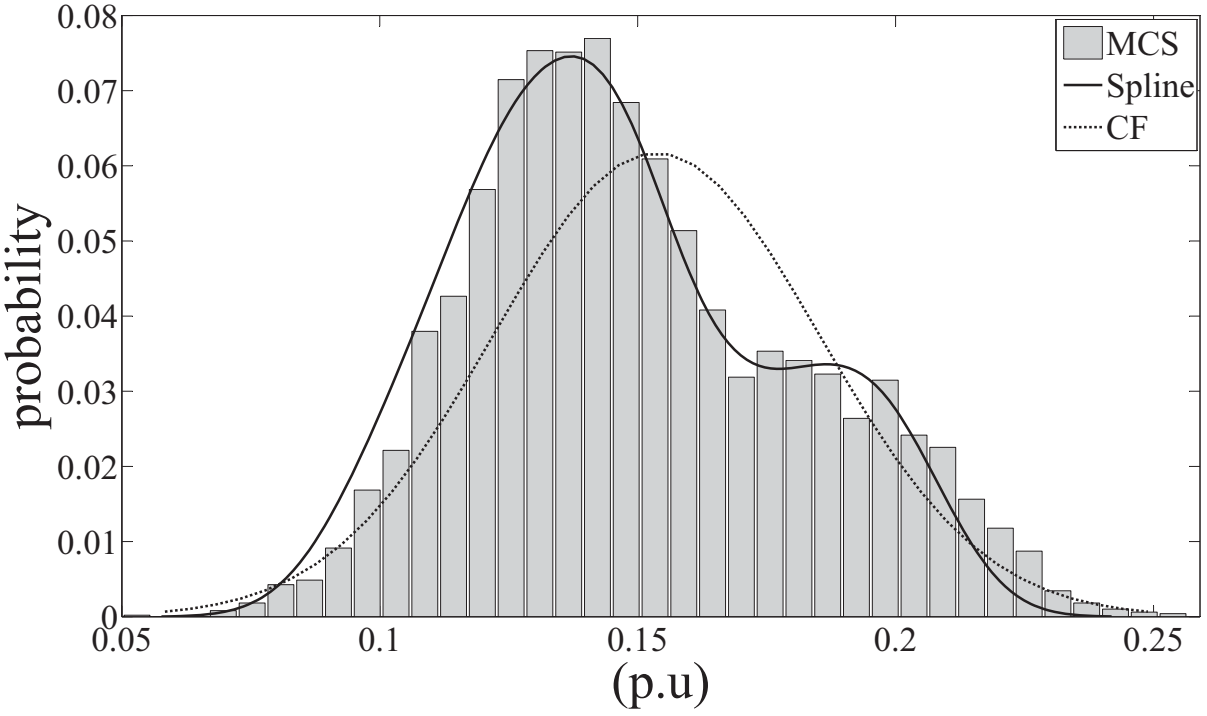

Figure 3.13: PDF of reactive power flow in the line between the buses 12-88

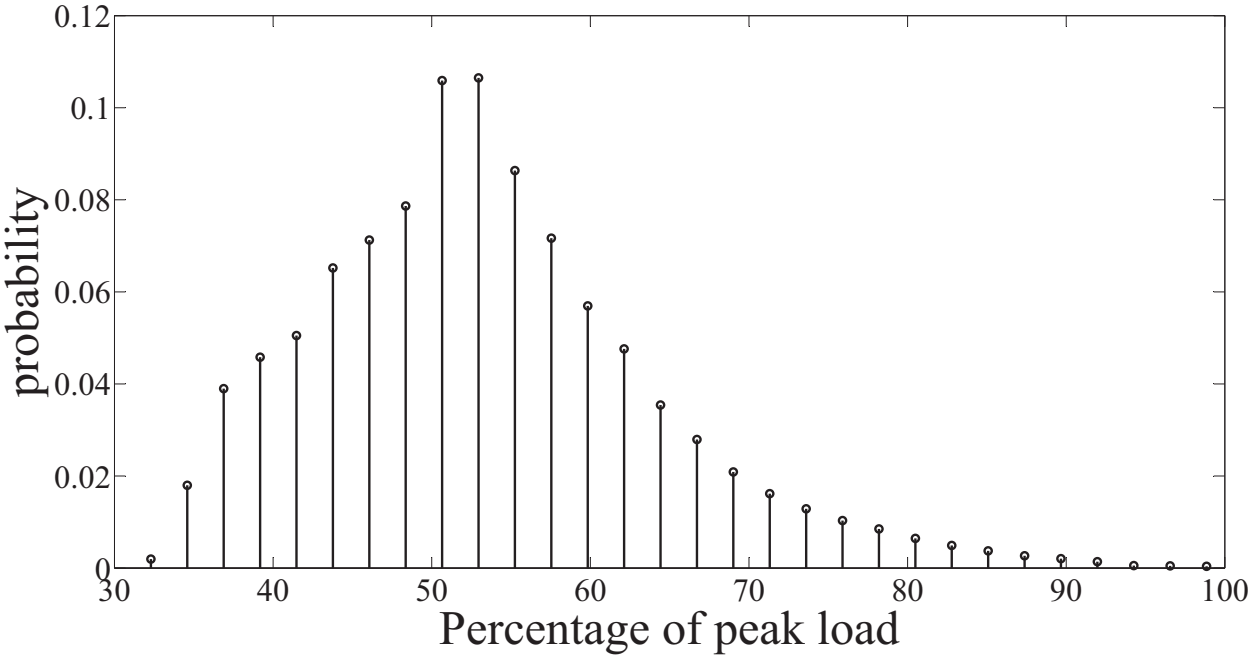

Figure 3.14: PJM load probability distribution function

For the 118 bus system, the loads at bus nos. 2 to 38 are considered to have normal distribution with the loads at bus numbers {14,15,17,18} correlated with each other. Loads at the bus nos. 39

to 78 are considered to have non-normal IEEE distribution with loads at bus numbers {48,49,51,52} correlated with each other and loads at the bus nos. 79 to 118 are assumed to have PJM load distribution in which loads at bus numbers {81,82,83,84} are considered to be correlated with each other. With this load distribution, the PLF of the system has been carried out by 7PEM using the procedure outlined in Section 3.3 and MCS as well. As a representative case, the PDF of voltage magnitude at generator bus no. 20 for 118 bus system is shown in Fig. 3.15 and the corresponding PDF of generator reactive power is shown in Fig. 3.16. The specified voltage magnitude at bus no. 20 is 0.953 p.u and the lower and upper generator reactive power limits are -0.08 p.u and 0.24 p.u respectively. In this case, the probability of violation of upper reactive power limit is more as compared to the violation of lower limit and therefore, the probability that the voltage magnitude is less than the specified value of 0.953 p.u. should be more. This is also clearly observed in the PDF of the bus voltage magnitude shown in Fig. 3.15. In this case, the multimodal PDF obtained for both voltage magnitude and generator reactive power by spline based reconstruction method is in close agreement with the corresponding PDFs obtained by MCS study.

Similar observations about the efficacy of spline based PDF estimation method can be made from the PDF of active power flow in the line between the buses 46-47 and PDF of reactive power flow in the line between the buses 31-18, as shown in Figs. 3.17 and 3.18 respectively.

For the IEEE-300 bus system, the loads at bus nos. 2 to 100 are considered to have normal distribution with loads at bus numbers {14,15,17,18} correlated with each other. Loads at bus nos. 101 to 200 are considered to have non-normal IEEE distribution with loads at bus numbers {106,107,108,109} correlated with each other and loads at bus nos. 201 to 300 are assumed to have PJM load distribution in which the loads at bus numbers {239,240,241,242} are considered to be correlated with each other. As a representative case, the PDF of voltage magnitude at bus no. 16 and the corresponding PDF of reactive power using MCS, Cornish-Fisher and spline based reconstruction method (using 7PEM), is shown in Figs. 3.19 and 3.20 respectively. The specified voltage at bus no. 16 is 0.952 p.u and the lower and upper generator reactive power limits are -0.1 p.u and 0.3 p.u respectively. In this case, the probability of upper reactive power limit violation is more as compared to the lower reactive power limit violation and therefore, the probability that the voltage magnitude is less than the specified value of 0.952 p.u. should be more. This is also evident in the PDF of the bus voltage magnitude as shown in Fig. 3.19. In this case also, the PDF of voltage magnitude and generator reactive power obtained by using spline based reconstruction method is in close agreement with PDF obtained from MCS study.

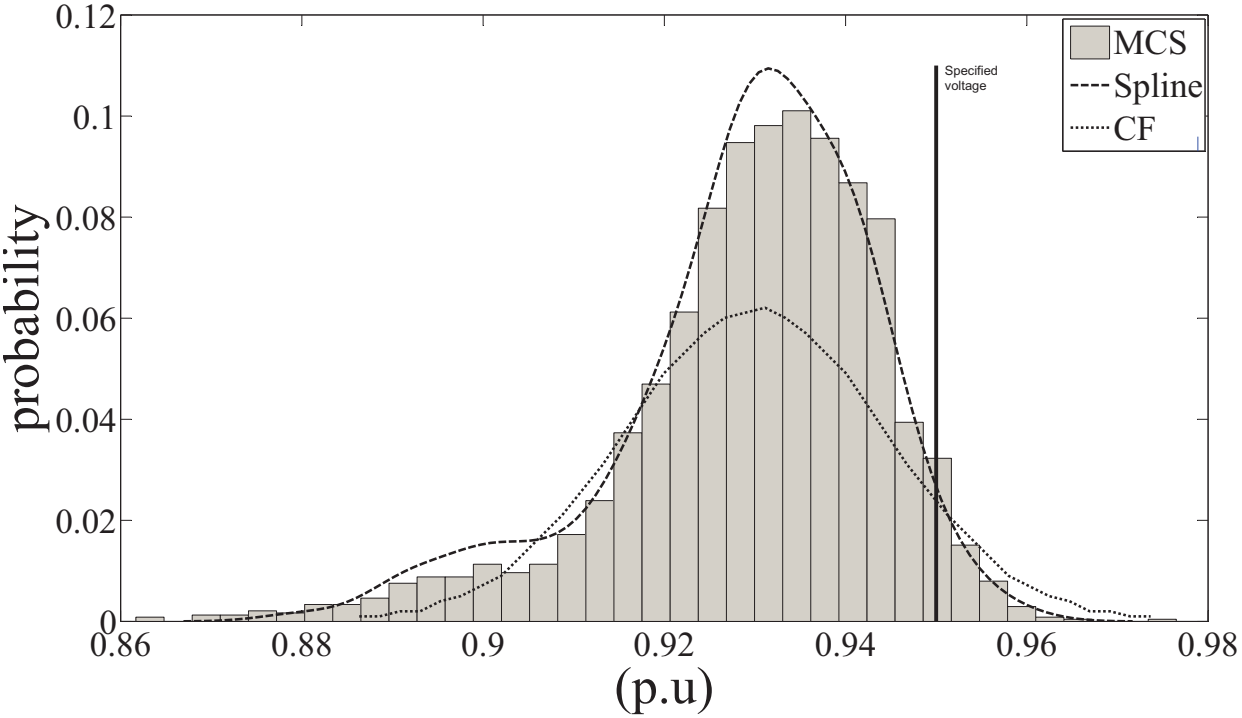

Figure 3.15: PDF of voltage magnitude at bus no. 20

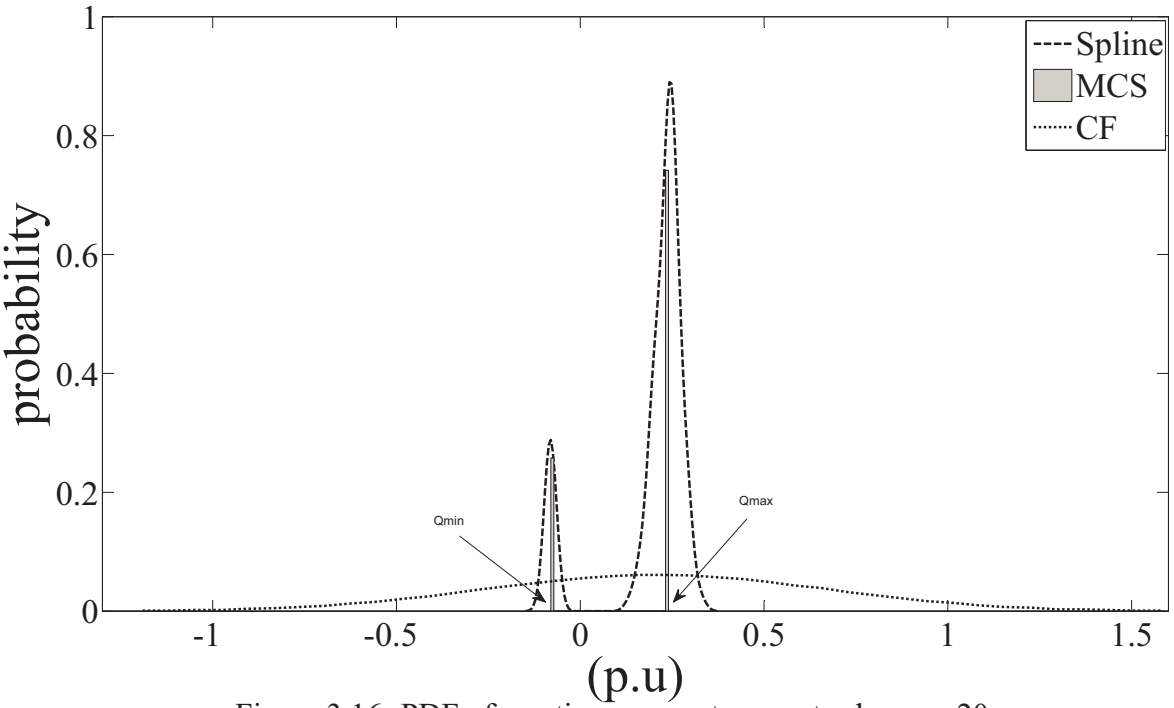

Figure 3.16: PDF of reactive power at generator bus no. 20

3.5 Consideration of slack bus power limit

In all the above studies, following the standard procedure of load flow, the real power outputs of all the generators except the slack bus have been kept fixed. As a result, the slack bus absorbs (generates)

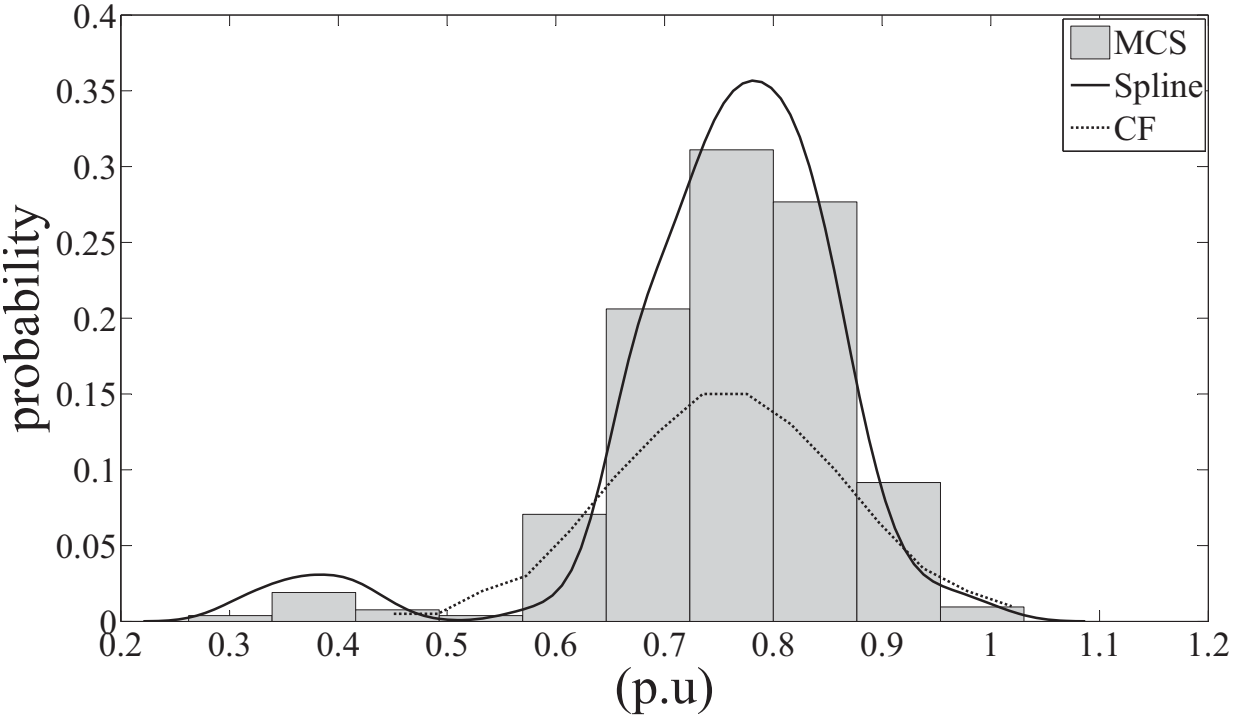

Figure 3.17: PDF of active power flow in the line between the buses 46-47

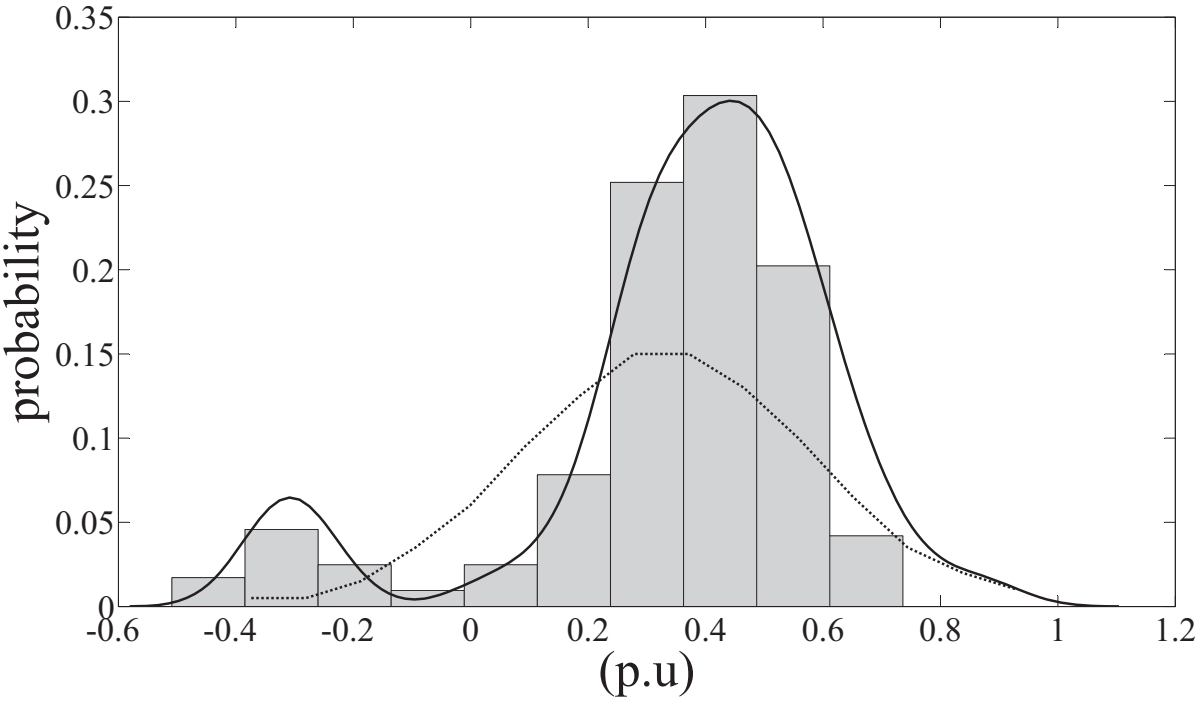

Figure 3.18: PDF of reactive power flow in the line between the buses 31-18

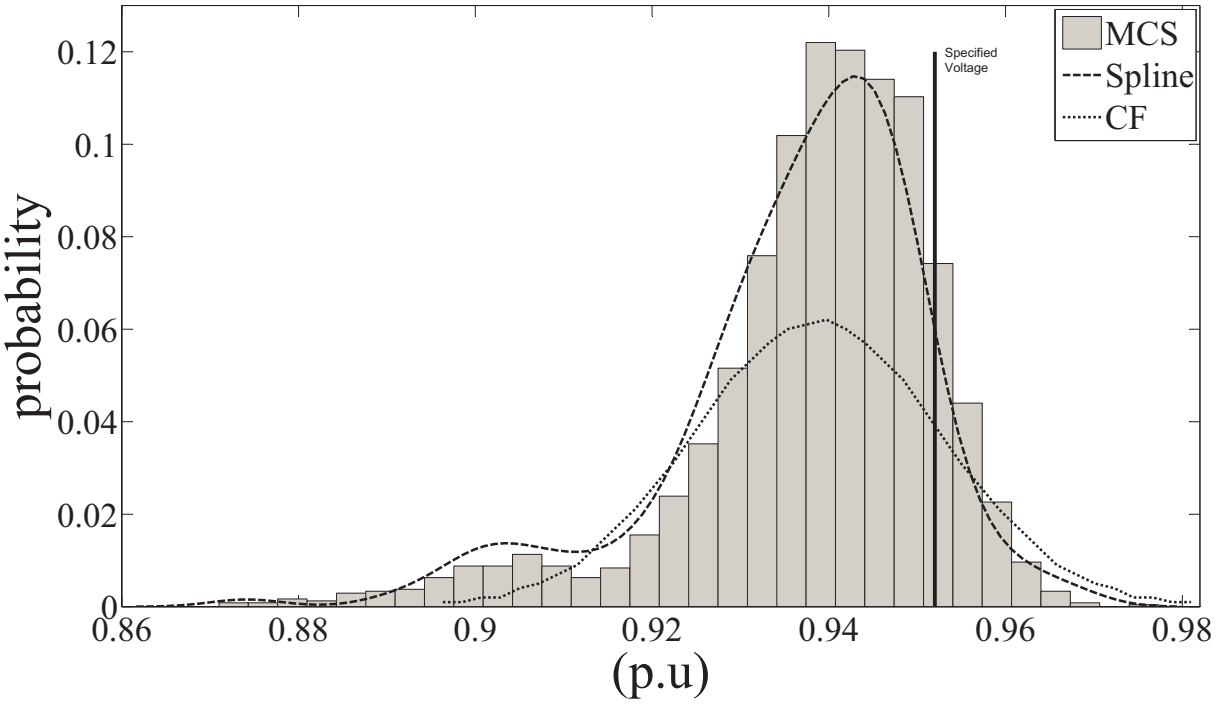

Figure 3.19: PDF of voltage magnitude at bus no. 16

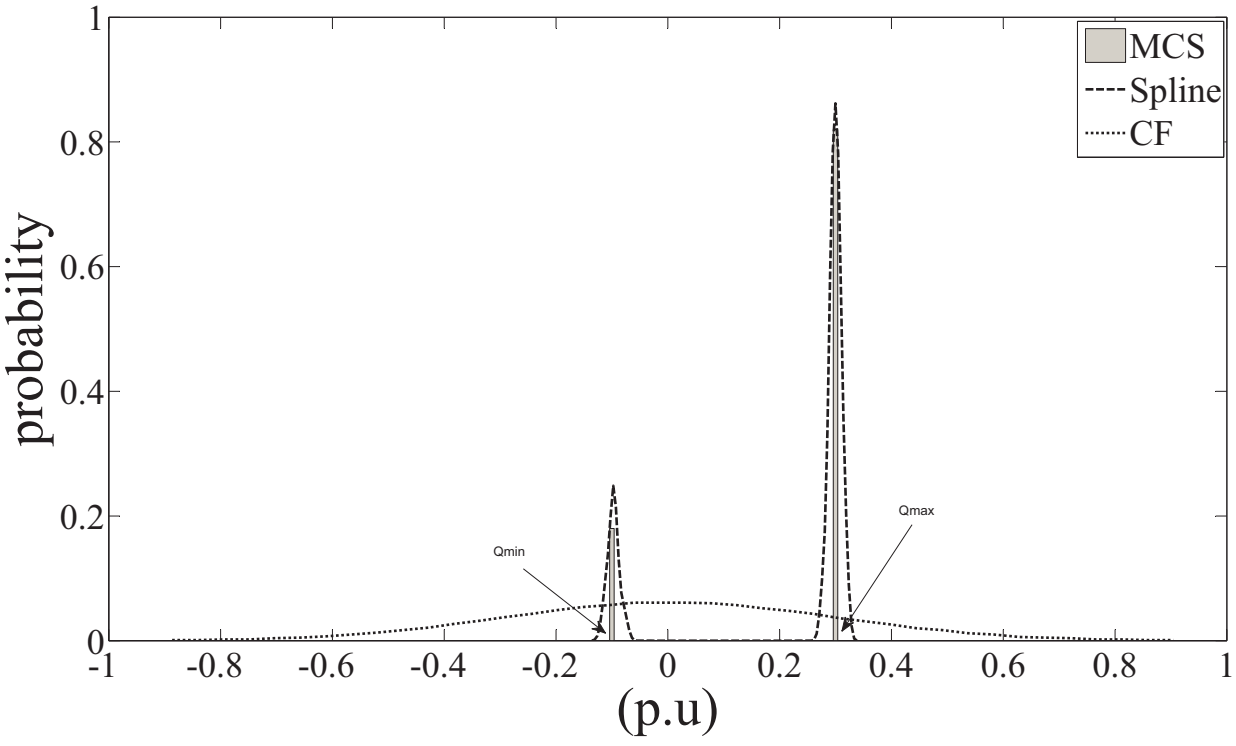

Figure 3.20: PDF of reactive power at generator bus no. 16

all uncertainities in the total load of the system and thus, it has the widest possible variations of real power among all the generators. If the rating of the slack bus generator is adequately high to cover this wide variation (which has so far been assumed in this study), then the solution obtained by the PLF is feasible. On the other hand, if the rating of the slack bus is not enough to cover the entire variation, then sometimes the slack generator would hit the maximum real power limit. In that case, following the procedure of [87, 88], the slack bus real power is fixed at the specified limit and the bus active power generation is relaxed for another generator which then is treated as the new slack bus. For a generator bus to act as the new slack bus, it must have the highest reserve margin (from current generation or consumption level). By swapping the slack bus with the other generator bus, the number of equations and unknowns remain the same and the load flow is run again to obtain the new results and if the generated power required from the new slack bus is more than its limit, then another generator bus is used as the new slack bus and the process continues untill the powers generated by all the generators are within their corresponding limits.

In the present case, with mixed and correlated loads as explained in the previous section, the active power limit for the slack bus (bus no. 1) in 118 bus system is 8.052 p.u. [89]. It can be seen from Fig. 3.21 (a) that the required slack bus generation crosses the generation limit and hence the procedure described for limiting the slack bus generation is adopted and bus no. 27 (having highest reserve margin) is selected as the new slack bus. The resulting PDF at bus no. 1 after imposing the active power limit at bus no. 1 is also shown in Fig. 3.21 (b). From Fig. 3.21 (b), it is clear that the maximum active power produced by slack bus is limited to 8.052 p.u. and remaining burden is shared by bus no. 27.

As a representative case, the statistical parameters of the voltage magnitude at bus number 16 in 118 bus system (with and without slack bus constraints) are given in Table 3.4. From this table it is observed that the difference in the moments estimated using 7PEM and MCS is quite less. Thus, the 7PEM method is capable of satisfactorily determining the statistical parameters with mixed and correlated loads for the 118 bus system with and without considering generation limits.

For IEEE-300 bus system the active power limit corresponding to the slack bus (bus no. 1) is 20.73 p.u. [89]. It can be seen from Fig. 3.22 (a) that the required slack bus generation crosses the generation limit and hence bus no. 118 is selected as the new slack bus as it has the highest reserve margin. The resulting PDF at bus no. 1 after imposing the active power limit at bus no. 1 is also shown in Fig. 3.22 (b). It is clear from Fig. 3.22 that the maximum active power produced by slack bus is limited to 20.73 p.u. and remaining burden is shared by bus no. 118.

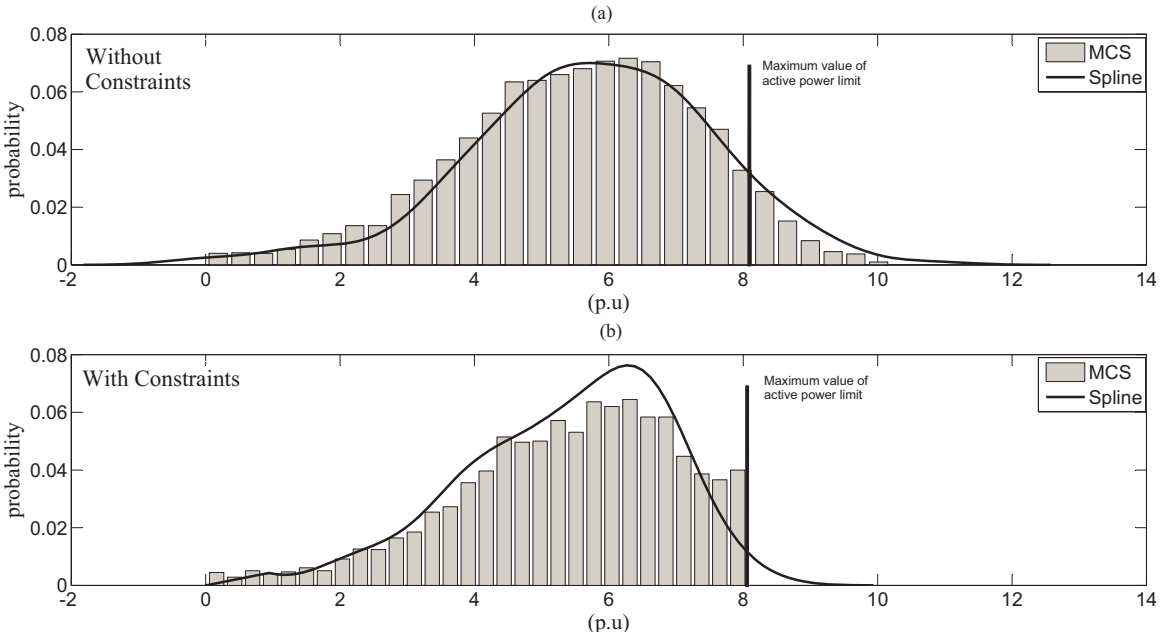

Figure 3.21: PDF of active power generation at slack bus for 118 bus system with and without constraints

Table 3.4: Statistical parameters of the voltage magnitude at bus no. 16

Schemes	**Without slack bus constraint**				**With slack bus constraint**			
	μ	σ	sk	ku	μ	σ	sk	ku
7PEM	0.93605	0.0164	3.2631	4.5189	0.93375	0.0132	3.3311	4.5731
MCS	0.93612	0.0172	3.2704	4.5083	0.93379	0.0145	3.3566	4.6573

Again, as a representative case, the statistical parameters of voltage magnitude at bus no. 64 in the 300 bus system with mixed and correlated loads, without and with slack bus constraints (with 7PEM and MCS) are given in Table 3.5. From Table 3.5, it is clear that the difference in the results obtained by 7PEM and MCS (without and with slack bus constraints) is very less. Hence, the point estimate based PLF (7PEM) can also satisfactorily be used for determining the statistical parameters in 300 bus system with mixed and correlated loads.

In all the above cases, it has been found that the 7PEM method is capable of computing the PDFs of any desired quantity quite accurately in conjunction with spline based reconstruction technique. A comparison of the computational times required by 7PEM method vis-à-vis the MCS studies is given in Table 3.6.

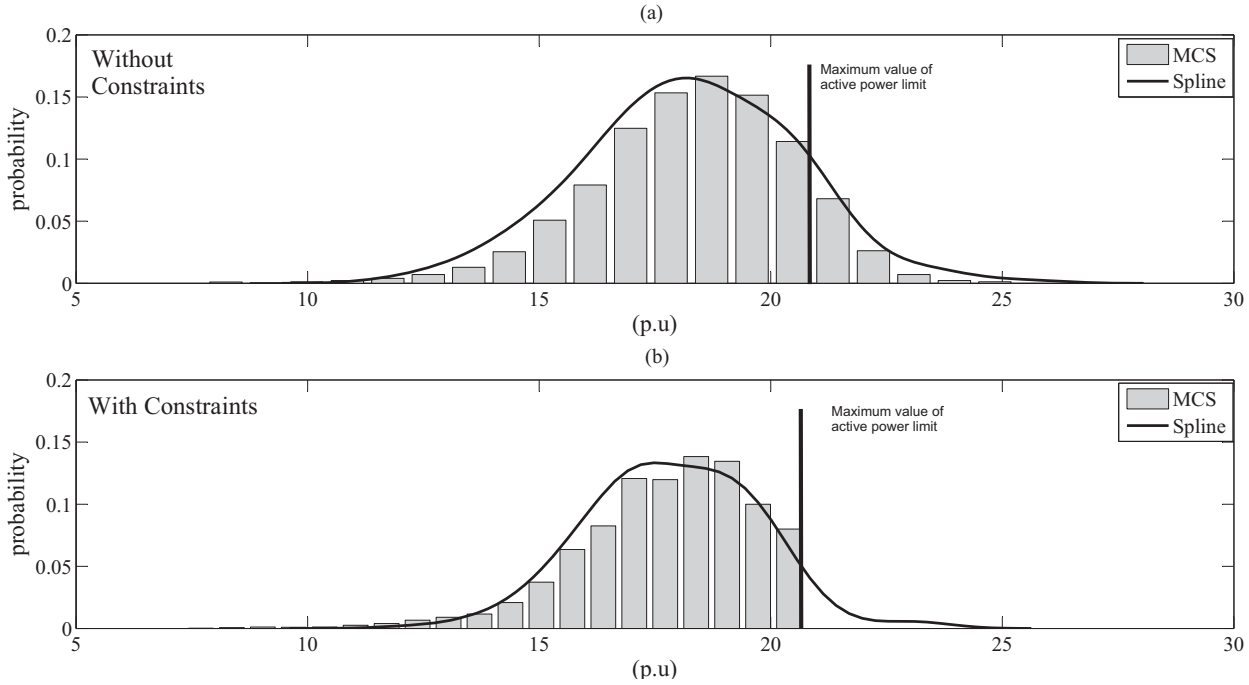

Figure 3.22: PDF of active power generation at slack bus for 300 bus system with and without constraints

Table 3.5: Statistical parameters of the voltage magnitude at bus no. 64

Schemes	**Without slack bus constraint**				**With slack bus constraint**			
	μ	σ	sk	ku	μ	σ	sk	ku
7PEM	0.99622	0.0051	3.034	2.404	0.99562	0.0056	4.0274	4.8509
MCS	0.99650	0.0042	3.065	2.569	0.99577	0.0065	4.0626	4.8629

Table 3.6: Computational time required for simulation studies (in seconds)

Type of loads	**With normal loads**		**With mixed loads**	
Test case/scheme	**7PEM**	**MCS**	**7PEM**	**MCS**
IEEE-118 bus system	194.259	21597	254.652	29974
IEEE-300 bus system	301.184	53466	408.172	66795

It can be seen from this table that it takes approximately six hours for the IEEE-118 bus system and fifteen hours for the IEEE-300 bus system to complete the MCS study with 100000 deterministic load flow solutions, while the time taken by 7PEM method for both IEEE-118 and IEEE-300 bus system is less than 6 minutes in case of normal loads. For mixed loads, time taken by 7PEM method for both 118 and 300 bus system is less than 7 minutes, which is much less as compared to that taken by MCS.

3.6 Conclusion

In this chapter, a spline based method for the reconstruction of multimodal distribution from the moments (obtained from PLF with PEM) is explained in detail. The procedure for the inclusion of correlation between the loads and the incorporation of slack bus power limit in PLF has also been explained. The developed procedure has been tested on IEEE-118 and 300 bus systems and the results show that the suggested procedure accurately determines the statistical parameter of the variables of interest. Further, the moments obtained using the developed procedure in conjunction with spline based reconstruction method can be used to construct the PDF of desired variable of interest with reasonable accuracy. To include the uncertainties of wind power generation in PLF, detailed wind generation models have been included in the PLF procedure as described in the next chapter.

Chapter 4: Probabilistic load flow with wind generation

This chapter describes a probabilistic load flow method for power systems with wind generators using different types of wind generation models. The effect of the wind power injection on the voltage profile of the system has been discussed. The correlation between wind generators has also been included in the probabilistic load flow and the developed method has been tested on IEEE-118 and IEEE-300 bus systems.

In recent years, renewable energy resources, such as wind generation, have become an integral part of electrical generation and their penetration level in the system is continuing to increase [90,91]. For the successful integration of wind energy to the grid, proper models of wind turbine generators (WTGs) need to be used to analyze the impact of wind power on the power system operation. The power generation of WTGs is a function of wind speed which is unpredictable in nature. Fig. 4.1 shows a typical histogram of wind data of a site [78]. From the histogram, it can be seen that the

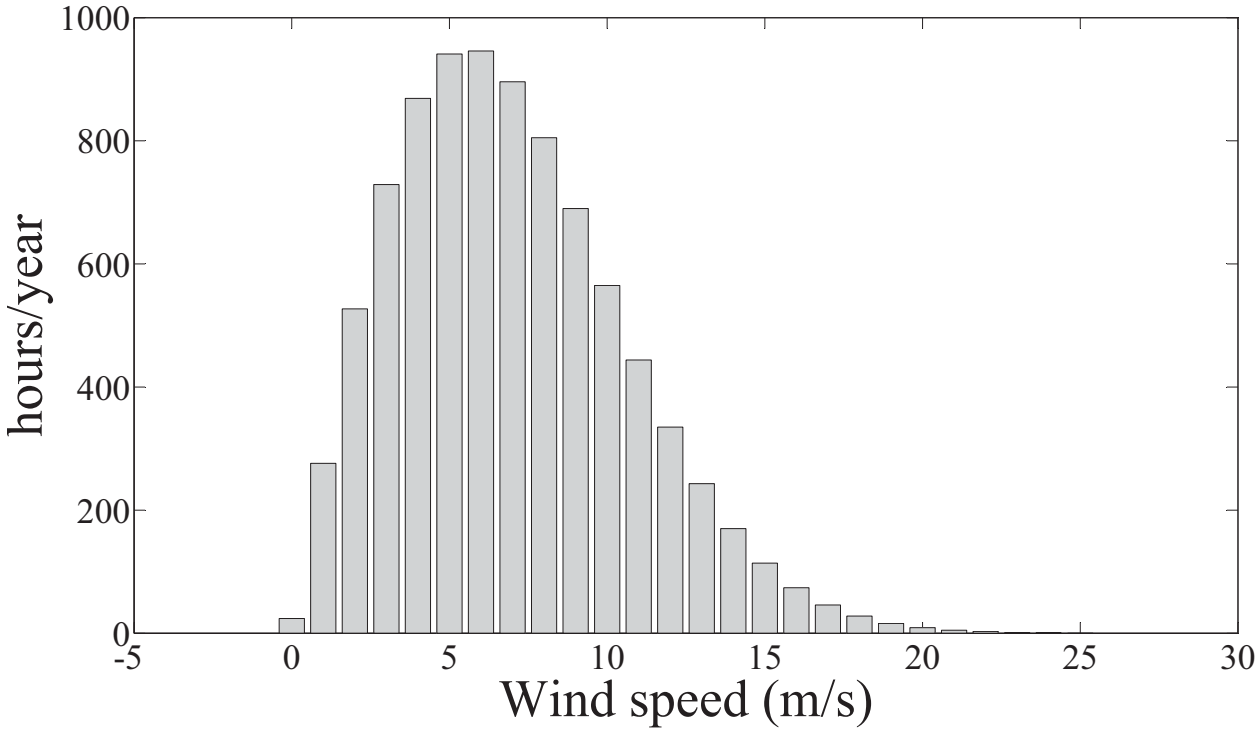

Figure 4.1: Histogram of wind data

wind speed varies over a large range with different frequencies of occurrence.

Hence, to determine the impact of varying wind power injection on the power grid, the analysis

needs to be carried out from a probabilistic point of view. For this purpose, a probabilistic power generation model of WTG needs to be developed [92]. This is done by using the PDF of the wind speed and wind speed-power output characteristics of WTG. The steps for obtaining the PDF of wind speed are discussed next.

4.1 PDF of wind speed

The information displayed in discrete histogram (as obtained from a site data shown in Fig. 4.1) can also be represented as a continuous PDF shown in Fig. 4.2.

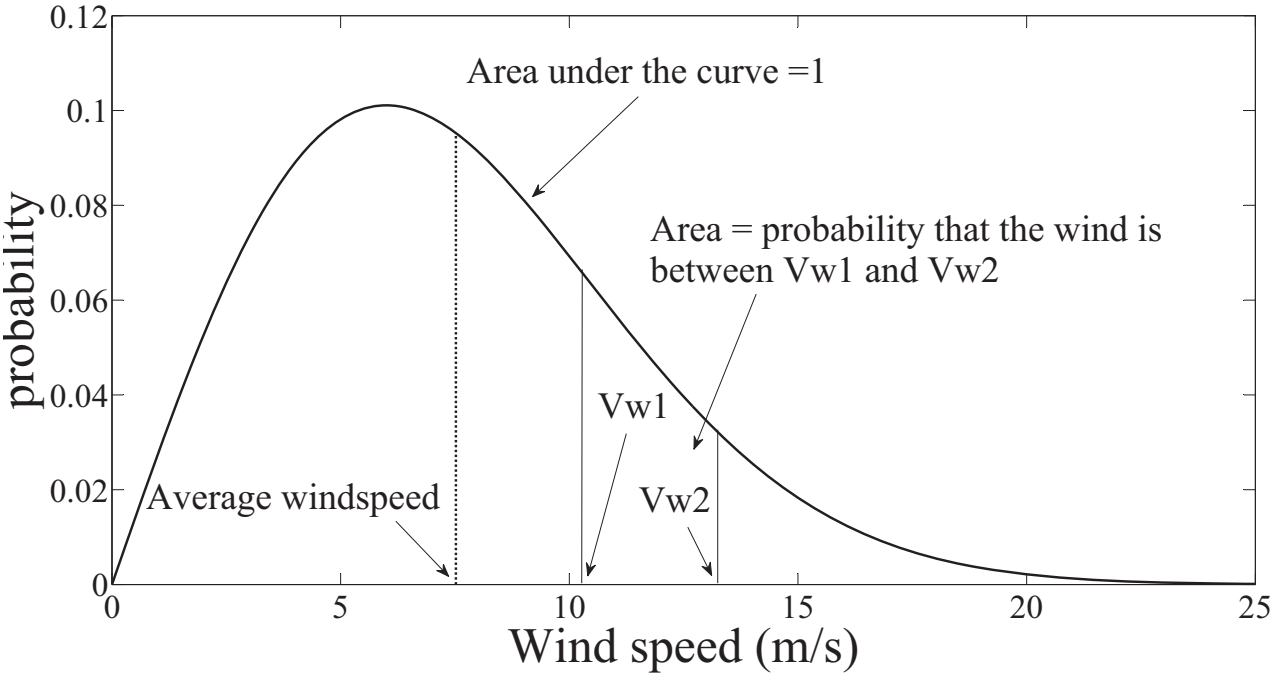

Figure 4.2: PDF of wind speed

The defining feature of such a PDF is that the area between any two wind speeds is the probability that the wind speed lies between these two limits. Let $f_{V_w}(V_w)$ be the probability associated with a wind velocity V_w. Then the probability that the wind speed lies between the two limits V_{w1} and V_{w2} is

$$\text{probability}(V_{w1} \leq V_w \leq V_{w2}) = \int_{V_{w1}}^{V_{w2}} f_{V_w}(V_w) dV_w \tag{4.1}$$

Also note that

$$\text{probability}(0 \leq V_w \leq \infty) = \int_{0}^{\infty} f_{V_w}(V_w) dV_w = 1 \tag{4.2}$$

The average wind speed μ_{v_w} and the number of hours per year that the wind speed lies between wind

speeds $V_{w1}$and V_{w2} are obtained by using eq. (4.3) and eq. (4.4) respectively.

$$\mu_{v_w} = \int_0^\infty V_w . f_{V_w}(V_w) dV_w \tag{4.3}$$

$$\text{hours/year } (V_{w1} \leq V_w \leq V_{w2}) = 8760 \int_{V_{w1}}^{V_{w2}} f_{V_w}(V_w) dV_w \tag{4.4}$$

Usually, the PDF of wind speed is given by Weibull PDF which is expressed as [78];

$$f_{V_w}(V_w) = \frac{k}{c}\left(\frac{V_w}{c}\right)^{k-1} \exp\left[-\left(\frac{V_w}{c}\right)^k\right];\ 0 \leq V_w \leq V_{w_{max}} \tag{4.5}$$

where, c is the scale parameter and k is the shape parameter. A change in the scale parameter has the same effect on the distribution as a change of the abscissa scale. Increasing the value of c while holding k constant has the effect of stretching out the PDF. The shape parameter controls the shape of the PDF, as shown in Fig. 4.3. In this figure, the scale parameter is fixed at $c = 6$.

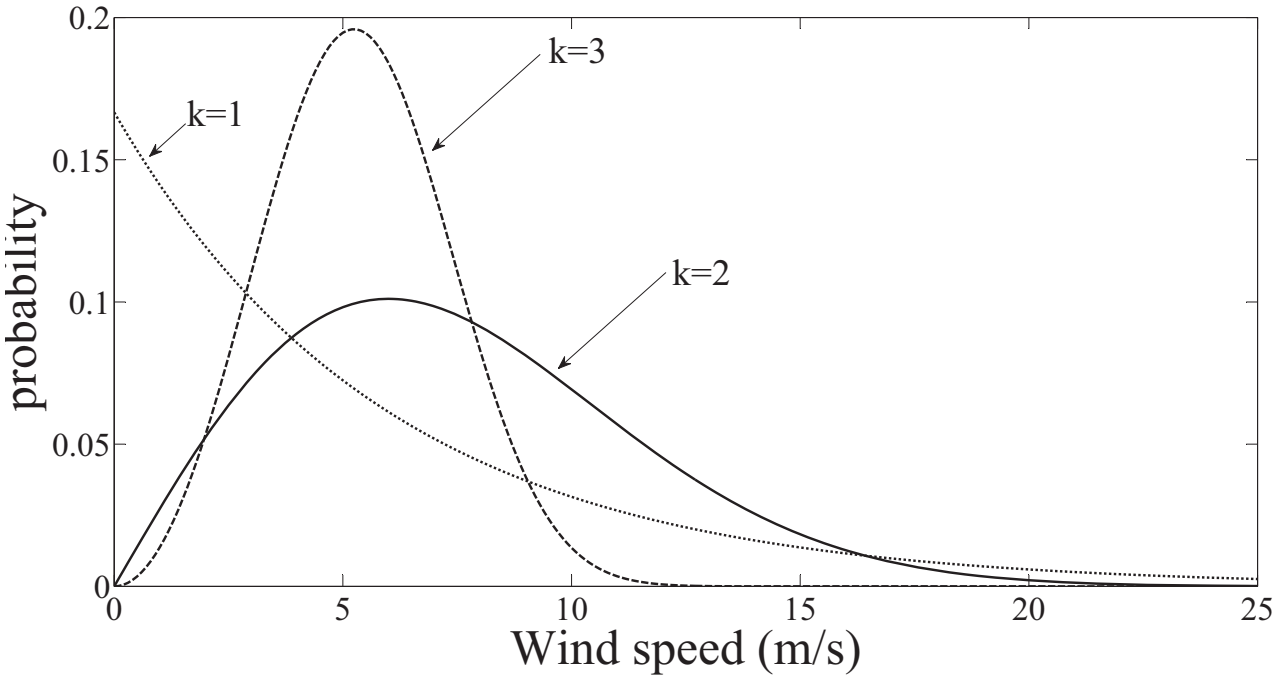

Figure 4.3: Weibull PDF of wind speed for different shape parameters

From the Fig. 4.3, it can be observed that for $k = 1$, the PDF resembles the exponential decay function. As for most of the time wind speeds are low (for $k = 1$), sites with such a wind speed distribution are not suitable for wind turbine installation. For $k = 2$, it is observed from Fig. 4.3 that there are regions in which the wind blows consistently, and there are periods during which wind

blows much faster. However, the probability of such periods (with high wind speed) is comparatively less. For $k = 3$, the PDF resembles a bell shaped curve in which the wind speed being more than a certain value (10 m/s in Fig. 4.3) is quite less.

Hence, $k = 2$ gives the most suitable PDF for a wind turbine site, as it has periods of consistent wind speeds with periods of low and high wind speed as well. For $k = 2$, the Weibull PDF is known as Rayleigh PDF (given by eq. (4.6)) and is generally the preferred distribution function for modelling of wind speeds [78].

$$f_{V_w}(V_w) = \frac{2V_w}{c^2}\exp\left[-\left(\frac{V_w}{c}\right)^2\right];\ 0 \leq V_w \leq V_{w_{max}} \tag{4.6}$$

4.1.1 Windfarms

Once a site with a suitable wind speed profile is identified, a wind farm with large number of wind turbines is constructed to fully exploit the wind potential of the site. In a wind farm, the wind turbines are installed in rectangular arrays with only few long rows perpendicular to the winds, each row having many turbines. Recommended spacing between turbines within a row is 3-5 times of rotor diameter and a spacing of 5-9 times of rotor diameter between the rows [78] (as shown in Fig. 4.4).

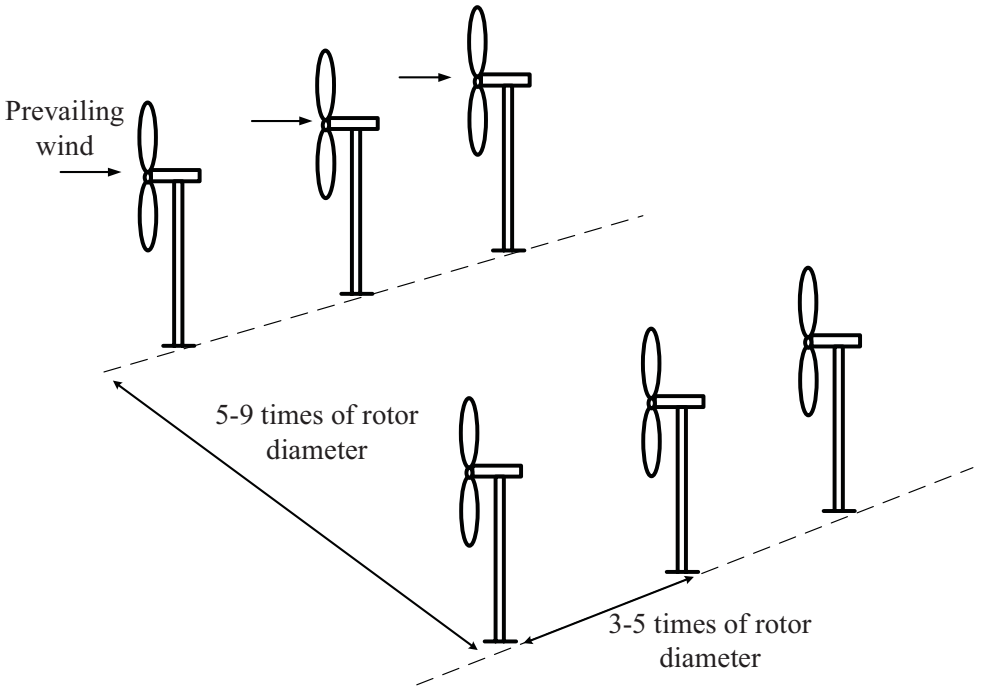

Figure 4.4: Wind farm with optimum spacing

4.1.2 Idealized wind turbine power output curve

For assessing the impact of wind turbines on the electric grid, a relationship between the wind speed and the generated electrical power output is needed. This relationship is called the wind turbine power output curve. A typical wind turbine power output curve with quadratic approximation is shown in Fig. 4.5. The corresponding power output expressions are given in eq. (4.7) [37].

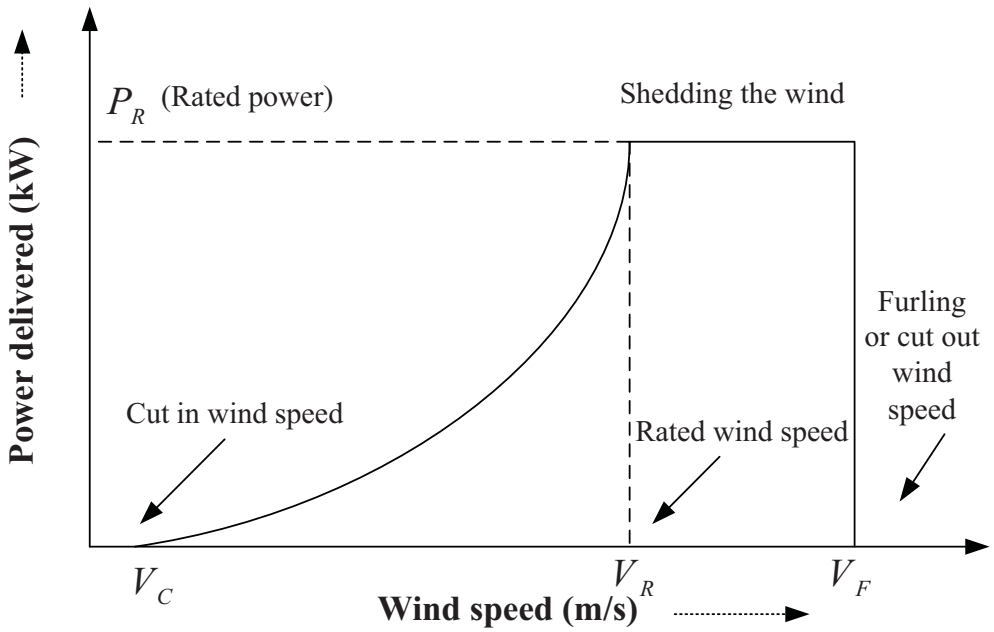

Figure 4.5: Idealized power output curve

$$P = \begin{cases} 0 \ ; & V_w \leq V_c \\ P_R \dfrac{V_w^2 - V_c^2}{V_R^2 - V_c^2}; & V_c < V_w \leq V_R \\ P_R \ ; & V_R < V_w \leq V_F \\ 0 \ ; & V_F < V_w \end{cases} \tag{4.7}$$

where, P_R is the rated power of turbine, while V_c, V_R, and V_F are cut in, rated and cut out speeds of the turbine respectively.

The cut-in wind speed (V_c) is the minimum speed required to generate power from wind turbines. The speeds below the cut-in speed may not have the required power to overcome friction in the drive train of the wind turbine or if the generator is rotating, there is not enough wind power input to offset the power required by the generator field winding. When the speed is greater than V_c, the power output increases till the rated speed is reached. Rated speed (V_R) is the speed when the generator is

delivering its full designed power output i.e the rated power (P_R).

If the wind speed exceeds the cut-out wind speed (V_F), there is a possibility of damage to the turbine and generator. Hence, for the wind speed above V_F, the wind turbine is shut down and the power output above cut-out speed will obviously be zero.

The effect of rotor diameter and generator size on the power curve is shown in Figs. 4.6 (a) and (b) respectively [78]. Increasing the rotor diameter shifts the power curve upwards so that rated

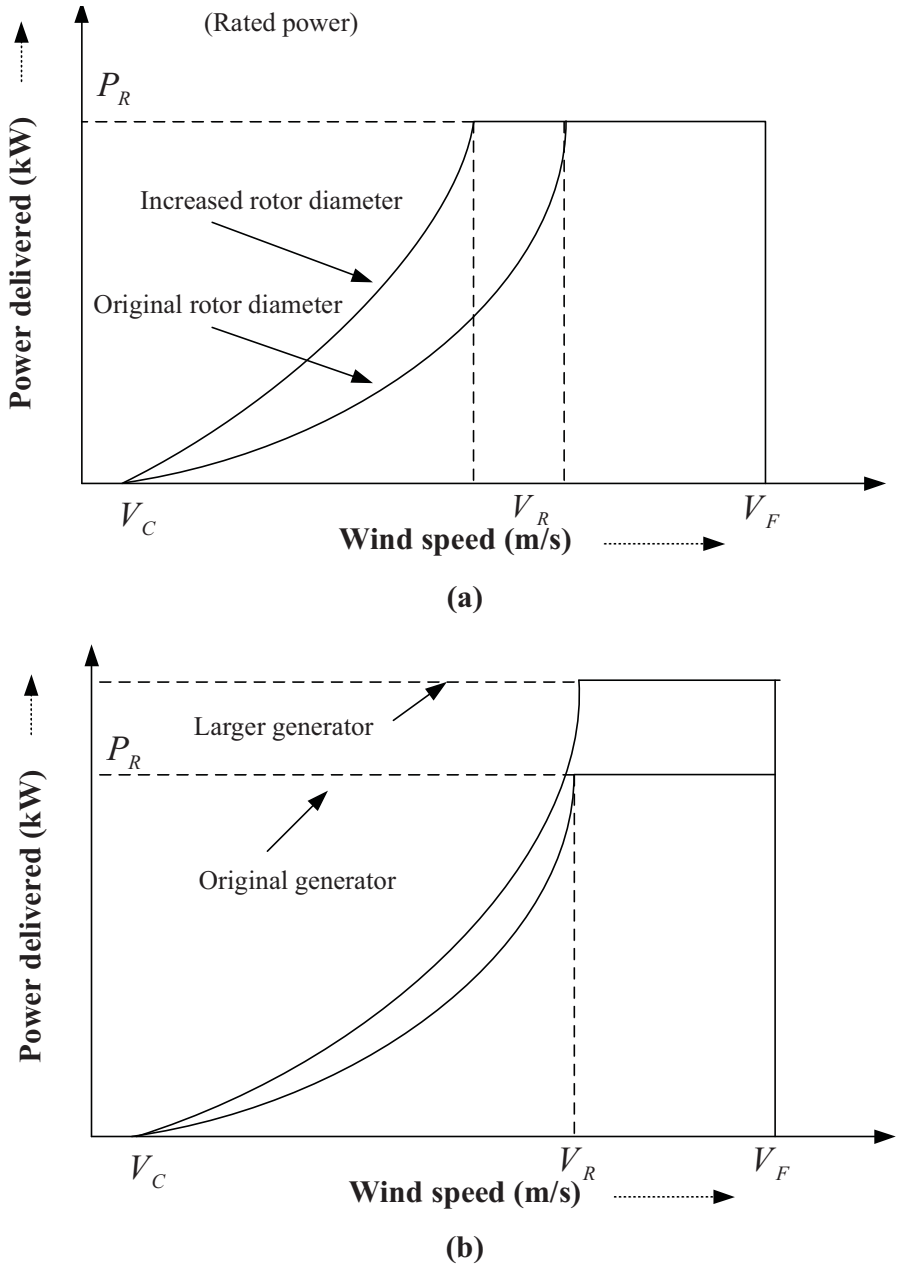

Figure 4.6: Effect of rotor diameter and generator size on wind turbine power output curve

power is reached at lower wind speeds (Figs. 4.6 (a)) and increasing the generator size increases the

rated power output (Figs. 4.6 (a)). The wind turbine power output curve is usually provided by the manufacturer.

4.2 Wind Generation Models

As, induction generators and synchronous generators are used in wind energy systems [93], in this work, four different models of wind generators have been considered. For each of these models, the active power output (P) for a given wind speed V_w can be obtained from the power output curve provided by the manufacturer. The equivalent circuit of an induction generator is shown in Fig. 4.7, in which I_1 is the stator current, I_2 is the rotor current, I_m is the magnetizing current, V_t is the terminal voltage magnitude, s is the slip, R_1 is the stator resistance, R_2 is the rotor resistance, X_{l1} is the stator leakage reactance, X_{l2} is the rotor leakage reactance and X_m is the magnetizing reactance of the induction machine.

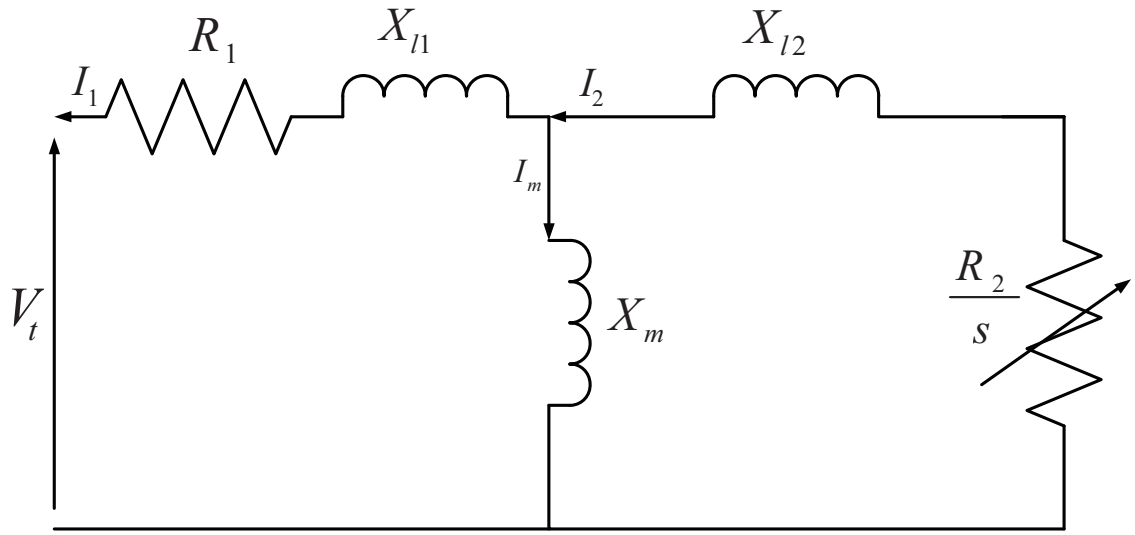

Figure 4.7: Induction machine equivalent circuit

4.2.1 Simple PQ model of Induction Generator

In this model, the generator reactive power Q is obtained by the following expression [94].

$$Q \approx V_t^2 \frac{X_c - X_m}{X_c X_m} + \frac{X}{V_t^2} P^2 \tag{4.8}$$

where, X is the sum of stator and rotor leakage reactances and X_c is the reactance of capacitor bank connected at the terminal of the generator. However, it is to be noted that, the stator and rotor resistances have been neglected in eq. (4.8).

4.2.2 Doubly fed induction generator model

A doubly fed induction generator (DFIG) model consists of an asynchronous generator with a wound rotor and slip rings. A rotor circuit is connected to the converter through the slip rings. In this case, the reactive power consumed (absorbed) depends upon the operating power factor (lead or lag) and can be obtained as [95],

$$Q = P\sqrt{\frac{1 - cos^2\theta}{cos\theta}} \tag{4.9}$$

4.2.3 Pitch regulated Induction Generator

In this case, as the wind speed varies the pitch angle controller regulates the wind turbine blade angle [96]. In this model, for the calculated value of generated P, a quadratic equation involving induction generator slip (s) is solved to compute the value of slip. The quadratic equation is written as [96]:

$$as^2 + bs + c = 0 \tag{4.10}$$

where,

$a = PR_1^2\left(X_{l2} + X_m\right)^2 + P\left(X_m X_{l2} + X_{l1}\left(X_{l2} + Xm\right)\right)^2 - V_t^2 R_1 (X_{l2} + X_m)^2$

$b = 2PR_1R_2X_m^2 - V_t^2 R_2 X_m^2$ and

$c = PR_2^2\left(X_{l1} + Xm\right)^2 + P\left(R_1R_2\right)^2 - V_t^2 R_1 R_2^2$

From eq. (4.10), the slip is calculated as,

$$s = min\left|\frac{-b \pm \sqrt{b^2 - 4ac}}{2a}\right| \tag{4.11}$$

Knowing s, the generator Q is computed as [96];

$$Q = \frac{X_m X_{l2} s^2\left(X_m + X_{l2}\right) + X_{l1} s^2\left(X_m + X_{l2}\right)^2 + \quad R_2^2\left(X_m + X_{l1}\right)}{\left[R_2R_1 + s\left(X_m^2 - \left(X_m + X_{l2}\right)\left(X_m + X_{l1}\right)\right)\right]^2 \quad + \left[R_2\left(X_m + X_{l1}\right) + sR_1\left(X_m + X_{l2}\right)\right]^2} V_t^2 \tag{4.12}$$

4.2.4 Semi variable speed Induction Generator

This type of induction generator consists of a pitch controlled wind turbine and wound rotor induction generator. The rotor circuit of the induction generator is connected to a variable resistance whose value is varied by power electronic devices [96]. In this case, the rotor resistance is unknown and its value is controlled by the controller. To determine the value of rotor resistance, the quadratic equation given in eq. (4.10) is recasted in terms of R_2/s (denoted as R_{eq}). Hence, even when the R_2

and s are unknown the quantity R_2/s can be computed by solving the quadratic equation involving R_{eq}. The quadratic equation for R_{eq} can be written as [96]:

$$aR_{eq}^2 + bR_{eq} + c = 0 \tag{4.13}$$

where,

$a = P\left(R_1^2 + (X_{l1} + X_m)^2\right) - V_t^2 R_1^2$

$b = 2R_1 P X_m^2 - X_m^2 V_t^2$

and

$c = PR_1^2 (X_{l2} + X_m)^2 + P\left(X_m^2 - (X_m + X_{l2})(X_m + X_{l1})\right)^2 - R_1 (X_m + X_{l2})^2 V_t^2$

From eq. (4.13), R_{eq} is computed as;

$$R_{eq} = max \left| \frac{-b \pm \sqrt{b^2 - 4ac}}{2a} \right| \tag{4.14}$$

Knowing R_{eq}, Q can be computed as

$$Q = \frac{R_{eq}^2 (X_m + X_{l1}) - (X_m + X_{l2})\left(X_m^2 - (X_m + X_{l2})(X_m + X_{l1})\right)}{\left[R_{eq}R_1 + \left(X_m^2 - (X_m + X_{l2})(X_m + X_{l1})\right)\right]^2 \quad + \left[R_{eq}(X_m + X_{l1}) + R_1 (X_m + X_{l2})\right]^2} V_t^2 \tag{4.15}$$

4.3 Inclusion of wind speed uncertainty into the PLF

As the first step towards the inclusion of wind speed uncertainty in PLF, either the available wind speed data of the site is collected or the wind speed data is generated using Rayleigh distribution with appropriate shape and scale parameters. From the wind speed data, the active power output of a generator is obtained by using the wind speed power curve of the turbine. From the power generation data obtained, PDF of the available or output power of WTGs is obtained using frequency counting technique. Next, the points and weights corresponding to the active power output PDF are generated as discussed in the Section 2.4. The active power generated by the WTG are represented as negative load in PEM. The reactive power injection at the buses where WTGs are connected is initially taken as zero.

Once the points and weights of generated WTG power corresponding to 3PEM, 5PEM and 7PEM are estimated, the following procedure is adopted for PLF:

1. Form the input matrices $\boldsymbol{X_1}, \boldsymbol{X_2}, .., \boldsymbol{X_k}$ as explained in Chapter 3;

$$\boldsymbol{X_k} = \begin{bmatrix} x_{1,k} & \mu_{x2} & \dots & \mu_{xn} \\ \mu_{x1} & x_{2,k} & \dots & \mu_{xn} \\ \vdots & \vdots & \ddots & \vdots \\ \mu_{x1} & \mu_{x2} & \dots & x_{n,k} \end{bmatrix} \tag{4.16}$$

where, $k = 1, .., m$, $m = 2, 4$ and 6 for 3PEM, 5PEM and 7PEM respectively. In this work, only 7PEM has been used, hence $m = 6$.

2. For each row of $\boldsymbol{X_k}$, a deterministic load flow is carried out. In each iteration of load flow, with the last updated voltage magnitude and the active power at the buses where WTGs is connected, the reactive power consumed/absorbed by WTGs is calculated (by the wind generation models explained in Section 4.2). For load flow calculation, the generated active power is considered as equivalent negative active load while the reactive power absorbed is treated as equivalent positive reactive load. With these equivalent active and reactive loads, the voltages are updated and the iterations are continued till the load flow is converged.

3. Repeat step 2 for all the rows of the matrices $\boldsymbol{X_1}, \boldsymbol{X_2}, .., \boldsymbol{X_k}$. As a result, a total of 'nm' load flow computations would be carried out.

4. For each output variable of interest $y_{i,lk}$ the j^{th} moment is calculated as,

$$E(y_{i,lk}^j) = \sum_{l=1}^{n} \sum_{k=1}^{m} w_{l,k} E\left[(y_{i,lk})^j \right], \quad j = 1, .., \text{no. of moments.} \tag{4.17}$$

In this work, first eight moments have been used. It is to be noted that in eq. (4.17), $y_{i,lk}$ denotes the value of i^{th} variable of interest corresponding to $(lk)^{th}$ load flow where $l = 1, ...n$ and $k = 1, ...m$.

5. Lastly, a deterministic load flow is carried out with a vector $\boldsymbol{X_{mean}} = [\mu_{x_1}, \mu_{x_2}, ..., \mu_{x_l}, , .., \mu_{x_n}]$, and let $y_{i,\mu}$ denotes the value of i^{th} output variable of interest corresponding to this load flow. The moment $E(y_{i,lk}^j)$ is then updated as:

$$E(y_{i,lk}^j) = E(y_{i,lk}^j) + w_\mu \left(y_{i,\mu} \right)^j \tag{4.18}$$

6. Using the above calculated moments, the CDF and PDF of y_i is computed using spline based reconstruction method.

4.4 Results

For assessing the effect of connecting WTGs on the system and calculating the PDFs of bus voltages, line power flows, reactive power absorbed by the wind generators, all the four types of wind generator models described in Section 4.2 have been incorporated in PLF. The PLF has been solved by using 7PEM method and the results obtained by these methods have also been compared with those obtained by the Monte Carlo simulation studies. For investigating the feasibility of the proposed methods, some loads have been considered as correlated and the correlation between WTGs has also been included. It is to be noted that any correlation between wind and load has been neglected. The hourly wind speed data for the wind farms, for a period of one year, has been taken from [97] with the wind speed distributions as shown in Fig. 4.8. All the studies in this work have been carried out on the IEEE-118 and IEEE-300 bus systems [80].

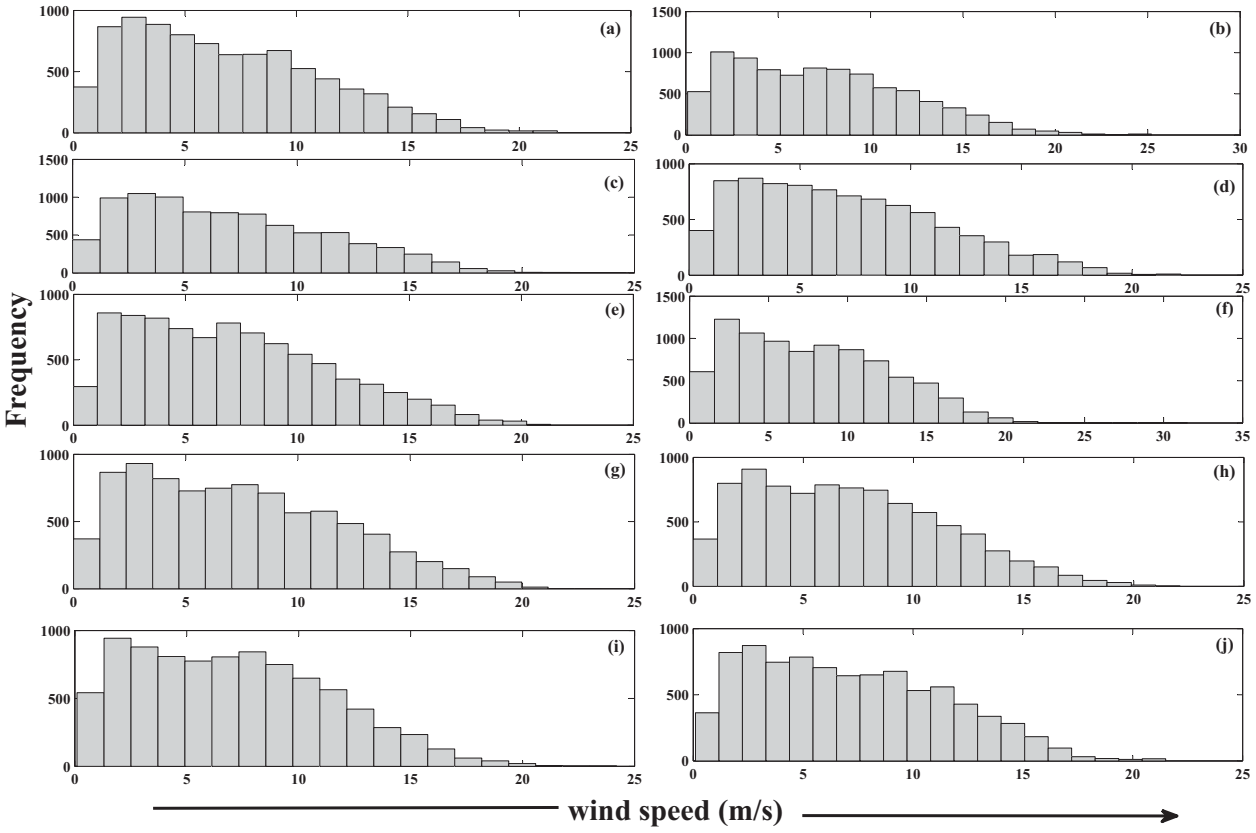

Figure 4.8: Wind speed distributions of the 10 wind farms

In this work, a total of 10 wind farms have been considered. In each wind farm, it has been

assumed that there are W number of WTGs which are distributed in 10 clusters. Therefore, in each cluster there are W/10 wind turbine generators. The wind turbine generators in each cluster are subjected to same wind speed at any given instant, while the wind speeds experienced by the WTGs in other clusters of the wind farm at that instant are different. As the clusters within a wind farm are assumed to be located in geographical proximity, the wind speeds experienced by these clusters are correlated with each other. From the wind speed data (Fig. 4.8), a representative wind speed correlation matrix of the clusters of a wind farm is given in eq. (4.19) and the scatter plot of the wind speeds of first two WTGs in a cluster with a correlation coefficient of 0.909 is shown in Fig. 4.9.

$$\boldsymbol{P_{wind}} = \begin{bmatrix} 1 & 0.909 & 0.847 & 0.792 & 0.749 & 0.714 & 0.686 & 0.659 & 0.635 & 0.616 \\ 0.909 & 1 & 0.929 & 0.871 & 0.822 & 0.777 & 0.746 & 0.719 & 0.692 & 0.670 \\ 0.847 & 0.929 & 1 & 0.936 & 0.884 & 0.839 & 0.803 & 0.773 & 0.742 & 0.718 \\ 0.792 & 0.871 & 0.936 & 1 & 0.946 & 0.899 & 0.861 & 0.828 & 0.797 & 0.767 \\ 0.749 & 0.822 & 0.884 & 0.946 & 1 & 0.953 & 0.912 & 0.878 & 0.845 & 0.814 \\ 0.714 & 0.777 & 0.839 & 0.899 & 0.953 & 1 & 0.959 & 0.922 & 0.889 & 0.857 \\ 0.686 & 0.746 & 0.803 & 0.861 & 0.912 & 0.959 & 1 & 0.961 & 0.927 & 0.893 \\ 0.659 & 0.719 & 0.773 & 0.828 & 0.878 & 0.922 & 0.961 & 1 & 0.964 & 0.931 \\ 0.635 & 0.692 & 0.742 & 0.797 & 0.845 & 0.889 & 0.927 & 0.964 & 1 & 0.968 \\ 0.616 & 0.670 & 0.718 & 0.767 & 0.814 & 0.857 & 0.893 & 0.931 & 0.968 & 1 \end{bmatrix} \tag{4.19}$$

From the wind speed faced by all the clusters of a wind farm, the aggregate power generated by the farm has been calculated using the wind power speed curve given in eq. (4.7) for all 8760 hours in a year (by multiplying the power output of a cluster with the number of WTGs in a cluster). From these calculated hourly power output of the farm, the corresponding PDF of the power output of each cluster has also been determined as shown in Fig. 4.10.

4.4.1 IEEE-118 bus system

For IEEE-118 bus system the 10 farms have been assumed to be located at these following 10 buses: 94 to 98, 108, 109, 114, 115, 117. The details of these wind farms are given in Table 4.1. It is to be noted that the distribution of different type of WTGs among different buses as shown in Table 4.1,

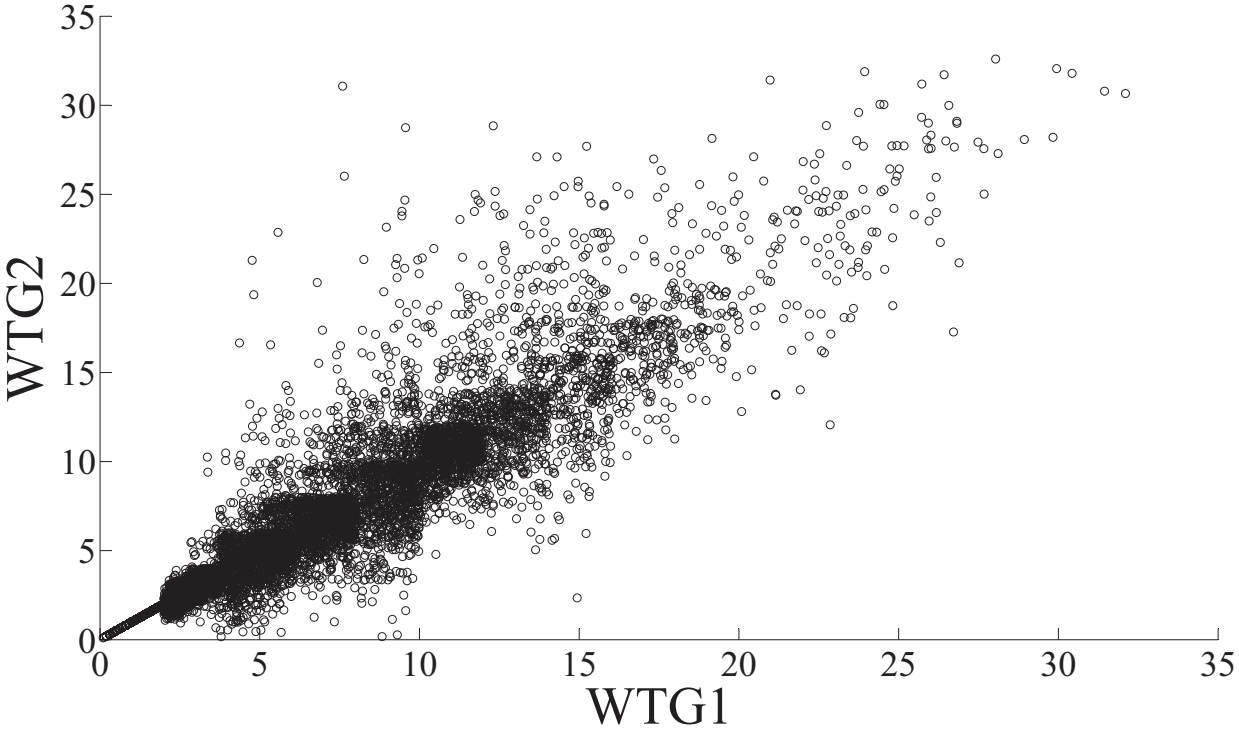

Figure 4.9: Scatter plot of the wind speeds (m/s) of first two WTGs in a cluster

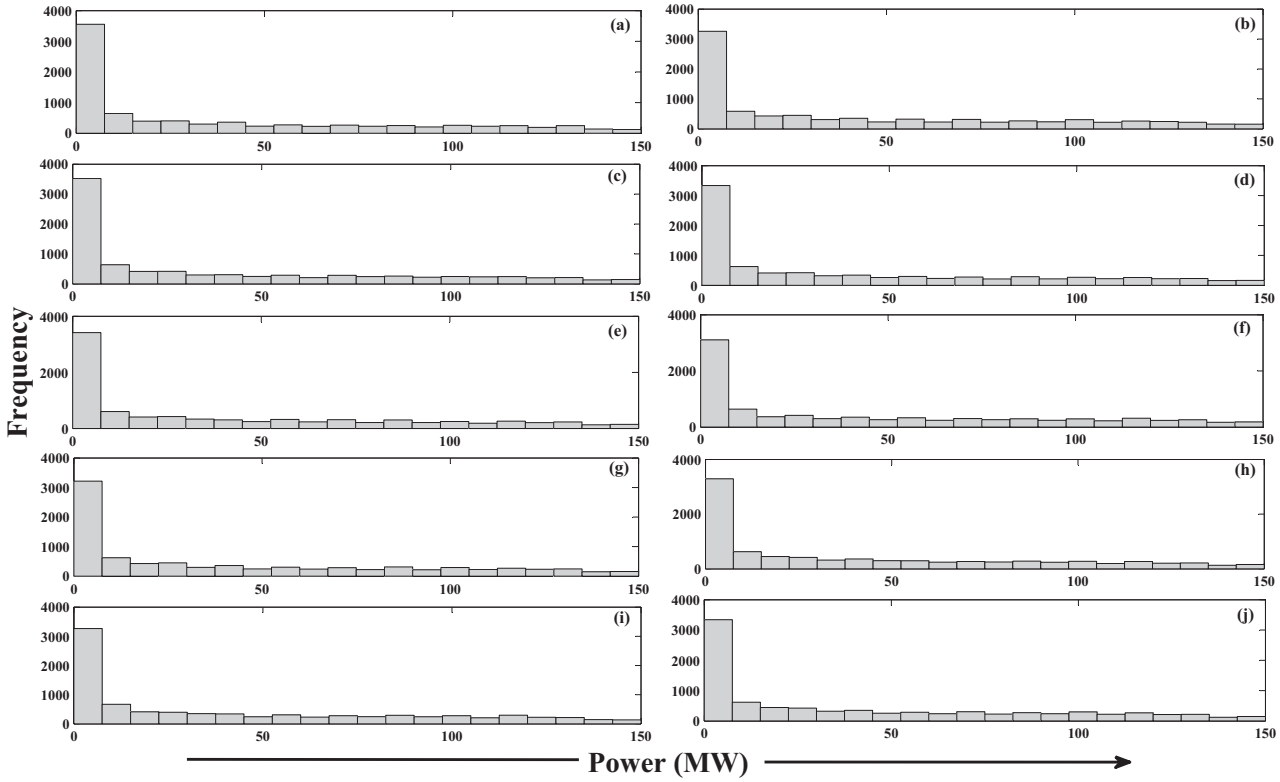

Figure 4.10: Wind power output distributions for the cluster of a wind farm

Table 4.1: Details of the wind farms in IEEE-118 bus system

Bus no.	Type of WTGs	No. of WTGs	WTG rating (kW)
94	PQ	300	500
95	PQ	300	500
96	PQ	300	500
97	Pitch Regulated	150	1000
98	Pitch Regulated	150	1000
108	Pitch Regulated	150	1000
109	Semi Variable speed	300	500
114	Semi Variable speed	300	500
115	DFIG	150	1000
117	DFIG	150	1000

has been assumed totally arbitrarily, any other distribution could have been assumed as well. Further, in this work the wind farms are assumed to be located far away from each other and as a result, no correlation is assumed among the wind speeds experienced by the wind farms.

The generator parameters of WTGs for pitch regulated fixed speed model and for semi variable speed induction generator are given in Appendix C [96] and for simple PQ model, the parameters are given in [94]. For DFIG, unity power factor operation has been assumed.

For each of the buses where the wind turbine is connected, the wind turbine power curve has been assumed to have quadratic approximation as given in eq. (4.7). The parameters of power curves are:- $V_c = 3\ m/s$, $V_R = 12\ m/s$ and $V_F = 20\ m/s$. These parameters have been assumed to be the same for all the WTGs connected to the system.

For modeling the uncertainties in the loads, the active power and the reactive power consumed by the loads connected at bus nos. 1 to 50 have been assumed to have non-normal distribution with a PDF as shown in Fig. 3.7, which represents the PDF of IEEE Reliability test system hourly load data [85].

The rest of loads from bus nos. 51 to 118 have been assumed to be normally distributed with mean values equal to 1.5 times the load data given in Appendix B [80] and the standard deviation

equal to 10% of the corresponding mean value of the load. This enhancement of load from base loading condition has been done to simulate the practical future scenario of the load. The active and reactive power loads at bus nos. 81 to 84 have been assumed to be correlated with each other and the correlation matrix is given in eq. (3.22).

The PDF of reactive power consumption at bus nos. 96 and 97 by using 7PEM with Cornish-fisher (CF) series and with spline based reconstruction technique are shown in Fig. 4.11 and Fig. 4.12 respectively.

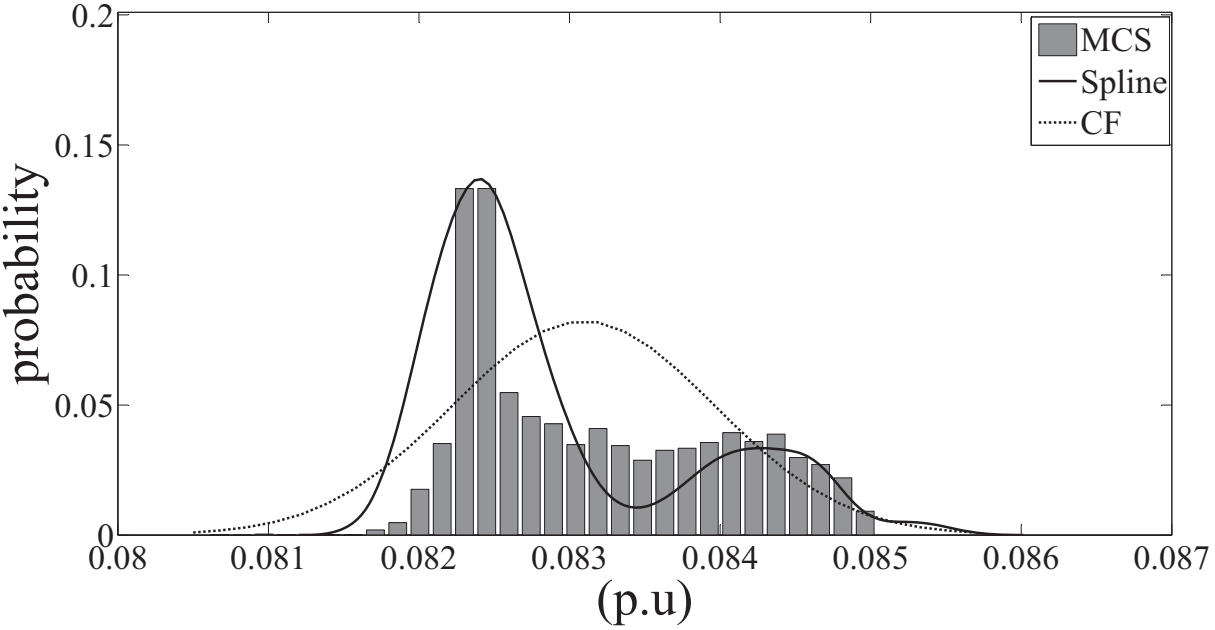

Figure 4.11: PDF of reactive power consumption at bus no. 96

Further for the purpose of comparison, PDFs has also been computed with the results of MCS study. The MCS study has been carried out by performing deterministic load flow 100000 times with random variations of the wind speeds and loads within their respective ranges. The PDFs of reactive power consumption at bus nos. 97 and 98 obtained with MCS studies are also shown in Fig. 4.11 and Fig. 4.12 respectively.

It is clearly evident from the Figs. 4.11 and 4.12 that the PDF obtained by using PEM and the spline based technique is in closer proximity with that obtained by MCS (as compared to the PDF obtained by Cornish-Fisher series).

Similarly, the PDFs of voltage magnitude at bus no. 114, active power flow in line between bus no. 60-61, reactive power flow in line between bus no. 36-38 obtained with MCS, CF series and Spline based reconstruction method (both obtained using 7PEM based PLF), are shown in Figs. 4.13

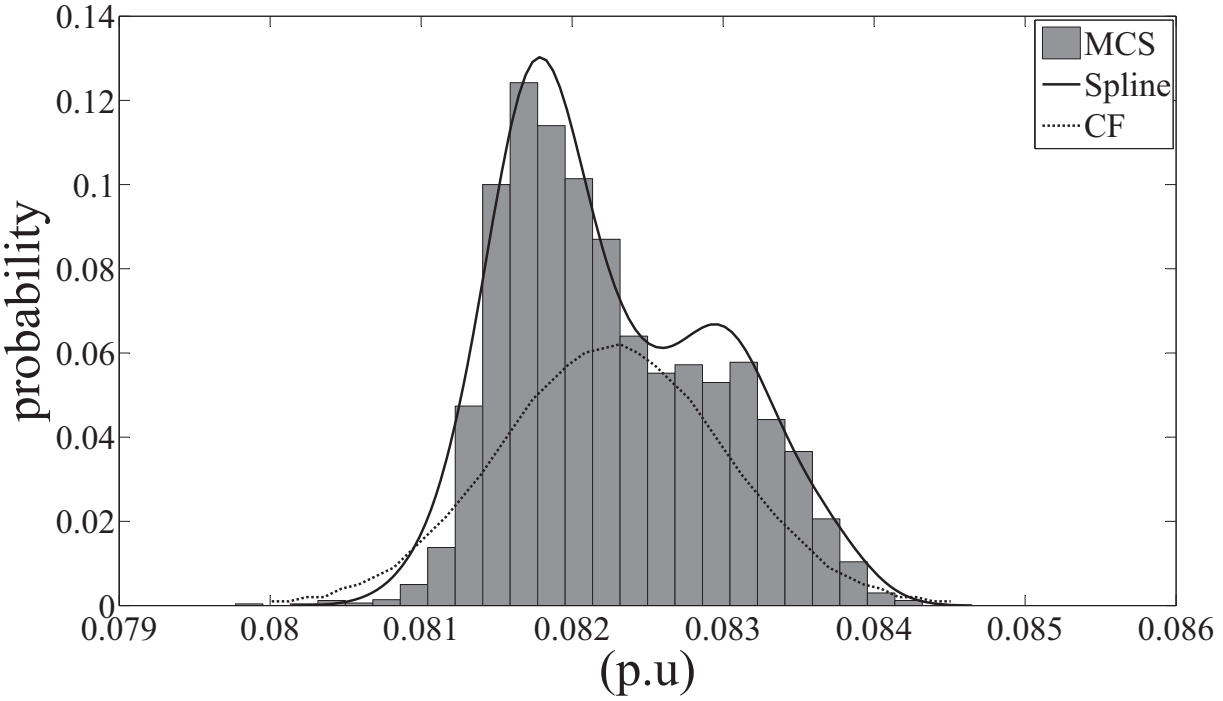

Figure 4.12: PDF of reactive power consumption at bus no. 97

to 4.15 respectively. Again it can be observed that the spline based reconstruction method is able to approximate the PDF much better as compared to Cornish-Fisher series.

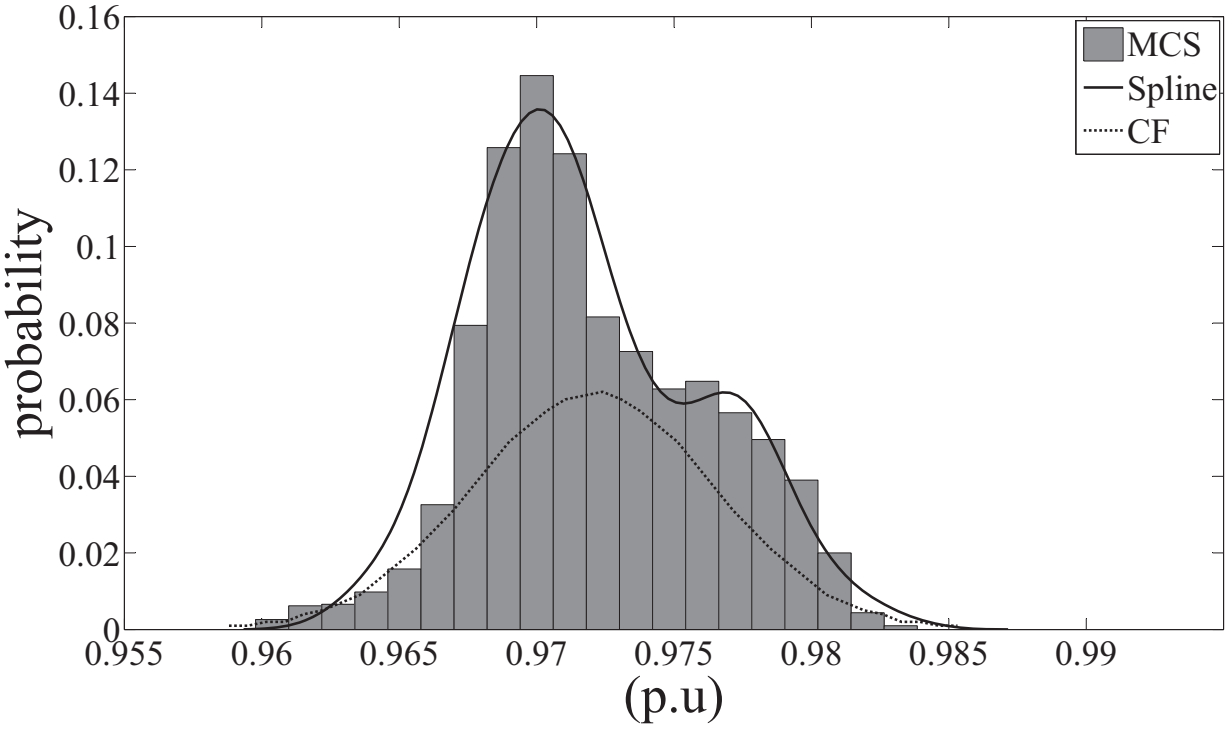

Figure 4.13: PDF of voltage at bus no. 114

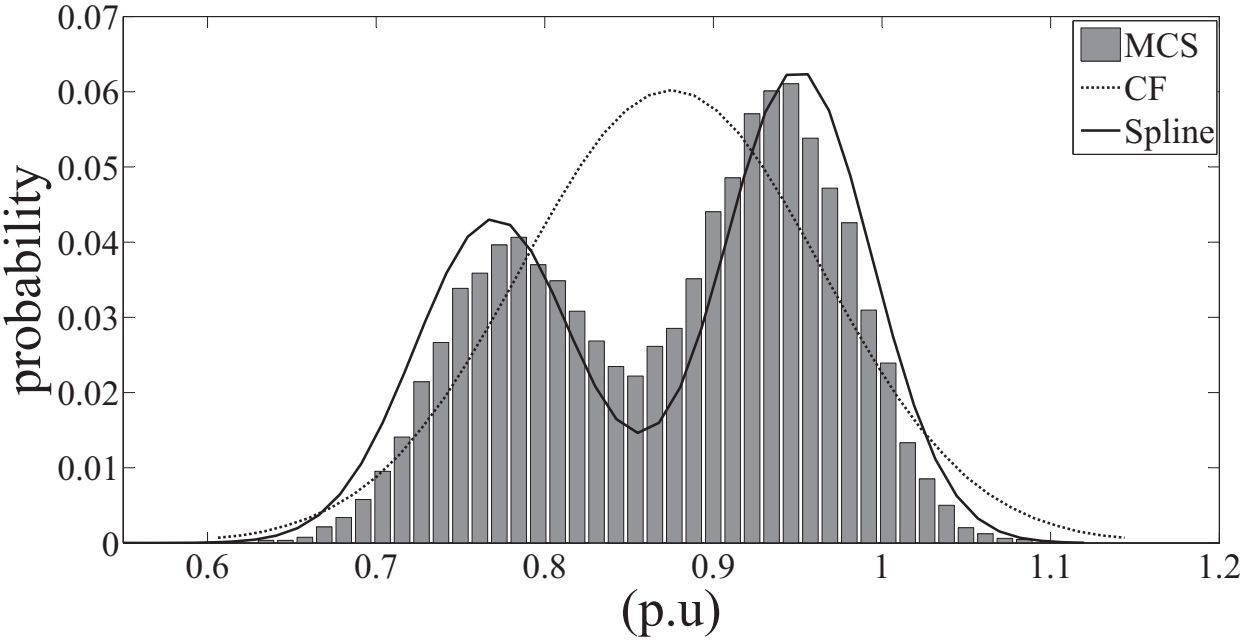

Figure 4.14: PDF of active power flow in line between bus no. 60 and 61

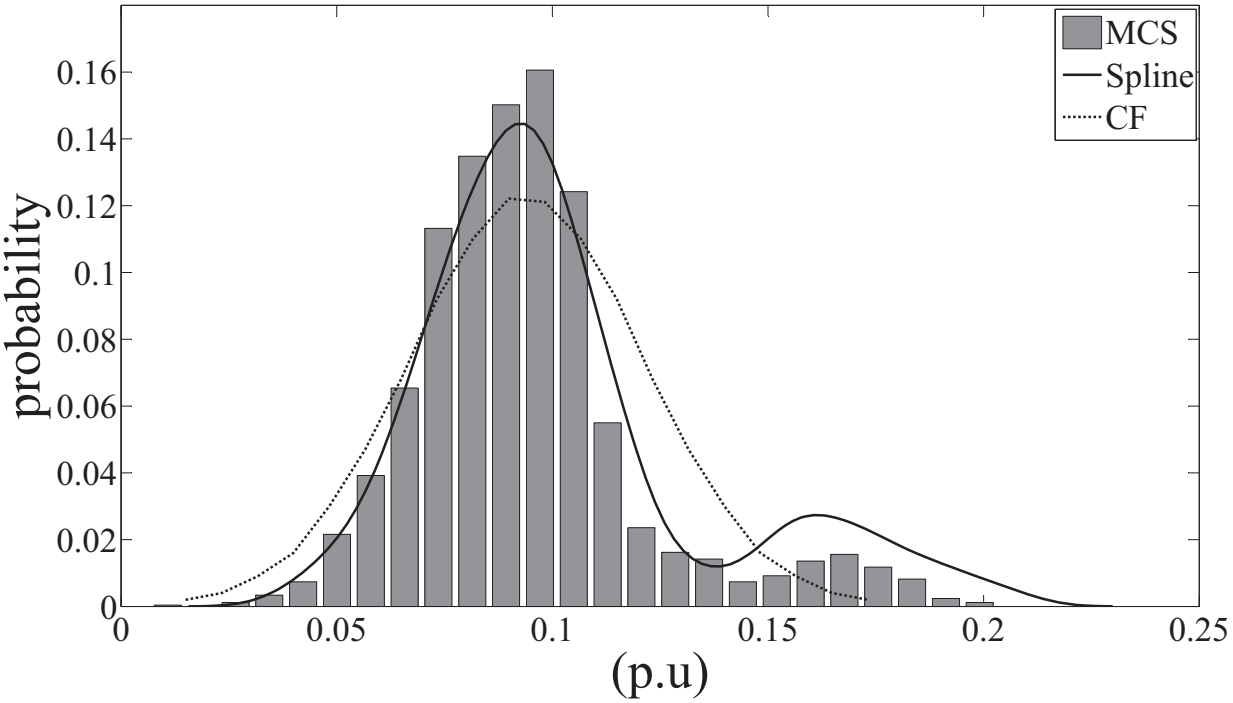

Figure 4.15: PDF of reactive power flow in line between bus no. 36 and 38

From Figs. 4.11- 4.15 (taken as representative cases), it is seen that the PDFs are multimodal in nature and the spline based method is able to reconstruct the multimodal PDFs much better as compared to the Cornish-Fisher series. Thus, the spline based reconstruction technique that utilizes

the moments obtained from 7PEM based PLF is more suitable for computing the PDF of the variables of interest in a system with large penetration of WTGs which also contains both continuous normal and discrete non-normal loads.

The impact of adding WTGs on the voltage profile of the system is shown in Fig. 4.16 in which only the mean values of bus voltages are plotted for all the buses. From this figure, it is observed that the voltage profile of the entire system is improved when WGTs are connected to the system. The PDFs of voltage at bus 76 (as a representative case) with WTGs and without WTGs, plotted

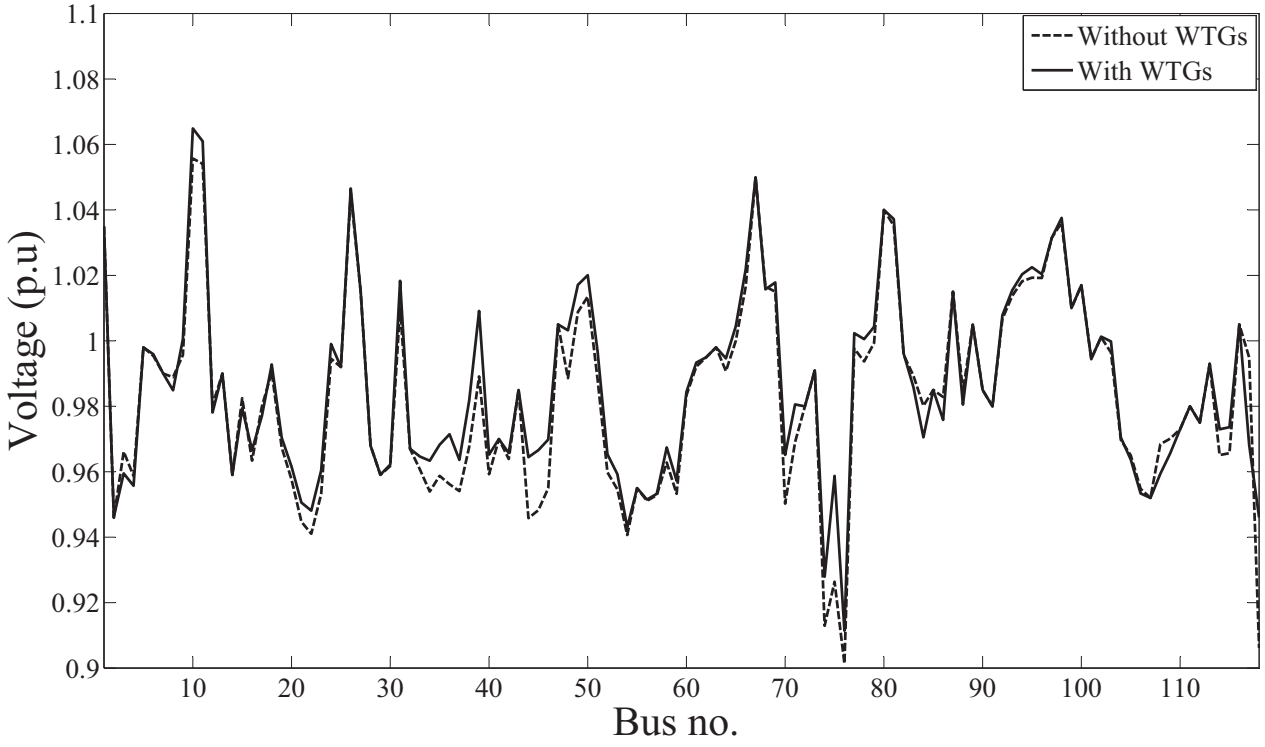

Figure 4.16: Voltage profile of the system with and without WTGs

with MCS and Spline based reconstruction method are shown in Fig. 4.17. From this figure, it is observed that the voltage PDF at this bus is shifted to higher voltage range indicating a higher average bus voltages (an indication of improved system voltage profile). Further, it can also be seen that the PDF obtained by Spline based reconstruction method matches well with the PDF obtained by MCS. Similar results have also been observed for other buses in the system.

4.4.2 IEEE-300 bus system

For IEEE-300 bus system, the load distribution and the correlation among the loads is assumed to be the same as given in Section 3.4.3 in Chapter 3. In this system also 10 farms have been assumed to

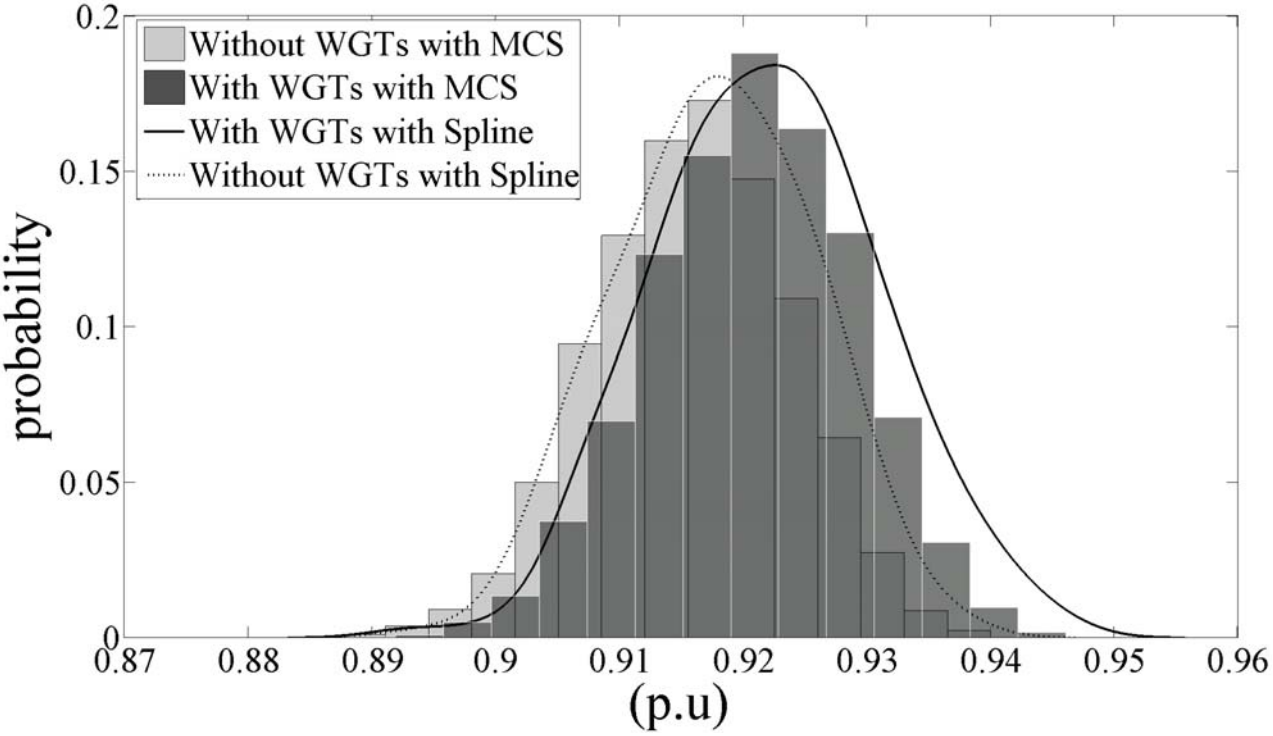

Figure 4.17: Voltage PDFs at the bus no 76 with and without WGTs

be located at 10 buses from bus no. 106 to 115. The details of these wind farms are given in Table 4.2.

Table 4.2: Details of the wind farms in IEEE-300 bus system

Bus no.	**Type of WTGs**	**No. of WTGs**	**WTG rating (kW)**
106	PQ	300	500
107	PQ	300	500
108	PQ	300	500
109	Pitch Regulated	150	1000
110	Pitch Regulated	150	1000
111	Pitch Regulated	150	1000
112	Semi Variable speed	300	500
113	Semi Variable speed	300	500
114	DFIG	150	1000
115	DFIG	150	1000

The PDFs of reactive power consumption at bus no. 113 by using 7PEM based PLF with Cornish-fisher (CF) series and with spline based reconstruction technique are shown in Fig. 4.18. For comparison purposes the PDF has also been computed with MCS and is shown in Fig. 4.18. It is observed from the Fig. 4.18 that the PDF obtained by the spline based technique is in closer proximity to the PDF obtained by MCS (as compared to the PDFs obtained by Cornish-Fisher series).

Similarly, the PDFs of the voltage magnitude at bus no. 247 and active power flow in line between bus nos. 32-266 obtained with MCS, CF series and Spline based reconstruction method are shown in Fig. 4.19 and Fig. 4.20 respectively.

The PDFs of voltage at bus 172 (as a representative case) with WTGs and without WTGs, obtained using MCS and Spline based reconstruction method are shown in Fig. 4.21.

From this figure, it is observed that the PDF of voltage at this bus is shifted to higher voltage range and the bus voltage PDF obtained from spline based reconstruction technique compares quite well with the PDF obtained from MCS. The shifting of PDF of voltage is due to the improvement in the voltage profile of the system and similar results are observed for other buses in the system also.

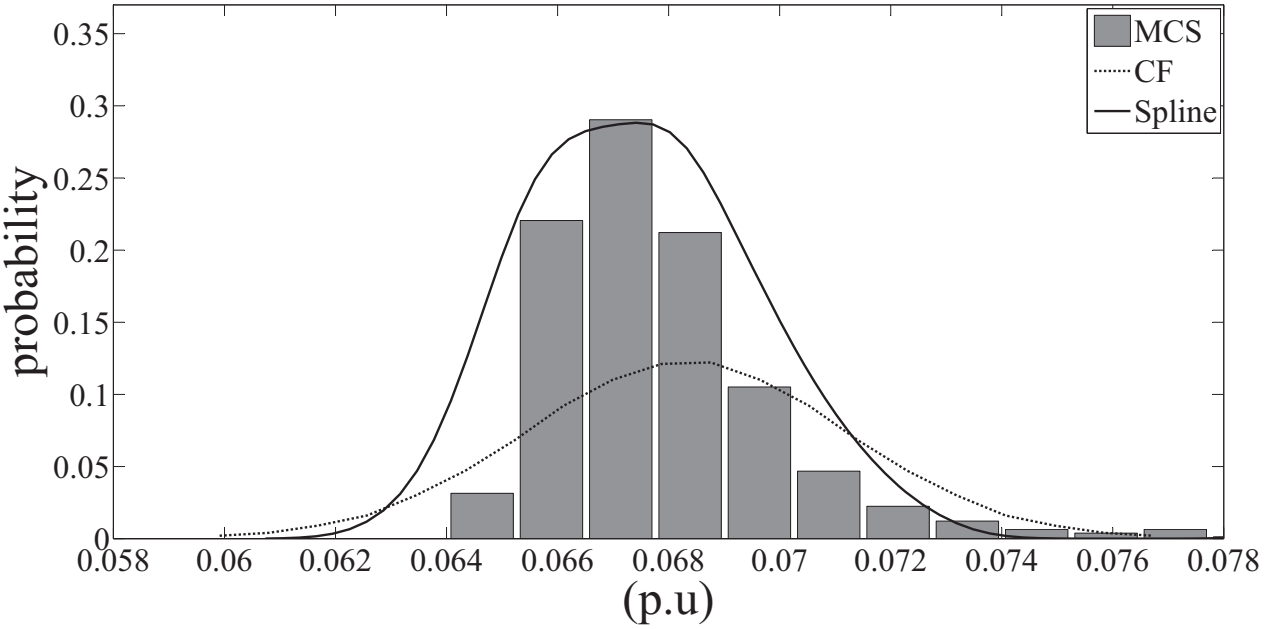

Figure 4.18: PDF of reactive power consumption at bus no. 113

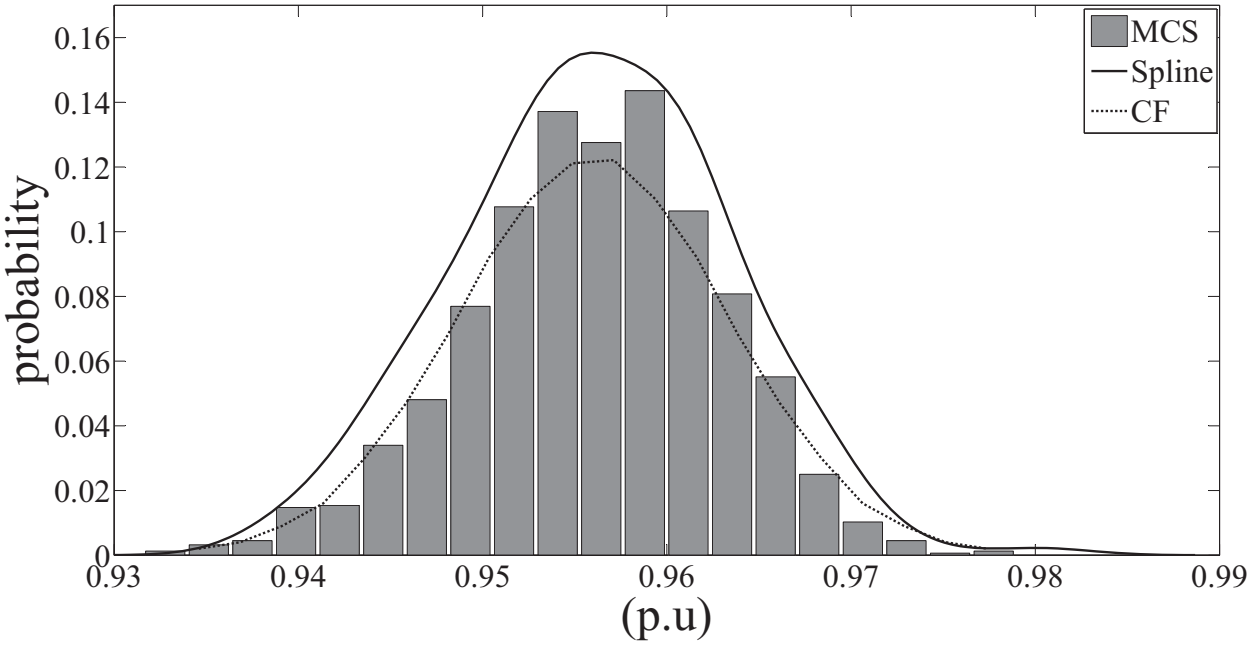

Figure 4.19: PDF of voltage at bus no. 247

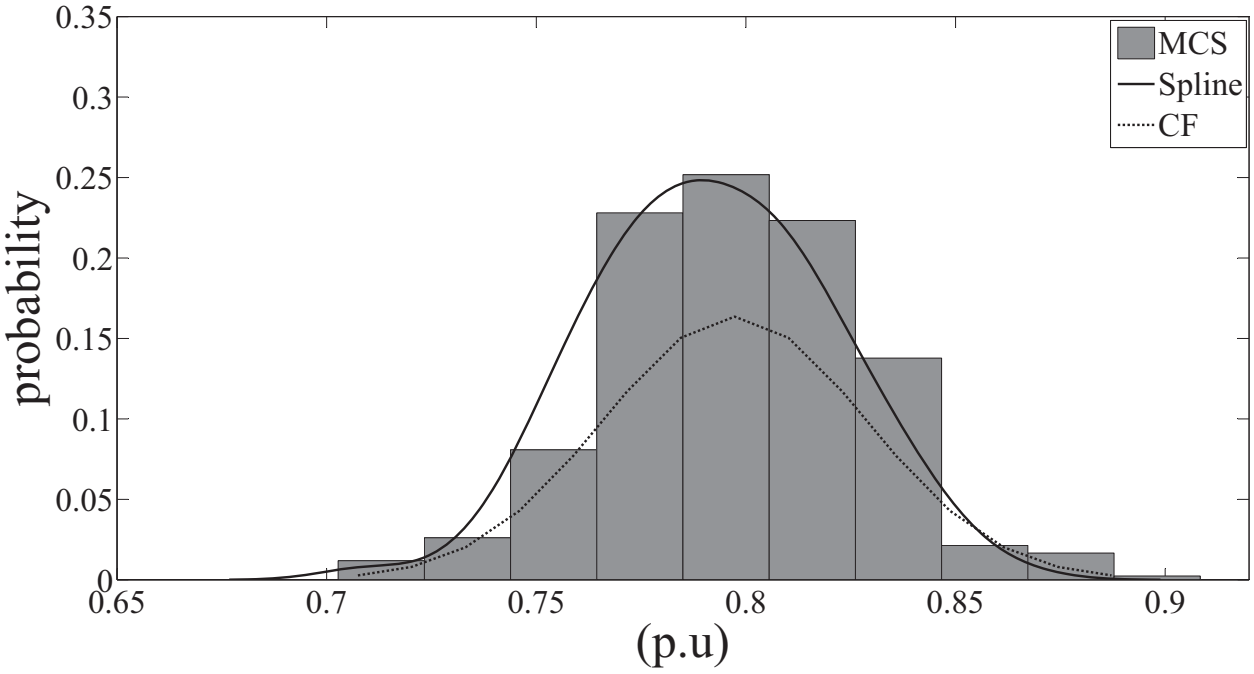

Figure 4.20: PDF of active power flow in line between bus no. 32 and 266

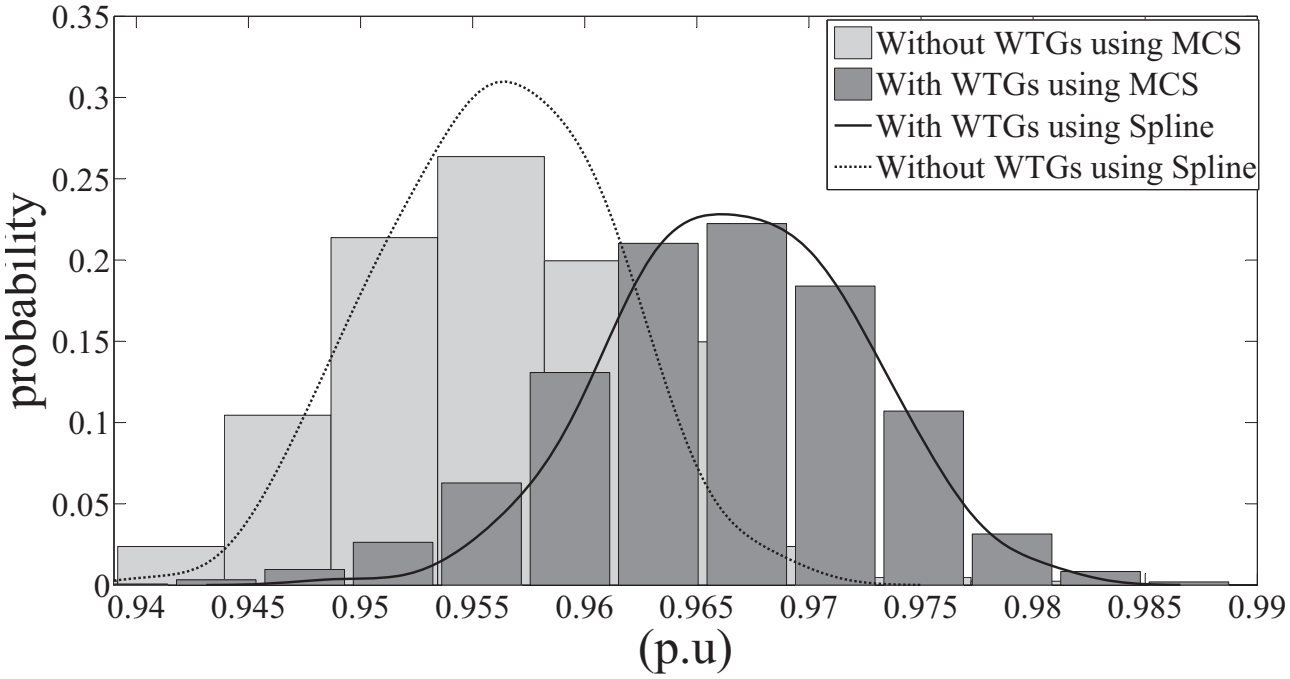

Figure 4.21: Voltage PDFs at the bus no 172 with and without WGT

4.5 Conclusion

In this chapter, 7PEM based PLF incorporating the uncertain wind generation into the power system has been explained in detail along with the different WTGs models. The correlation between the WTGs within the same wind farm and between the loads has also been taken into consideration. The validity of this method has been tested on the IEEE-118 and IEEE-300 bus systems with mixed loads (loads with normal and discrete PDFs). From the obtained results on the two systems, it can be concluded that spline based reconstruction technique in conjunction with 7PEM based PLF is suitable for carrying out probabilistic load flow studies on power systems with embedded wind power generation. With the integration of WTGs in the power system, reactive power management is an important issue. In the next chapter, a method for optimal reactive power planning having wind power generation in power systems has been proposed.

Chapter 5: Reactive power planning using PLF

In this chapter, an optimal probabilistic method for reactive power planning considering uncertain loads and intermittent wind generation is proposed. Four types of wind generator models have been considered in this work. The objective of the planning strategy adopted is to maximize the annual profit of the utility. To maximize the profit, a modified PSOGSA optimization technique has been developed. The performance of this developed technique has been compared with those obtained by GA, GSA and PSOGSA. Upon extensive simulation studies on the IEEE-30, IEEE-57 and IEEE-118 bus systems, it has been found that the performance of the modified PSOGSA technique is superior to those of other methods in terms of the value of the objective function and reproducibility of results.

It is well known that the optimal adjustment of the reactive power control devices such as shunt capacitors and transformer taps are required for the security and the economic operation of the power system which is accomplished by optimal reactive power planning (ORPP) [53–59, 98–100].

Linear-programming, decomposition techniques and heuristic technique for reactive power planning are reported in [53], [54] and [56] respectively, while, application of evolutionary programming and simulated annealing is proposed in [57] and [58]. An extensive review of reactive power planning techniques with objectives, constraints and different algorithms used, is given in [59].

However, in [53–59] the loads in reactive power planning problem are considered to be deterministic. It is to be noted that uncertainties always exist in the power system loads. A stochastic reactive power planning method considering the uncertainty of loads is described in [60–62].

However, in all the above works wind generation has not been considered. Now, because of random and wide variation of wind velocity, the power output from a wind turbine generator (WTG) is intermittent and of fluctuating nature. When this fluctuating power is injected into the grid, it causes variations in bus voltages and line power flows of transmission system. These variations are going to be quite significant in the future (if not already) because of significant and increasing penetration of WTGs in the grid. With the increase in the penetration of WTGs in the system, the reactive power planning has to be carried out considering the uncertainties of the wind power generation also.

However, in the literature, only one reference [64] has addressed this issue, in which a cumulant based stochastic reactive power planning technique for distribution system is proposed while considering high wind penetration in the distribution grid. However, a simple power injection model of the WTG has been considered and as a result, the reactive power absorbed by the WTG was not

accounted for in this work. Further, the loads have been assumed to be normally distributed and independent of each other. In the next section the reactive power planning strategy is discussed taking into account the above two issues. In the subsequent sections, the different optimization methods used in this work for solving the reactive power planning problem are discussed.

5.1 Reactive Power planning strategy

The basic objective adopted in this work for reactive power planning is to maximize the profit of the utility for the entire year, as described in eq. (5.1), by choosing appropriate values of the control variables (shunt capacitors and transformer taps). The profit of the utility is defined as the extra savings earned by the utility on account of reduction in power loss owing to the placement and installation of extra capacitors in the system and the choice of appropriate control variables minus the capital cost of the extra capacitors installed in the system. The reduction in loss is computed as the difference of loss in the base system (with only WTGs and the given settings of capacitors and transformer taps i.e. the uncoordinated system) and the augmented system (with WTGs and coordinated values of all the control variables along with the settings of the extra capacitors installed in the system (if any) i.e. with coordinated control variables). Consequently, mathematically the objective function can be expressed as;

$$max\left\{((P_b - P_c) \times E_n \times 8760) - (M_c \times C_w)\right\} \tag{5.1}$$

subject to:

$$\begin{aligned} pr(V_{min} \leq V^k \leq V_{max}) &\geq 0.9999 \,\forall\, k = 1, ...N \\ pr(Q^g_{min} \leq Q^g \leq Q^g_{max}) &\geq 0.9999 \,\forall\, g = 1, ...N_{gen} \\ pr(|I^l_{line}| \leq |I_{rated}|^l) &\geq 0.9999 \,\forall\, l = 1, ...nl \\ U^i_{min} \leq U_i \leq U^i_{max} &\,\forall\, i = 1, ...n_{ct} \end{aligned} \tag{5.2}$$

In the above expressions, $C_w = \sum_{i=1}^{nG} C_i$ is the total capacitive MVAR installed in the system, C_i is the MVAR required at i^{th} bus, nG is the number of buses where extra capacitors can be installed and is obtained as $nG = N - N_{gen} - N_{cap} - N_{trans}$, in which, N is the total number of buses in the system, N_{gen} is the total number of generator buses, N_{cap} is the total number of buses at which capacitors are already existing and N_{trans} is the total number of transformer buses. Further, E_n is the cost of energy/MWhr, M_c is the capital cost of capacitor/MVAR , P_b is the mean value of total power loss in the system with wind generators and the base values of the control variables

(uncoordinated system as given in system data), P_c is the mean value of total calculated power loss in the system with wind generators and the optimized values of the control variables, V^k is the voltage magnitude of k^{th} bus, Q^g is the reactive power generation of g^{th} synchronous generator, $|I^l_{line}|$ is the l^{th} line current magnitude and U_i is the i^{th} control variable. V_{min} and V_{max} are the minimum and the maximum values of the bus voltages respectively, Q^g_{min} and Q^g_{max} are the specified minimum and the maximum values of the g^{th} synchronous generator reactive power respectively, $|I_{rated}|^l$ is the rated value of the current magnitude in l^{th} line and U^i_{min} and U^i_{max} are the specified minimum and the maximum values of i^{th} control variables respectively. Also, $pr()$ denotes the probability of the event given inside the parenthesis. Lastly, nl and n_{ct} denote the number of lines and number of control variables in the system respectively.

5.2 Meta-heuristic optimization methods for reactive Power planning

Traditionally, classical techniques of optimization have been widely used in optimization problems. However, in modern power systems problems, the objective functions and constraints are complex, non-smooth and non-differentiable and therefore, classical approaches fail to deal with this situation satisfactorily. To overcome the drawback of classical techniques, evolutionary algorithms, such as genetic algorithm (GA) and gravitational search algorithm (GSA) have been applied for reactive power planning in [62] and [69] respectively. To further improve the performance of GSA, a new hybrid algorithm is proposed in [70] in which Particle Swarm Optimization (PSO) is combined with GSA. This new algorithm is called PSOGSA and the main idea is to integrate the ability of exploitation in PSO with the ability of exploration in GSA to combine the strengths of both the algorithms.

A brief review of different optimization algorithms used in the present work is given below.

5.2.1 Genetic algorithm

Genetic algorithm is an optimization algorithm based on the genetics and the mechanisms of natural selection [101]. A solution generated by genetic algorithm is called a chromosome, while collection of chromosome is referred to as a population. A chromosome is composed of genes and its value can be either numerical, binary, symbols or characters depending on the nature of the problem. GA based optimization methods are robust, and operate on the encoded string of the problem parameters rather than the actual parameters of the problem and each string of a chromosome completely describes one possible candidate solution to the problem. A population of solutions rather than a single solution is used by GA in its search, which allows it to explore several areas of the search space and reduce the

probability of finding local optima. It only requires the evaluation of the fitness function and assigns a quality value to every solution produced. Also, it does not require any prior knowledge or specific details of the function to be optimized (such as smoothness, convexity, unimodality, or existence of derivatives).

The main steps of GA are [102]:

1. Initial population generation:- Initially, a population of binary strings is randomly created, each of which represents one feasible solution, satisfying the given constraints.

2. Evaluation of fitness:- Each candidate solution is tested for the value of the fitness, i.e., the fitness values of the candidate solutions are evaluated.

3. Selection and reproduction:- It creates a new population from old one. In this step, two chromosomes are selected from the parent population based on their fitness values. Solutions with high fitness values have a high probability of contributing new offspring to the next generation. Some of the important selection procedures which have been proposed are roulette-wheel selection, stochastic universal selection, ranking selection and tournament selection [102].

4. Crossover:- The function of the crossover operator is to generate new or child chromosomes from two parent chromosomes by combining the information extracted from the parents. It involves swapping the bits after a position, which is chosen randomly in the two strings to be swapped. It can be done at a single position (single crossover), or at a number of different positions (multiple crossover). Typically, the probability for crossover ranges from 0.6 to 0.95.

5. Mutation:- This step is responsible for the injection of new information in the solution process. It involves selecting a string and a bit position (within a string) at random and changing it from 1 to 0 or vice-versa. This is generally done to escape from a local minima or maxima. The mutation is applied with a very small probability (between 0.0001 and 0.001) to every bit of the chromosome. After this, the new generation is complete and the procedure is started again with the evaluation of fitness of the population.

The flowchart of different steps of GA is shown in the Fig. 5.1. GA has been used extensively for solving power system optimization problems [103, 104]. Next, we discuss another meta-heustric optimization method, namely Gravitational search algorithm.

5.2.2 Gravitational search algorithm

The tendency of masses to accelerate towards each other is called gravitation and it acts between separated particles without any intermediary or delay. According to Newton′s law of gravity, each particle attracts other particle with a force (gravitational force), which is directly proportional to the product of their masses and inversely proportional to the square of the distance between them [105, 106].

$$F = G\left(\frac{M_1 M_2}{R^2}\right) \tag{5.3}$$

where, F is the gravitational force magnitude, M_1 and M_2 are the masses of the first and second particles, respectively, G is the gravitational constant, and R is the distance between the two particles.

Following Newton′s second law (eq. (5.4)), when a force F is applied to a particle, the magnitude of its acceleration a depends only on the force and its mass M.

$$a = \frac{F}{M} \tag{5.4}$$

Hence, from eqs. (5.3) and (5.4), there is an attracting gravitational force among all particles of the universe, in which the effect of the closer and the bigger particle is high as shown in Fig. 5.2. In this figure, a_1 is the acceleration caused by the overall force F_1 that acts on M_1 and F_{1j} is the force that acts on M_1 from M_j.

Also, the value of gravitational constant G depends on the actual age of the universe and is given by:

$$G(t) = G(t_0)\left(\frac{t_0}{t}\right)^{\beta}, \quad \beta < 1 \tag{5.5}$$

where, $G(t)$ and $G(t_0)$ are the gravitational constants at a time t and t_0 (at the beginning of the universe) respectively. Eq. (5.5) shows the reduction of gravitational constant with age, owing to the effect of reduction in gravity with time.

In GSA algorithm, the performance of the objects is measured by their masses which communicate with each other using gravitational force. The heavy masses move more slowly than the lighter ones and correspond to good solutions, which in turn improves the exploitation ability of the algorithm. In GSA, mass of each object has four specifications: position, inertial mass, active gravitational mass and passive gravitational mass.

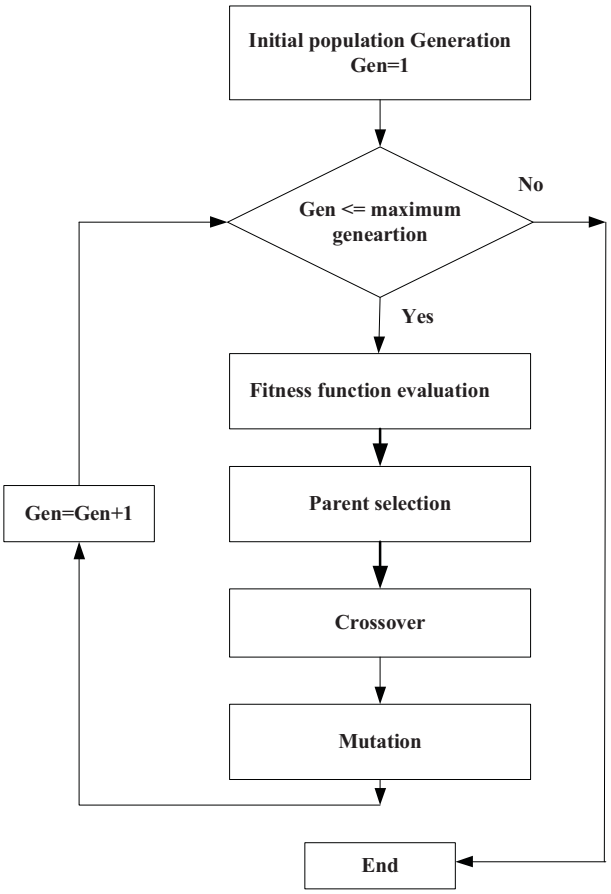

Figure 5.1: Flowchart of GA

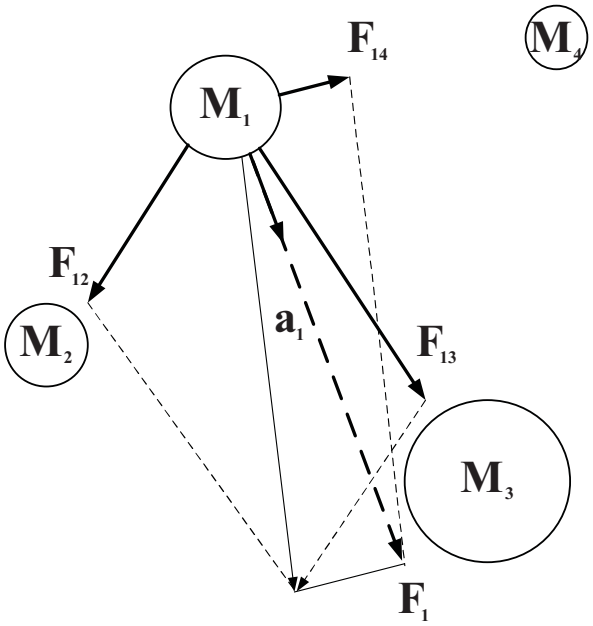

Figure 5.2: Acceleration of the mass along the resultant force that acts on it due to other nearby masses

Active gravitational mass (M_a) is the measure of the strength of the gravitational field due to a specific object. The object with large active gravitational mass has stronger gravitational field. The measure of the strength of an object's interaction with gravitational field is called passive gravitational mass (M_p). The object with a larger passive gravitational mass experiences a larger force. Inertial mass (M_i) is the measure of an object's resistance to change its state of motion, when a force is applied. The change in the motion of an object with a large inertial mass is less.

Now Newton′s first and the second law can be rewritten as:

$$F_{ij} = G\left(\frac{M_{aj}M_{pi}}{R^2}\right) \tag{5.6}$$

$$a_i = \frac{F_{ij}}{M_{ii}} \tag{5.7}$$

From eqs. (5.6) and (5.7), the gravitational force F_{ij} (exerted by mass j on mass i) is proportional to the product of the active gravitational mass of mass j (M_{aj}) and passive gravitational mass of mass i (M_{pi}), and inversely proportional to the square of the distance between them. Also, acceleration a_i is proportional to F_{ij} and inversely proportional to inertia mass M_{ii} of the mass i.

The position of each mass corresponds to a solution of the problem. The solution space is navigated by properly adjusting the inertial and gravitational masses (determined using a fitness function). The masses obey the following laws:

Law of gravity: As given in eq. (5.3) but R^2 in denominator is replaced by R [105].

Law of motion: The present velocity of any mass is equal to the variation in the velocity (calculated by using eq. (5.7)) and the sum of the fraction of its previous velocity.

Given a system with N agents (N number of masses), the position of i^{th} agent in search space (which represents a solution to the problem) is described as follows:

$$\boldsymbol{X_i} = \left(x_i^1, x_i^2, .., x_i^d, .., x_i^n\right), \quad \text{for } i = 1, 2, 3..., N \tag{5.8}$$

where, x_i^d represents the position of the i^{th} agent in the d^{th} dimension and n is the dimension of the problem in space.

The force acting on mass i due to mass j at any specific time t in the d^{th} dimension is given by:

$$F_{ij}^d(t) = G(t)\left(\frac{M_{aj}(t)M_{pi}(t)}{R_{ij}(t)+\epsilon}\right)\left(x_j^d(t) - x_i^d(t)\right) \tag{5.9}$$

$$R_{ij}(t) = ||x_i(t), x_j(t)||^2 \tag{5.10}$$

where, M_{aj} is the active gravitational mass of the agent j, M_{pi} is the passive gravitational mass of the agent i, $R_{ij}(t)$ is the Euclidian distance between i and j agents (as given in eq. (5.10)) at any specific time t. $x_i^d(t)$ and $x_j^d(t)$ are the positions of mass i and mass j respectively at any specific time t, $G(t)$ is the gravitational constant at time t, and ϵ is a small constant of the order of 10^{-16}.

The total force acting on agent i in the dimension d is a weighted (randomly using $rand_j$ in eq. (5.11)) sum of all the other d^{th} components of the forces exerted by the other agents as given in eq. (5.11).

$$F_i^d(t) = \sum_{j=1\ j\neq i}^{n} rand_j F_{ij}^d(t) \tag{5.11}$$

In eq. (5.11), $rand_j$ is randomly generated weight corresponding to agent j. Now, following the law of the motion, the acceleration $a_i^d(t)$ of agent i at time t in d^{th} dimension is given by:

$$a_i^d(t) = \frac{F_i^d(t)}{M_{ii}(t)} \tag{5.12}$$

The next step is to find the new velocity and position of the agent. The new velocity is obtained by adding the fraction of its current velocity to its current acceleration and the new position is the sum of the current position and next velocity of that agent. Given the velocity $v_i^d(t)$ and the acceleration $a_i^d(t)$ at time t the values of velocity and the position are calculated for the time instance $t+1$. These operations are written as:

$$v_i^d(t+1) = rand_i v_i^d(t) + a_i^d(t) \tag{5.13}$$

$$x_i^d(t+1) = x_i^d(t) + v_i^d(t+1) \tag{5.14}$$

where, $v_i^d(t)$ and $x_i^d(t)$ are the velocity and position of an agent at time t in d^{th} dimension respectively, and $rand_i$ is a random number (between [0,1]) to impart a randomized characteristic to the search.

The gravitational constant G is initialized randomly at the starting, and then it decreases with time i.e. G is a function of the initial value G_0 and time t and is given by:

$$G(t) = G_0 e^{-\alpha t/Iter_{max}} \tag{5.15}$$

where, G_0 is initial value of gravitational constant, α is a user specified constant and $Iter_{max}$ is the total number of iterations (analogous to the total age of system).

Gravitational and inertia masses are simply calculated by the fitness evaluation. A heavier mass means a more efficient agent concerning the solution it represents. The gravitational and inertial masses are assumed to be equal and are calculated as:

$$M_{ai} = M_{pi} = M_{ii} = M_i,\ i = 1, 2, ...N \tag{5.16}$$

$$m_i(t) = \frac{fit_i(t) - worst(t)}{best(t) - worst(t)} \tag{5.17}$$

$$M_i(t) = \frac{m_i(t)}{\sum_{j=1}^{N} m_j(t)} \tag{5.18}$$

where, $fit_i(t)$ represents the fitness value of the agent i at time t, $best(t)$ and $worst(t)$ represent the strongest and weakest agents respectively (with regard to their fitness). For a minimization and maximization problems, $best(t)$ and $worst(t)$ are calculated using eqs. (5.19) and (5.20) respectively.

$$\begin{aligned} best(t) &= \min_{j\in\{1,2...,N\}} (fit_j(t)) \\ worst(t) &= \max_{j\in\{1,2...,N\}} (fit_j(t)) \end{aligned} \tag{5.19}$$

$$\begin{aligned} best(t) &= \max_{j\in\{1,2...,N\}} (fit_j(t)) \\ worst(t) &= \min_{j\in\{1,2...,N\}} (fit_j(t)) \end{aligned} \tag{5.20}$$

To avoid the algorithm from getting trapped in a local optimum, the exploration must be used at beginning. As the iterations proceed exploration must fade out and exploitation must fade in. The performance of GSA is improved by controlling exploration and exploitation only when the K_{best} agents will attract the others. K_{best} is a function of time, with an initial value K_0 at the beginning and decreasing with time. In such a way, at the beginning, all agents apply the force, and as time passes, K_{best} is decreased linearly and at the end there will be just one agent applying force to the others. Therefore, eq. (5.11) could be modified as:

$$F_i^d(t) = \sum_{j\in K_{best}}^{N} \sum_{j\neq i} rand_j F_{ij}^d(t) \tag{5.21}$$

where, K_{best} is the set of first K_0 agents with the biggest mass and best fitness value. The steps of GSA are shown in the flowchart given in Fig. 5.3.

The steps for applying GSA to the reactive power planning problem of a power system are explained next. The control variables in this case are reactive power outputs of the shunt capacitors and tap positions of the tap changing transformers. These control variables constitute the individual position of masses in a complete solution set.

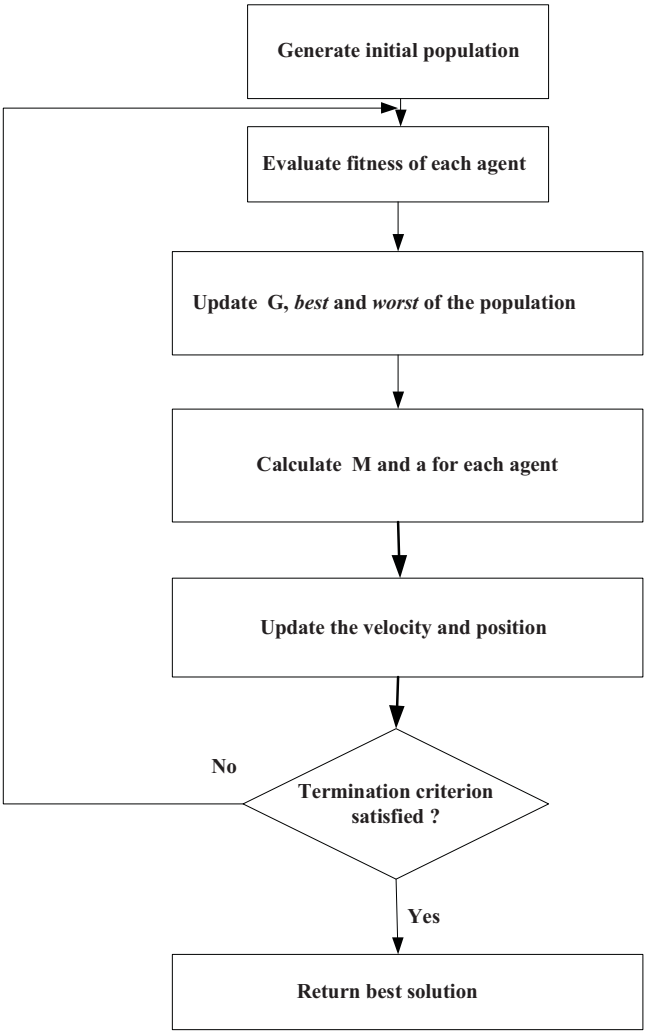

Figure 5.3: The flowchart of GSA method

Let us consider that there are N number of masses and position of any agent i is given by eq. (5.8). The agent matrix formed by several agents together is given as:

$$\boldsymbol{X} = \begin{bmatrix} x_1^1 & x_1^2 & \dots & x_1^d & \dots & x_1^n \\ x_2^1 & x_2^2 & \dots & x_2^d & \dots & x_2^n \\ \vdots & \vdots & \ddots & \vdots & \ddots & \vdots \\ x_i^1 & x_i^2 & \dots & x_i^d & \dots & x_i^n \\ x_N^1 & x_N^2 & \dots & x_N^d & \dots & x_N^n \end{bmatrix} \tag{5.22}$$

The different steps to be taken to solve this problem are:

1. Initialize G_0, α and $Iter_{max}$

2. The initial position of each agent is randomly selected within the specified lower and upper bounds of control variables. A total of N numbers of agents are generated (as given in eq. (5.22)) in which each set represents a potential solution.

3. Run the PEM based PLF using each individual set of the agent matrix to check whether the obtained solution satisfies the inequality constraints of eq. (5.2) or not. Discard the corresponding population set if it does not satisfy these constraints and re-initialize such an agent set.

4. Calculate the fitness function value of an agent set using eq. (5.1) for each member of matrix $\boldsymbol{X}$.

5. For each set of agents, update the values of $G(t)$, $best(t)$, $worst(t)$ and $M_i(t)$.

6. Calculate the total force on i^{th} agent in different directions using eq. (5.21).

7. Obtain the acceleration and velocity of each agent using eqs. (5.12) and (5.13) respectively and update the position of each agent using eq. (5.14).

8. Repeat steps 2 to 7 until the maximum number of iterations are performed. The algorithm returns the values of positions of the corresponding agent set at specified dimensions in the final iteration (i.e position of transformer taps and reactive power injected by the capacitors) which is the best solution of the optimization problem.

However, to improve the performance of GSA, PSOGSA is proposed in [70] which combines the property of the exploitation in PSO and exploration in GSA i.e. it combines the strength of both the algorithms.

5.2.3 PSOGSA method for optimization

Particle swarm optimization is an evolutionary computation technique proposed by Kennedy and Eberhart [107] and is motivated by the social behavior of flock of birds. It uses a number of particles as candidate solutions which move in the search-space. The movements of these particles are guided by their own best known position in the search-space as well as the entire flock′s best known position. It is mathematically modeled as:

$$x_i^d(t+1) = x_i^d(t) + v_i^d(t+1) \tag{5.23}$$

$$v_i^d(t+1) = w(t)v_i^d(t) + c_1 r_{i1}\left(pbest_i^d - x_i^d(t)\right) + c_2 r_{i2}\left(gbest^d - x_i^d(t)\right) \tag{5.24}$$

where, r_{i1} and r_{i2} are the random variables in the range [0,1], $w(t)$ is the inertia weight, c_1 and c_2 are positive constants, $v_i^d(t)$ and $x_i^d(t)$ are the velocity and position of an agent at time t in d^{th} dimension respectively. $\boldsymbol{X_i} = (x_i^1, x_i^2, .., x_i^d, ..x_i^n)$ and $\boldsymbol{V_i} = (v_i^1, v_i^2, .., v_i^d, ..v_i^n)$ represent the position and velocity of i^{th} particle, respectively. $pbest_i = (pbest_i^1, pbest_i^2, ..., pbest_i^n)$ and $gbest = (gbest^1, gbest^2, ..., gbest^n)$ represents the best previous position of i^{th} particle and best previous position among all the particles in the population, respectively.

In eq. (5.24), the first term $w(t)v_i^d(t)$ provides the exploration ability to PSO, while the second term $c_1 r_{i1}\left(pbest_i^d - x_i^d(t)\right) + c_2 r_{i2}\left(gbest^d - x_i^d(t)\right)$ represents private thinking and collaborations of particles respectively. In PSO, the particles are placed randomly in a problem space and velocities of particles are calculated in each iteration, and subsequently position of masses are calculated using eq. (5.23) i.e, each particle tries to modify its position ($\boldsymbol{X_i}$) using the distance between the current position and $pbest_i$, and the distance between the current position and $gbest$. In power system applications, various versions of PSO have been successfully used [108–114].

PSOGSA, is a low-level co-evolutionary heterogeneous hybrid optimization method [70]. It combines the functionality of PSO and GSA algorithms which run in parallel, to produce the final result. The basic idea is to combine the ability of social thinking ($gbest$) in PSO with the local search capability of GSA. The velocity of i^{th} agent at time $t+1$ is found out as:

$$v_i^d(t+1) = w(t)v_i^d(t) + c_1' \times rand_i \times a_i^d(t) + c_2' \times rand_i' \times \left(gbest^d - x_i^d(t)\right) \tag{5.25}$$

Next, the position of the i^{th} agent at time $t+1$ is calculated as:

$$x_i^d(t+1) = x_i^d(t) + v_i^d(t+1) \tag{5.26}$$

where, $v_i^d(t)$ is the velocity and $x_i^d(t)$ is the position of agent i at iteration t in d^{th} dimension, c_j' is the weighting factor and $rand_i$ and $rand_i'$ are the random numbers between 0 and 1, $w(t)$ is the weighting function and a_i^d is the acceleration of i^{th} agent in d^{th} dimension at iteration t.

In this method, initially, all agents are initialized randomly and are considered as potential candidate solutions. Next, the gravitational force, resultant forces among agents, the acceleration of the particles and the gravitational constant are calculated using eqs. (5.9), (5.11), (5.12) and (5.15) respectively. Best solution obtained so far should be updated in each iteration and the velocities and

positions of the agents are updated using eqs. (5.25) and (5.26) respectively. The process of updating velocities and positions continues till the stopping criterion is met. The flowchart of PSOGSA method is given in Fig. 5.4

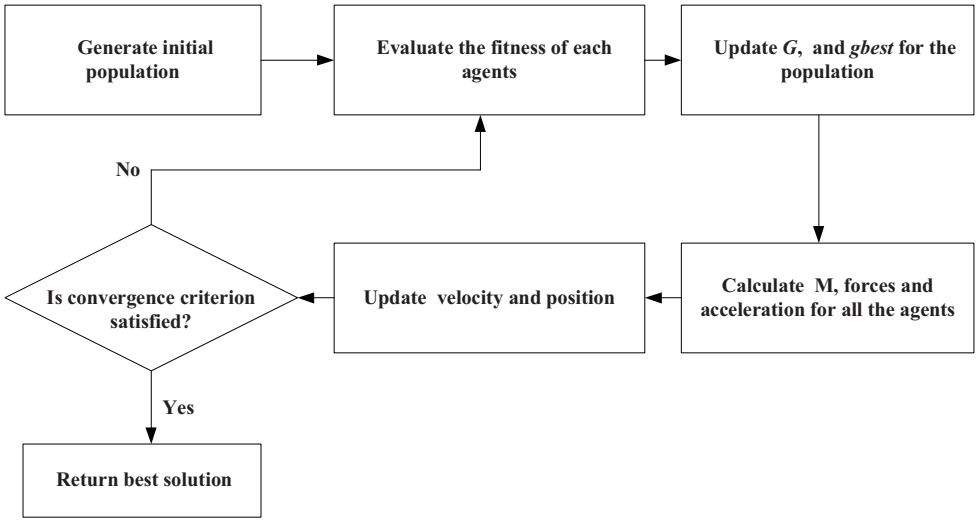

Figure 5.4: Flowchart of PSOGSA

In this work, all the three methods, namely, GA, GSA and PSOGSA have been applied for solving the reactive power planning problem. However, as will be shown in the next section, all these three methods suffer from the problem of repeatability, i.e. if these techniques are run repeatedly, they tend to produce different results on each run. To overcome this limitation, in this work a new modified PSOGSA (henceforth termed as MPSOGSA) is proposed.

The steps involved in MPSOGSA are as follows:

Step 1: Generate initial population of size N and initialize the velocity and acceleration. Set $count\_temp = 0$, $count\_gsa = 0$ and sys_best to a low value for maximization problem or to a high value for a minimization problem.

Step 2: If $(count\_gsa <= iter\_f)$ then proceed to step 3, else stop and print final result.

Step 3: If $(count\_gsa > iter\_m)$ then go to step 4, else go to step 5.

Step 4: Mutate the best agent obtained so far.

Step 5: Evaluate all the agents in the population.

Step 6: Is the best solution obtained in step 5 better than sys_best ? if so, go to step 7, else go

to step 8.

Step 7: Update sys_best with the best solution and set $count\_temp = 0$ and $count\_gsa = 0$. Go to step 9.

Step 8: Update $count\_temp = count\_temp + 1$ and $count\_gsa = count\_gsa + 1$.

Step 9: Update the velocity and position of all the agents in the population.

Step 10: If $(count\_temp >= iter\_N)$ then go to step 11, else go back to step 2.

Step 11: Create a new population of size N-1 and add the best solution obtained so far to this population. Go back to step 2.

As can be seen from above discussion, the heart of MPSOGSA is the basic PSOGSA. However, for preventing the solution from being stuck in the local optimum, two additional operations are introduced;

i) Generation of a new population, retaining the best solution obtained so far, if the solution does not improve for '$iter\_N$' number of iterations and

ii) Applying mutation to the best solution obtained so far if it does not improve for '$iter\_m$' iterations.

In this work the values of $iter\_f = 20,\ iter\_m = 10,\ iter\_N = 5$ and N = 15 have been used. The flowchart of MPSOGSA method is given in Fig. 5.5.

5.3 Results and discussion

For reactive power planning, all the wind generator models described in Section 4.2 of Chapter 4 have been incorporated in PLF. The PLF has been solved by using 7PEM method. For investigating the feasibility of the proposed method, some loads have been considered as correlated and the correlation between WTGs has also been considered. It is to be noted that any correlation between the WTGs and loads has been neglected in this work. All the studies in this work have been carried out on the IEEE-30, IEEE-57 and IEEE-118 bus systems [80]. In this work, a total of 2, 4 and 10 wind farms have been considered for IEEE-30, IEEE-57 and IEEE-118 bus systems respectively.

For IEEE-30 bus system, the two wind farms are assumed to be located at bus no. 23 (PQ type) and 24 (Pitch Regulated type). For IEEE-57 bus system, the four wind farms are assumed to be connected at bus no. 37 (PQ type), 38 (Pitch regulated type), 39 (Semi variable speed type) and 40 (DFIG). Lastly, the 10 farms for IEEE-118 bus system have been assumed to be located at the

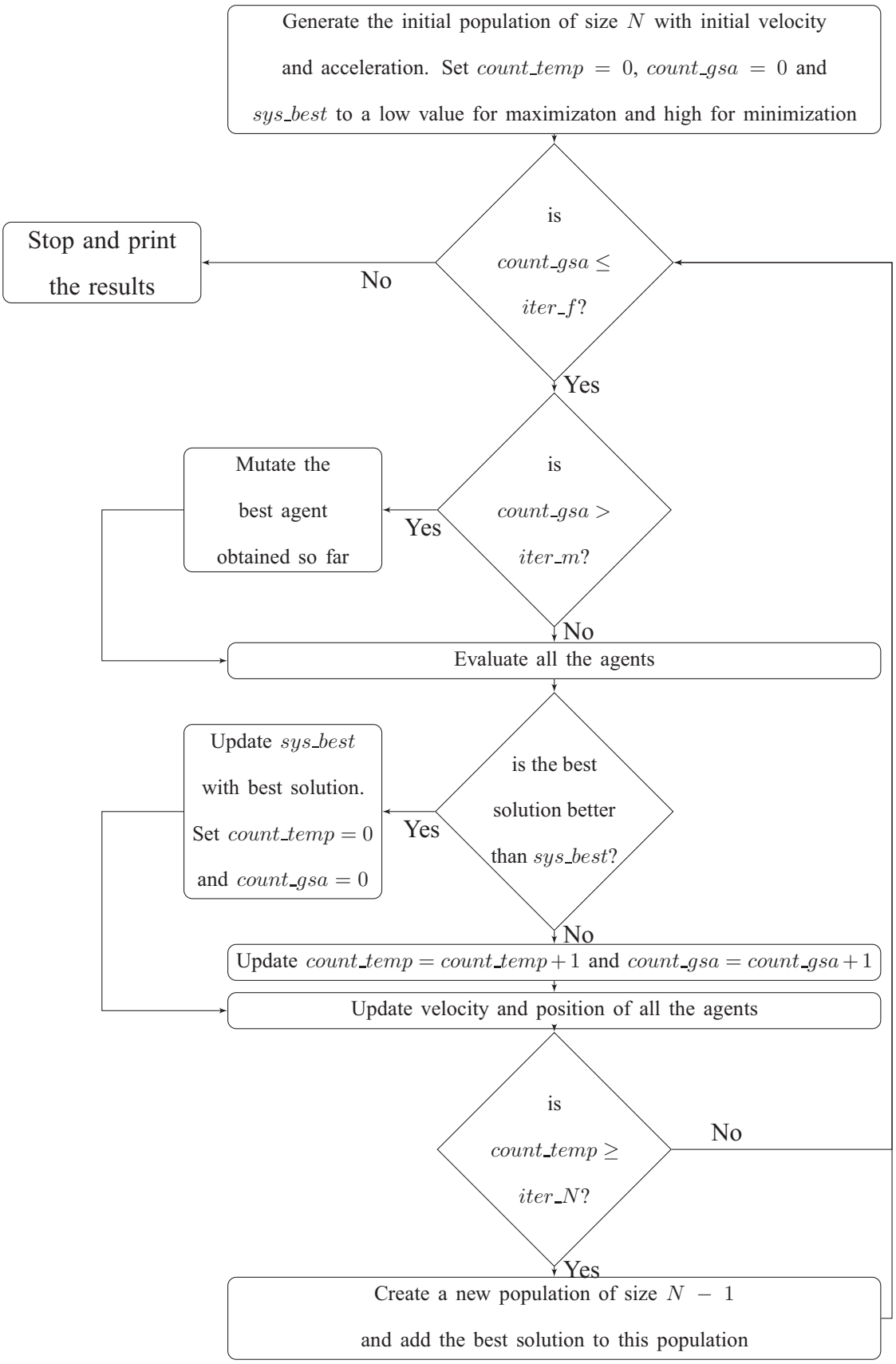

Figure 5.5: Flowchart of MPSOGSA technique

following 10 buses: 94 to 98, 108, 109, 114, 115, 117. The details of these wind farms for IEEE-118 bus system are given in Table 4.1.

It is to be noted that for both IEEE-30 and IEEE-57 bus system, the rating and number of WTGs in each type of wind farm have been assumed to be the same as given in Table 4.1. The wind turbine power curve parameters have been assumed to be the same as discussed in Section 4.4 of Chapter 4.

For modeling the load uncertainties, a non-normal PDF for the load active and reactive powers has been assumed at bus nos. 1 to 15 of IEEE-30 bus system, at bus nos. 1 to 20 of IEEE-57 bus system and at bus nos. 1 to 50 of IEEE-118 bus system. This PDF represents the PDF of IEEE Reliability test system hourly load data [85]. Further, for the loads at the remaining buses of these systems, a normal PDF has been assumed with a standard deviation of 10% of the mean value of load (which is increased to 1.5 times the base load data). This enhancement of load from base loading condition has been done to simulate the possible future scenario of the load. The loads at bus nos. 16 to 19, 20 to 23 and 81 to 84 for IEEE-30, IEEE-57 and IEEE-118 bus system respectively, have been assumed to be correlated with each other and the correlation matrix is given in eq. (3.22).

Towards the reactive power planning for the whole year, initially, the mean value of power loss (P_b) in the base case probabilistic load flow including WTGs has been calculated with the settings of capacitors and transformer taps as given in [80]. Subsequently, the objective function given in eq. (5.1) has been maximized by using GA, GSA, PSOGSA and MPSOGSA. In this case the decision variables are the the taps of the transformers already existing in the system (at the locations given in [80]) and the values of capacitor MVARs to be installed at the buses, as explained in Section 5.1. Hence, the total number of decision variables for IEEE-30, IEEE-57 and IEEE-118 bus system are 23, 41 and 58 respectively. The minimum and maximum voltage limits have been taken as 0.95 and 1.05 p.u respectively. The minimum and maximum transformer tap settings have been taken as 0.90 and 1.10 respectively, with a step of 0.01. The capacitor cost has been taken as 90 USD/kVAR [64] and energy cost has been taken as 0.09 USD/kWhr. The range of MVAR injected at buses is [0 2] p.u with a step of 0.05 p.u. All the decision variables have been taken as discrete variables.

As the optimization algorithm proceeds, the variables are checked for constraints given in eq. (5.2). The probability of variables remaining within the limits is obtained by finding the area under the PDF between the minimum and the maximum limits. The PDF is obtained using Cornish-Fisher expansion series with the help of the moments calculated by 7PEM. It is to be noted that in this chapter, spline based technique has not been used for reconstructing the PDF as it is quite computational intensive method. Now, in GA, GSA, PSOGSA and MPSOGSA, the algorithm runs for several gen-

erations and in each generation, several candidate solutions (depending upon the population size) need to be evaluated. Therefore, if spline based reconstruction technique is used to determine the PDF for each candidate solution in every generation, then the overall time taken by either of these four heuristic methods for determining the final solution would be prohibitively large. To reduce this overall time required for finding the solution, Cornish-Fisher expansion series has been used in this chapter instead of spline based technique. After the PDF is obtained, the area between the minimum and the maximum limits is calculated. If this area is more than the threshold limit (0.9999 as given in eq. (5.2)), then the solution is considered to be acceptable, otherwise not.

For GA, the following parameters have been chosen: maximum generation = 150, population size = 20, mutation rate = 0.90, crossover rate = 0.20, while for GSA, PSOGSA and MPSOGSA, the parameters chosen are: population size = 20, weighting factor C_1 = 0.5, weighting factor C_2 = 1.5, maximum iteration = 150.

Each of these four methods has been executed three times to investigate the repeatability of the solutions. Tables 5.1, 5.2 and 5.3 show the fitness function values obtained for these four methods corresponding to these three runs for IEEE-30, IEEE-57 and IEEE-118 bus system respectively.

Table 5.1: Final values of fitness function for three runs in IEEE-30 bus system

Run no.	**GA**	**GSA**	**PSOGSA**	**MPSOGSA**
1	1.193e+009	2.927e+008	2.595e+009	2.828e+009
2	1.623e+009	3.301e+008	2.545e+009	2.828e+009
3	1.429e+009	2.577e+007	2.696e+009	2.828e+009

Table 5.2: Final values of fitness function for three runs in IEEE-57 bus system

Run no.	**GA**	**GSA**	**PSOGSA**	**MPSOGSA**
1	4.332e+009	1.028e+009	5.028e+009	5.570e+009
2	4.183e+009	1.017e+009	5.201e+009	5.570e+009
3	4.212e+009	1.030e+009	4.395e+009	5.570e+009

It is observed from these tables, that for different runs of GA, GSA and PSOGSA, the fitness

Table 5.3: Final values of fitness function for three runs in IEEE-118 bus system

Run no.	GA	GSA	PSOGSA	MPSOGSA
1	7.521e+009	6.040e+009	9.214e+009	1.070e+010
2	7.428e+009	6.002e+009	9.086e+009	1.070e+010
3	7.841e+009	5.018e+009	9.148e+009	1.070e+010

function has different values, while MPSOGSA always produces the same result. Further, it is also observed from these tables that among these four methods, MPSOGSA technique gives the maximum value of the profit earned by the utility in each case for the three systems studied.

Figs. 5.6, 5.7 and 5.8 show the variations of the objective functions with iterations for all these four methods corresponding to the three test systems, respectively.

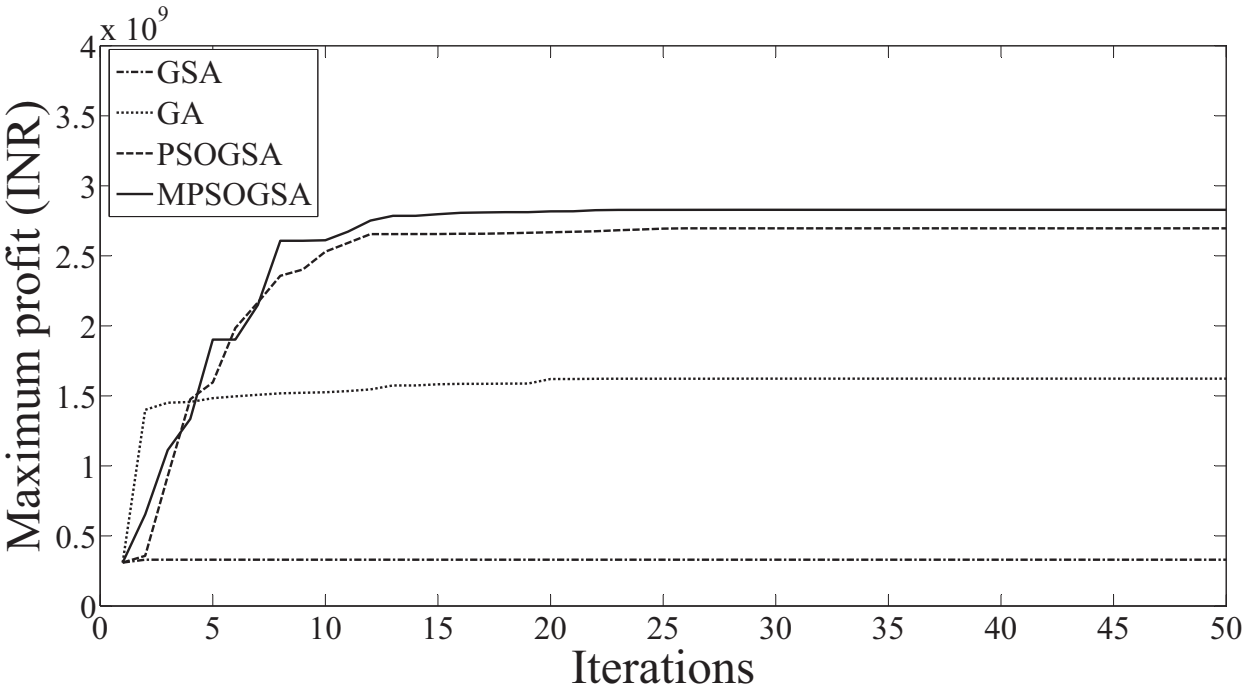

Figure 5.6: Convergence characteristics of different optimization methods for IEEE-30 bus system

It can be seen from these figures that, in all the cases the value of objective function obtained by MPSOGSA is better than the value of the objective function given by the other three methods i.e. GA, GSA and PSOGSA. Therefore, MPSOGSA is found to be the most suitable method in this work as it gives the best value of the objective function while maintaining the repeatability of the results. It is to be noted that in Tables 5.1, 5.2 and 5.3 and Figs. 5.6, 5.7 and 5.8, the values of the

objective function are given in Indian Rupees (INR), by assuming the USD-INR exchange rate as 60 INR/USD.

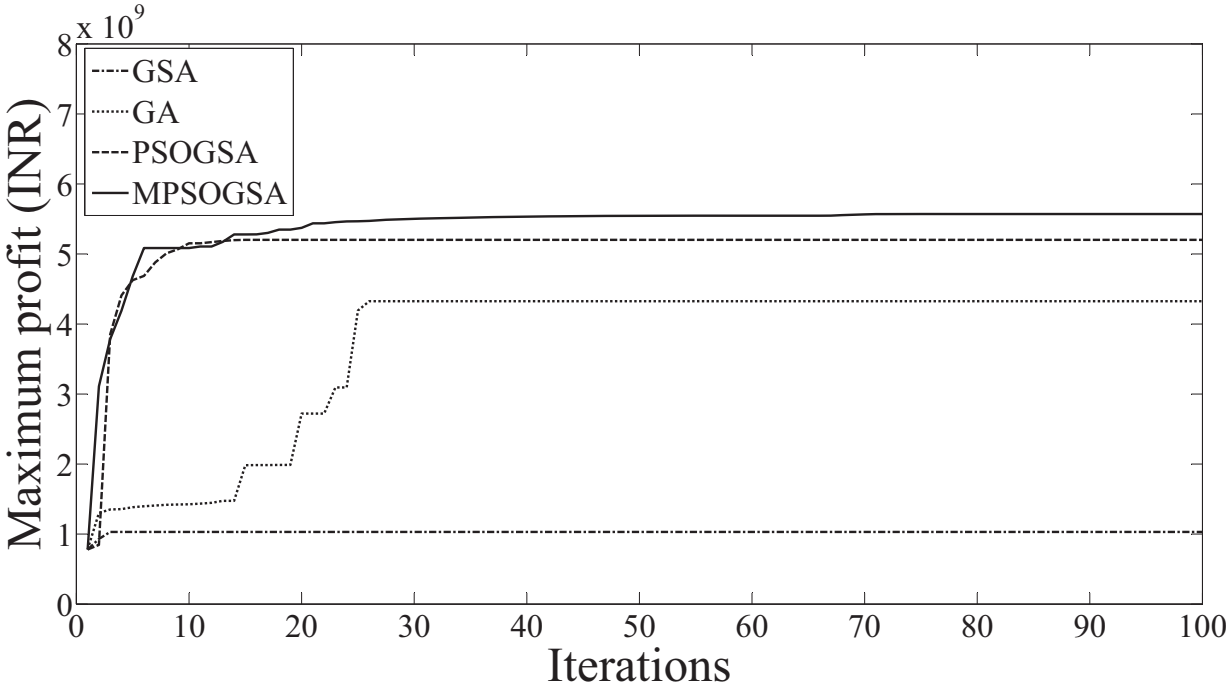

Figure 5.7: Convergence characteristics of different optimization methods for IEEE-57 bus system

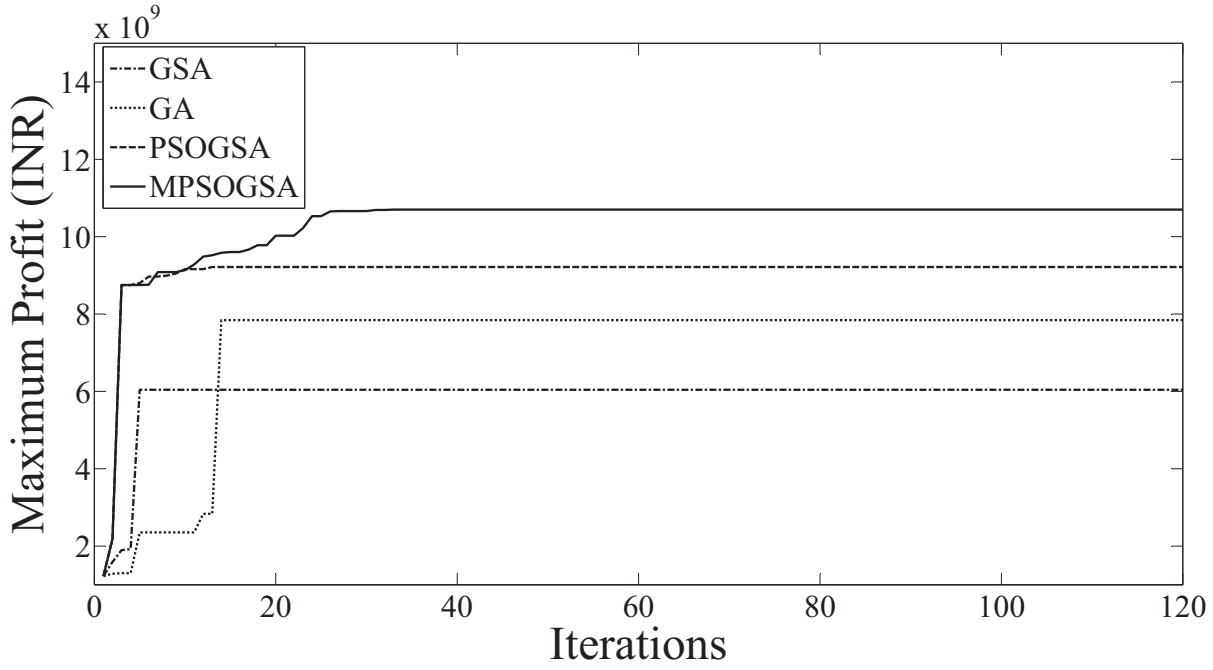

Figure 5.8: Convergence characteristics of different optimization methods for IEEE-118 bus system

The final values of the decision variables (obtained by MPSOGSA) for IEEE-30, IEEE-57 and IEEE-118 bus system are given in Tables 5.4, 5.5 and 5.6 respectively, in which C_i is the value of MVAR injected at i^{th} bus (in p.u) and T_{k-j} is the value of transformer tap settings connected between the k^{th} and j^{th} bus. Only the decision variables with non-zero values are given in these tables.

Table 5.4: Decision variables for IEEE-30 bus system obtained using MPSOGSA

Decision variables	**Final value**	**Decision variables**	**Final value**
C_{21} (p.u)	0.05	T_{9-10}	0.92
T_{6-9}	1.04	T_{4-12}	0.92
T_{6-10}	0.94	T_{12-13}	0.94
T_{9-11}	1.04	T_{27-28}	0.97

Table 5.5: Decision variables for IEEE-57 bus system obtained using MPSOGSA

Decision variables	**Final value**	**Decision variables**	**Final value**
T_{4-17}	0.92	T_{41-43}	1.08
T_{4-18}	0.92	T_{15-45}	0.92
T_{21-20}	1.08	T_{14-46}	0.92
T_{24-23}	0.92	T_{10-51}	0.92
T_{24-25}	0.92	T_{13-49}	0.92
T_{24-26}	1.01	T_{11-43}	0.92
T_{7-29}	0.92	T_{40-56}	1.08
T_{34-32}	0.92	T_{39-57}	1.08
T_{11-41}	0.92	T_{9-55}	0.94

The effect of the adopted reactive power planning strategy on the bus voltage for IEEE-30 bus system is shown in Fig. 5.9 in which the PDFs of voltage magnitude at bus 7 (as a representative case) with coordinated control variables (after implementing the settings of the capacitors and

the transformer taps obtained by the optimization algorithm) and with base values of the control

Table 5.6: Decision variables for IEEE-118 bus system obtained using MPSOGSA

Decision variables	**Final value**	**Decision variables**	**Final value**
C_3 (p.u)	0.15	C_{96} (p.u)	0.05
C_4 (p.u)	0.1	C_{101} (p.u)	0.3
C_8 (p.u)	0.1	C_{102} (p.u)	0.1
C_{22} (p.u)	0.25	C_{109} (p.u)	0.2
C_{23} (p.u)	0.05	C_{114} (p.u)	0.05
C_{29} (p.u)	0.3	C_{117} (p.u)	0.1
C_{30} (p.u)	0.05	C_{118} (p.u)	0.3
C_{36} (p.u)	0.3	T_{9-6}	1.06
C_{52} (p.u)	0.25	T_{27-26}	0.95
C_{58} (p.u)	0.15	T_{65-62}	1.07
C_{61} (p.u)	0.3	T_{66-67}	1.08
C_{78} (p.u)	0.15	T_{69-1}	1.07
C_{84} (p.u)	0.3	T_{81-80}	1.0
C_{88} (p.u)	0.05	T_{31-18}	1.07
C_{93} (p.u)	0.05	T_{39-38}	1.08
C_{94} (p.u)	0.25	T_{64-60}	1.05

variables are compared. The PDF of bus voltage magnitude has been obtained using spline based reconstruction technique.

From this figure, it is observed that for the uncoordinated case, the probability that the bus voltage violates the lower limit (of 0.95 p.u) is high, while for the coordinated control case, the entire PDF of bus voltage magnitude lies well within the limits and the probability of limits being violated is practically zero. Further, a marked improvement in the expected value of bus voltage magnitude can

also been seen indicating an improvement in the system voltage profile. Similar trends in the voltage magnitude PDFs at bus no. 18 and bus no. 53 (shown in Figs. 5.10 and 5.11), are observed for IEEE-57 and IEEE-118 bus system respectively (taken as representative cases).

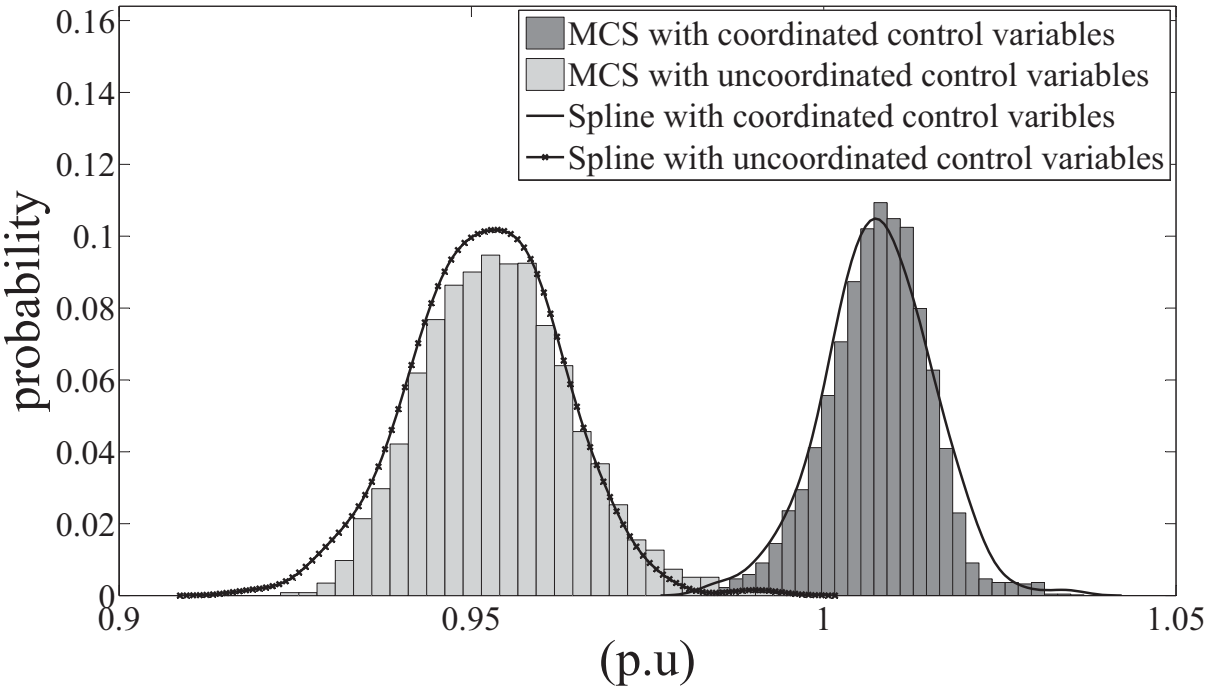

Figure 5.9: Voltage magnitude PDF at bus no. 7 with coordinated and uncoordinated control variables in IEEE-30 bus system

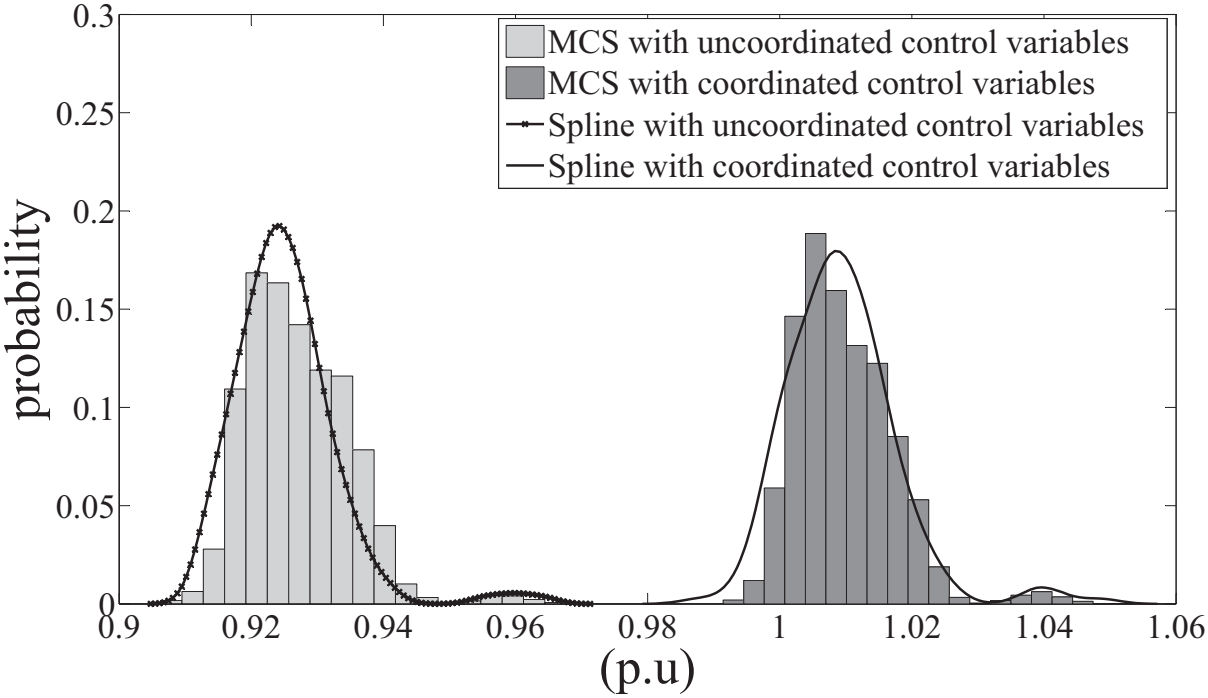

Figure 5.10: Voltage magnitude PDF at bus no. 18 with coordinated and uncoordinated control variables in IEEE-57 bus system

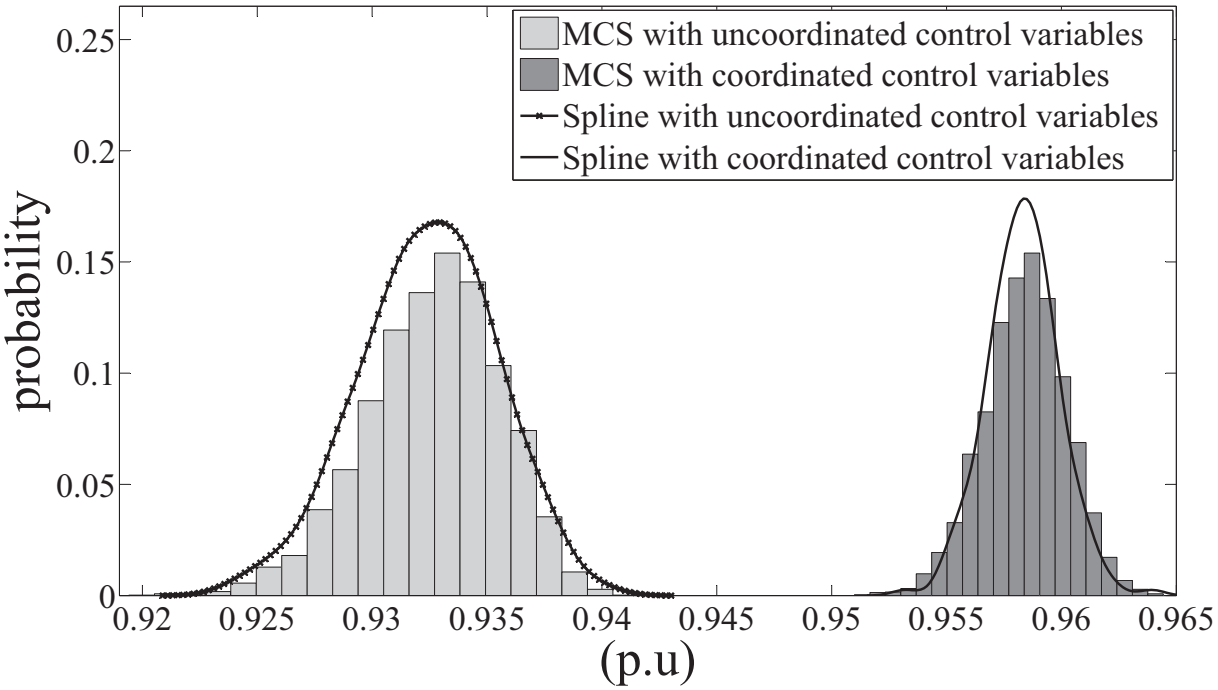

Figure 5.11: Voltage magnitude PDF at bus no. 53 with coordinated and uncoordinated control variables in IEEE-118 bus system

Therefore, the developed reactive power planning strategy will help the utilities to maximize their profits when WTGs are connected to the system, while operating their systems within various system constraints in the face of uncertainties.

5.4 Conclusion

In this chapter, a stochastic reactive power planning strategy is proposed to maximize the profit of the utility while satisfying the operating constraints of the power system in the presence of WTGs and various uncertainties in the system. Further, to solve the optimization problem a modified version of PSOGSA has also been proposed. From the studies carried out on three different power systems, it is concluded that the proposed MPOGSA technique gives the best result in terms of maximum profit of the utility and repeatability as compared to GA, GSA and PSOGSA. So far in this work, neither line nor generator outage has been considered. Hence, in the next chapter, line and generator outages are been considered in PEM based PLF method.

Chapter 6: PLF considering generator and line outages

In this chapter, generator and line outages have been incorporated in the PEM based PLF for the contingency analysis of power system. The method has been validated on IEEE-30 and IEEE-118 bus systems with WTGs considering generator and line outages.

In the previous chapters, the network configuration of the power system has been assumed to be fixed and, consequently, the probability of the basic configuration of the system has been assumed to be unity, and the probability of losing any network element, such as transmission line, transformer, generator etc., has been neglected. However, changes do occur in the network configuration because of generator and line outages owing to faults, overloads and routine maintenance. Hence, the assumption of fixed constant network configuration is unrealistic, particularly when the power generation and load uncertainties are significant.

Any change in the power system configuration will alter the set of functions relating inputs and outputs and, consequently, probability distributions (PDF and CDF) of output variables will change. This may have a significant effect on technical and economic decisions related to the power system. To compute the new probability distributions of the output variables, the outages need to be modeled. The outages are modeled as random variables and as a result, each network configuration has an associated probability of occurrence [67]. To calculate the probabilities of occurrence of different network configurations, probabilistic models of generators and transmission line outages are required which are discussed next.

6.1 Modelling of generator outage

If the generators are considered as 100% reliable, then they have only one state i.e. the state in which generator is generating its rated output. Such generators deliver their full output with a probability equal to unity. In this work, small generators have been modelled as single-state generators. In practice, the generators have finite failure probabilities. In the simplest form, a generator can be modelled as a two-state component having an up state (rated output state) and a down state (zero output state) with both the states having finite probability of occurrence such that the sum total of the probabilities corresponding to these two states is equal to unity.

The basic parameter representing the outage characteristic of a generator is its forced outage rate (FOR), the probability of generator being in down state which is generally denoted by q [21]. Let the capacity of i^{th} generator be C_i MW and its FOR be q_i, then pr^{gen}, the probability of generation

capacity X_a^{gen} being available is given by

$$pr^{gen}(X_a^{gen} = x_i^{gen}) = \left.\begin{array}{ll} q_i\ ; & x_i^{gen} = 0 \\ 1 - q_i\ ; & x_i^{gen} = C_i \end{array}\right\} \tag{6.1}$$

From this equation, it is inferred that the probability of the available capacity of generator being 0 is equal to q_i and the probability of available capacity equal to C_i is $1 - q_i$. For some applications it is more convenient to use outage capacity X_0^{gen} of a generator for assessing the reliability of electrical power system [21]. The two-states of outage capacity based generator model is given as

$$pr^{gen}(X_0^{gen} = x_i^{gen}) = \left.\begin{array}{ll} 1 - q_i\ ; & x_i^{gen} = 0 \\ q_i\ ; & x_i^{gen} = C_i \end{array}\right\} \tag{6.2}$$

The capacity outage probability function of eq. (6.2) implies that the probability of capacity outage equal to C_i MW is q_i and the probability of capacity outage equal to zero is $1 - q_i$. Thus, eqs. (6.1) and (6.2) are complementary.

The probabilistic model of the generator discussed above is a two-state model. Some of the generating units (especially large thermal generators) have multiple auxiliaries. Also, in thermal power generator units, the turbine and the boiler units are comparatively more complex and have multiple stages. Further, the failure of few ancillary components in the power generating units may not result in total shutdown of the generator but will only cause a reduction in the output power of the generator unit. Therefore, besides up state (normal operation) and down state (failure state), a generator unit may also have derated operating states depending on the number of functional auxiliary units.

Up and down states signify that the generator is working either at full capacity or at zero capacity, respectively, while a derated state signifies that the generator is working at a reduced capacity. Hence, while building the probabilistic model of a generation unit, the number of derated states, their power generation capacities and associated probabilities must also be also known, a priori. Consequently, the probability distribution of generator output power is no longer a simple two-state model but a multi-state model representing its power output in different possible states of operation and their associated probability of occurrence.

The probability distributions of available capacity for a two state and a multi-state generator are shown in Fig. 6.1. In Fig. 6.1(a), the i^{th} generator has two states having capacities $c_{i1}(= 0)$ and $c_{i2}(= C_i =$ the rated generator capacity$)$ and corresponding probabilities of occurrences p_{i1} and $p_{i2}(= q_i)$, respectively. In Fig. 6.1(b), the i^{th} generator has n states i.e. multiple states

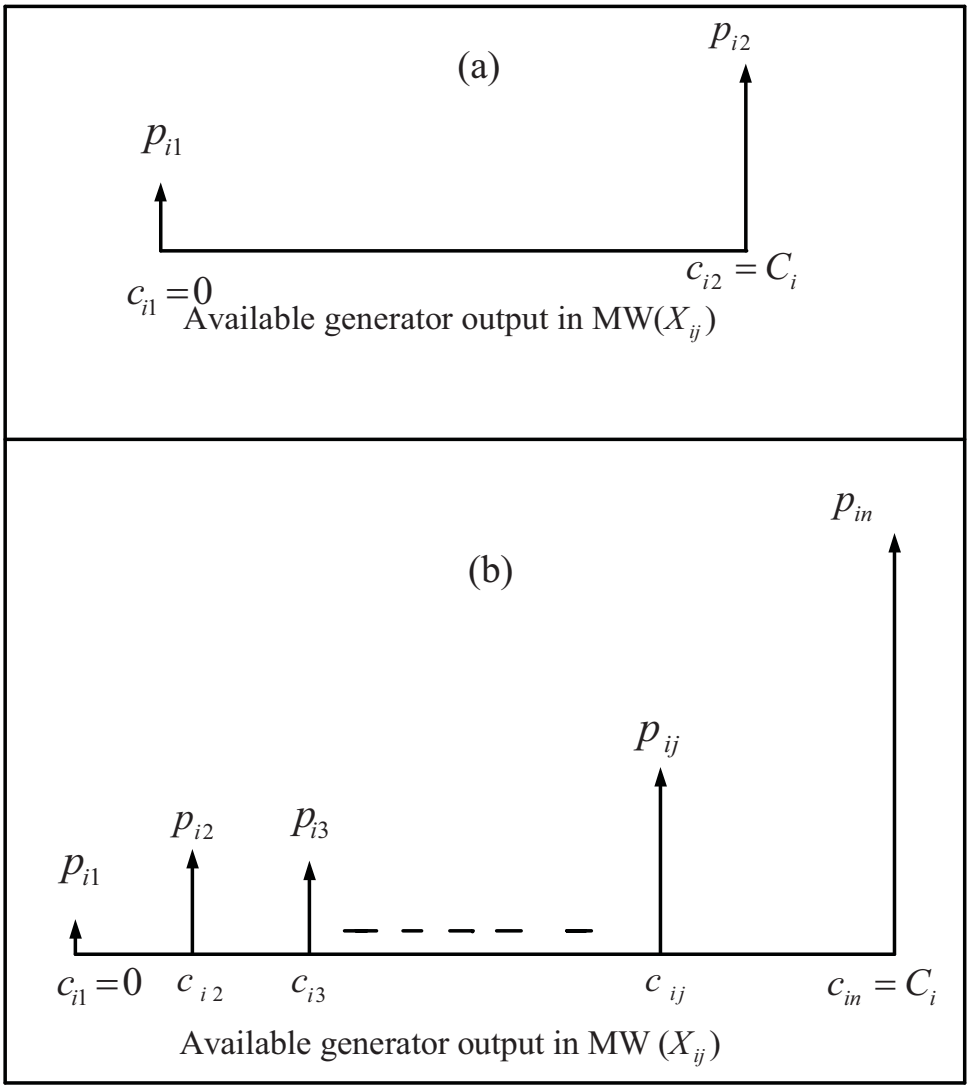

Figure 6.1: Generator available capacity probability distribution for (a) two-state generator (b) multi-state generator

having capacities $c_{i1}(= 0)$, c_{i2},.,c_{ij},., $c_{in}(= C_i)$ and the corresponding probabilities p_{i1},p_{i2},.., p_{in}, respectively. However, in both the cases

$$\sum_{j=1}^{\text{no. of states}} p_{ij} = 1 \tag{6.3}$$

In the present work, the multi-state generator model with five states has been used.

In the PEM based PLF, when the outages of 's' multi-state generators is included, the vector $\boldsymbol{X_k}$

(eq. (2.47)) in Section 2.6 of Chapter 2 is augmented as:

$$\boldsymbol{X_k} = \begin{bmatrix} x_{1,k} & \mu_2 & \dots & \mu_n & \mu_{gm1} & \dots & \mu_{gms} \\ \mu_1 & x_{2,k} & \dots & \mu_n & \mu_{gm1} & \dots & \mu_{gms} \\ \vdots & \vdots & \ddots & \vdots & \vdots & \vdots & \vdots \\ \mu_1 & \mu_2 & \dots & x_{n,k} & \mu_{gm1} & \dots & \mu_{gms} \\ \mu_1 & \mu_2 & \dots & \mu_n & x_{gm1,k} & \dots & \mu_{gms} \\ \vdots & \vdots & \vdots & \vdots & \vdots & \ddots & \vdots \\ \mu_1 & \mu_2 & \dots & \mu_n & \mu_{gm1} & \dots & x_{gms,k} \end{bmatrix} \tag{6.4}$$

where, $gm1, ..., gms$ are the multi-state generators, $k = 1, .., m$ where $m = 2, 4$ and 6 for 3PEM, 5PEM and 7PEM, respectively.

6.2 Modelling of line outage

In power system operation, the transmission line and transformer outages are termed as contingencies which could sometimes lead to the collapse of the entire power system. The task of power engineers becomes more challenging due to the continuous variation in demand for electrical energy, as they have to ensure a secure and an efficient power dispatch to the consumer under all operating conditions. Contingency analysis is one of the major tools for security assessment of a power system, which enables the power system operators to foresee the impact of a contingency on power system operation and chalk out a course of suitable measures to ensure system integrity. Such an analysis can be used to save the electrical power system by preventing other cascade events and is used for Static Security Assessment (SSA), mainly based on the transmission line or transformer power flow security (i.e. overloading of transformer or transmission line) and voltage security (i.e. voltage stability) [115]. A contingency set is a group of probable line or transformer outages. The outage of any single component (generator, transformer, transmission line) is called an $N-1$ contingency while the simultaneous outage of any two components is called an $N-2$ contingency.

In this work, a new PEM-based PLF method that takes line outages (contingencies) into account is proposed for bulk power system. Let a contingency be considered in which k^{th} transmission line is out of service and the probability of occurrence for the network configuration for this k^{th}network state is $pr_f(A_k)$ [116], where A_k is the k^{th} network configuration and $pr_f(A_k)$is the probability of occurrence of k^{th} network configuration. It is also assumed that all such possible network configu-

rations due to line outages are mutually exclusive. It is to be noted that $\sum_{i=1}^{n} pr_f(A_i) = 1$, where 'n' is the total number of mutually exclusive events. Assuming that the outage of each component is independent of other components, the probability of k^{th} network configuration is given by

$$pr_f(A_k) = \prod_{i=1}^{n_{av,k}} (1 - q_{i,k}) \prod_{j=1}^{n_{uav,k}} (q_{j,k}) \tag{6.5}$$

where, $q_{i,k}$ is the unavailability of the i^{th} network element for k^{th} configuration, $n_{av,k}$ and $n_{uav,k}$ are the number of available and unavailable network elements for k^{th} configuration, respectively.

6.2.1 PLF with line contingencies

For n mutually exclusive events $A_1, A_2, ..., A_n$, with $\sum_{i=1}^{n} pr_f(A_i) = 1$, the probability of an arbitrary event B_i, is given as:

$$P(B_i) = P(B_i|A_1)pr_f(A_1) + P(B_i|A_2)pr_f(A_2) + ... + P(B_i|A_k)pr_f(A_k) + .. + P(B_i|A_n)pr_f(A_n) \tag{6.6}$$

In eq. (6.6), B_i, represents the output variables of interest, $P(B_i)$ represents the total probability of the output variables of interest and $P(B_i|A_k)$ is the probability of B_i when the k^{th} network configuration with a probability $pr_f(A_k)$ occurs. Eq. (6.6) can be recasted in terms of moments of PDF of output variables of interest (as explained in Appendix A) as

$$m_f^j(B_i) = m_f^j(B_i|A_1)pr_f(A_1)+m_f^j(B_i|A_2)pr_f(A_2)+...+m_f^j(B_i|A_k)pr_f(A_k)+...+m_f^j(B_i|A_n)pr_f(A_n) \tag{6.7}$$

where, $m_f^j(B_i)$ represents the j^{th} moment of the variable B_i of interest and $m_f^j(B_i|A_k)$ is the j^{th} moment of output variables of interest when k^{th} network configuration occurs. The j^{th} moment, $m_f^j(B_i|A_k)$ can be obtained by using the PEM based PLF for k^{th} network configuration.

However, in a real power system, it is not practical to evaluate all the possible configurations and the corresponding probabilities, in an N transmission line system, there are up to 2^N possible network configurations. To simplify the problem and to reduce the computational burden, it is usually assumed that a maximum of 2 components can fail simultaneously. Hence, only $N-1$ and $N-2$ contingencies are usually considered, which is sufficient for most of power system operations and planning requirement. The steps involved in the PEM based PLF method considering the line outages are given below.

1. Calculate the probabilities of occurrence of the following network configurations (using eq. (6.5)):

(a) Without any line outage denoted as $(pr_f^0(A_{k_0}))$ with $k_0 = 1$ only.

(b) With $N-1$ contingencies denoted as $(pr_f^{N-1}(A_{k_1}))$ for k_1 possible configurations, where $k_1 = {}^{N_{tl}}\mathrm{C}_1$.

(c) With $N-2$ contingencies denoted as $(pr_f^{N-2}(A_{k_2}))$ for k_2 possible configurations, where $k_2 = {}^{N_{tl}}\mathrm{C}_2$.

where, N_{tl} is the total number of transmission lines in the system.

2. Perform the PLF (as explained in Section 2.6 of Chapter 2) and obtain the moments of the output variables of interest denoted as $(E^0(y^j_{i,lk}))$ without any line outage.

3. Perform the PLF for all possible $N-1$ contingencies and obtain the j^{th} moments of the output variables of interest denoted as $(E^{N-1}(y^j_{i,lk}))$.

4. Perform the PLF for all possible $N-2$ contingencies and obtain the moments of the output variables of interest denoted as $(E^{N-2}(y^j_{i,lk}))$.

5. Following eq. (6.7), add the product of moments and the configuration probability, to obtain the j^{th} moments $m^j_f(B_i)$ of the output variables of interest as:

$$m^j_f(B_i) = pr^0_f(A_{k_0}) \times E^0(y^j_{i,lk}) + \sum_{k_1=1}^{N_{tl}\mathrm{C}_1} pr^{N-1}_f(A_{k_1}) \times E^{N-1}(y^j_{i,lk}) + \sum_{k_2=1}^{N_{tl}\mathrm{C}_2} pr^{N-2}_f(A_{k_2}) \times E^{N-2}(y^j_{i,lk}) \tag{6.8}$$

It is to be noted as $j = 1, 2..., 8$, as only first eight moments have been used in this work.

6. Obtain the PDF of the output variables of interest using the calculated moments and spline based reconstruction method.

6.3 Results and discussion

The procedure discussed above has been applied to different test systems. The performance of the developed method has been evaluated for the following cases.

1. Considering outages of conventional generators only, without WTGs.

2. Considering line outages only, without WTGs.

3. Considering simultaneous generator and line outages without WTGs.

4. Considering simultaneous generator and line outages with WTGs.

6.3.1 PLF considering outages of conventional generators only, without WTG

For calculating the distributions of the variables of interest with only generator outages, the generator outages are included in the PEM based PLF. The simulation studies have been carried out in IEEE-118 bus system and this system has been modified accordingly for the analysis. In this system, the generators with specified generation $<$ 35 MW have been modeled as single-state units, while the generators having specified generation $\geq$ 35 MW have been considered as multi-state generators with five states. The outage data for multi-state generator model used in this work is given in Table 6.1 [117].

Table 6.1: Available generation probability data of generating units

Model 1		**Model 2**	
% of rated output	**State probability**	**% of rated output**	**State probability**
100	0.881	100	0.868
75	0.01	75	0.04
50	0.04	50	0.022
25	0.029	25	0.03
0	0.04	0	0.04

In Table 6.1, the generator output states (in percentage of rated output) and associated state probability have been specified for two multi-state models. Model 1 has been used for generator with rated output $<$ 220 MW, while Model 2 has been used for generators with rated output $\geq$ 220 MW. Out of the 53 generators in the system, 15 generators have rated capacity $>$ 35 MW and hence, have been modeled as multi-state units, and the remaining generators have been modeled as single-state units. Out of these 15 generators, generators at bus nos. 11, 26, 27, 50, 66, 67, 80, 89, 100 use multi-state model 1, while generator at bus nos. 13, 55, 60, 62, 103, 111 use multi-state model 2. The probability distribution of the available capacity of some of the multistate generators for IEEE-118 bus system (as a representative case) is shown in Fig. 6.2.

Since the probability distribution of the generator available capacity has only five states, it is not possible to estimate this PDF using 7PEM, as the roots obtained by solving eq. (2.36) turn out to be complex numbers. The roots represent the estimated locations of real random variable (generated

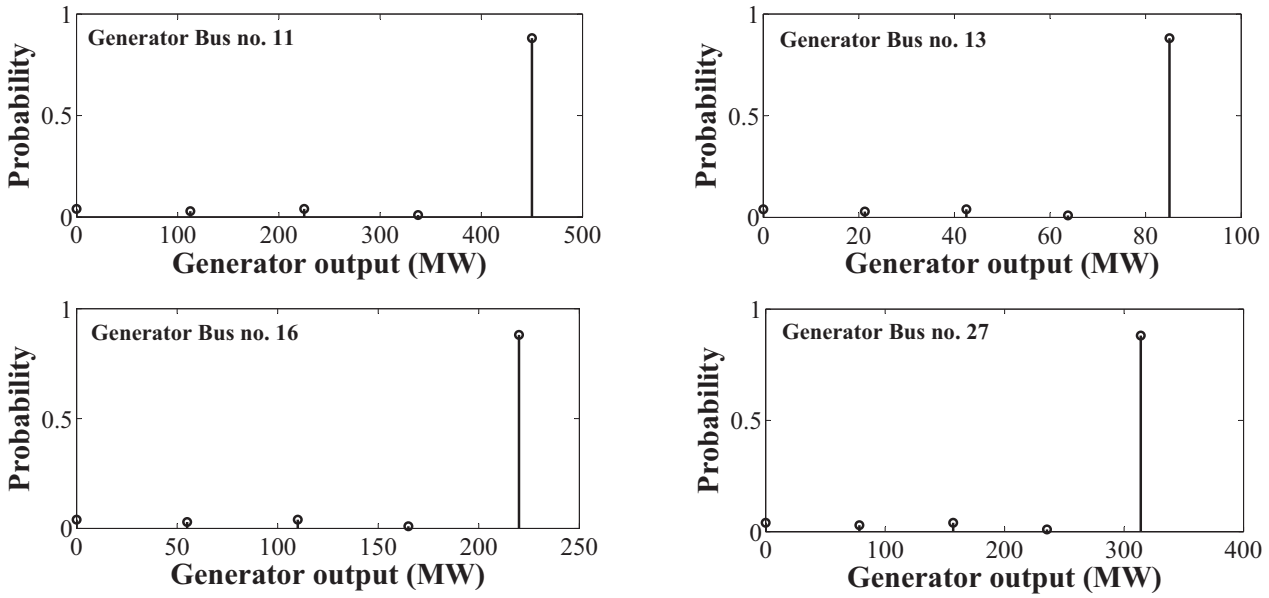

Figure 6.2: Available capacity probability distribution of generators

real power in this case) and hence cannot be complex in nature. As a result, a 7 point estimate of a discrete PDF having only 5 discrete values of random variables cannot be made. Hence, for this estimation 5PEM is used, in which the roots calculated by solving eq. (2.31) and corresponding locations obtained are real in nature. Therefore, the PLF has been solved by using 5PEM method and the results obtained by this method have also been compared with those obtained by the Monte Carlo simulation (MCS) studies. For modeling the variations in bus loads, mixed probability distributions (normal and discrete), as described in Chapter 3 have been used.

The PDF of the voltage at bus no. 34 (taken as a representative case) is shown in Fig. 6.3. From this figure, it is seen that the PLF with 5PEM and spline based reconstruction technique gives a PDF which compares well with the PDF obtained through MCS.

Similarly, the PDF of active and reactive power flow in the lines connected between bus no. 2 and 3 and between bus nos. 35 and 37 estimated using the proposed method and MCS (shown in Fig. 6.4 and Fig. 6.5 respectively) are in good agreement. Thus, the proposed PEM based PLF method, in conjuction with spline based PDF reconstruction, gives good results when generator outages are also considered. With the inclusion of generator outage rates in PEM based PLF, the number of random variables is increased, which in turn increases the computational burden. However, the computational time taken by the PEM is still very less as compared to that taken by MCS, as shown in Table 6.2.

Hence, generator outages can be efficiently and effectively included into the proposed PLF using PEM.

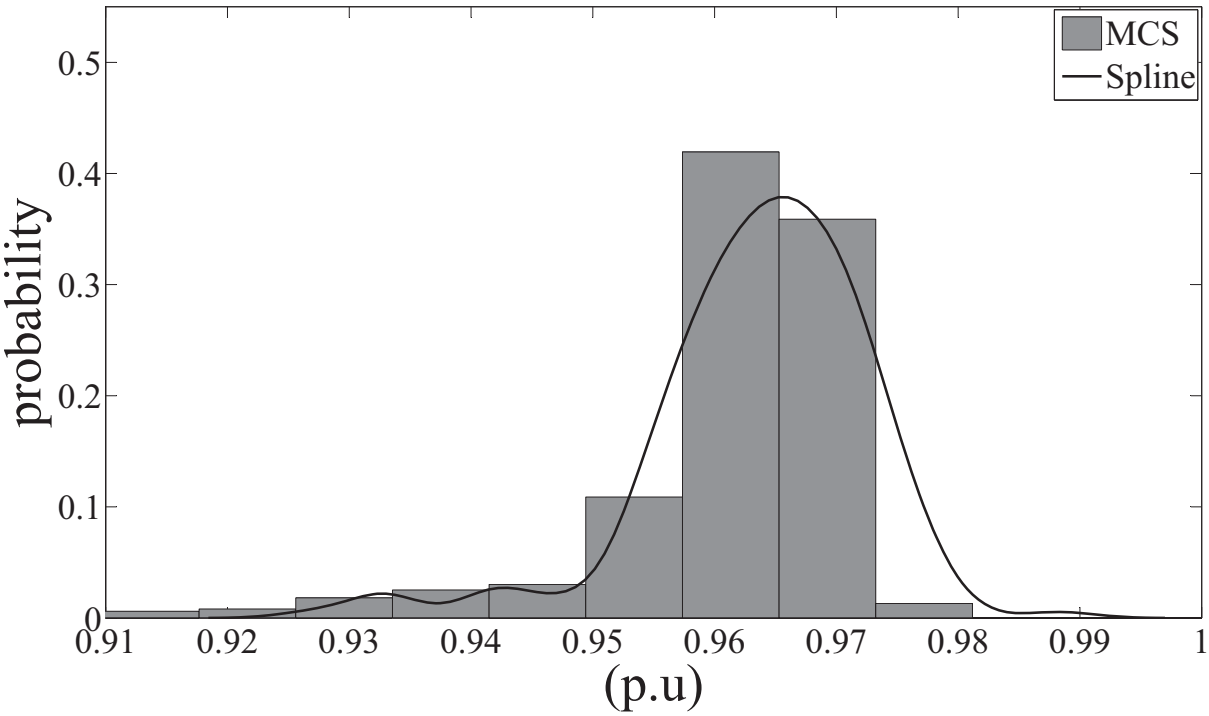

Figure 6.3: PDF of voltage at bus no. 34 considering generator outages only

Table 6.2: Time required for simulation studies (in seconds)

Test case/scheme	**5PEM**	**MCS**
IEEE-118 bus system	210.182	28794

6.3.2 PLF considering line outages only, without WTG

In this case, the simulation studies have been carried out on both IEEE-30 and IEEE-118 bus system. For IEEE-30 bus system both $N-1$ and $N-2$ contingencies have been considered. However, for IEEE-118 bus system, only $N-1$ contingencies have been considered as the number of $N-2$ contingencies is ${}^{186}\mathrm{C}_2 = 17205$, which is quite large. In fact, the time required for computing the moments using PEM for one configuration is 201.52 sec. Therefore, for a total of 17205 configurations, the time required for computing the moments would be 3467151.6 seconds (963.09 hours). Because of this requirement of high computational time, $N-2$ contingencies have not been considered in the 118 bus system. However, the basic procedure for considering $N-2$ contingencies is illustrated in IEEE-30 bus system which can be easily replicated for IEEE-118 bus system. Further, for MCS study, the total computational requirement for studying $N-1$ and $N-2$ contingencies becomes

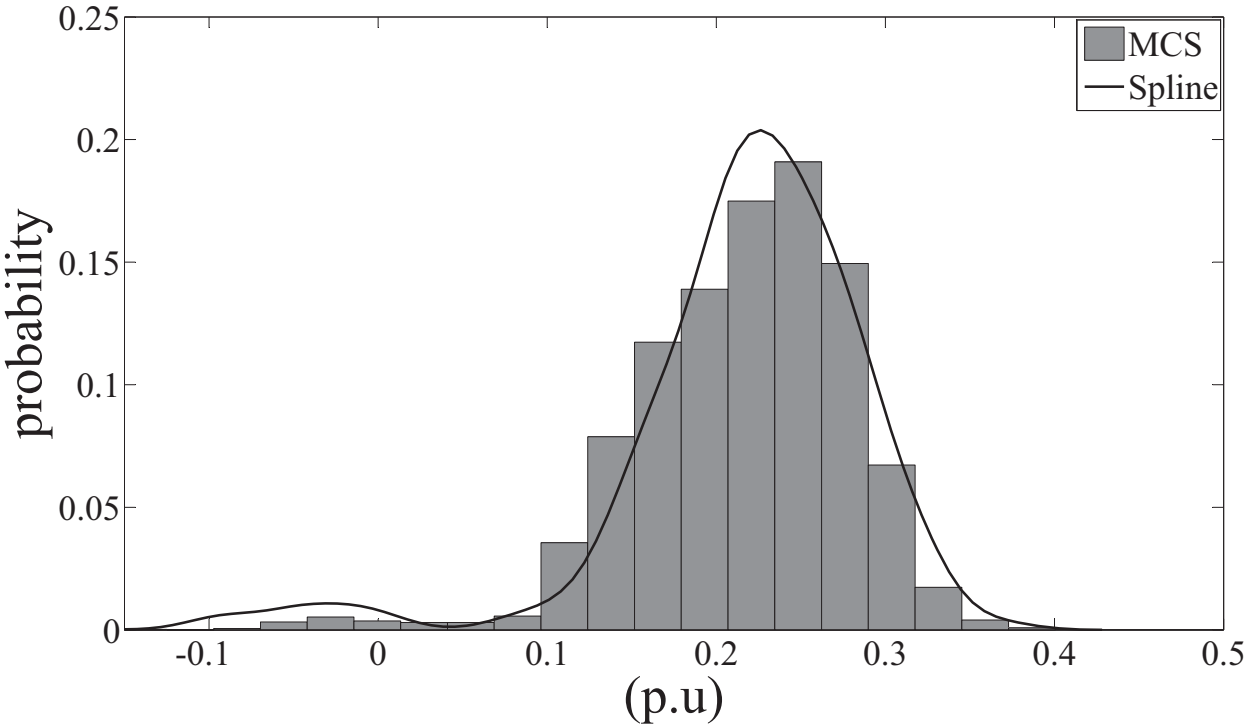

Figure 6.4: PDF of active power flow in the line between bus no. 2 and 3 considering generator outages only

prohibitively large. Therefore, the results of PLF with PEM and spline based reconstruction method only are presented.

For IEEE-30 bus system (given in Appendix B), the probability of a line being available is assumed to be 0.99. If N_{tl} is the total number of transmission lines in the system and p_{av} and p_{uav} are the probability of availability and unavailability of the transmission line respectively, then the total probability of a system state with N_{out} number of outaged lines is given by $p_{av}^{N_{tl}-N_{out}} \times p_{uav}^{N_{out}}$. The PLF analysis incorporating the line outages involves the following steps:

- The number of transmission lines in the IEEE-30 bus system is 41. First, the PLF is carried out without considering line outages and the moments thus obtained are multiplied by the configuration probability, which in this case is $0.99^{41} \times 0.01^{0} = 0.66228$.

- Next, the PLF is run for all possible $N-1$ contingencies and the moments obtained in each case are multiplied by the configuration probability, which is $0.99^{40} \times 0.01^{1} = 0.0066897$ for every configuration. For IEEE-30 bus system, there are a total of 41 $(N-1)$ contingencies.

- In the next step, the PLF is run for all possible $N-2$ contingencies and the moments obtained in each case are multiplied by the configuration probability, which is $0.99^{39} \times 0.01^{2} = 6.7573e-$

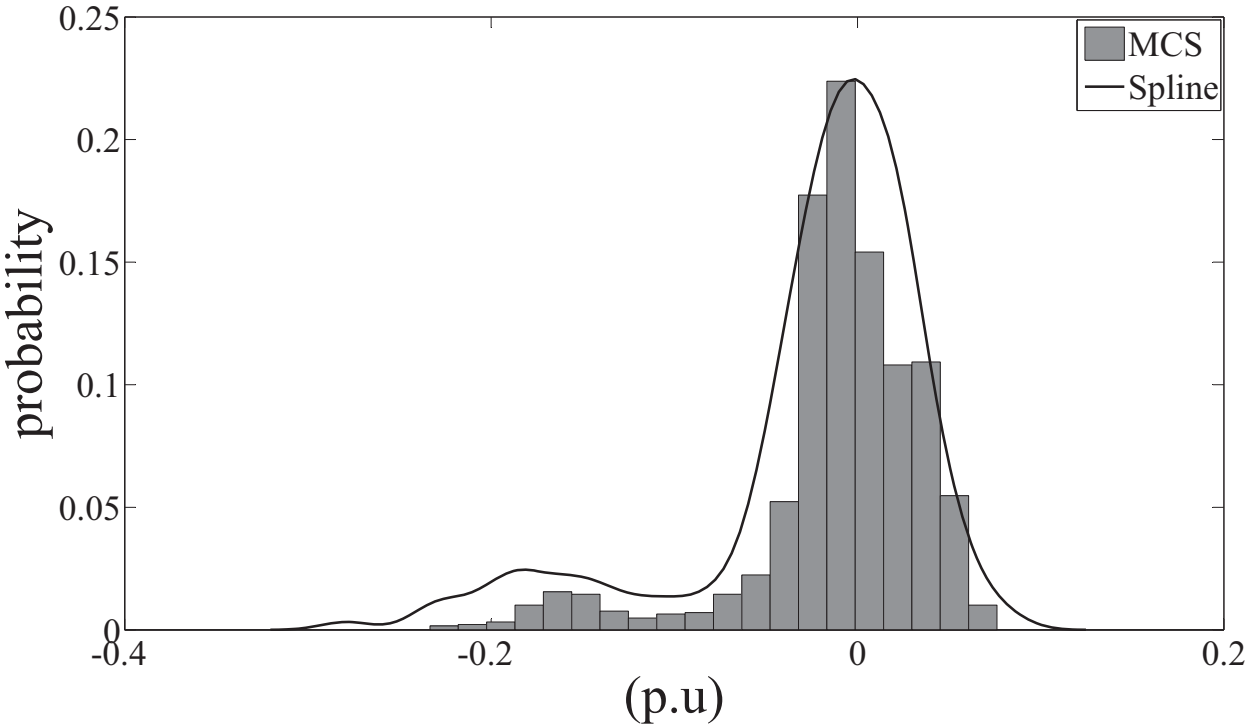

Figure 6.5: PDF of reactive power flow in the line between bus no. 35 and 37 considering generator outages only

005 for every configuration. For IEEE-30 bus system, there are a total of 820 numbers of $(N-2)$ contingencies.

- Finally, the product of moments and the configuration probability is added (following eq. (6.7)), to obtain the final moments from which the probability distributions of desired variables of interest can be obtained using spline based reconstruction method. It is to be noted that for any system, $\sum_{k=0}^{N_{tl}} pr(N-k)^{N_{tl}}\mathrm{C}_k = 1$, where, $pr(N-k)$ denotes the probability of a single configuration having $(N-k)$ contingency. However, in 30 bus system, it has been assumed that for $(N-k)$ contingencies, where $k > 2$, the system would fail to operate. Nevertheless, the total probability of all such contingencies can be calculated as, $\sum_{k=3}^{N_{tl}} pr(N-k)^{N_{tl}}\mathrm{C}_k = 1-\sum_{k=0}^{2} pr(N-k)^{N_{tl}}\mathrm{C}_k = 1-(0.66228+41\times 0.0066897+820\times 6.7573\times 10^{-05}) = 0.0080.$

Fig. 6.6 shows the PDFs of bus voltage of bus no. 30 with and without line outages. The statistical parameters (mean and standard deviation) of bus voltage for these two cases are given in Table 6.3. It can be seen from Fig. 6.6 that the PDF of bus voltage with line outages has a larger spread towards the lower voltage levels as compared to the PDF obtained without any line outage. This fact is also clearly observable in the values of mean and standard deviation of bus voltage as

shown in Table 6.3. This indicates that for some contingencies, voltage at bus no. 30 can become low and fall below 0.8 p.u level. Also, with contingencies considered, the PDF has a solitary pulse having a probability of approximately 0.08 corresponding to the bus voltage = 0 p.u.

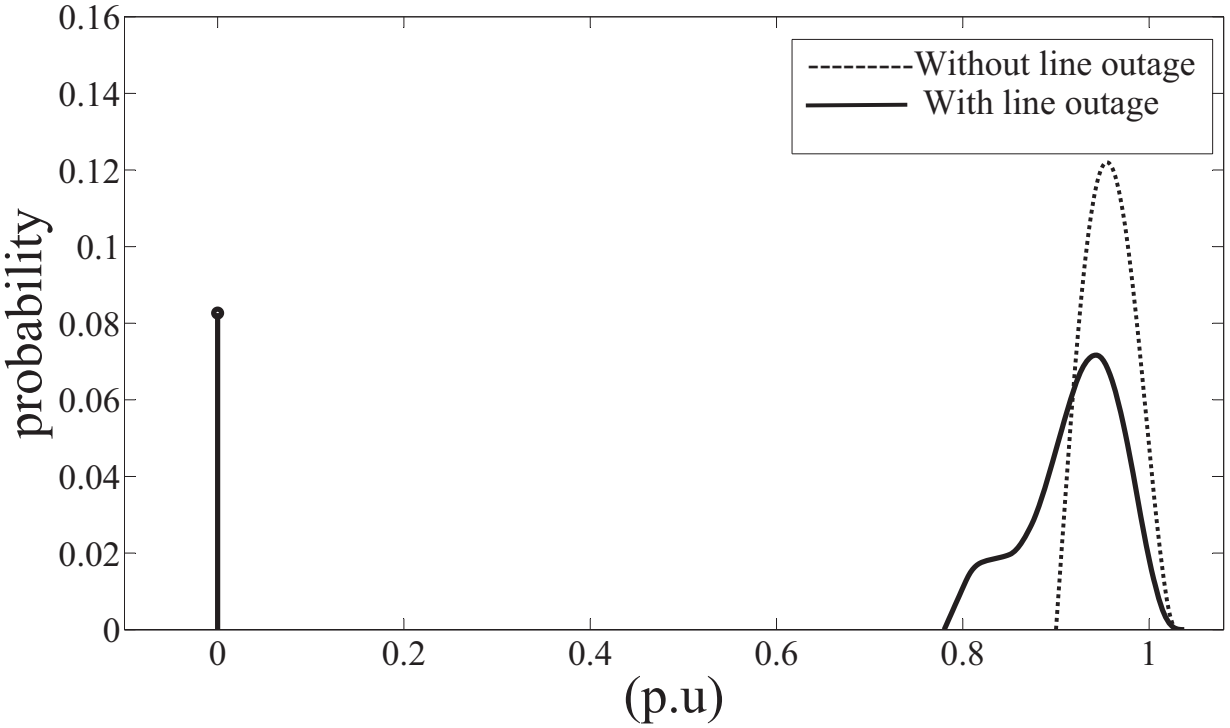

Figure 6.6: PDF of voltage at bus no. 30 with and without line outage

Table 6.3: Statistical parameters of voltage at bus no. 30

Case/Parameters	Mean	Standard deviation
Without line outages	0.9650	0.0377
With line outages	0.9089	0.0748

This corresponds to unconverged load flow cases, and can be interpreted as the probability that the system will collapse under the contingencies considered. It can also be observed that with line outages, bus voltage varies over a large range as compared to the case without any outage and hence, the probability of bus voltage remaining between the specified limits (0.95 and 1.05 p.u) also reduces. It is to be noted that in Fig. 6.6, the PDF of bus voltage has been plotted considering only up to $(N-2)$ contingencies. It has already been mentioned that the system operation would fail for

$(N-3)$ contingencies and beyond. Therefore, to depict the true PDF of the system considering all possible contingencies, the probability of the bus voltage equal to 0 p.u would have to be augmented by the value of 0.0080.

With the contingencies considered, there is a redistribution of power flow over the lines. This is observed in the PDFs of active and reactive power flow (with and without line outages) for lines between bus no. 9 and 10, and between bus nos. 7 and 5 as shown in Figs. 6.7 and 6.8, respectively.

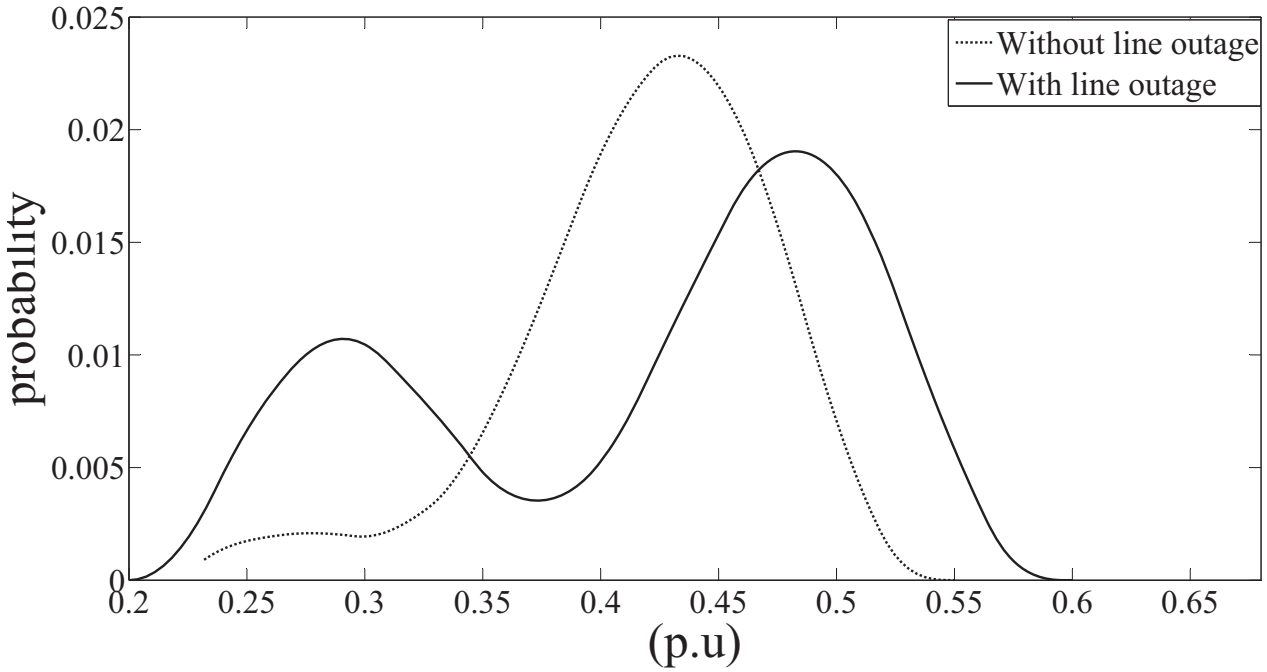

Figure 6.7: PDF of active power flow in the line between bus no. 9 and 10

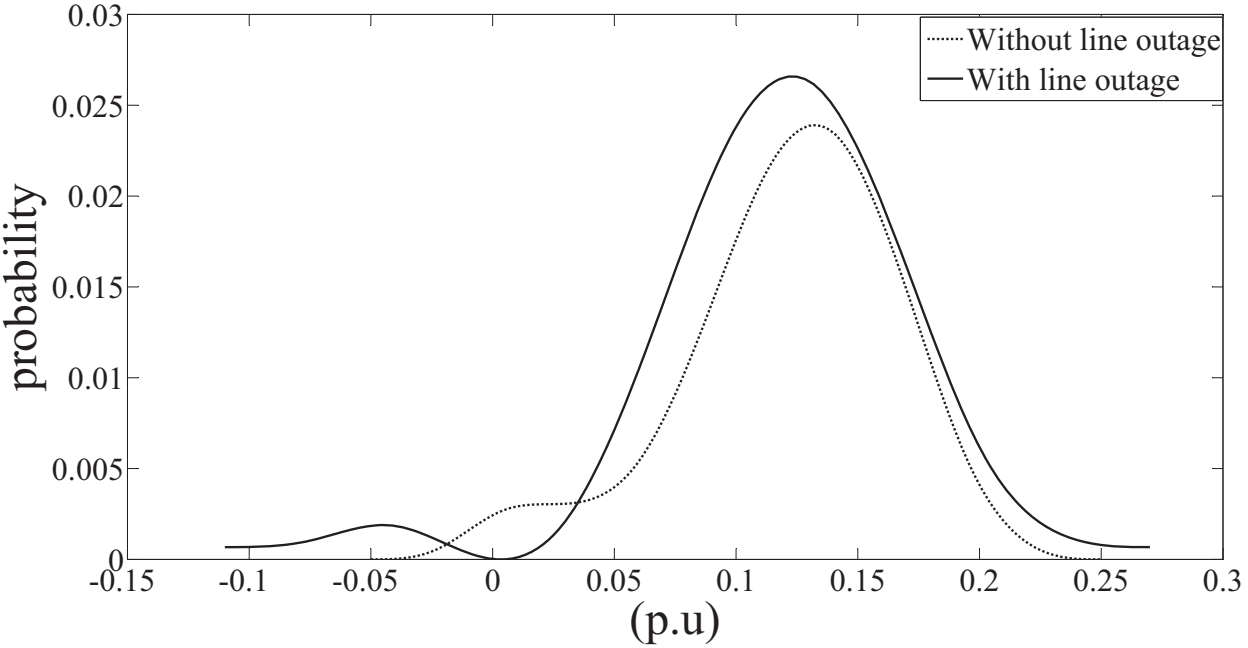

Figure 6.8: PDF of reactive power flow in the line between bus no. 7 and 5

Similarly, for IEEE-118 bus system, the probability of availability of a line has been assumed to be 0.99 for all the lines. However, as discussed earlier, in this case only up to $N-1$ contingencies have been considered as number of possible combinations of $N-2$ contingencies are extremely large (17205). The analysis involves the following steps:

- The number of transmission lines in the IEEE-118 bus system is 186. First, the PLF is carried out without any line outage and the moments thus obtained are multiplied by the configuration probability, which is $0.99^{186} \times 0.01^{0} = 0.15422$.

- Next, the PLF is run for all possible $N-1$ contingencies and the moments obtained in each case are multiplied by the configuration probability, which is $0.99^{185} \times 0.01^{1} = 0.0015578$ for every configuration. For IEEE-118 bus case there are 186 $(N-1)$ contingencies.

- Finally, product of moments and the configuration probability are added (following eq. (6.7)), to obtain the final moments from which the probability distributions of desired variables of interest can be obtained using spline based reconstruction method. Again, in this case also, the total probability of all $(N-k)$ contingencies, where $k>1$, can be calculated as, $\sum_{k=2}^{N_{tl}} pr(N-k)^{N_{tl}}\mathrm{C}_k = 1-(0.15422+186\times 0.0015578) = 0.5560$

The PDF of voltage at bus number 66 with and without line outage is shown in Fig. 6.9 and the relevant statistical parametres are given in Table 6.4.

From Fig. 6.9, it is observed that for $(N-1)$ contingency, the probability of system collapse (unconverged load flow cases) is 0.138. Further, it is also observed that the expected minimum and maximum voltage magnitude in the system (with $(N-1)$ contingency) are 0.5 and 0.8 p.u. only. Clearly, the system cannot operate at this low voltage level as the undervoltage relays would trip the transmission lines at this low voltage level. Table 6.4 also confirms that the mean value of the voltage reduces drastically because of $(N-1)$ contingencies.

For validating the results of the proposed PLF method, efforts were made to run MCS considering line outages. For one run of MCS, the time required for IEEE-30 bus system, considering up to $N-2$ contingencies, was 68.5 minutes. For IEEE-118 bus system, one run of MCS, considering $N-1$ contingencies only, required 614.2 minutes. For obtaining reasonably accurate results, a large number of MCS are required. Even for a modest 10000 MCS runs, the time required will be about 102366 hours for the IEEE-118 bus system. In the previous chapter 100000 MCS runs have been done. Thus, the time required for carrying out the MCS study is prohibitively large and hence has

not been carried out.

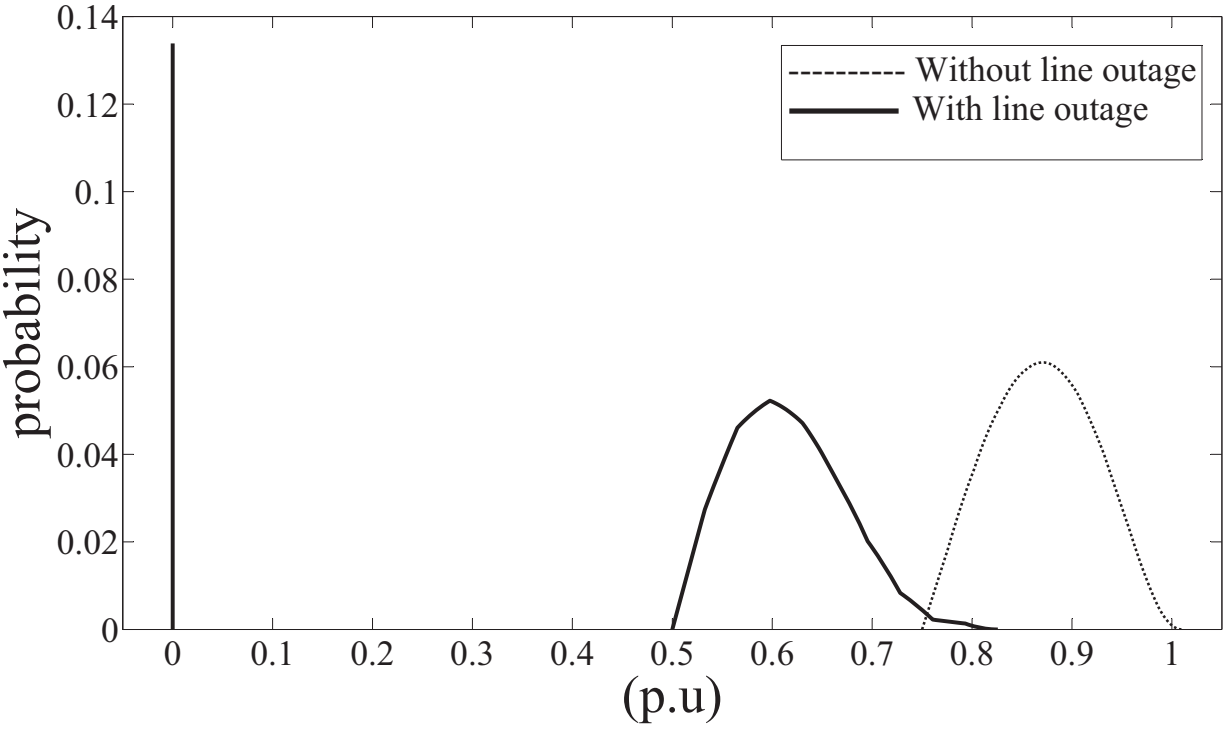

Figure 6.9: PDF of voltage at bus no. 66 without and with line outage

Table 6.4: Statistical parameters of voltage at bus no. 66

Case/Parameters	Mean	Standard deviation
Without line outages	0.8800	0.0755
With line outages	0.6629	0.0946

6.3.3 PLF considering simultaneous line and generator outages, without WTG

In this case, both generator and line outages have been included, using the procedure explained in the previous sections. The resulting PDF of the voltage at bus no. 30 (for IEEE-30 bus system) is shown in the Fig. 6.10. From this figure, it is observed that when both generator and line outages are considered, there is a further reduction in the minimum values of bus voltage (as compared to the case when only line outages are considered as shown in Fig. 6.6). The mean and the standard deviation values in this case are 0.7750 and 0.1480 respectively. Thus, while the mean value is reduced, the spread of the PDF is also increased (as compared to the case with only line outage). The

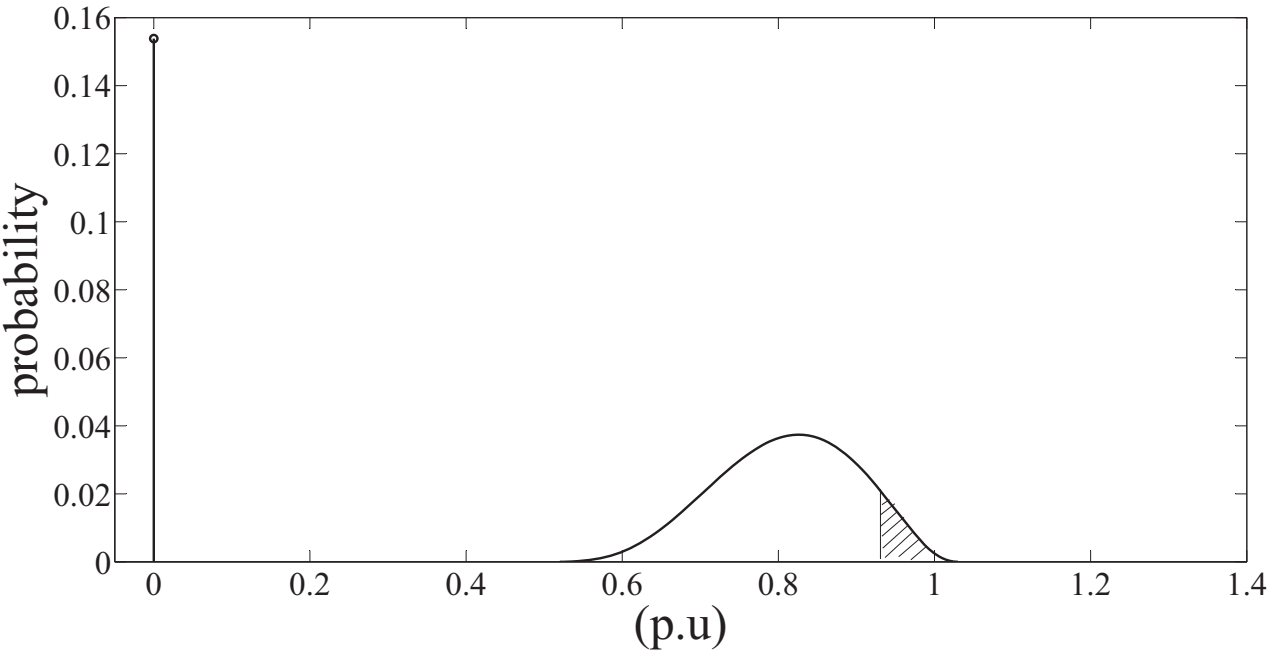

Figure 6.10: PDF of voltage at bus no. 30 considering simultaneous generator and line outages for IEEE-30 bus system

shaded area represents the probability that the system voltage will be between the specified limits of 0.95-1.05 p.u. This area is very small and indicates that the probability of the system operating successfully under generator and line outage conditions is very small. In this case also, there is a considerable amount of possibility that the undervoltage relays would trip the transmission lines. Also, as observed from Fig. 6.10, the probability of system collapse also increases as evident from the increase in the probability of zero voltage.

Similar observations are made for IEEE-118 bus system, in which the minimum voltage level decreases from 0.5 p.u in the previous case (with line outage only) to 0.48 p.u., as shown in Fig. 6.11. The mean and the standard deviation in this case are 0.6329 p.u. and 0.0996 p.u. respectively indicating a further shift in the PDF towards left as well as increase in the spread, as compared to the case with line outage only (with the mean and standard deviation of 0.6629 p.u. and 0.0946 p.u. respectively). Again, as before, in this case also, it would not be possible to operate the system as the undervoltage relays would trip the lines.

From the above analysis, it is evident that the proposed PEM based PLF along with spline based reconstruction method can be successfully applied to the analysis of power systems for considering simultaneous outages of generator and transmission lines.

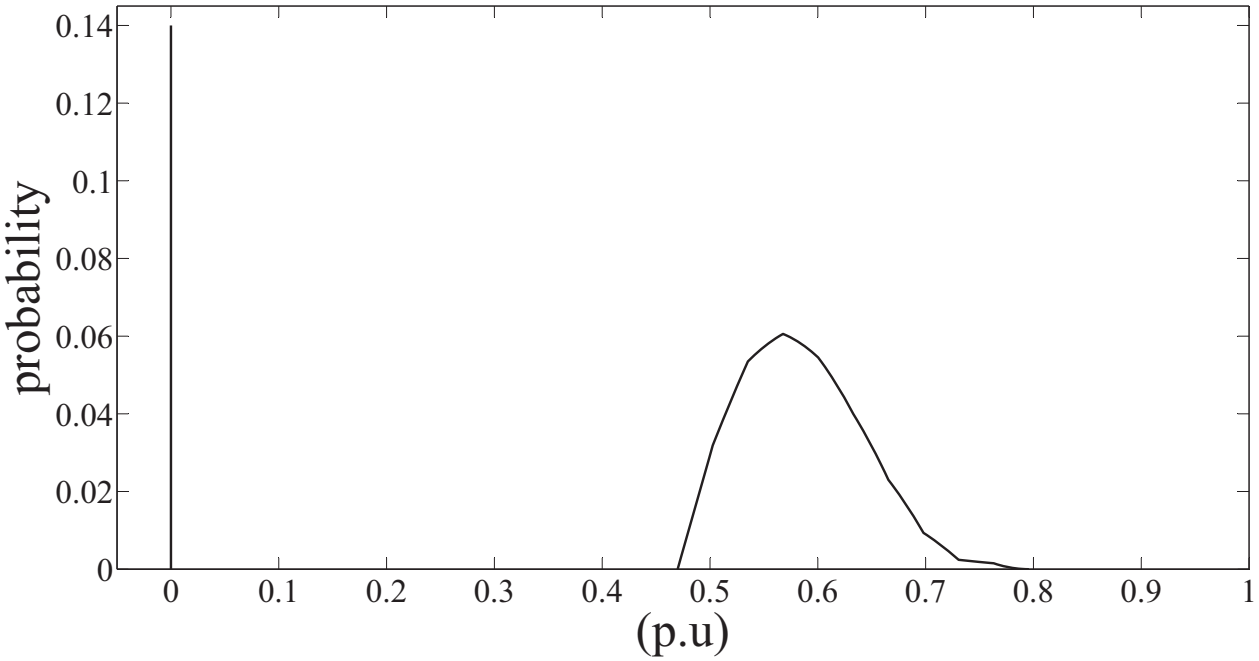

Figure 6.11: PDF of voltage at bus no. 66 with simultaneous generator and line outages for IEEE-118 bus system

6.3.4 PLF considering simultaneous line and generator outages with uncertain wind power generation

In this case WTGs as explained in Chapter 5 have been included in the IEEE-118 bus system. The resulting PDF of voltage at bus no. 66 is shown in Fig. 6.12. The comparison of statistical parameters of bus voltage for different cases is given in Table 6.5.

The mean and standard deviation in this case are 0.8 p.u. and 0.0871 p.u. respectively. From Fig. 6.12 and Table 6.5 (taken as a representative case), it is observed that the overall voltage profile of the system has improved in the presence of WTGs as compared to the voltage profile without any WTG (shown in Fig. 6.11) in terms of both increased mean value and reduced standard deviation. Thus, it can be observed that though the addition of WTGs in the system helps to improve the system performance under generator and/or line outages, the bus voltages are still well below the minimum allowable operating limit.

For IEEE-300 bus system, the generators having specified generation $<$ 100 MW are considered as single-state generators and generator having specified generation $\geq$ 100 MW are considered as multi-state generators with five states. As explained in Section 6.3.1, two different generator models (shown in Table 6.1) have been used to modify the generator data. Model 1 has been used for the

generators with specified generation $\leq$ 400 MW and model 2 has been used for the generators with specified generation $>$ 400 MW. Out of the 55 generators in the system, 46 generators have been modelled as multi-state units and rest as single-state generators.

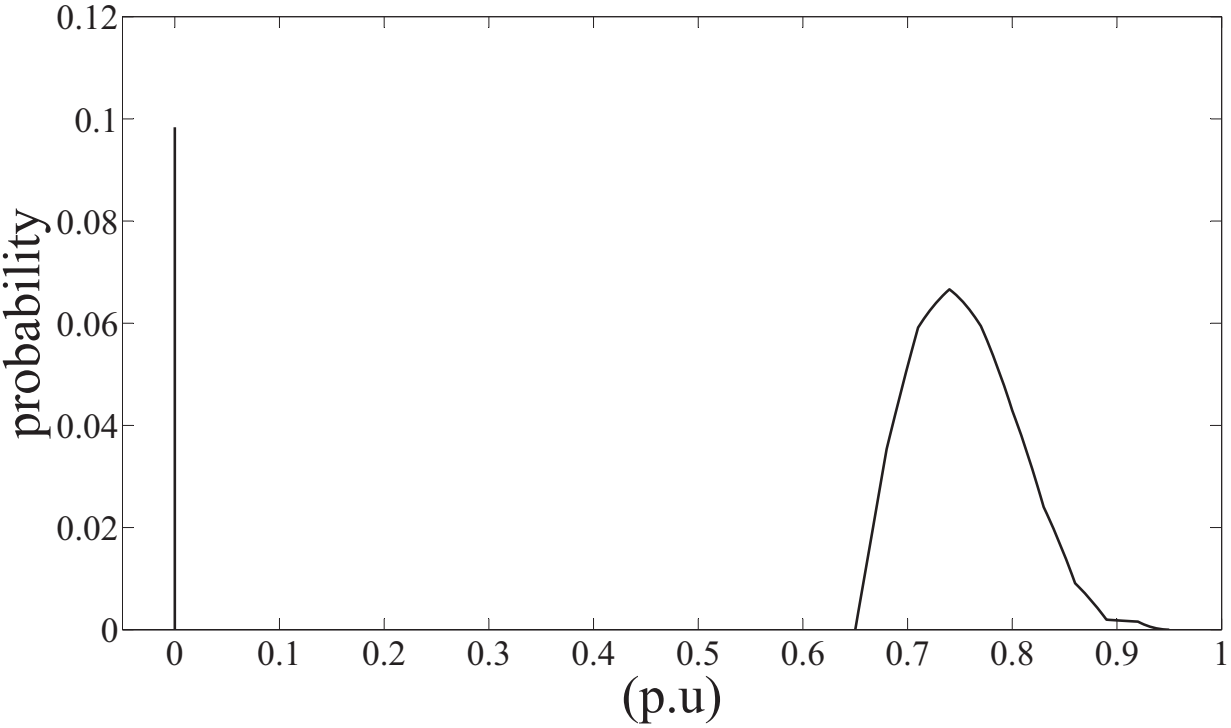

Figure 6.12: PDF of voltage at bus no. 66 with WTG and simultaneous generator and line outages for IEEE-118 bus system

Table 6.5: Statistical parameters of voltage at bus no. 66 of IEEE-118 bus system for different cases

Case/Parameters	Mean	Standard deviation
Without line outages	0.8800	0.0755
With line outages	0.6629	0.0946
With line and generator outages	0.6329	0.0996
With line and generator outages including WTGs	0.8000	0.0871

Out of 46 generators, the generators at bus no. 2, 3, 5, 7, 8, 11, 12, 13, 14, 15, 16, 18, 24, 27, 28, 29, 30, 32, 35, 40, 41, 42, 43, 48, 49, 50 and 51 have been represented by model 1 and

the generators at bus no. 6, 9, 19, 20, 21, 22, 23, 26, 31, 33, 34, 37, 38, 39, 44, 45, 52, 53 and 54 have been represented by model 2. The WTG data and the correlation between the loads and between the WTGs is same as considered in Chapter 5. Further, the probability of line availability has been assumed to be as 0.99 and the analysis up to $(N-1)$ contingencies (total 411 in number) has only been carried out. Due to the large number of $N-2$ contingencies (84255), they have not been considered. Therefore, the probability of the network configuration without any line outage is calculated as $0.99^{411} \times 0.01^{0} = 0.016072$ and for $N-1$ contingency, it is $0.99^{410} \times 0.01^{1} = 0.00016234$ for every line outage. Again, as before, the total probability of all $(n-k)$ contingencies, where $k > 1$, is given by $\sum_{k=2}^{N_{tl}} pr(N-k)^{N_{tl}}\mathrm{C}_k = 1 - (0.016072 + 411 \times 0.00016234) = 0.9172$.

The PDFs of the voltage magnitude at bus number 271 with and without outages are shown in Fig. 6.13 and the relevant statistical parameters are given in Table 6.6.

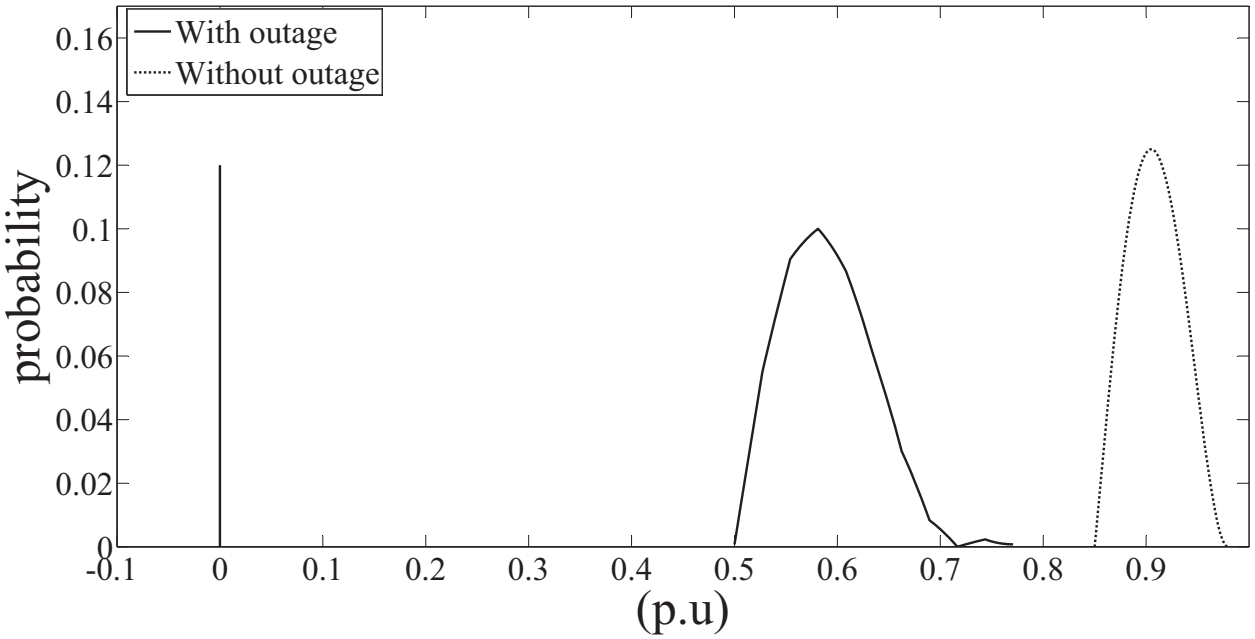

Figure 6.13: PDF of voltage at bus no. 271 without and with simultaneous generator and line outage

Table 6.6: Statistical parameters of voltage at bus no. 271

Case/Parameters	Mean	Standard deviation
Without line and generator outages	0.9150	0.0377
With line and generator outages	0.6354	0.0786

From Fig. 6.13 and Table 6.6, it is observed that voltage PDF is shifted towards the left along with the increase in the spread of PDF i.e. there is a reduction in the voltage level with simultaneous line and generator outage case as compared to the case without any outage. The reduction in voltage can be attributed to a reduction in the reactive power flow in the line between bus no. 268 and 271 due to outages as shown in Fig. 6.14.

Further, because of the simultaneous outages of transmission lines and generators, the active and reactive power flows in some of the lines are significantly modified, as evident from Figs. 6.14 - 6.16.

In the above analysis, the probability of availability of a line has been assumed to be 0.99 for all the lines and loading on the buses have been assumed to be 1.5 times the base loading condition for IEEE-118 bus system and 1.05 times the base loading condition for IEEE-300 bus system. For these values of loading and line availability, both the systems have very low probability of operating successfully with outages. In the next section, the effect of change in the availability of a line and the bus loadings has been studied.

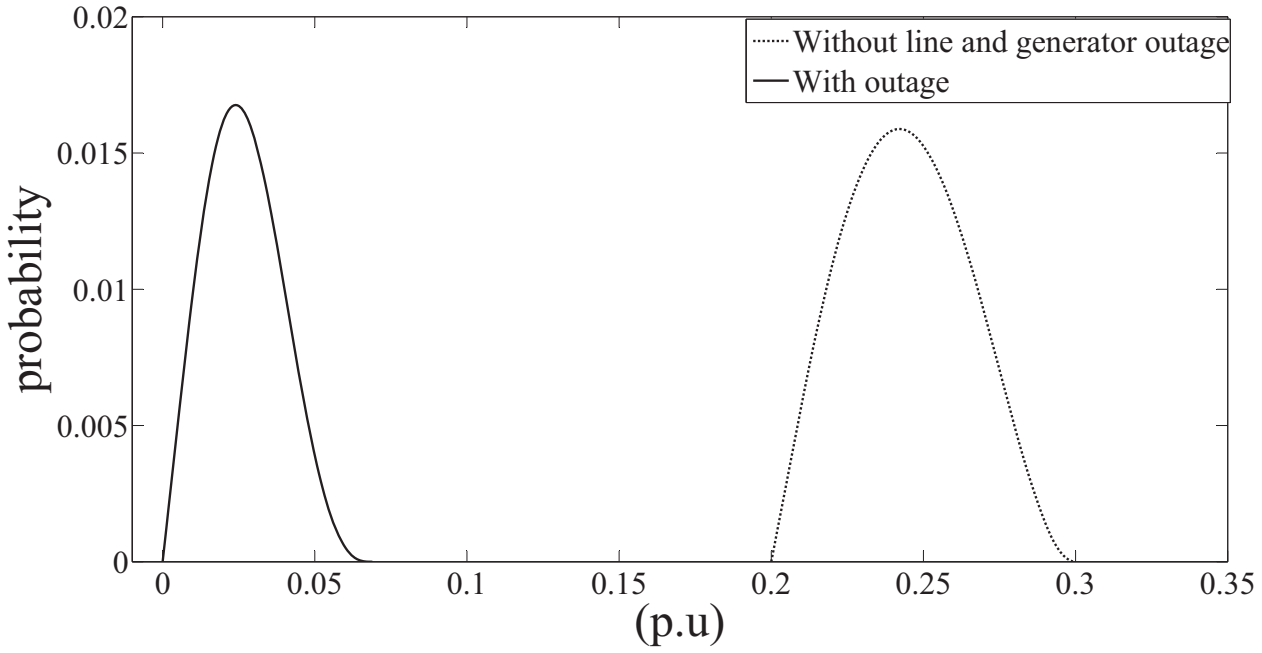

Figure 6.14: PDF of reactive power flow in line between the bus no. 268 and 271

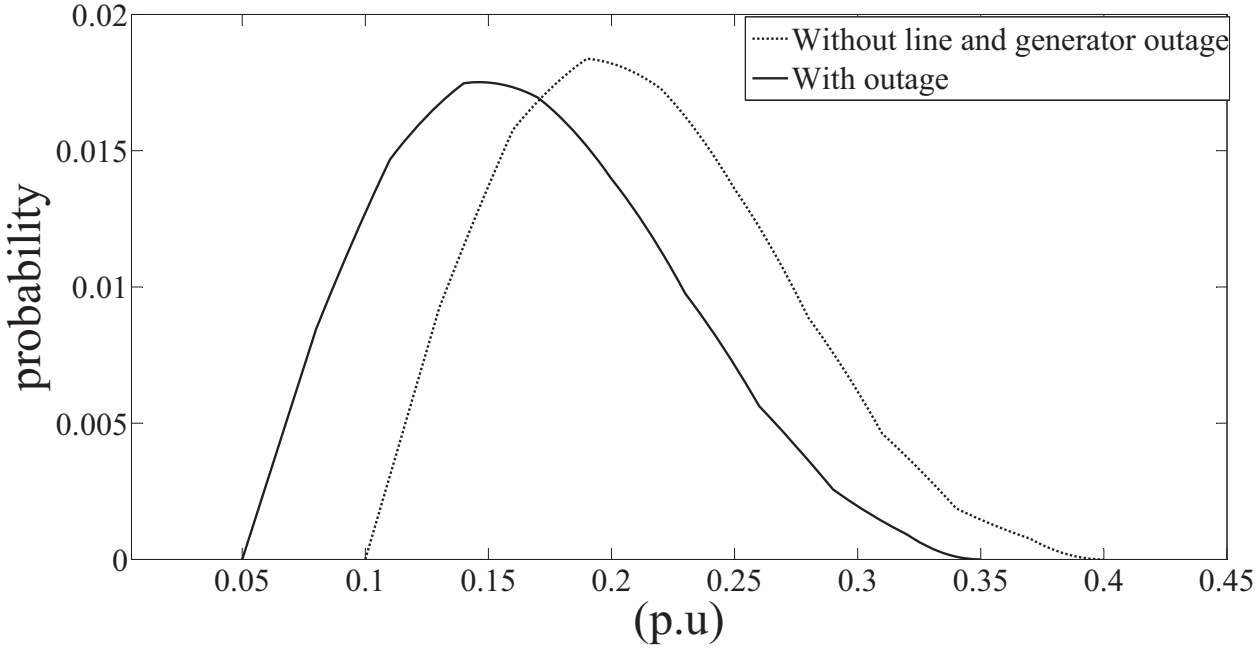

Figure 6.15: PDF of active power flow in line between the bus no. 266 and 271

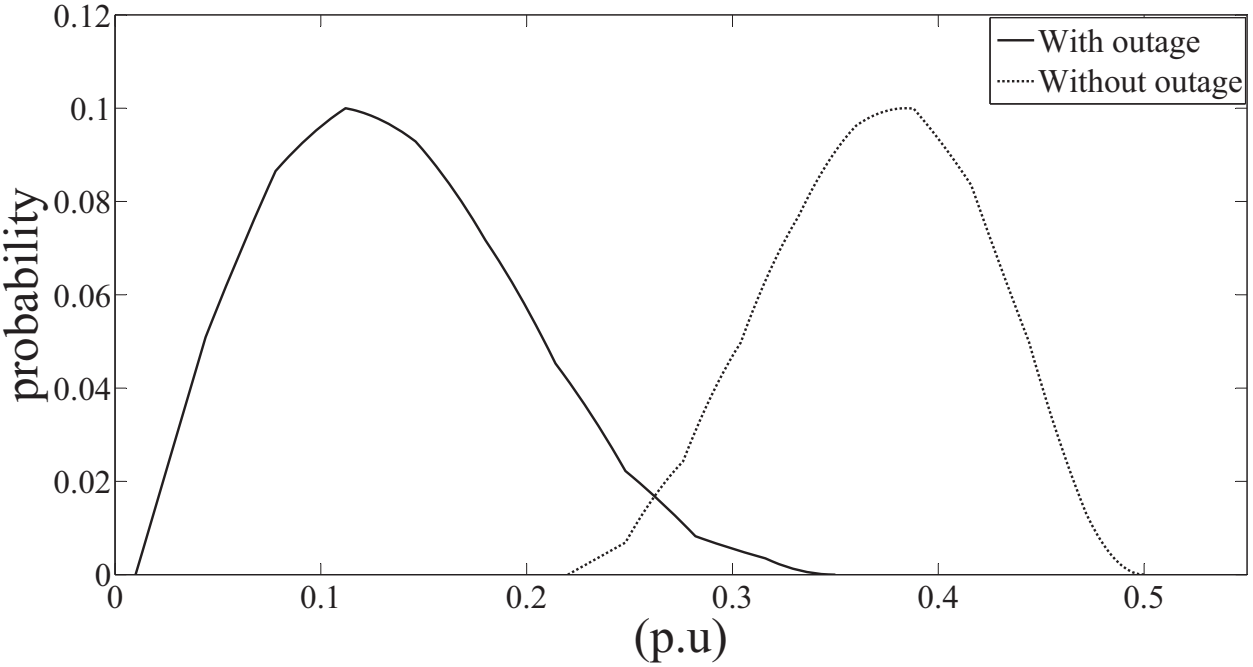

Figure 6.16: PDF of reactive power flow in line between the bus no. 266 and 270

6.4 Effect of variation in line availability and loading on system operation

6.4.1 Effect of variation in the probability of line availability

In this case, for IEEE-118 bus system, the probability of availability of a line has been assumed to be 0.998 [118] for all the lines. The analysis involves the following steps:

- The number of transmission lines in the IEEE-118 bus system is 186. First, the PLF is carried out without any line outage and the moments thus obtained are multiplied by the configuration probability, which is $0.998^{186} \times 0.002^{0} = 0.6891$.
- Next, the PLF is run for all possible $N-1$ contingencies and the moments obtained in each case are multiplied by the configuration probability, which is $0.998^{185} \times 0.002^{1} = 0.001381$ for every configuration. For IEEE-118 bus case there are 186 $(N-1)$ contingencies.
- Finally, product of moments and the configuration probability are added (following eq. (6.7)), to obtain the final moments from which the probability distributions of desired variables of interest can be obtained using spline based reconstruction method. Again, in this case also, the total probability of all $(N-k)$ contingencies, where $k > 1$, can be calculated as, $\sum_{k=2}^{N_{tl}} pr(N-k)^{N_{tl}}\mathrm{C}_k = 1 - (0.6891 + 186 \times 0.001381) = 0.054034$

The PDF of voltage at bus no. 66 with outage is shown in Fig. 6.17.

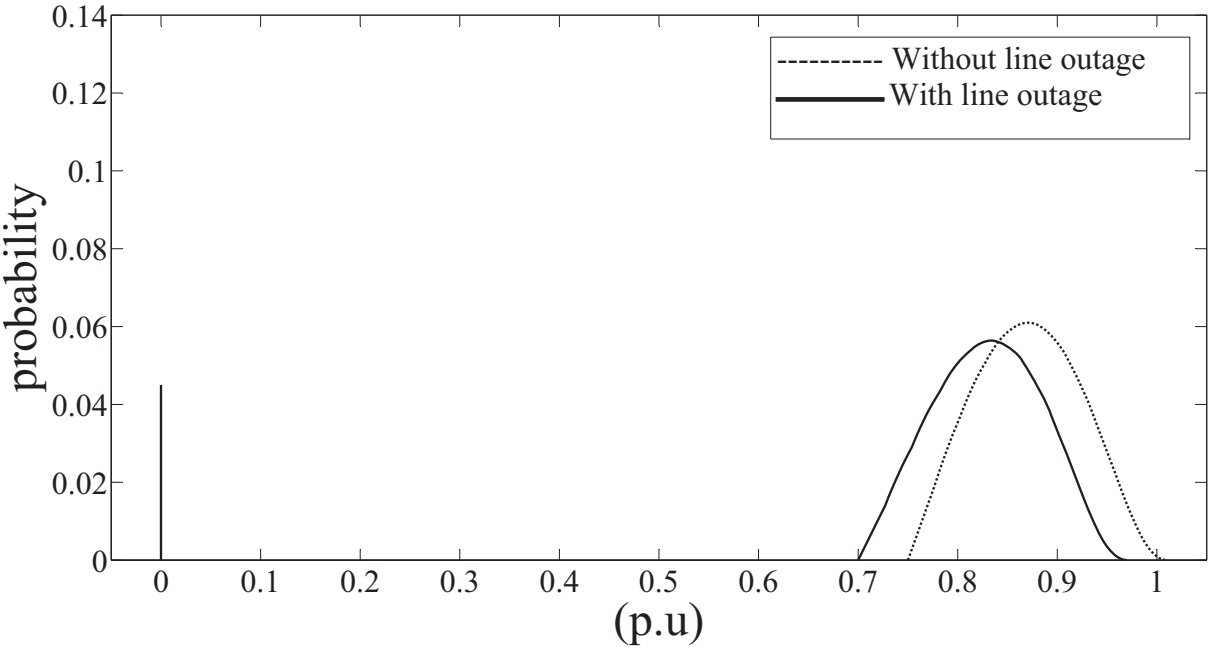

Figure 6.17: PDF of voltage at bus no. 66 with line outage only for IEEE-118 bus system

The PDFs of voltage of bus no. 66 for the three cases (line outage only, line and generator outage, line and generator outage with WTG) for a line availability of 0.998 are shown in Figs. 6.17- 6.19. The average and the standard deviation of the voltage of the bus no. 66 for two different values of probability of line availability (0.99 and 0.998) is given in Table 6.5 and 6.7 respectively. From the figures and the tables, it can be seen that the system reliability has improved when the probability of line availability is 0.998 as compared to the probability value of 0.99. The probability of the system collapse (represented by the height of the impulse at V=0 p.u) has also reduced considerably. Similar observations have also been made for other bus voltages.

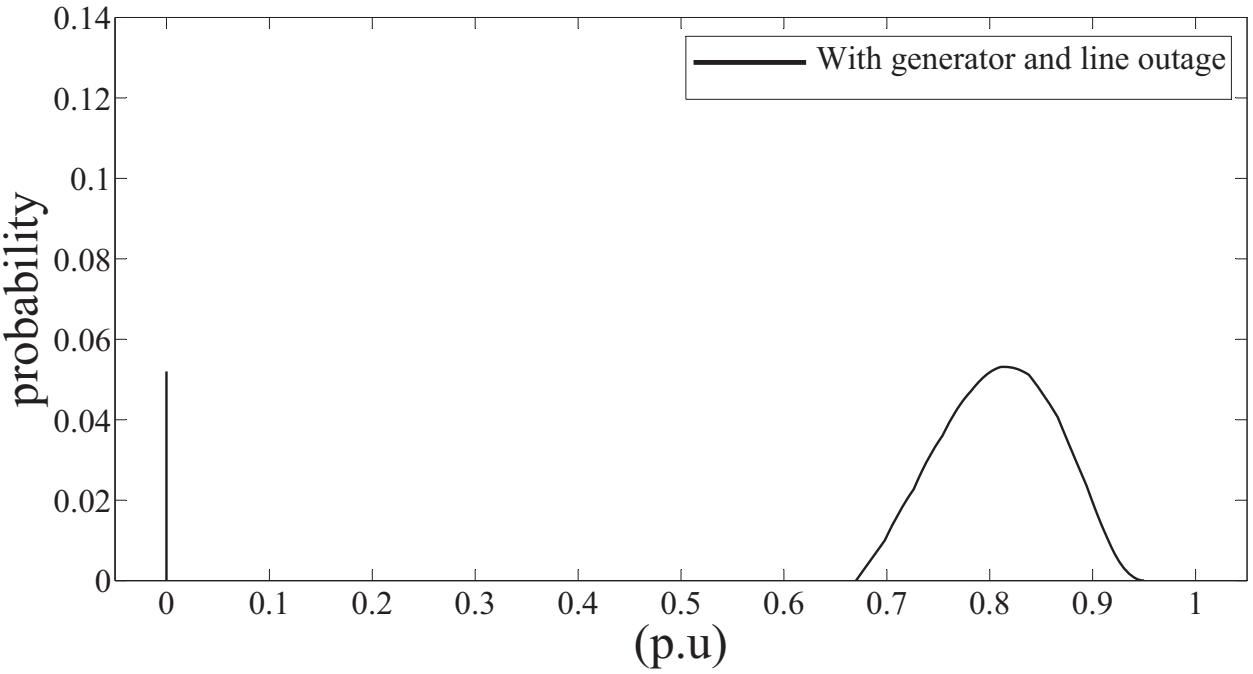

Figure 6.18: PDF of voltage at bus no. 66 with line and generator outage for IEEE-118 bus system

For IEEE-300 bus system also, the probability of line availability has been assumed to be as 0.998. Therefore, the probability of the network configuration without any line outage is calculated as $0.998^{411} \times 0.002^{0} = 0.43919$ and for $N-1$ contingency, it is $0.998^{410} \times 0.002^{1} = 0.00088014$ for every line outage. Again, as before, the total probability of all $(n-k)$ contingencies, where $k > 1$, is given by $\sum_{k=2}^{N_{tl}} pr(N-k)^{N_{tl}}\mathrm{C}_k = 1 - (0.43919 + 411 \times 0.00088014) = 0.19907$.

Fig. 6.20 shows the PDF of voltage at bus 271 for this case. From this figure, it is observed that the shift towards the left and the spread of PDF is much less as compared to the previous case shown in Fig. 6.13 (with a probability of line availability 0.99), indicating an improvement in system performance.

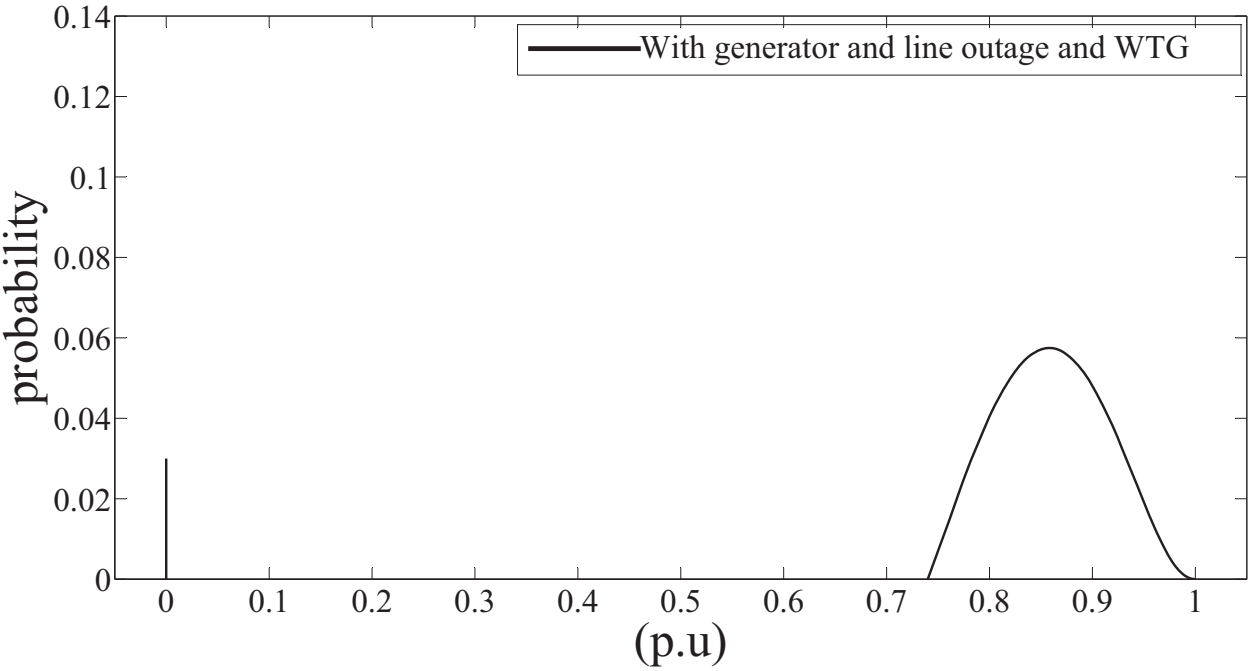

Figure 6.19: PDF of voltage at bus no. 66 with WTG for IEEE-118 bus system

Table 6.7: Statistical parameters of voltage at bus no. 66 of IEEE-118 bus system for different cases with a probability of availability as 0.998

Case/Parameters	Mean	Standard deviation
Without line outages	0.8800	0.0755
With line outages	0.8350	0.0784
With line and generator outages	0.8100	0.0813
With line and generator outages including WTGs	0.8700	0.0756

6.4.2 Effect of change in the system loading conditions

In the previous cases bus loading has been taken as 1.5 times the base loading condition for IEEE-118 bus system. In this case, the bus loading has been taken as the given base loading condition and the probability of availability of line is assumed to be as 0.998.

The PDFs of voltage at bus no. 66 for all the four cases is shown in the Fig. 6.21 and the statistical parameters are given in Table 6.8.

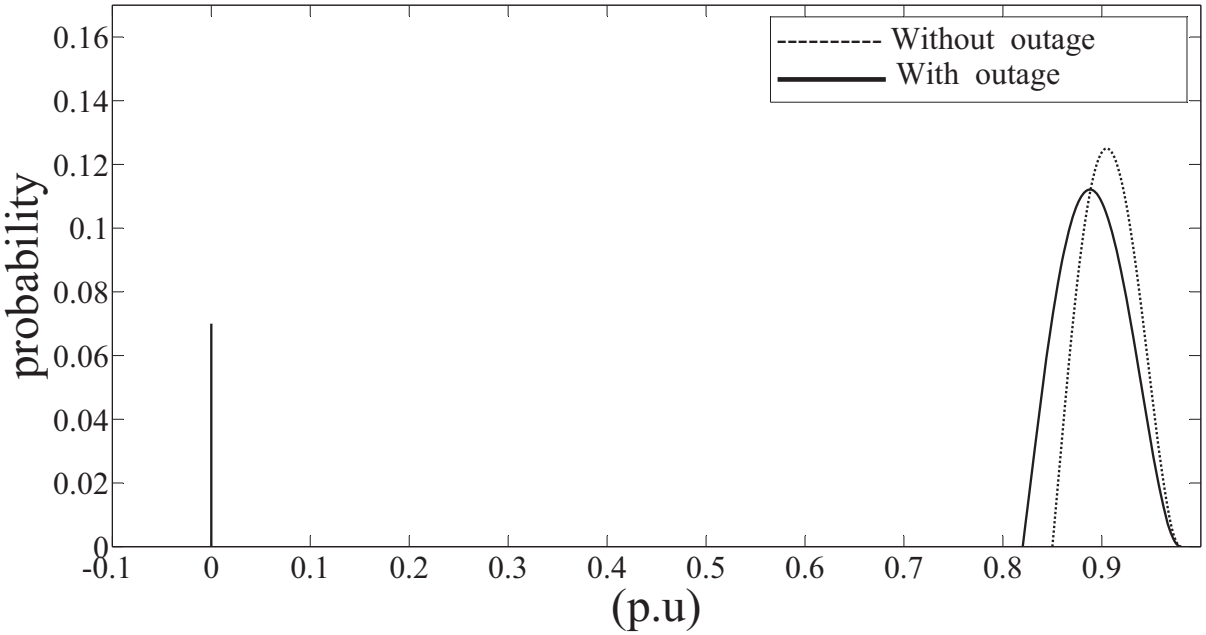

Figure 6.20: PDF of voltage at bus no. 271 without and with outage

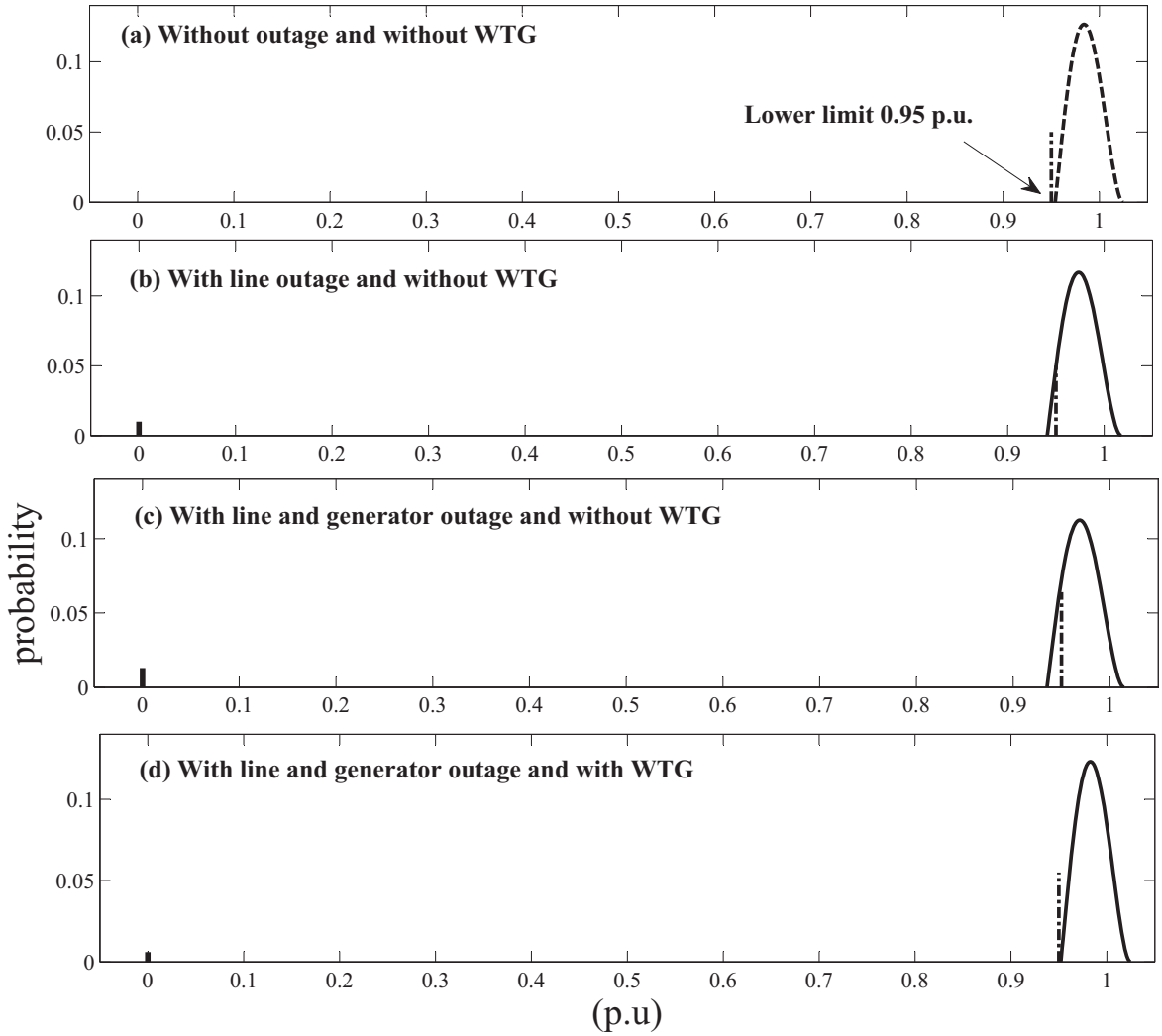

Figure 6.21: Effect of the change in the system loading on the voltage of bus no. 66 for all the four cases

Table 6.8: Statistical parameters of voltage at bus no. 66 of IEEE-118 bus system for different cases

Case/Parameters	Mean	Standard deviation
Without line outages	0.9895	0.0206
With line outages	0.9795	0.0224
With line and generator outages	0.9750	0.0232
With line and generator outages including WTGs	0.9885	0.0212

From Fig. 6.21 and Table 6.8, it is observed that for this loading condition the PDF of bus voltage is well within the maximum and minimum voltage limits without any outage (Fig. 6.21 (a)), violates the lower limit slightly with only line outage (Fig. 6.21 (b)), drifts further towards the left increasingly violating the lower limit with line and generator outage (Fig. 6.21 (c)), and finally is again within the limits when the WTG is included (Fig. 6.21 (d)). This trend was also observed for the other buses of the system and the voltage magnitudes were within the specified limits. Hence, in the presence of WTGs the system can operate safely under base loading condition, as compared to the previous case of increased loading condition (Fig. 6.19).

From Fig. 6.22, similar observations can be made for the IEEE-300 bus system with the base loading condition and the availability of line as 0.998.

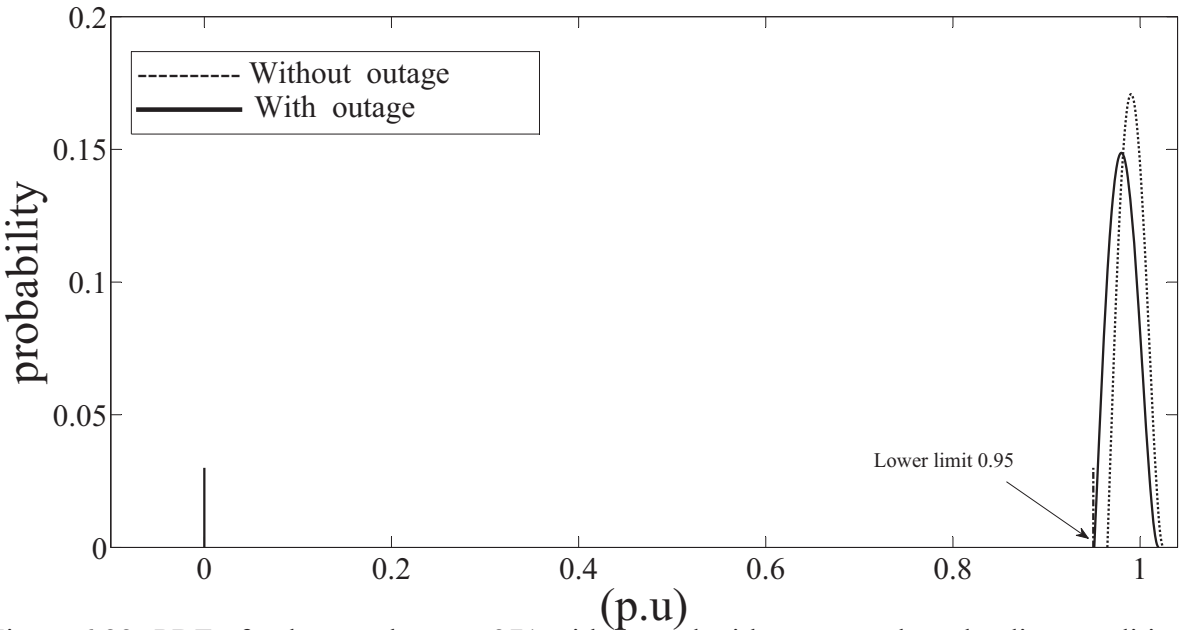

Figure 6.22: PDF of voltage at bus no. 271 without and with outage at base loading condition, with WTGs

In this case also, the system can operate safely with WTG as the bus voltage magnitudes are well within the upper and lower limits.

From the study carried out on different systems, it is evident that the developed PEM based PLF method is suitable for carrying out contingency analysis of the power system, with embedded wind generation and generation uncertainty.

6.5 Conclusion

In this chapter, a PEM based PLF method has been developed to analyse the effect of generator and line outages in the system with WTGs. The analysis also considers the uncertainty in wind generation, correlation between the loads as well as the correlation between the wind generators. Further, spline based technique has been used for reconstructing the PDFs. The method has been tested on IEEE-30, IEEE-118 and IEEE-300 bus systems. The results obtained establish the suitability and efficiency of the developed technique. In the next chapter, the major contributions made in this work and suggestions for future work are presented.

Chapter 7: Conclusion and scope for future work

This chapter summarizes the major contributions of the work and suggests directions for the future investigations.

7.1 Conclusions

Based on the work reported in this thesis, the following conclusions are drawn:

- For computing the moments of variables of interest, seven point PEM (7PEM) is most accurate as compared to three PEM (3PEM) or five PEM (5PEM). Further, 7PEM is well suited for including the limit on the active power of the slack bus as well the limits on the reactive power generation/absorption of all the generators.

- GC or CF series can reconstruct the PDF or CDF of unimodal variables of interest quite accurately. However, for multi-modal distributions, the performance of both the series is not satisfactory.

- For reconstructing the PDF or CDF of multimodal variables of interest, spline based method is an accurate and attractive method.

- PEM based load flow technique can be appropriately modified to include the detailed models of the WTGS considering correlations among the loads as well as among the WTGs.

- PEM based load flow method can be effectively used for probabilistic reactive power planning under uncertain environment. Further, a new technique, namely, MPSOGSA gives the best results in comparison to those obtained by GA, GSA and PSOGSA and also ensures the repeatability of the results.

- PEM based load flow method can also be effectively used for contingency analysis under uncertain generation and load conditions.

7.2 Scope for future work

- In this work, a simple model of the DFIG has been considered. For more realistic assessment of the power system, detailed model of the DFIG should be included in the PEM based PLF.

- In this work, brute force method for MCS has been adopted, which is quite time consuming. However, in the literature, different efficient techniques have been proposed to speed up the

MCS process. It would be illuminating to explore the performance these techniques vis-a-vis the proposed PEM based PLF.

- In this work, only spline based PDF reconstruction method has been used for reconstructing the multimodal PDFs. However, it would informative to explore application of other methods such as GMM, KDE etc. for this same purpose.
- In this work, probabilistic reactive power planning has been carried out without considering any contingencies. However, to enhance the security of the system, it would be better to consider the contingencies also during probabilistic reactive power planning exercise.
- The PEM based PLF can be explored for bulk power system reliability evaluation.

Bibliography

[1] W. El-Khattam and M. M. A. Salama, "Distributed generation technologies, definitions and benefits", *Electric Power Systems Research*, vol. 71, no. 2, pp. 119–128, Oct. 2004.

[2] G. J. Anders, *Probability Concepts in Electric Power Systems*, New York: Wiley, 1990.

[3] B. Borkowska, "Probabilistic load flow", *IEEE Transactions on Power Apparatus and Systems*, vol. PAS-93, no. 3, pp. 752–759, May 1974.

[4] R.N. Allan, B. Borkowska, and C.H. Grigg, "Probabilistic analysis of power flows", *Proceedings of the Institution of Electrical Engineers*, vol. 121, no. 12, pp. 1551–1556, Dec. 1974.

[5] N. D. Hatziargyriou, T. S. Karakatsanis, and M. Papadopoulos, "Probabilistic load flow in distribution system containing dispersed wind power generation", *IEEE Transactions on Power Systems*, vol. 8, no. 1, pp. 159–165, Feb. 1993.

[6] A. C. Melhorn, A. Dimitrovski, and K. Tomsovic, "Three phase probabilistic load flow in radial distribution networks", in *Proceedings of the 12th International Conference on Probabilistic Methods Applied to Power, Istanbul, Turkey*, June 10-14 2012.

[7] W. El-Khattam, Y. G. Hegazy, and M. M. A. Salama, "Investigating distributed generation systems performance using monte carlo simulation", *IEEE Transactions on Power Systems*, vol. 21, no. 2, pp. 524–532, May 2006.

[8] R.N. Allan, A.M. Leite da Silva, and R.C. Burchett, "Evaluation methods and accuracy in probabilistic load flow solutions", *IEEE Transactions on Power Apparatus and Systems*, vol. PAS-100, no. 5, pp. 2539–2546, May 1981.

[9] H. Yu, C. Y. Chung, K. P. Wong, H. W. Lee, and J. H. Zhang, "Probabilistic load flow evaluation with hybrid latin hypercube sampling and cholesky decomposition", *IEEE Transactions on Power Systems*, vol. 24, no. 2, pp. 661–667, May 2009.

[10] Yan Chen, Jinyu Wen, and Shijie Cheng, "Probabilistic load flow method based on nataf transformation and latin hypercube sampling", *IEEE Transactions sustainable energy*, vol. 4, no. 2, pp. 294–301, April 2013.

[11] Defu Cai, Dongyuan Shi, and Jinfu Chen, "Probabilistic load flow computation with polynomial normal transformation and latin hypercube sampling", *IET Generation Transmission Distribution*, vol. 7, no. 5, pp. 474–482, 2013.

[12] Defu Cai, Dongyuan Shi, and Jinfu Chen, "Probabilistic load flow computation using copula and latin hypercube sampling", *IET Generation Transmission Distribution*, vol. 8, no. 9, pp. 1539–1549, 2014.

[13] Defu Cai, Dongyuan Shi, and Jinfu Chen, "Probabilistic load flow with correlated input random variables using uniform design sampling", *International Journal of Electrical Power and Energy Systems*, vol. 63, pp. 105–112, 2014.

[14] R.N. Allan and M.R.G. Al-Shakarchi, "Probabilistic a.c. load flow", *Proceedings of the Institution of Electrical Engineers*, vol. 123, no. 6, pp. 531–536, June 1976.

[15] A. P. S. Meliopoulos, G. J. Cokkinides, and X. Y. Chao, "A new probabilistic power flow analysis method", *IEEE Transactions on Power Systems*, vol. 5, no. 1, pp. 182–190, Feb. 1990.

[16] R. N. Allan, C. H. Grigg, and M. R. G. Al-Shakarchi, "Numerical techniques in probabilistic load flow problems", *International Journal for Numerical Methods in Engineering*, vol. 10, no. 4, pp. 853–860, 1976.

[17] R. N. Allan and A. M Leite da Silva, "Probabilistic load flow using multilinearisations", *Proceedings of the Institution of Electrical Engineers*, vol. 128, no. 5, pp. 280–287, Sept. 1981.

[18] A. M Leite da Silva and V. L. Arienti, "Probabilistic load flow by multilinear simulation algorithm", *Proceedings of the Institution of Electrical Engineers*, vol. 137, no. 4, pp. 276–282, July 1990.

[19] M. Brucoli, F. Torelli, and R. Napoli, "Quadratic probabilistic load flow with linearly modeled dispatch", *International Journal of Electrical Power and Energy Systems*, vol. 7, no. 3, pp. 138–146, July 1985.

[20] X. Li, X. Chen, X. Yin, T. Xiang, and H. Liu, "The algorithm of probabilistic load flow retaining nonlinearity", *International Conference on Power System Technology*, vol. 4, pp. 2111–2115, 2002.

[21] Xi. Wang, Y. Song, and M. Irving, *Modern Power Systems Analysis*, Springer, 2009.

[22] Pei Zhang and S.T. Lee, "Probabilistic load flow computation using the method of combined cumulants and Gram-Charlier expansion", *IEEE Transactions on Power Systems*, vol. 19, no. 1, pp. 676–682, Feb. 2004.

[23] T. Williams and C. Crawford, "Probabilistic load flow modeling comparing maximum entropy and gram-charlier probability density function reconstructions", *IEEE Transactions on Power Systems*, vol. 28, no. 1, pp. 272–280, Feb. 2013.

[24] D. Villanueva, A. E. Feijo, and J. L. Pazos, "An analytical method to solve the probabilistic load flow considering load demand correlation using the dc load flow", *Electric Power Systems Research*, vol. 110, pp. 1–8, 2014.

[25] H. P. Hong, "An efficient point estimate method for probabilistic analysis", *Reliability Engineering and System Safety*, vol. 59, no. 3, pp. 261–267, 1998.

[26] Chun-Lien Su and Chan-Nan Lu, "Two-point estimate method for quantifying transfer capability uncertainty", *IEEE Transactions on Power Systems*, vol. 20, no. 2, pp. 573–579, May 2005.

[27] J. M. Morales and J. Perez-Ruiz, "Point estimate schemes to solve the probabilistic power flow", *IEEE Transactions on Power Systems*, vol. 22, no. 4, pp. 1594–1601, Nov. 2007.

[28] Chun-Lien Su, "Probabilistic load-flow computation using point estimate method", *IEEE Transactions on Power Systems*, vol. 20, no. 4, pp. 1843–1851, Nov. 2005.

[29] J. Usaola, "Probabilistic load flow with wind production uncertainty using cumulants and Cornish-Fisher expansion", *International Journal of Electrical Power and Energy Systems*, vol. 31, no. 9, pp. 474–481, Oct. 2009.

[30] J. Usaola, "Probabilistic load flow in systems with wind generation", *IET Generation, Transmission and Distribution*, vol. 3, no. 12, pp. 1031–1041, Dec. 2009.

[31] G. Valverde, A. T. Saric, and V. Terzija, "Probabilistic load flow with non-gaussian correlated random variables using gaussian mixture models", *IET generation, transmission and distribution*, vol. 6, no. 7, pp. 701–709, 2012.

[32] Cristina Carmona-Delgado, Esther Romero-Ramos, and J. Riquelme-Santos, "Probabilistic load flow with versatile non-gaussian power injections", *Electric Power Systems Research*, vol. 119, pp. 266–277, 2015.

[33] N. Soleimanpour and M. Mohammadi, "Probabilistic load flow by using nonparametric density estimators", *IEEE Transactions on Power systems*, vol. 28, no. 4, pp. 3747–3755, Nov. 2013.

[34] J.A. Carta, P. Ramirez, and S. Velazquez, "A review of wind speed probability distributions used in wind energy analysis: Case studies in the Canary Islands", *Renewable and Sustainable Energy Reviews*, vol. 13, no. 5, pp. 933–955, June 2009.

[35] J. Usaola, "Probabilistic load flow with correlated wind power injections", *Electric Power Systems Research*, vol. 80, no. 5, pp. 528–536, May 2010.

[36] Y. Yuan, J. Zhou, P. Ju, and J. Feuchtwang, "Probabilistic load flow computation of a power system containing wind farms using the method of combined cumulants and Gram- Charlier expansion", *IET Renewable Power Generation*, vol. 5, no. 6, pp. 448–454, Nov. 2011.

[37] D. Villanueva, J. L. Pazos, and A. Feijoo, "Probabilistic load flow including wind power generation", *IEEE Transactions on Power Systems*, vol. 26, no. 3, pp. 1659–1667, Aug. 2011.

[38] Can Chen, Wenchuan Wu, Boming Zhang, and Hongbin Sun, "Correlated probabilistic load flow using a point estimate method with nataf transformation", *International Journal of Electrical Power and Energy Systems*, vol. 65, pp. 325–333, 2015.

[39] Xiaomeng Ai, Jinyu Wen, Tong Wu, and Wei-Jen Lee, "A discrete point estimate method for probabilistic load flow based on the measured data of wind power", in *IEEE Industry Applications Society Annual Meeting*, 2012, pp. 1–7.

[40] J. M. Morales, L. Baringo, A. J. Conejo, and R. Minguez, "Probabilistic power flow with correlated wind sources", *IET Generation, Transmission and Distribution*, vol. 4, no. 5, pp. 641–651, May 2010.

[41] J. M. Morales, R. Minguez, and A. J. Conejo, "A methodology to generate statistically dependent wind speed scenarios", *Applied Energy*, vol. 87, no. 3, pp. 843–855, March 2010.

[42] A. E. Feijoo, J. Cidras, and J. L. G. Dornelas, "Wind speed simulation in wind farms for steady-state security assessment of electrical power systems", *IEEE Transactions on Energy Conversion*, vol. 14, no. 4, pp. 592–598, Dec. 1999.

[43] Andres Feijoo, Daniel Villanueva, Jose Luis Pazos, and Robert Sobolewski, "Simulation of correlated wind speeds: A review", *Renewable and Sustainable Energy Reviews*, vol. 15, no. 6, pp. 2826–2832, Aug. 2011.

[44] P. F. Correia and J. M. Ferreira de Jesus, "Simulation of correlated wind speed and power variates in wind parks", *Electric Power Systems Research*, vol. 80, no. 5, pp. 592–598, Nov. 2010.

[45] Z. Qin, W. Li, and X. Xiong, "Generation system reliability evaluation incorporating correlations of wind speeds with different distributions", *IEEE Transactions on Power Systems*, vol. 28, no. 1, pp. 551–558, Feb. 2013.

[46] G. Papaefthymiou, P. H. Schavemaker, L. Sluis, W. L. Kling, D. Kurowicka, and R. M. Cooke, "Integration of stochastic generation in power systems", *Electrical Power and Energy Systems*, vol. 28, pp. 655–667, Aug. 2005.

[47] R. N. Allan and Al Shakarchi, "Linear dependence in nodal power in probabilistic a.c. load flow", *Proceedings of the Institution of Electrical Engineers*, vol. 124, no. 6, pp. 529–534, June 1977.

[48] A. M. Leite da Silva, V.L. Arienti, and R. N. Allan, "Probabilistic load flow considering dependence between input nodal powers", *IEEE Transactions on Power Apparatus and Systems*, vol. 103, no. 6, pp. 1524–1530, June 1984.

[49] R. N. Allan, C. H. Grigg, D. A. Newey, and R. F. Simmons, "Probabilistic power-flow techniques extended and applied to operational decision making", *Proceedings of the Institution of Electrical Engineers*, vol. 123, no. 12, pp. 1317–1324, Dec. 1976.

[50] A. M. Leite da Silva, S. M. P. Ribeiro, V. L. Arienti, R. N. Allan, and M. B. Do Coutto Filho, "Probabilistic load flow techniques applied to power system expansion planning", *IEEE Transactions on Power Systems*, vol. 5, no. 4, pp. 1047–1053, Nov. 1990.

[51] S. K. Parida, S. C. Srivastava, and S. N. Singh, "A review on reactive power management in electricity markets", *International Journal of Energy Sector Management*, vol. 5, no. 2, pp. 201–214, 2011.

[52] S. K. Parida, S. N. Singh, and S. C. Srivastava, "A hybrid approach toward security-constrained reactive power planning in electricity markets", *Electric Power Components and Systems*, vol. 36, no. 6, pp. 649–663, May. 2008.

[53] K. Iba, H. Suzuki, K. I. Suzuki, and K. Suzuki, "Practical reactive power allocation/operation planning using successive linear programming", *IEEE Transactions on Power Systems*, vol. 3, no. 2, pp. 558–566, May 1988.

[54] M. K. Mangoli, K. Y. Lee, and Park Y. M., "Optimal long-term reactive power planning using decomposition techniques", *Electric Power Systems Research*, vol. 26, no. 1, pp. 41–52, Jan. 1993.

[55] D. Chattopadhyay, K. Bhattacharya, and J. Parikh, "Optimal reactive power planning and its spot-pricing: an integrated approach", *IEEE Transactions on Power Systems*, vol. 10, no. 4, pp. 2014–2020, Nov. 1995.

[56] J. R. S. Mantovani and A.V. Garcia, "A heuristic method for reactive power planning", *IEEE Transactions on Power Systems*, vol. 11, no. 1, pp. 68–74, Feb. 1996.

[57] L. L. Lai and J. T. Ma, "Application of evolutionary programming to reactive power planning-comparison with nonlinear programming approach", *IEEE Transactions on Power Systems*, vol. 12, no. 1, pp. 198–206, Feb. 1997.

[58] Y. T. Hsiao and Chiang H. D., "Applying network window schema and a simulated annealing technique to optimal var planning in large-scale power systems", *International Journal of Electrical Power & Energy Systems*, vol. 22, no. 1, pp. 1–8, Jan. 2000.

[59] W. Zhang, F. Li, and L. M. Tolbert, "Review of reactive power planning: Objectives, constraints, and algorithms", *IEEE Transactions on Power Systems*, vol. 22, no. 4, pp. 2177–2186, Oct. 2007.

[60] N. Yang, C. W. Yu, F. Wen, and C. Y. Chung, "An investigation of reactive power planning based on chance constrained programming", *International Journal of Electrical Power & Energy Systems*, vol. 29, no. 9, pp. 650–656, Nov. 2007.

[61] J. C. Lopez, J. Contreras, J. Munoz, and J. R. S. Mantovani, "A multi-stage stochastic nonlinear model for reactive power planning under contingencies", *IEEE Transactions on Power Systems*, vol. 28, no. 2, pp. 1503–1514, Apr. 2013.

[62] Z. Hua, X. Wang, and G. Taylor, "Stochastic optimal reactive power dispatch: Formulation and solution method", *International Journal of Electrical Power & Energy Systems*, vol. 32, no. 6, pp. 615–621, July 2010.

[63] T. S. Karakatsanis and N. D. Hatziargyriou, "Probabilistic constrained load flow based on sensitivity analysis", *IEEE Transactions on Power Systems*, vol. 9, no. 4, pp. 1853–1860, Nov. 1994.

[64] M. Dadkhah and B. Venkatesh, "Cumulant based stochastic reactive power planning method for distribution systems with wind generators", *IEEE Transactions on Power Systems*, vol. 27, no. 4, pp. 2351–2359, Nov. 2012.

[65] S. A. Arefifar and A. Y. I. Mohamed, "Probabilistic optimal reactive power planning in distribution systems with renewable resources in grid-connected and islanded modes", *IEEE Transactions on industrial electronics*, vol. 61, no. 11, pp. 5830–5839, Nov. 2014.

[66] K. Zou, K. M. Agalgaonkar, A. P. Muttaqi, and S. Perera, "Distribution system planning with incorporating dg reactive capability and system uncertainties", *IEEE Transactions on Sustainable Energy*, vol. 3, no. 1, pp. 112–123, 2012.

[67] A. M Leite da Silva, R. N. Allan, S.M. Soares, and V.L. Arienti, "Probabilistic load flow considering network outages", *IEE Proceedings on Generation Transmission and Distribution*, vol. 132, no. 3, pp. 139–145, May 1985.

[68] Z. Hu and X. Wang, "A probabilistic load flow method considering branch outages", *IEEE Transactions on Power Systems*, vol. 21, no. 2, pp. 507–514, May 2006.

[69] A. Bhattacharya and P. K. Roy, "Solution of multi-objective optimal power flow using gravitational search algorithm", *IET Generation, Transmission and Distribution*, vol. 6, no. 8, pp. 751–763, Aug. 2012.

[70] S. Mirjalili and S.Z.M. Hashim, "A new hybrid psogsa algorithm for function optimization", *International Conference on Computer and Information Application (ICCIA 2010)*, , no. 5, pp. 374–377, Dec. 2010.

[71] W. L. Martinez and A. R. Martinez, *Computational statistics handbook with matlab*, Chapman and Hall/CRC, 2002.

[72] Chun-Lien Su and Chan-Nan Lu, "Two-point estimate method for quantifying transfer capability uncertainty", *IEEE Transactions on Power Systems*, vol. 20, no. 2, pp. 573–579, May 2005.

[73] P. Caramia, G. Carpinelli, and P. Varilone, "Point estimate schemes for probabilistic three-phase load flow", *Electric Power Systems Research*, vol. 80, no. 2, pp. 168 –175, Feb. 2010.

[74] J. Usaola, "Probabilistic load flow in systems with high wind power penetration", *Departamento de Ingeniera Elctrica, Universidad Carlos III de Madrid*, Aug. 2008.

[75] Allen C. Miller and Thomas R. Rice, "Discrete approximations of probability distributions", *Management Science*, vol. 29, no. 3, pp. 352–362, March 1983.

[76] A. Stuart, K. Ord, and Arnold S., *Kendalls advanced theory of statistics*, New York: Wiley, 1994.

[77] G. W. Hill and A. W. Davis, " Generalized Asymptotic Expansions of Cornish-Fisher Type ", *The Annals of Mathematical Statistics*, vol. 39, no. 4, pp. 1107–1380, 1968.

[78] G. M Masters, *Renewable and efficient electrical power systems*, Wiley-Interscience, 2004.

[79] S. Blinnikov and R. Moessner, "Expansions for nearly gaussian distributions", *Astronomy and Astrophysics*, vol. 130, pp. 193–205, 1998.

[80] "Power Systems Test Case Archive (Online), available@ http://www.ee. washington.edu/research/pstca.".

[81] *Matlab 7.5*, Mathworks, US.

[82] C. Rose and M.D. Smith, *MathStatica: Mathematical Statistics with Mathematica*, Springer-Verlag: New York, 2002.

[83] J. Fan and Q. Yao, *Nonlinear time series*, vol. 2, Springer, 2002.

[84] V. John, I. Angelov, A. A. Oncul, and D. Thevenin, "Techniques for the reconstruction of a distribution from a finite number of its moments", *Chemical Engineering Science*, vol. 62, no. 11, pp. 2890–2904, June 2007.

[85] "The IEEE Reliability Test System - 1996", *IEEE Transactions on Power Systems*, vol. 14, no. 3, pp. 1010–1020, Aug. 1999.

[86] "PJM load data (online), available@ http://www.pjm.com".

[87] A Dimitrovski and K. Tomsovic, "Slack bus treatment in load flow solutions with uncertain nodal powers", *International Journal of Electrical Power and Energy Systems*, vol. 27, no. 9-10, pp. 614–619, Dec. 2005.

[88] A. Dimitrovski and K Tomsovic, "Uncertainty in load flow modeling: Application of the boundary load flow", *Automation of Electric Power Systems*, vol. 29, no. 16, pp. 6–15, Aug. 2005.

[89] R. D. Zimmerman, C. E. Murillo-Sanchez, and R. J. Thomas, "Matpower: Steady- state operations, planning and analysis tools for power systems research and education", *IEEE Transactions on Power Systems*, vol. 26, no. 1, pp. 12–19, Feb. 2011.

[90] Shikha, T. S. Bhatti, and D. P. Kothari, "Wind energy conversion systems as a distributed source of generation", *Journal of Energy Engineering*, vol. 129, no. 3, pp. 69–80, Feb. 2003.

[91] R. C Bansal, T. S. Bhatti, and D. P. Kothari, "On some of the design aspects of wind energy conversion systems", *Energy conversion and management*, vol. 43, no. 16, pp. 2175–2187, Nov. 2002.

[92] M. H. Ahmed, K. Bhattacharya, and M. M. A. Salama, "Probabilistic distribution load flow with different wind turbine models", *IEEE Transactions on Power Systems*, vol. 28, no. 2, pp. 1540–1549, May 2013.

[93] R. C. Bansal, T. S. Bhatti, and D. P. Kothari, "Bibliography on the application of induction generators in nonconventional energy systems", *IEEE Transactions on Energy Conversion*, vol. 18, no. 3, pp. 433–439, Sept. 2003.

[94] A.E. Feijoo and J. Cidras, "Modeling of wind farms in the load flow analysis", *IEEE Transactions on Power Systems*, vol. 15, no. 1, pp. 110–115, Feb. 2000.

[95] M. Zhao, Z. Chen, and F. Blaabjerg, "Load flow analysis for variable speed offshore wind farms", *IET Renewable Power Generation*, vol. 3, no. 2, pp. 120–132, June 2009.

[96] K.C. Divya and P.S. Nagendra Rao, "Models for wind turbine generating systems and their application in load flow studies", *Electric Power Systems Research*, vol. 76, no. 9-10, pp. 844–856, June 2006.

[97] *http://www.vortex.es/samples/sample_series.txt.*

[98] D. Das, "Reactive power compensation for radial distribution networks using genetic algorithm", *International journal of electrical power and energy systems*, vol. 24, no. 7, pp. 573–581, Oct. 2002.

[99] D. Das, "Optimal placement of capacitors in radial distribution system using a fuzzy-ga method", *International Journal of Electrical Power and Energy Systems*, vol. 30, no. 6, pp. 361–367, June 2008.

[100] H. Barot and K. Bhattacharya, "Optimal reactive power planning and compensation effects on transmission loss components", in *IEEE Power Engineering Society General Meeting*. IEEE, 2007, pp. 1–7.

[101] A. G. Bakirtzis, P. N. Biskas, C. E. Zoumas, and V. Petridis, "Optimal power flow by enhanced genetic algorithm", *IEEE Transactions on power systems*, vol. 17, no. 2, pp. 229–235, May 2002.

[102] K. Y. Lee, X. Bai, and Y Park, "Optimization method for reactive power planning by using a modified simple genetic algorithm", *IEEE Transactions on power systems*, vol. 10, no. 4, pp. 1843–1850, Nov. 1995.

[103] B. Bhattacharyya and S. K. Goswami, "Reactive power optimization through evolutionary techniques: A comparative study of the ga, de and pso algorithms", *Intelligent Automation and Soft Computing*, vol. 13, no. 4, pp. 453–461, 2007.

[104] S. P. Singh, C. Kistanna, and A. R. Rao, "Optimal capacitor allocation in distribution systems using genetic algorithm", *International Journal of Computer Systems Science & Engineering*, vol. 23, no. 5, pp. 387–394, 2008.

[105] E. Rashedi, H. Nezamabadi-pour, and S. Saryazdi, " GSA: A Gravitational Search Algorithm", *Information Sciences*, vol. 179, no. 13, pp. 2232–2248, June 2009.

[106] S. Duman, Y. Sonmez, Guvenc U., and N. Yorukeren, "Optimal reactive power dispatch using a gravitational search algorithm", *IET Generation, Transmission and Distribution*, vol. 6, no. 6, pp. 563–576, June 2012.

[107] J. Kennedy and R. C. Eberhart, "Particle swarm optimization", *Proceedings of IEEE international conference on neural networks*, vol. 4, pp. 1942–1948, 1995.

[108] S. Ganguly, N. C. Sahoo, and D. Das, "Mono-and multi-objective planning of electrical distribution networks using particle swarm optimization", *Applied Soft Computing*, vol. 11, no. 2, pp. 2391–2405, June 2011.

[109] S. Ganguly, N. C. Sahoo, and D. Das, "Multi-objective particle swarm optimization based on fuzzy-pareto-dominance for possibilistic planning of electrical distribution systems incorporating distributed generation", *Fuzzy Sets and Systems*, vol. 213, pp. 47–73, June 2013.

[110] P. Acharjee and S. K. Goswami, "Chaotic particle swarm optimization based robust load flow", *International journal of electrical power and energy systems*, vol. 32, no. 2, pp. 141–146, Feb. 2010.

[111] P. Acharjee and S. K. Goswami, "A decoupled power flow algorithm using particle swarm optimization technique", *Energy Conversion and Management*, vol. 50, no. 9, pp. 2351–2360, Sept. 2009.

[112] S. P. Singh and A. R. Rao, "Optimal allocation of capacitors in distribution systems using particle swarm optimization", *International Journal of Electrical Power and Energy Systems*, vol. 43, no. 1, pp. 1267–1275, July 2012.

[113] N. Jain, S. N. Singh, and S. C. Srivastava, "Pso based placement of multiple wind dgs and capacitors utilizing probabilistic load flow model", *Swarm and Evolutionary Computation*, vol. 19, pp. 15–24, Dec. 2014.

[114] S. Dutta and S. P. Singh, "Optimal rescheduling of generators for congestion management based on particle swarm optimization", *IEEE Transactions on Power Systems*, vol. 23, no. 4, pp. 1560–1569, Nov. 2008.

[115] H. R. Baghaee and M. Abedi, "Calculation of weighting factors of static security indices used in contingency ranking of power systems based on fuzzy logic and analytical hierarchy process", *Electrical Power and Energy Systems*, vol. 33, no. 4, pp. 855–860, May 2011.

[116] M. L. Zhao, Y. Dong, and T. K. Saha, "Probabilistic load flow method considering transmission network contingency", *IEEE Power Engineering Society General Meeting*, pp. 1–6, 2007.

[117] M. Prabhat, R. Balasubramanian, and K. S. P Rao, "A new fourier method for evaluating generation system reliability indices", *IEEE Transactions on Power Systems*, vol. 1, no. 3, pp. 88–94, Aug. 1986.

[118] "Outage and Reliability Reports, Automatic Transmission Line Outage Counts and Durations, available@ http://transmission.bpa.gov/Business/Operations/Outages/default.aspx".

[119] Z. Lubosny, *Wind Turbine Operation in Electric Power Systems Advanced Modeling*, Springer Verlag, 2003.

Publications from the research work

Journals

- N. Gupta, V. Pant, and B. Das, Probabilistic load flow incorporating generator reactive power limit violations with spline based reconstruction method, Electric Power Systems Research, vol. 106, pp. 203- 213, Jan 2014.

Under Review

- N. Gupta, V. Pant, and B. Das, Probabilistic optimal reactive power planning with wind generation, Submitted to IEEE Transactions on Sustainable Energy.

International Conferences

- N. Gupta, A complete probabilistic power flow solution for transmission system, IEEE Fifth Power India Conference, pp. 1- 6, Dec. 2012.

Appendix A

- **Random Variable**

If the outcome of a random experiment can be described by one numerical variable, and this numerical value is determined by a certain probability, then the variable is named a random variable (RV). The random variable X can be classified into a discrete random variable and a continuous random variable according to its different possible values. For continuous random variables, the probability density function (PDF) $f_X(x)$, is defined as [2, 21]

$$f_X(x) = \lim_{\Delta x \to 0} \frac{1}{\Delta x} P(x < X < x + \Delta x) \tag{A.1}$$

eq. (A.1) can be expressed as;

$$P(x < X < x + \Delta x) \approx f_X(x)\Delta x \tag{A.2}$$

which is the probability under the condition that random variable X is in the interval $(x, x + \Delta x)$ as $\Delta x \longrightarrow 0$. Obviously, the probability of random variable X lying in the interval between a and b is given by

$$P(a < X \leq b) = \int_a^b f_X(x)d(x) \tag{A.3}$$

The cumulative distribution function $F_X(x)$ can be written as

$$F_X(x) = \int_{-\infty}^{x} f_X(x)d(x), \text{ or } f_X(x) = \frac{dF_X(x)}{dx} \tag{A.4}$$

For a discrete random variable X having n discrete values $x_i (i = 1, 2, ..., n)$ and its probability density function and cumulative distribution function are given by eq. (A.5) and eq. (A.6) respectively.

$$p(x) = \left\{ \begin{array}{rl} P(X = x_i) & x = x_i \\ 0 & x \neq x_i \end{array} \right\} \tag{A.5}$$

$$F(x) = \sum_{x_i \leq x} p(x_i) \tag{A.6}$$

The PDFs of discrete and continuous random variables are given in Fig. A.1(a) and (b) respectively.

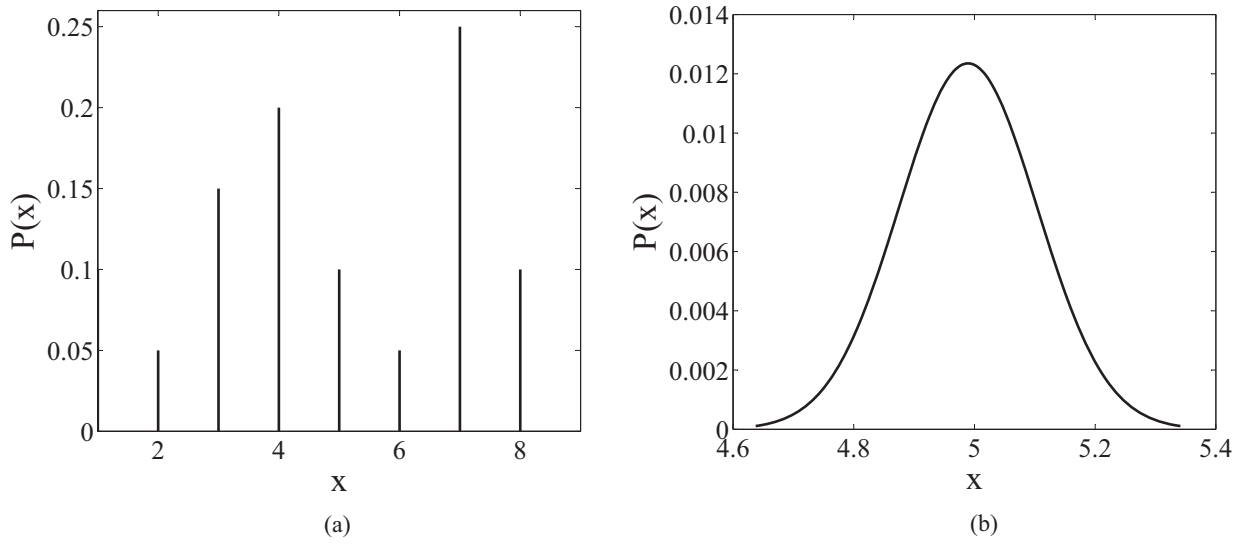

Figure A.1: PDFs of discrete and continuous random variables

- **Moments and cumulants**

Let $f_X(x)$ be the probability density function for the continuous RV x, then the Moment Generating Function (MGF) is given by

$$MGF(t) = \int_{-\infty}^{\infty} f_X(x) e^{tx} dx \tag{A.7}$$

With the assumption of finite moments, the MGF can be represented by Maclaurin series expansion

$$MGF(t) = \sum_{n=0}^{\infty} m_n \frac{t^n}{n!} \tag{A.8}$$

where, m_n is the n^{th} moments about origin and can be obtained as

$$m_n = \int_{-\infty}^{\infty} x^n f_X(x) dx, \quad (n = 0, 1....) \tag{A.9}$$

when n=1, then m_1 is the mean or expected value μ. The central moment M_n can be obtained as:

$$M_n = \int_{-\infty}^{\infty} (x - \mu)^n f_X(x) dx \tag{A.10}$$

Cumulants are most easily defined through the cumulant generating function (CGF) which is the logarithm of MGF. The CGF is given by

$$CGF(t) = lnMGF(t) \tag{A.11}$$

or

$$CGF(t) = \sum_{n=1}^{\infty} \kappa_n \frac{t^n}{n!} \tag{A.12}$$

where, κ_n are the cumulants and are given by

$$\kappa_n = CGF^n(0), \quad (n = 1, 2....) \tag{A.13}$$

Now, the recurrence relation for moments is obtained from

$$MGF(t) = \sum_{n=1}^{\infty} m_n \frac{t^n}{n!} = exp\left(\sum_{n=1}^{\infty} \kappa_n \frac{t^n}{n!}\right) \tag{A.14}$$

By taking the n^{th} order derivatives at $t = 0$, we get

$$m_{n+1} = \sum_{p=0}^{n} \binom{n}{p} m_{n-p}\kappa_{p+1} \tag{A.15}$$

The first four raw moments are related to the cumulants by

$$\begin{aligned} m_1 &= \kappa_1 \\ m_2 &= \kappa_1^2 + \kappa_2 \\ m_3 &= \kappa_1^3 + 3\kappa_1\kappa_2 + \kappa_3 \\ m_4 &= \kappa_1^4 + 6\kappa_1^2\kappa_2 + 3\kappa_2^2 + 4\kappa_1\kappa_3 + \kappa_4 \end{aligned} \tag{A.16}$$

Eq. A.15 can be solved for κ_{n+1} i.e cumulants in terms of moments

$$\kappa_{n+1} = m_{n+1} - \sum_{p=0}^{n-1} \binom{n}{p} m_{n-p}\kappa_{p+1} \tag{A.17}$$

The first four cumulants in terms of moments are given by

$$\begin{aligned} \kappa_1 &= m_1 = \mu \\ \kappa_2 &= m_2 - m_1^2 = \sigma^2 \\ \kappa_3 &= 2m_1^3 - 3m_1m_2 + m_3 = \gamma_1\sigma^3 \\ \kappa_4 &= -6m_1^4 + 12m_1^2m_2 - 3m_2^2 - 4m_1m_3 + m_4 = \gamma_2\sigma^4 \end{aligned} \tag{A.18}$$

where, μ is the mean, σ is the standard deviation, γ_1 is the skewness, γ_2 is the kurtosis of a random variable and $\binom{n}{p}$ is the binomial coefficient ${}^n\mathrm{C}_p$.

Similar relations can also be found between the cumulants and central moments (M_n), and the

first eight cumulants in terms of central moments are given by

$$\begin{aligned}
\kappa_1 &= M_1 = 0 \\
\kappa_2 &= M_2 \\
\kappa_3 &= M_3 \\
\kappa_4 &= M_4 - 3M_2^2 \\
\kappa_5 &= M_5 - 10M_3M - 2 \\
\kappa_6 &= M_6 - 15M_4M_2 - 10M_3^2 + 30M_2^3 \\
\kappa_7 &= M_7 - 21M_3M_2^2 - 35M_4M_3 + 210M_3M_2^2 \\
\kappa_8 &= M_8 - 28M_3^2M_2 - 56M_5M_3 - 35M_4^2 + 420M_4M_2^2 + 560M_3^3M_2 - 630M_2^4
\end{aligned} \tag{A.19}$$

- **Gram-Charlier expansion series**

By using the normalized cumulants, the distribution of the random variable by Gram-Charlier series can be obtained by [21]:

$$F_X(x) = \int_x^\infty \phi(x)dx + \frac{g_3}{3!}\phi^{(2)}(x) - \frac{g_4}{4!}\phi^{(3)}(x) - \frac{g_5}{5!}\phi^{(4)}(x) - \frac{g_6 + 10g_3^2}{6!}\phi^{(5)}(x) - \frac{g_7 + 35g_3g_4}{7!}\phi^{(6)}(x) + ... \tag{A.20}$$

where, $F_X(x)$ is the probability when the random variable has a value greater than or equal to x, g_n is the normalized cumulant of order n, and can be obtained from the cumulants and standard deviation of RV as.

$$g_n = K_n/\sigma^n \tag{A.21}$$

$\phi(x)$ is the standard normal density function:

$$\phi(x) = \frac{1}{\sqrt{2\pi}} e^{-\frac{1}{2}x^2} \tag{A.22}$$

$\phi^n(x)$ $(n = 1, 2, ...)$ is the n^{th} order derivative of $\phi(x)$.

$$\phi^n(x) = \left(\frac{d}{dx}\right)^n \phi(x) = (-1)^n H_n(x)\phi(x) \tag{A.23}$$

where, $H_n(x)$ is the Hermite polynomial, and is defined by the Rodrigues formula as

$$H_n(x) = (-1)^n e^{x^2} \frac{d^n}{dx^n} e^{-x^2} \tag{A.24}$$

The first eight Hermite polynomial are:

$$\begin{aligned}
H_0(x) &= 1 \\
H_1(x) &= x \\
H_2(x) &= x^2 - 1 \\
H_3(x) &= x^3 - 3x \\
H_4(x) &= x^4 - 6x^2 + 3 \\
H_5(x) &= x^5 - 10x^3 + 15x \\
H_6(x) &= x^6 - 15x^3 + 45x^2 - 15 \\
H_7(x) &= x^7 - 21x^5 + 105x^3 - 105x \\
H_8(x) &= x^8 - 28x^6 + 210x^4 - 420x^2 - 105
\end{aligned} \tag{A.25}$$

Now, eq.(A.20) can be written as

$$F_X(x) = \int_x^\infty \phi(x)dx + \phi(\bar{x}) \left(\frac{g_3}{3!} H_2(\bar{x}) + \frac{g_4}{4!} H_3(\bar{x}) + \frac{g_5}{5!} H_4(\bar{x}) + \frac{g_6 + 10g_3^2}{6!} H_5(\bar{x}) .... \right) \tag{A.26}$$

where, $\bar{x} = (x - \mu)/\sigma$

Finally, the PDF of a variable can be obtained by differentiating eq.(A.26), with respect to x, as shown below.

$$f_X(x) = \phi(x) \left(1 + \frac{g_3}{3!} H_3(\bar{x}) + \frac{g_4}{4!} H_4(\bar{x}) + \frac{g_5}{5!} H_5(\bar{x}) + \frac{g_6 + 10g_3^2}{6!} H_6(\bar{x}) + \frac{g_7 + 35g_3g_4}{7!} H_6(\bar{x}) + ... \right) \tag{A.27}$$

- **Quantile of a distribution function**

The p_{th} quantile of a random variable X is the value q_p, such that

$$F(q_p) = P(X \leq q_p) = p \tag{A.28}$$

where, $0 < p < 1$.

For a continuous distribution function $f_X(x)$ it can be obtained by solving

$$p = \int_{-\infty}^{q_p} f_X(x)dx \tag{A.29}$$

for q_p, or by using the inverse of CDF as;

$$q_p = F^{-1}(p) \tag{A.30}$$

Examples of quantiles are quartiles, denoted by $q_{0.25}$, $q_{0.5}$, $q_{0.75}$, in which the distribution is divided into four equal segments.

- **Sum of two PDFs with their configuration probability**

Let us consider two PDFs as shown in Fig. A.2 (a) and (b) having their respective probability configurations as $p(A_1)$ and $p(A_2)$.

When these two are convolve together , distribution as shown in Fig. A.2 (c) is obtained with the final j^{th} moment $m^j(B)$ of the output variable B as as;

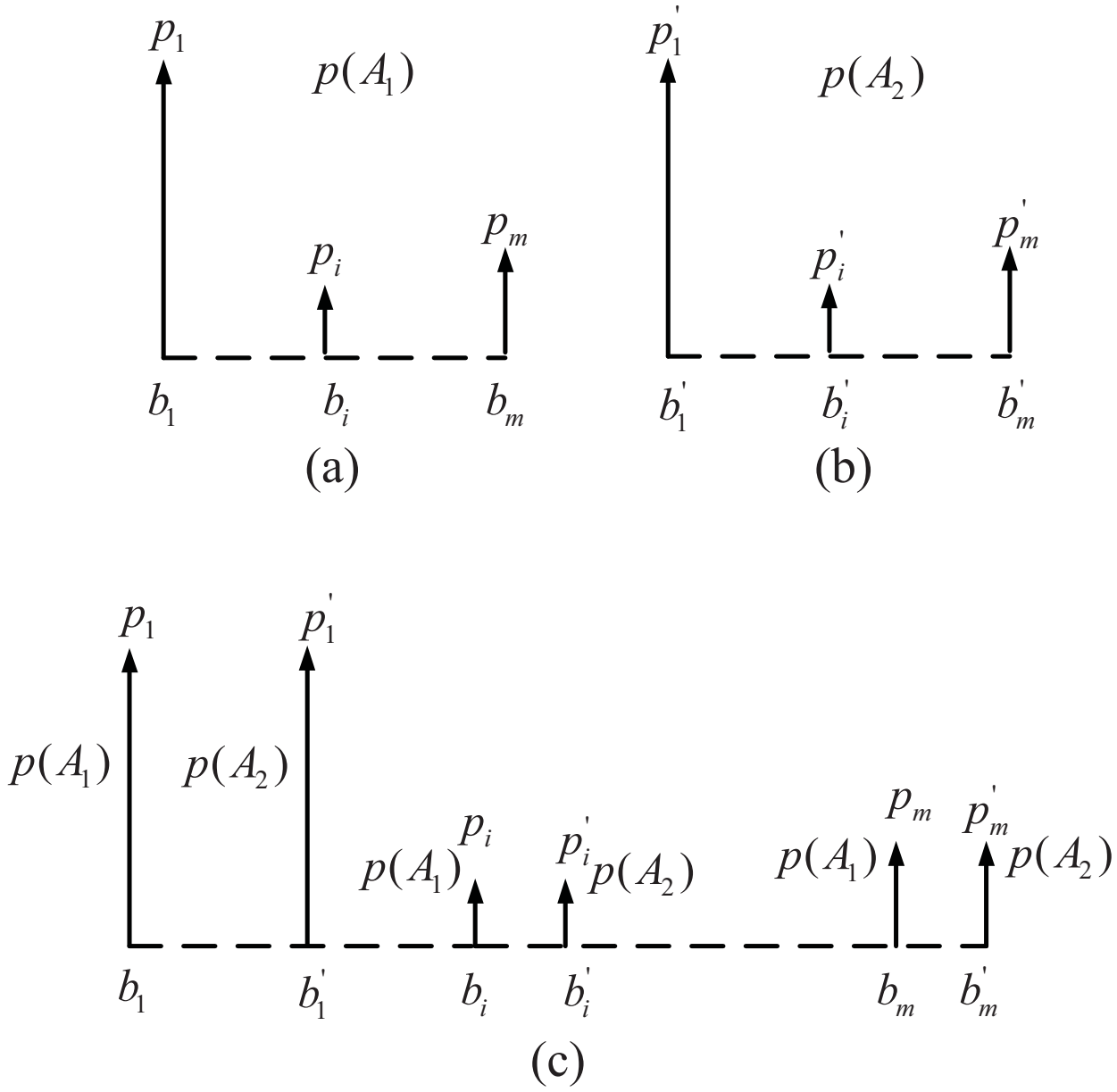

Figure A.2: Convolution of PDFs

$$
\begin{aligned}
m^j(B) =& b_1^j p(A_1)p_1 + ... + b_i^j p(A_1)p_i + ... + b_m^j p(A_1)p_m \\
&+ b_1^{'j} p(A_2)p_1^{'} + ... + b_i^{'j} p(A_2)p_i^{'} + ... + b_m^{'j} p(A_2)p_m^{'} \\
=& p(A_1)(b_1^j p_1 + ... + b_i^j p_i + ... + b_m^j p_m) \\
&+ p(A_2)(b_1^{'j} p_1^{'} + ... + b_i^{'j} p_i^{'} + ... + b_m^{'j} p_m^{'}) \\
=& p(A_1)m^j(B/A_1) + p(A_2)m^j(B/A_2)
\end{aligned}
\tag{A.31}
$$

where, $m^j(B/A_1) = (b_1^j p_1 + ... + b_i^j p_i + ... + b_m^j p_m)$ for the configuration A_1 and $m^j(B/A_2) = (b_1^{'j} p_1^{'} + ... + b_i^{'j} p_i^{'} + ... + b_m^{'j} p_m^{'})$ for the configuration A_2.

For k number of configurations, we have

$$
\begin{aligned}
m^j(B) =& p(A_1)m^j(B/A_1) + p(A_2)m^j(B/A_2) + ... + p(A_k)m^j(B/A_k) \\
=& \sum_{n=1}^{k} p(A_n)m^j(B/A_n)
\end{aligned}
\tag{A.32}
$$

Appendix B

- **Data of IEEE-118 Bus Test System**

The system data is taken from [80]. The load, generator, transformer, shunt capacitor/reactor and transmission line data are provided in the table respectively. The data is on 100 MVA base.

Bus load data

Bus no.	Load		Bus no.	Load	
	Real (MW)	Reactive (MVAR)		Real (MW)	Reactive (MVAR)
1	0.0	0.0	60	277	113
2	51	27	61	78	3
3	20	9	62	0.0	0.0
4	39	10	63	77	14
5	30	12	64	0.0	0.0
6	0.0	0.0	65	0.0	0.0
7	52	22	66	0.0	0.0
8	19	2	67	39	18
9	0.0	0.0	68	28	7
10	0.0	0.0	69	0.0	0.0
11	0.0	0.0	70	66	20
12	70	23	71	0.0	0.0
13	47	10	72	0.0	0.0
14	34	16	73	0.0	0.0
15	14	1	74	68	27
16	90	30	75	47	11

Bus no.	Load		Bus no.	Load	
	Real (MW)	Reactive (MVAR)		Real (MW)	Reactive (MVAR)
17	25	10	76	68	36
18	11	3	77	61	28
19	60	34	78	71	26
20	45	25	79	39	32
21	18	3	80	130	26
22	14	8	81	0.0	0.0
23	10	5	82	54	27
24	7	3	83	20	10
25	0.0	0.0	84	11	7
26	0.0	0.0	85	24	15
27	0.0	0.0	86	21	10
28	62	13	87	0.0	0.0
29	17	7	88	48	10
30	24	4	89	0.0	0.0
31	0.0	0.0	90	78	42
32	43	27	91	0.0	0.0
33	59	23	92	65	10
34	23	9	93	12	7
35	59	26	94	30	16
36	33	9	95	42	31

Bus no.	Load		Bus no.	Load	
	Real (MW)	Reactive (MVAR)		Real (MW)	Reactive (MVAR)
37	31	17	96	38	15
38	0.0	0.0	97	15	9
39	0.0	0.0	98	34	8
40	27	11	99	0.0	0.0
41	20	23	100	37	18
42	37	10	101	22	15
43	37	23	102	5	3
44	18	7	103	23	16
45	16	8	104	38	25
46	53	22	105	31	26
47	28	10	106	43	16
48	34	0.0	107	28	12
49	20	11	108	2	1
50	87	30	109	8	3
51	17	4	110	39	30
52	17	8	111	0.0	0.0
52	0.0	5	112	25	13
54	23	11	113	0.0	0.0
55	113	32	114	8	3
56	63	22	115	22	7

Bus no.	Load		Bus no.	Load	
	Real (MW)	Reactive (MVAR)		Real (MW)	Reactive (MVAR)
57	84	18	116	0.0	0.0
58	12	3	117	20	8
59	12	3	118	33	15

Transmission line data

Line no.	From bus no.	To bus no.	Series impedance (p.u)		Half line charging suceptance (p.u)	Line Rating (p.u)
			Resistance	Reactance		
1	2	3	0.0303	0.0999	0.0254	1.75
2	2	4	0.0129	0.0424	0.01082	1.75
3	5	6	0.00176	0.00798	0.0021	5
4	4	6	0.0241	0.108	0.0284	1.75
5	6	7	0.0119	0.054	0.01426	1.75
6	7	8	0.00459	0.0208	0.0055	1.75
7	9	10	0.00244	0.0305	1.162	5
9	10	11	0.00258	0.0322	1.23	5
10	5	12	0.0209	0.0688	0.01748	1.75
11	6	12	0.0203	0.0682	0.01738	1.75
12	12	13	0.00595	0.0196	0.00502	1.75
13	3	13	0.0187	0.0616	0.01572	1.75
14	4	13	0.0484	0.16	0.0406	1.75

Line no.	From bus no.	To bus no.	Series impedance (p.u)		Half line charging suceptance (p.u)	Line Rating (p.u)
			Resistance	Reactance		
15	8	13	0.00862	0.034	0.00874	1.75
16	12	14	0.02225	0.0731	0.01876	1.75
17	13	15	0.0215	0.0707	0.01816	1.75
18	14	16	0.0744	0.2444	0.06268	1.75
19	15	16	0.0595	0.195	0.0502	1.75
20	13	17	0.0212	0.0834	0.0214	1.75
21	16	18	0.0132	0.0437	0.0444	5
22	17	18	0.0454	0.1801	0.0466	1.75
23	18	19	0.0123	0.0505	0.01298	1.75
24	19	20	0.01119	0.0493	0.01142	1.75
25	20	21	0.0252	0.117	0.0298	1.75
26	16	20	0.012	0.0394	0.0101	1.75
27	21	22	0.0183	0.0849	0.0216	1.75
28	22	23	0.0209	0.097	0.0246	1.75
29	23	24	0.0342	0.159	0.0404	1.75
30	24	25	0.0135	0.0492	0.0498	1.75
31	24	26	0.0156	0.08	0.0864	5
33	26	28	0.0318	0.163	0.1764	5
34	28	29	0.01913	0.0855	0.0216	1.75
35	29	30	0.0237	0.0943	0.0238	1.75
37	9	31	0.00431	0.0504	0.514	1.75

Line no.	From bus no.	To bus no.	Series impedance (p.u)		Half line charging suceptance (p.u)	Line Rating (p.u)
			Resistance	Reactance		
38	27	31	0.00799	0.086	0.908	5
39	18	32	0.0474	0.1563	0.0399	1.75
40	30	32	0.0108	0.0331	0.0083	1.75
41	24	33	0.0317	0.1153	0.1173	1.4
42	32	33	0.0298	0.0985	0.0251	1.75
43	28	33	0.0229	0.0755	0.01926	1.75
44	16	34	0.038	0.1244	0.03194	1.75
45	20	35	0.0752	0.247	0.0632	1.75
46	36	37	0.00224	0.0102	0.00268	1.75
47	36	38	0.011	0.0497	0.01318	1.75
48	34	38	0.0415	0.142	0.0366	1.75
49	35	37	0.00871	0.0268	0.00568	1.75
50	35	38	0.00256	0.0094	0.00984	5
52	38	40	0.0321	0.106	0.027	1.75
53	38	41	0.0593	0.168	0.042	1.75
54	31	39	0.00464	0.054	0.422	1.75
55	40	41	0.0184	0.0605	0.01552	1.75
56	41	42	0.0145	0.0487	0.01222	1.75
57	41	43	0.0555	0.183	0.0466	1.75
58	42	43	0.041	0.135	0.0344	1.75
59	44	45	0.0608	0.2454	0.06068	1.75

Line no.	From bus no.	To bus no.	Series impedance (p.u)		Half line charging suceptance (p.u)	Line Rating (p.u)
			Resistance	Reactance		
60	35	44	0.0413	0.1681	0.04226	1.75
61	45	46	0.0224	0.0901	0.0224	1.75
62	46	47	0.04	0.1356	0.0332	1.75
63	47	48	0.038	0.127	0.0316	1.75
64	47	49	0.0601	0.189	0.0472	1.75
65	48	50	0.0191	0.0625	0.01604	1.75
66	43	50	0.0715	0.323	0.086	1.75
67	43	50	0.0715	0.323	0.086	1.75
68	46	50	0.0684	0.186	0.0444	1.75
69	49	50	0.0179	0.0505	0.01258	1.75
70	50	51	0.0267	0.0752	0.01874	1.75
71	50	52	0.0486	0.137	0.0342	1.75
72	52	53	0.0203	0.0588	0.01396	1.75
73	53	54	0.0405	0.1635	0.04058	1.75
74	54	55	0.0263	0.122	0.031	1.75
75	50	55	0.073	0.289	0.0738	1.75
76	50	55	0.0869	0.291	0.073	1.75
77	55	56	0.0169	0.0707	0.0202	1.75
78	55	57	0.00275	0.00955	0.00732	1.75
79	56	57	0.00488	0.0151	0.00374	1.75
80	57	58	0.0343	0.0966	0.0242	1.75

Line no.	From bus no.	To bus no.	Series impedance (p.u)		Half line charging suceptance (p.u)	Line Rating (p.u)
			Resistance	Reactance		
81	51	58	0.0474	0.134	0.0332	1.75
82	57	59	0.0343	0.0966	0.0242	1.75
83	52	59	0.0255	0.0719	0.01788	1.75
84	55	60	0.0503	0.2293	0.0598	1.75
85	57	60	0.0825	0.251	0.0569	1.75
86	57	60	0.0803	0.239	0.0536	1.75
87	56	60	0.04739	0.2158	0.05646	1.75
88	60	61	0.0317	0.145	0.0376	1.75
89	60	62	0.0328	0.15	0.0388	1.75
90	61	62	0.00264	0.0135	0.01456	5
91	61	63	0.0123	0.0561	0.01468	1.75
92	62	63	0.00824	0.0376	0.0098	1.75
94	64	65	0.00172	0.02	0.216	5
96	39	66	0.00901	0.0986	1.046	5
97	65	66	0.00269	0.0302	0.38	5
98	50	67	0.018	0.0919	0.0248	5
99	50	67	0.018	0.0919	0.0248	5
100	63	67	0.0482	0.218	0.0578	1.75
101	63	68	0.0258	0.117	0.031	1.75
103	67	68	0.0224	0.1015	0.02682	1.75
104	66	69	0.00138	0.016	0.638	5

Line no.	From bus no.	To bus no.	Series impedance (p.u)		Half line charging suceptance (p.u)	Line Rating (p.u)
			Resistance	Reactance		
105	48	1	0.0844	0.2778	0.07092	1.75
106	50	1	0.0985	0.324	0.0828	1.75
108	1	70	0.03	0.127	0.122	5
109	25	70	0.00221	0.4115	0.10198	1.75
110	70	71	0.00882	0.0355	0.00878	1.75
111	25	72	0.0488	0.196	0.0488	1.75
112	71	72	0.0446	0.18	0.04444	1.75
113	71	73	0.00866	0.0454	0.01178	1.75
114	70	74	0.0401	0.1323	0.03368	1.75
115	70	75	0.0428	0.141	0.036	1.75
116	1	75	0.0405	0.122	0.124	5
117	74	75	0.0123	0.0406	0.01034	1.75
118	76	77	0.0444	0.148	0.0368	1.75
119	1	77	0.0309	0.101	0.1038	1.75
120	75	77	0.0601	0.1999	0.04978	1.75
121	77	78	0.00376	0.0124	0.01264	1.75
122	78	79	0.00546	0.0244	0.00648	1.75
123	77	80	0.017	0.0485	0.0472	5
124	77	80	0.0294	0.105	0.0228	5
125	79	80	0.0156	0.0704	0.0187	1.75
126	69	81	0.00175	0.0202	0.808	5

Line no.	From bus no.	To bus no.	Series impedance (p.u)		Half line charging suceptance (p.u)	Line Rating (p.u)
			Resistance	Reactance		
128	77	82	0.0298	0.0853	0.08174	2
129	82	83	0.0112	0.03665	0.03796	2
130	83	84	0.0625	0.132	0.0258	1.75
131	83	85	0.043	0.148	0.0348	1.75
132	84	85	0.0302	0.0641	0.01234	1.75
133	85	86	0.035	0.123	0.0276	5
134	86	87	0.02828	0.2074	0.0445	5
135	85	88	0.02	0.102	0.0276	1.75
136	85	89	0.0239	0.173	0.047	1.75
137	88	89	0.0139	0.0712	0.01934	5
138	89	90	0.0518	0.188	0.0528	5
139	89	90	0.0238	0.0997	0.106	5
140	90	91	0.0254	0.0836	0.0214	1.75
141	89	92	0.0099	0.0505	0.0548	5
142	89	92	0.0393	0.1581	0.0414	5
143	91	92	0.0387	0.1272	0.03268	1.75
144	92	93	0.0258	0.0848	0.0218	1.75
145	92	94	0.0481	0.158	0.0406	1.75
146	93	94	0.0223	0.0732	0.01876	1.75
147	94	95	0.0132	0.0434	0.0111	1.75
148	80	96	0.0356	0.182	0.0494	1.75

Line no.	From bus no.	To bus no.	Series impedance (p.u)		Half line charging suceptance (p.u)	Line Rating (p.u)
			Resistance	Reactance		
149	82	96	0.0162	0.053	0.0544	1.75
150	94	96	0.0269	0.0869	0.023	1.75
151	80	97	0.0183	0.0934	0.0254	1.75
152	80	98	0.0238	0.108	0.0286	1.75
153	80	99	0.0454	0.206	0.0546	2
154	92	100	0.0648	0.295	0.0472	1.75
155	94	100	0.0178	0.058	0.0604	1.75
156	95	96	0.0171	0.0547	0.01474	1.75
157	96	97	0.0173	0.0885	0.024	1.75
158	98	100	0.0397	0.179	0.0476	1.75
159	99	100	0.018	0.0813	0.0216	1.75
160	100	101	0.0277	0.1262	0.0328	1.75
161	92	102	0.0123	0.0559	0.01464	1.75
162	101	102	0.0246	0.112	0.0294	1.75
163	100	103	0.016	0.0525	0.0536	5
164	100	104	0.0451	0.204	0.0541	1.75
165	103	104	0.0466	0.1584	0.0407	1.75
166	103	105	0.0535	0.1625	0.0408	1.75
167	100	106	0.0605	0.229	0.062	1.75
168	104	105	0.00994	0.0378	0.00986	1.75
169	105	106	0.014	0.0547	0.01434	1.75

Line no.	From bus no.	To bus no.	Series impedance (p.u)		Half line charging suceptance (p.u)	Line Rating (p.u)
			Resistance	Reactance		
170	105	107	0.053	0.183	0.0472	1.75
171	105	108	0.0261	0.0703	0.01844	1.75
172	106	107	0.053	0.183	0.0472	1.75
173	108	109	0.0105	0.0288	0.0076	1.75
174	103	110	0.03906	0.1813	0.0461	1.75
175	109	110	0.0278	0.0762	0.0202	1.75
176	110	111	0.022	0.0755	0.02	1.75
177	110	112	0.0247	0.064	0.062	1.75
178	18	113	0.00913	0.0301	0.00768	1.75
179	33	113	0.0615	0.203	0.0518	5
180	33	114	0.0135	0.0612	0.01628	1.75
181	28	115	0.0164	0.0741	0.01972	1.75
182	114	115	0.0023	0.0104	0.00276	1.75
183	69	116	0.00034	0.00405	0.164	5
184	13	117	0.0329	0.14	0.0358	1.75
185	75	118	0.0145	0.0481	0.01198	1.75
186	76	118	0.0164	0.0544	0.01356	1.75

Transformer data

Line no.	Transformer no.	Between buses		Series impedance (p.u)		Taps
		From bus no.	To bus no.	Resistance	Reactance	
8	1	9	6	0.0	0.0267	0.985
32	2	27	26	0.0	0.0382	0.960
36	3	31	18	0.0	0.0388	0.960
51	4	39	38	0.0	0.0375	0.935
93	5	64	60	0.0	0.0386	0.960
95	6	65	62	0.0	0.0268	0.985
102	7	66	67	0.0	0.0370	0.935
107	8	69	1	0.0	0.0370	0.935
127	9	81	80	0.0	0.0370	0.935

Generation data

Gen.	Bus no.	Vsp (p.u)	Generation		Reactive power limits	
			Real (MW)	Reactive (MVAR)	Min. (MVAR)	Max. (MVAR)
G1	1	1.035	0.0	0.0	0.0	0.0
G2	2	0.955	0.0	0.0	-5	15
G3	5	0.998	-9	0.0	-300	300
G4	7	0.99	0.0	0.0	-13	50
G5	9	1.015	-28	0.0	-300	300
G6	11	1.08	450	0.0	-147	200
G7	13	0.99	85	0.0	-35	120
G8	16	0.97	0.0	0.0	-10	30

Gen.	Bus no.	Vsp (p.u)	Generation		Reactive power limits	
			Real (MW)	Reactive (MVAR)	Min. (MVAR)	Max. (MVAR)
G9	19	0.973	0.0	0.0	-16	50
G10	20	0.953	0.0	0.0	-8	24
G11	25	0.992	-13	0.0	-300	300
G12	26	1.05	220	0.0	-47	140
G13	27	1.015	314	0.0	-1000	1000
G14	28	0.968	-9	0.0	-300	300
G15	32	0.967	7	0.0	-300	300
G16	33	0.964	0.0	0.0	-14	42
G17	35	0.986	0.0	0.0	-8	24
G18	37	0.98	0.0	0.0	-8	24
G19	41	0.97	-46	0.0	-300	300
G20	43	0.985	-59	0.0	-300	300
G21	47	1.005	19	0.0	-100	100
G22	50	1.025	204	0.0	-85	210
G23	55	0.955	48	0.0	-300	300
G24	56	0.952	0.0	0.0	-8	23
G25	57	0.954	0.0	0.0	-8	15
G26	60	0.985	155	0.0	-60	180
G27	62	0.995	160	0.0	-100	300
G28	63	0.998	0.0	0.0	-20	20

Gen.	Bus no.	Vsp (p.u)	Generation		Reactive power limits	
			Real (MW)	Reactive (MVAR)	Min. (MVAR)	Max. (MVAR)
G29	66	1.005	391	0.0	-67	200
G30	67	1.05	392	0.0	-67	200
G31	70	0.984	0.0	0.0	-10	32
G32	72	0.98	-12	0.0	-100	100
G33	73	0.991	-6	0.0	-100	100
G34	74	0.958	0.0	0.0	-6	9
G35	76	0.943	0.0	0.0	-8	23
G36	77	1.006	0.0	0.0	-20	70
G37	80	1.04	477	0.0	-165	280
G38	85	0.985	0.0	0.0	-8	23
G39	87	1.015	4	0.0	-100	1000
G40	89	1.005	607	0.0	-210	300
G41	90	0.985	-85	0.0	-300	300
G42	91	0.98	-10	0.0	-100	100
G43	92	0.993	0.0	0.0	-3	9
G44	99	1.01	-42	0.0	-100	100
G45	100	1.017	252	0.0	-50	155
G46	103	1.001	40	0.0	-15	40
G47	104	0.971	0.0	0.0	-8	23
G48	105	0.965	0.0	0.0	-8	23

Gen.	Bus no.	Vsp (p.u)	Generation		Reactive power limits	
			Real (MW)	Reactive (MVAR)	Min. (MVAR)	Max. (MVAR)
G49	107	0.952	-22	0.0	-200	200
G50	110	0.973	0.0	0.0	-8	23
G51	111	0.98	36	0.0	-100	1000
G52	112	0.975	-43	0.0	-100	1000
G53	113	0.993	-6	0.0	-100	200
G54	116	1.005	-184	0.0	-1000	1000

Bus injected MVAR

Bus no.	Injected MVAR		Bus no.	Injected MVAR	
	Capacitive	Inductive		Capacitive	Inductive
6	0.0	4	74	12	0.0
35	14	0.0	79	20	0.0
38	0.0	25	82	20	0.0
45	10	0.0	83	10	0.0
46	10	0.0	105	20	0.0
47	10	0.0	107	6	0.0
49	15	0.0	110	6	0.0

- **Data of IEEE-30 Bus Test System**

Bus load data

Bus no.	Load		Bus no.	Load	
	Real (MW)	Reactive (MVAR)		Real (MW)	Reactive (MVAR)
1	0	0	16	3.5	1.8
2	21.7	12.7	17	9	5.8
3	2.4	1.2	18	3.2	0.9
4	7.6	1.6	19	9.5	3.4
5	94.2	19	20	2.2	0.7
6	0	0	21	17.5	11.2
7	62.8	10.9	22	0	0
8	80	30	23	3.2	1.6
9	0	0	24	8.7	6.7
10	5.8	2	25	0	0
11	0	0	26	3.5	2.3
12	11.2	7.5	27	0	0
13	0	0	28	0	0
14	6.2	1.6	29	2.4	0.9
15	8.2	2.5	30	10.6	1.9

Transmission line data

Line no.	From bus no.	To bus no.	Series impedance (p.u)		Half line charging suceptance (p.u)	Line Rating (p.u)
			Resistance	Reactance		
1	1	2	0.0192	0.0575	0.0528	1.75
2	1	3	0.0452	0.1852	0.0408	1.75
3	2	4	0.057	0.1737	0.0368	1.75
4	3	4	0.0132	0.0379	0.0084	1.75
5	2	5	0.0472	0.1983	0.0418	1.75
6	2	6	0.0581	0.1763	0.0374	1.75
7	4	6	0.0119	0.0414	0.009	1.75
8	5	7	0.046	0.116	0.0204	1.75
9	6	7	0.0267	0.082	0.017	1.75
10	6	8	0.012	0.042	0.009	1.75
17	12	14	0.1231	0.2559	0	1.75
18	12	15	0.0662	0.1304	0	1.75
19	12	16	0.0945	0.1987	0	1.75
20	14	15	0.221	0.1997	0	1.75
21	16	17	0.0824	0.1932	0	1.75
22	15	18	0.107	0.2185	0	1.75
23	18	19	0.0639	0.1292	0	1.75
24	19	20	0.034	0.068	0	1.75
25	10	20	0.0936	0.209	0	1.75
26	10	17	0.0324	0.0845	0	1.75
27	10	21	0.0348	0.0749	0	1.75

Line no.	From bus no.	To bus no.	Series impedance (p.u)		Half line charging suceptance (p.u)	Line Rating (p.u)
			Resistance	Reactance		
28	10	22	0.0727	0.1499	0	1.75
29	21	22	0.0116	0.0236	0	1.75
30	15	23	0.1	0.202	0	1.75
31	22	24	0.115	0.179	0	1.75
32	23	24	0.132	0.27	0	1.75
33	24	25	0.1885	0.3292	0	1.75
34	25	26	0.2544	0.38	0	1.75
35	25	27	0.1093	0.2087	0	1.75
37	27	29	0.2198	0.4153	0	1.75
38	27	30	0.3202	0.6027	0	1.75
39	29	30	0.2399	0.4533	0	1.75
40	8	28	0.0636	0.2	0.0418	1.75
41	6	28	0.0169	0.0599	0.013	1.75

Transformer data

Line no.	Transformer no.	Between buses		Series impedance (p.u)		Taps
		From bus no.	To bus no.	Resistance	Reactance	
1	11	6	9	0.0	0.208	1
2	12	6	10	0.0	0.556	1
3	13	9	11	0.0	0.208	1
4	14	9	10	0.0	0.11	1
5	15	4	12	0.0	0.256	1
6	16	12	13	0.0	0.14	1
7	36	27	28	0.0	0.396	1

Generation data

Gen.	Bus no.	Vsp (p.u)	Generation		Reactive power limits	
			Real (MW)	Reactive (MVAR)	Min. (MVAR)	Max. (MVAR)
G1	1	1.05	0.0	0.0	0.0	0.0
G2	2	1.0338	21.7	12.7	-500	500
G3	5	1.0058	94.2	19	-500	4
G4	8	1.023	80	30	-500	500
G5	11	1.0913	0.0	0.0	-500	20
G6	13	1.0883	0.0	0.0	-500	15

Bus injected MVAR

Bus no.	Injected MVAR		Bus no.	Injected MVAR	
	Capacitive	Inductive		Capacitive	Inductive
10	19	0.0	24	4	0.0

Appendix C

Induction generator circuit parameters

Type of WTGs	**Pitch regulated fixed speed [96]**	**Semi-variable speed [119]**
Rating (MW)	1.0	0.5
Rated (kV)	0.69	0.69
$\boldsymbol{R_1}$	0.005986	0.005671
$\boldsymbol{X_{l1}}$	0.08212	0.15250
$\boldsymbol{R_2}$	0.01690	0.00462
$\boldsymbol{X_{l2}}$	0.107225	0.096618
$\boldsymbol{X_m}$	2.5561	2.8985
$\boldsymbol{cos\phi} = 1$		